Sea ice climate interactions in the Pliocene Arctic

Fergus William Howell

School of Earth and Environment

University of Leeds

Submitted in accordance with the requirements for the degree of

Doctor of Philosophy

September 2015

The candidate confirms that the work submitted is his own, except where work which has formed part of jointly authored publications has been included. The contribution of the candidate and the other authors to this work has been explicitly indicated below. The candidate confirms that appropriate credit has been given within the thesis where reference has been made to the work of others. The work in chapters 4 to 6 of the thesis has appeared in publications as follows:

Howell, F. W., Haywood, A. M., Dolan, A. M., Dowsett, H. J., Francis, J. E., Hill, D. J., Pickering, S. J., Pope, J. O., Salzmann, U., and Wade, B. S. (2014). "Can uncertainties in sea ice albedo reconcile patterns of data-model discord for the Pliocene and 20th/21st centuries?". Geophys. Res. Lett.. Work presented in this publication forms chapter 4 and appendix A. The candidate designed the experiment, ran the model simulations and analysed the results, created the figures and wrote the paper. The co-authors A.M., A.D., J.F. and B.W. designed the research and helped write the paper. H.D. designed the research and provided a portion of the temperature data. D.H. helped to write the paper. S.P. and J.P. provided modelling support. U.S. provided a portion of the temperature data.

Howell, F. W., Haywood, A. M., Otto-Bliesner, B. L., Bragg, F., Chan, W.-L., Chandler, M. A., Contoux, C., Kamae, Y., Abe-Ouchi, A., Rosenbloom, N. A., Stepanek, C. and Zhang, Z.. "Assessment of simulations of Arctic sea ice in the PlioMIP models". Submitted to Climate of the Past. Revision of "Arctic sea ice in the PlioMIP ensemble: is model performance for modern climates a reliable guide to performance for the past or the future?", published in Climate of the Past Discussions (2015). Work presented in this publication forms chapter 5. The candidate analysed the results, created the figures and wrote the paper. A.H. and B. O-B. designed the research and helped to write the paper. C.C. and C.S. ran model simulations

and helped to write the paper. F.B., W-L.C., M.C., Y.K., A.A-O., N.R. and Z.Z. ran model simulations.

Howell, F. W., Haywood, A. M., and Pickering, S. J. "Sensitivity of Pliocene Arctic climate to orbital forcing, atmospheric CO_2 and sea ice albedo parameterisation", In preparation for submission to Earth and Planetary Science Letters. The manuscript for this submission forms chapter 6. The candidate designed the experiment, ran the model simulations and analysed the results, created the figures and wrote the paper. A.H. designed the research and helped write the paper. S.P. provided modelling support.

This copy has been supplied on the understanding that it is copyright material and that no quotation from the thesis may be published without proper acknowledgement.

©2015 The University of Leeds and Fergus William Howell.

The right of Fergus William Howell to be identified as Author of this work has been asserted by him in accordance with the Copyright, Designs and Patents Act 1988.

Acknowledgements

I would like to thank my PhD supervisor, Alan Haywood, for his encouragement and guidance throughout my PhD. I would also like to thank my co-supervisors Harry Dowsett, Bridget Wade and Jane Francis for all their help. I am very grateful to Steven Pickering for all the hours of computational support he has provided. I acknowledge the Natural Environment Research Council for the funding provided for this project, and the United States Geological Survey for the CASE Award financial assistance.

I would like to thank all the PlioMIP participants for providing data and feedback for the PlioMIP sea ice paper. Additional thanks to anyone who has been a co-author on a paper with me for their advice. Thanks to everyone in the modelling and palaeo@Leeds groups for their support and input. Thank you in particular to James Pope for his help and patience in teaching me how to perform the computer simulations.

Thank you all of my friends and family who have given me valuable support throughout my PhD. I owe a lot to Hannah, for her encouragement and for keeping me sane towards the end. Thanks most of all to my Mum and Dad, for everything they have done for me.

Abstract

The mid-Pliocene Warm Period (mPWP, 3.264 to 3.025 Myr ago) has been extensively studied through the use of general circulation models (GCMs). Whilst the output from these simulations replicates closely many of the patterns of the climate of the interval indicated by proxy data, at northern high latitudes the reconstructed proxy data temperatures exceed the model temperatures by over 15°C for some sites. This data-model discrepancy highlights the importance of focusing on model representation of processes that strongly affect the northern high latitude climates. Arctic sea ice exerts a strong influence on the Arctic climate, largely due to the ice-albedo feedback mechanism, and by creating an insulating layer between the ocean and the atmosphere. Interest in Arctic sea ice and its representation in climate models has been enhanced in recent years due to the rapid decline in the September minimum sea ice extent that has been observed since the advent of satellite observations in 1979.

This thesis describes the results from simulations of the mPWP with the GCM HadCM3, focusing on the simulated Arctic temperatures and sea ice. A change to the parameterisation of sea ice albedo is implemented in the model, based on recent observations of changes in the albedo of Arctic sea ice. The results show mean annual surface air temperature (SAT) increases of up to 6°C, and mean annual sea surface temperature (SST) increases of up to 2°C, and the disappearance of Arctic sea ice in some summer months, but very small changes in the discrepancy between the model and proxy data temperatures. The sensitivity of simulated Arctic sea ice to orbital forcings and atmospheric CO_2 in HadCM3 is also explored, with the results suggesting that changes in orbital forcing are sufficient to change the simulated mid-Pliocene Arctic from perennial to seasonal sea ice, unless combined with lower CO_2 concentrations. Changes to orbits and

CO_2 are also combined with the alternative albedo parameterisation, and further data-model comparisons are performed, with the results continuing to show cooler model temperatures, but with a reduced gap.

Also shown are the simulated Arctic sea ice outputs from eight different GCMs as part of the Pliocene Modelling Intercomparison Project (PlioMIP). The comparison demonstrates the model dependency on the simulation of Arctic sea ice, as only half of the models simulate perennial Arctic sea ice in the mid-Pliocene. The dominant influences on the sea ice simulation in the ensemble are also discussed.

Abbreviations

ACEX	Arctic Coring Expedition
AGCM	Atmosphere-only General Circulation Model
AMO	Atlantic Multi-decadal Oscillation
AMOC	Atlantic Meridional Overturning Circulation
AOGCM	Atmosphere-Ocean coupled General Circulation Model
ASO	August, September, October
AVHRR	Advanced Very High Resolution Radiometer
BASISM	British Antarctic Survey Ice Sheet Model
BIOME	Offline vegetation model (Kaplan, 2001)
BP	Before Present
BWT	Bottom Water Temperature
CAM	Community Atmosphere Model
CCSM	Community Climate System Model
CICE	Los Alamos sea ice model
CLAMP	Climate-Leaf Analysis Multivariate Program
CMIP	Coupled Model Intercomparison Project
COSMOS	Comprehensive Earth System Model
CV	Coefficient of Variation
DJF	December, January, February
DMC	Data Model Comparison
DMI	Danish Meteorological Institute
DMS	Dimethyl Sulfide
DOT	Deep Ocean Temperature
DSDP	Deep Sea Drilling Project
EoMIP	Eocene Modelling Intercomparison Project
ETOP05	Earth Topography at a 5 minute spacing

EVP	Elastic-Viscous Plastic
FMA	February, March, April
GCM	General Circulation Model
GISS	Goddard Institute of Space Studies
GISST	Global sea-Ice and Sea Surface Temperature data set
HadAM	Hadley Centre Atmospheric Model
HadCM	Hadley Centre Coupled Model
HadISST	Hadley Centre Sea Ice and Sea Surface Temperature data set
HadOM	Hadley Centre Oceanic Model
HBI	Highly Branched Isoprenoids
HOPE	Hamburg Ocean Primitive Equation
IP_{25}	Ice Proxy with 25 carbon atoms
IPCC	Intergovernmental Panel on Climate Change
IPSLCM	Institut Pierre Simon Laplace Climate Model
JJA	June, July, August
LW	Longwave
MAM	March, April, May
MIROC	Model for Interdisciplinary Research on Climate
MJJ	May, June, July
MMCO	Mid-Miocene Climatic Optimum
MOSES	Met Office Surface Exchange Scheme
mPWP	mid-Pliocene Warm Period
MRI-CGCM	Meteorological Research Institute (Japan) Coupled General Circulation Model
MSA	Methane Sulfonic Acid
NADW	North Atlantic Deep Water
NAO	North Atlantic Oscillation
NCAR	National Center for Atmospheric Research

NDJ	November, December, January
NH	Northern Hemisphere
NorESM	Norwegian Earth System Model
ODP	Ocean Drilling Program
PlioMIP	Pliocene Modelling Intercomparison Project
PRISM	Pliocene Research, Interpretation and Synoptic Mapping
SAT	Surface Air Temperature
SCD	Squared Chord Distance
SD	Standard Deviation
SH	Southern Hemisphere
SHEBA	Surface Heat Budget of the Arctic ocean
SMMR	Scanning Multi-channel Microwave Radiometer
SON	September, October, November
SST	Sea Surface Temperature
SW	Shortwave
TEVIS	Tertiary Environmental Information System
THC	Thermohaline Circulation
TRIFFID	Top-down Representation of Interactive Foliage and Flora Including Dynamics
VP	Viscous-Plastic

Contents

1 Introduction **1**

1.1 Thesis rationale . . . 1

1.2 Aims and objectives . . . 2

1.3 The mid-Pliocene Warm Period . . . 3

1.4 Atmospheric CO_2 concentrations in the mPWP . . . 6

1.5 Reconstruction of mPWP temperatures . . . 8

1.5.1 Sea surface temperatures . . . 8

1.5.1.1 Faunal analysis . . . 9

1.5.1.2 Mg/Ca palaeothermometry . . . 11

1.5.1.3 Biomarkers . . . 12

1.5.1.4 TEX_{86} . . . 13

1.5.1.5 Time-slab SST calculation . . . 13

1.5.2 Deep ocean temperatures and circulation . . . 16

1.5.3 Surface air temperatures . . . 17

1.6 Other PRISM boundary conditions . . . 18

1.6.1 Sea level . . . 18

1.6.2 Topography . . . 19

1.6.3 Vegetation . . . 21

1.6.4 Land ice . . . 23

1.6.5 Sea ice . . . 24

1.7 Modelling the mPWP . . . 25

1.8 High-latitude data-model mismatch . . . 27

1.9 Milankovitch theory . . . 32

1.9.1 Eccentricity . . . 32

1.9.2 Obliquity . . . 32
1.9.3 Precession . . . 32

2 Sea ice **34**
2.1 Sea ice influence on climate . . . 34
2.1.1 The sea ice albedo effect . . . 37
2.1.2 Factors affecting sea ice behaviour . . . 39
2.2 Observations of sea ice . . . 42
2.2.1 History of observations . . . 42
2.2.2 Polar amplification . . . 44
2.3 Sea ice modelling . . . 46
2.4 Sea ice proxies . . . 51

3 Methods **59**
3.1 HadCM3 model description . . . 59
3.1.1 Model components and coupling . . . 59
3.1.1.1 Atmosphere component . . . 59
3.1.1.2 Ocean component . . . 60
3.1.1.3 Sea ice . . . 61
3.1.1.4 Atmosphere-ocean coupling . . . 63
3.1.2 Simulation of modern climate . . . 64
3.1.2.1 Temperatures . . . 64
3.1.2.2 Sea ice . . . 65
3.2 Experimental design . . . 66

4 Sensitivity of Pliocene Arctic climate to sea ice albedo **72**
Abstract . . . 72
4.1 Introduction . . . 73
4.2 Methods . . . 75
4.2.1 Model Description . . . 75
4.2.2 Experimental Set Up . . . 75
4.2.3 Model-Data Comparisons . . . 77
4.3 Results . . . 77
4.3.1 Pliocene Albedo Runs . . . 77

4.3.1.1 Annual . . . 77
4.3.1.2 Seasonal . . . 78
4.3.2 Transient Runs . . . 79
4.4 Discussion . . . 80
4.4.1 Pliocene Albedo Runs . . . 80
4.4.2 Transient Runs . . . 82
4.5 Conclusions . . . 84

References **85**

5 Assessment of simulations of Arctic sea ice in the PlioMIP models **91**

Abstract . . . 91
5.1 Introduction . . . 92
5.2 Methods . . . 95
5.2.1 PlioMIP experimental design . . . 95
5.2.2 Analysis of results . . . 95
5.3 Results . . . 96
5.3.1 Pre-industrial sea ice simulations . . . 96
5.3.1.1 Sea ice extent . . . 96
5.3.1.2 Sea ice thickness . . . 98
5.3.2 Pliocene simulations . . . 101
5.3.2.1 Sea ice extent . . . 101
5.3.2.2 Sea ice thickness . . . 104
5.3.3 Variability across the ensemble . . . 105
5.3.4 Correlation of sea ice characteristics in the ensemble . . . 107
5.4 Discussion . . . 111
5.4.1 Pre-industrial simulations . . . 111
5.4.2 Mid-Pliocene simulations . . . 113
5.4.3 Causes of PlioMIP ensemble variability . . . 116
5.4.3.1 Influence of the sea ice models . . . 116
5.4.3.2 Influence of the control simulation . . . 119
5.4.3.3 Influence of atmosphere and ocean on the sea ice simulation . . . 120

5.5 Conclusions 123

References **129**

6 Sensitivity of Pliocene Arctic climate to orbital forcing, atmospheric CO_2 and sea ice albedo parameterisation **138**

Abstract 138

6.1 Introduction 140

6.2 Methods 141

6.2.1 Model description 141

6.2.2 Experimental design 142

6.2.2.1 Orbital configurations 143

6.2.2.2 Atmospheric CO_2 concentrations 143

6.2.2.3 Minimum sea ice albedo 144

6.2.3 Data analysis techniques 144

6.2.3.1 Data-model comparison 144

6.2.3.2 Energy balance analysis 146

6.3 Results 146

6.3.1 Sea Ice 146

6.3.1.1 Sea ice extent 146

6.3.1.2 Sea ice thickness 149

6.3.2 Temperature changes 150

6.3.2.1 Annual and seasonal changes 150

6.3.2.2 Energy balance 153

6.3.2.3 Data-model comparison 154

6.4 Discussion 161

6.4.1 Sea ice 161

6.4.2 Temperatures 162

6.5 Conclusions 165

References **168**

7 Discussion and conclusions **175**
7.1 Summary . . . 175
7.2 Research questions . . . 176
7.2.1 . . . 176
7.2.2 . . . 179
7.2.3 . . . 180
7.3 Overall conclusions . . . 185
7.4 Future work . . . 186

A Appendix **188**
A.1 Sea Ice Model Description . . . 188
A.2 Experimental Set Up . . . 189
A.2.1 Experimental Design . . . 189
A.2.2 Boundary Conditions . . . 190
A.3 Delayed Warming Effect . . . 191

References **197**

B Appendix **200**

References **203**

List of Figures

1.1 Identifying the PRISM time slab 5
1.2 Proxy estimates of mid-Pliocene pCO_2 7
1.3 Location of PRISM marine data sites 9
1.4 Warm peak averaging example 14
1.5 Deep ocean temperature estimates 16
1.6 PRISM topographical reconstruction 19
1.7 Location of PRISM terrestrial data sites 21
1.8 BIOME4 results and classifications 22
1.9 Data-model comparison for mPWP SSTs 29
1.10 Data-model comparison for mPWP SATs and SSTs 30

2.1 Schematic of sea ice-climate interactions 35
2.2 Sea ice-albedo feedback schematic 38
2.3 Sea ice albedo observations 40
2.4 Observations of September Arctic sea ice extent boundaries 43
2.5 Arctic sea ice area annual cycle 44
2.6 IP_{25} schematic 52
2.7 MSA schematic 56

3.1 Albedo values used in simulations 67

4.1 Mean annual temperature anomalies for simulations with altered minimum sea ice albedo 76
4.2 Mean seasonal temperature anomalies for simulation with minimum sea ice albedo of 0.2 79

4.3 September Arctic sea ice extent for transient simulations with both standard and altered minimum sea ice albedo 80

5.1 Mean winter (FMA) and summer (ASO) pre-industrial sea ice concentrations for all models 97
5.2 Annual pre-industrial Arctic sea ice extent cycles for PlioMIP ensemble 98
5.3 Mean winter (FMA) and summer (ASO) pre-industrial sea ice thicknesses for all models 99
5.4 Root mean square errors and spatial pattern correlations of sea ice thicknesses 100
5.5 Mean winter (FMA) and summer (ASO) mid-Pliocene sea ice concentrations for all models 103
5.6 Annual mid-Pliocene Arctic sea ice extent cycles for PlioMIP ensemble 104
5.7 Mean winter (FMA) and summer (ASO) mid-Pliocene sea ice thicknesses for all models 106
5.8 Standard deviation of sea ice concentration and thicknesses for pre-industrial and mid-Pliocene simulations 107
5.9 Scatter plots of various pre-industrial and mid-Pliocene sea ice characteristics 109
5.10 Scatter plots of temperatures and sea ice extent and volume . . . 110
5.11 Mid-Pliocene sea ice proxy locations 115
5.12 10 m winds and sea ice thickness 127
5.13 HadCM3 ocean currents and sea ice thickness 128

6.1 Locations of marine and terrestrial proxy data sites 145
6.2 Annual sea ice extent cycle for all 30 ensemble members 148
6.3 Mean annual sea ice thickness anomalies for selected simulations . 150
6.4 Mean annual SAT anomalies for selected simulations 151
6.5 Mean annual SST anomalies for selected simulations 152
6.6 Mean seasonal SAT anomalies for the Jul_500_0.2 simulation . . . 153
6.7 Mean seasonal SST anomalies for the Jul_500_0.2 simulation . . . 154

6.8 Mean annual cycle in SAT differences between two groups of simulations . . . 157
6.9 Energy balance analysis of Arctic warming . . . 158
6.10 Zonal means of Arctic total cloud for selected simulations . . . 164

A.1 Albedo values used in simulations . . . 190
A.2 Mean seasonal net downward shortwave radiation flux anomalies . . . 192
A.3 Mean seasonal sea ice fraction anomalies . . . 193
A.4 Mean seasonal sea ice thickness anomalies . . . 193
A.5 Mean seasonal net upward longwave radiation flux anomalies . . . 194
A.6 Mean seasonal sensible heat flux anomalies . . . 194
A.7 Mean seasonal SAT anomalies with different orbital simulations . . . 195
A.8 Mean seasonal sea ice concentration anomalies with different orbital simulations . . . 195

B.1 10 m winds and sea ice thicknesses . . . 201
B.2 Ocean currents and sea ice thicknesses . . . 202

LIST OF FIGURES

Chapter 1

Introduction

1.1 Thesis rationale

Mean annual Arctic sea ice extent has decreased by an average of 3.5-4.1% per decade since the beginning of modern satellite-based observations of sea ice in 1979 (Vaughan *et al.*, 2013), whilst the September sea ice extent minimum has declined by 12.9% per decade in the same time period (Stroeve *et al.*, 2012b). The future rate of sea ice decline, and the timing of the potential disappearance of summer Arctic sea ice, is of great interest when assessing predictions of climate change by computer models, known as General Circulation Models (GCMs). As Arctic sea ice exerts a strong influence on northern high-latitude climates (e.g. (Dorn *et al.*, 2007; Liu *et al.*, 2009)), better understanding of the representation of sea ice processes in GCMs will help to improve not only the simulation of sea ice in the models, but also the effects on the wider climate.

In addition to present day and the future, GCMs are also used to simulate climates of the past, with the results used to provide an independent assessment of the performance of the models. The mid-Pliocene Warm Period (mPWP, 3.3 to 3.0 Ma, (Dowsett *et al.*, 2010)) is a period of time that has been frequently modelled (see section 1.7). When results from these modelling studies have been compared to proxy data reconstructions of the mid-Pliocene climate, they have shown that the models fail to simulate sufficiently warm temperatures at high northern latitudes (e.g. Dowsett *et al.* (2011); Haywood *et al.* (2013b); Salzmann *et al.* (2013)).

Analysing processes in the models which strongly influence high latitude temperatures may help to reveal areas where modifications to the model could produce greater agreement between mid-Pliocene model and proxy data. Given the influence of sea ice at high latitudes, then the modelling of sea ice is one process through which these improvements may be achieved.

1.2 Aims and objectives

The aim of this thesis is to investigate the nature of sea ice in the mid-Pliocene Warm Period, and its effect on the climate of northern high latitudes. This research will be done primarily by using the model HadCM3 (Gordon *et al.*, 2000). The thesis aims to quantify the impact of modifications to sea ice parameterisations, or boundary conditions that will have an influence on the simulation of sea ice, on high latitude temperatures. Additionally, the model dependency of mid-Pliocene Arctic sea ice simulation will be investigated.

More specifically, chapters 4-6 aim to provide answers for the following questions:

- Is it appropriate to use the same parameterisation of sea ice albedo for simulations of different climate states? Are there alternative parameterisations for the mid-Pliocene that can improve data-model disagreements? (Chapter 4)
- What is the spread between different models' simulation of the mid-Pliocene sea ice? How does the ensemble variability compare to the same models' simulation of the pre-industrial climate? (Chapter 5)
- To what extent can atmospheric CO_2 uncertainty and orbital variations influence the nature of simulated sea ice during the mPWP, and thereby high latitude temperatures? What is the optimal combination of these factors in the model? (Chapter 6)

The following objectives will be implemented in order to provide answers to the research questions:

- Run simulations of the mPWP with the model HadCM3, with varying combinations of minimum and maximum sea ice albedo, and compare results with proxy data reconstructions of SAT and SST.
- Use results from the Pliocene Modelling Intercomparison Project (PlioMIP) in order to assess the model dependency of simulation of mid-Pliocene Arctic sea ice.
- Run further HadCM3 mPWP simulations with orbital forcings with maximum insolation at different times of year. Combine these with changes to atmospheric CO_2 and sea ice albedo in order to determine the conditions under which HadCM3 simulates a sea ice-free Arctic summer, and perform further comparisons with SAT and SST proxy data reconstructions.

The rest of chapter 1 will provide an overview of the mPWP and past modelling efforts of this time period. Chapter 2 will discuss the history of observations and modelling of sea ice, and the development of proxies for past sea ice cover. Chapter 3 will outline a brief history of GCM development, in addition to a more detailed description of the HadCM3 model, and experimental designs for chapters 4, 5 and 6.

1.3 The mid-Pliocene Warm Period

The mid-Pliocene Warm Period (mPWP, 3.264 to 3.025 Myr ago (Dowsett *et al.*, 2010)) is a period of time within the Pliocene epoch, which lasted from 5.332 to 2.588 Myr ago (Gibbard *et al.*, 2010). The mPWP was a period of sustained global warmth, with annual temperatures estimated to have been 2-3°C greater than pre-industrial (Haywood *et al.*, 2013b). As the mPWP is, in geological terms, relatively recent, it is thought that there has been very little significant change in the continental configuration to present day, and all major gateway openings or closures had occurred by the start of the mPWP (Lunt *et al.*, 2010). Sea levels are estimated to have been 25 m higher than present day (Miller *et al.*, 2012). Proxy based atmospheric CO_2 estimates fall in to the range of 190 - 450 ppm (Martinez-Boti *et al.*, 2015), and so the mPWP is the most recent period

of earth history that may have experienced the CO_2 concentrations that are seen today.

The warming of 2-3°C estimated for the Pliocene is also considered the most likely estimate of the level of warming at the end of the 21st century (Collins *et al.*, 2013b). The mPWP is therefore an excellent time period in which to test the skill and effectiveness of GCMs at predicting the future climate. In comparison to the predicted climate at the end of the 21st century, the mPWP has a similar temperature increase in comparison to present day, with little difference in important boundary conditions such as the continental configuration, which reduces the number of variables to be taken in to account.

The PRISM (Pliocene Research, Interpretation and Synoptic Mapping) project is an 'internally consistent and comprehensive global synthesis of a past interval of relatively warm and stable climate', developed by the United States Geological Survey (Dowsett *et al.*, 2010). The reconstruction ranges over the interval from 3.264 Ma to 3.025 Ma (Dowsett *et al.*, 2010), for which the terms PRISM interval, mid-Pliocene, mPWP or PRISM time-slab are used interchangeably.

Figure 1.1 shows the PRISM interval on the geomagnetic polarity timescale of Berggren *et al.* (1995), and the benthic $\delta^{18}O$ (ratio between ^{16}O and ^{18}O, the two stable isotopes of oxygen) record of Lisiecki & Raymo (2005), where it lies between oxygen isotope stages M2/M1 and G21/G20. $\delta^{18}O$ can be used as a proxy for changes in ocean temperature, salinity and global ice volume (Lisiecki & Raymo, 2005). ^{16}O is preferentially evaporated in comparison to ^{18}O, due to being lighter, and thus precipitation has a lower $\delta^{18}O$ value than its source water. In periods of cooler global temperatures, snowfall accumulates on ice sheets, and so seawater becomes relatively enriched in ^{18}O, as more ^{16}O becomes trapped in the ice sheets. Ocean temperature also influences the degree of isotopic fractionation, with ^{16}O becoming more abundant in the carbonate shells of the foraminifera with cooler temperatures. Higher benthic $\delta^{18}O$ values are thus thought to indicate colder climates with larger ice volumes, with lighter excursions indicating warmer periods.

The PRISM time-slab is sufficiently long to be dependably identified and correlated between different marine sequences (Berggren *et al.*, 1995; Dowsett, 1989; Dowsett & Robinson, 2006), and is easily discriminated from the intervals it

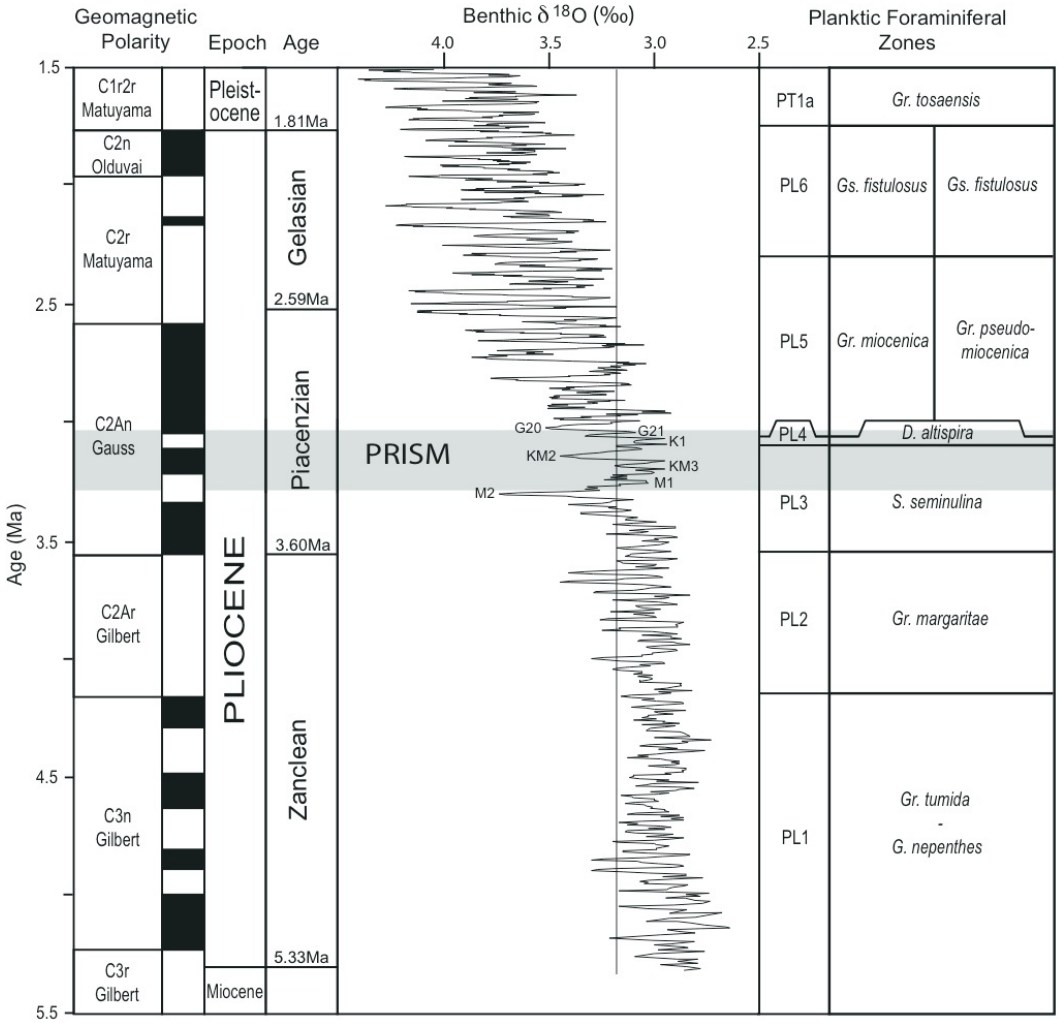

Figure 1.1: The PRISM time slab (shaded strip) on geomagnetic polarity, Lisiecki & Raymo (2005) benthic δ^{18}O record and planktic foraminiferal zones (Dowsett *et al.*, 2010).

is surrounded by (Dowsett *et al.*, 2005; Draut *et al.*, 2003; Lisiecki & Raymo, 2005; Shackleton *et al.*, 1995). The latest PRISM reconstruction, PRISM3D (Dowsett *et al.*, 2010) is the fourth generation of PRISM palaeoclimate reconstructions, after PRISM0 (Dowsett *et al.*, 1994), PRISM1 (Dowsett *et al.*, 1996) and PRISM2 (Dowsett *et al.*, 1999).

The PRISM reconstruction consists of data sets for SSTs (section 1.5.1), deep

ocean temperatures (section 1.5.2), as well as global sea level, topography, deep ocean temperature and circulation, vegetation, land ice and sea ice (section 1.6).

1.4 Atmospheric CO_2 concentrations in the mPWP

Estimates for atmospheric concentrations of CO_2 in the mPWP range from approximately 190 ppm to 450 ppm (e.g. Badger *et al.* (2013); Bartoli *et al.* (2009); Kürschner *et al.* (1996); Martinez-Boti *et al.* (2015); Pagani *et al.* (2010); Seki *et al.* (2010); Zhang *et al.* (2013a)). These estimates derive from analyses of stomatal density in fossil leaves, boron isotopic composition in planktic foraminifera, and carbon isotope composition in foraminifera and sedimentary alkenones. Figure 1.2 shows estimates of pCO_2 for 2.3 to 3.3 Myr ago gained from boron and carbon isotopic composition analysis.

Analysis of the frequency and size of stomata on fossil plant leaves by Kürschner *et al.* (1996), using observed inverse relationships between these indices and atmospheric pCO_2, produced estimates of mid-Pliocene CO_2 concentrations of 280 to 360 ppm.

Bartoli *et al.* (2009); Seki *et al.* (2010) and Martinez-Boti *et al.* (2015) all use data on boron isotopic composition in planktic foraminifera to calculate mid-Pliocene CO_2 concentrations. The ratios of ^{10}B to ^{11}B ($\delta^{11}B$) and B/Ca in the planktic foraminifera species *Globigerinoides ruber* is a function of the pH of seawater (Henehan *et al.*, 2013). Seawater pH is correlated with aqueous CO_2 concentrations, which are known to be a function of atmospheric CO_2, when the surface water is at or close to equilibrium with the atmosphere (Martinez-Boti *et al.*, 2015). $\delta^{11}B$ has been demonstrated to be an accurate recorder of atmospheric CO_2 concentrations (e.g. Foster (2008); Henehan *et al.* (2013); Hönisch & Hemming (2005)) over the past 130,000 years.

Analysis by Seki *et al.* (2010) of $\delta^{11}B$ and B/Ca ratios in two species of planktic foraminifera (*G. sacculifer and G. ruber*) from ODP (Ocean Drilling Program) site 999 in the Caribbean produced estimates of mid-Pliocene CO_2 of 340 to 450 ppm. Using $\delta^{11}B$ in *G. sacculifer* from the same site, Bartoli *et al.* (2009) estimate mid-Pliocene CO_2 to be 245 ppm to 420 ppm, and Martinez-Boti *et al.* (2015), using the same techniques and site, produce an estimate of 280 to 420 ppm.

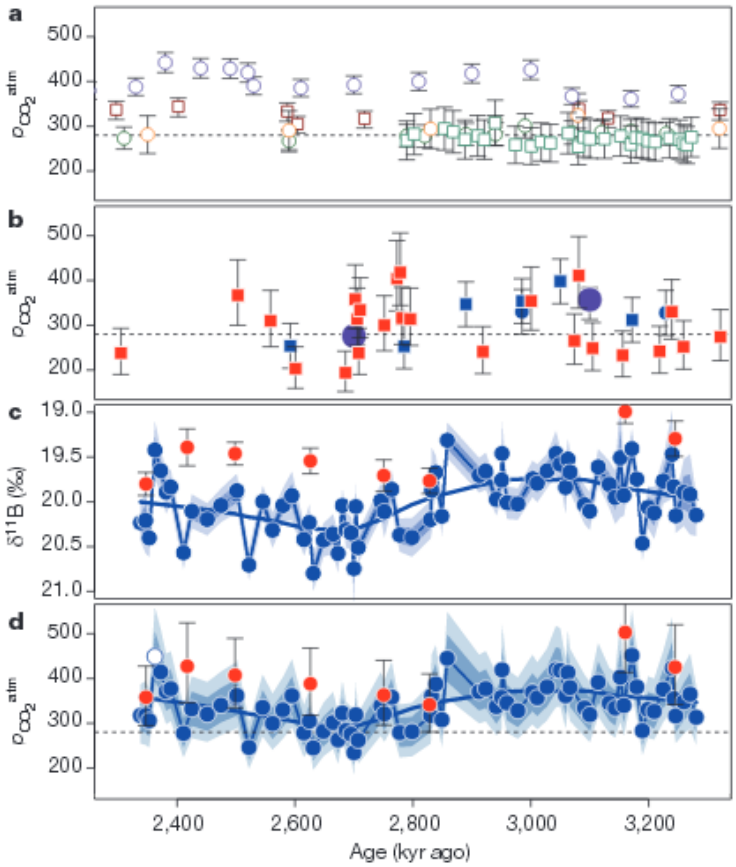

Figure 1.2: pCO_2 estimates of late Pliocene/early Plesitocene based on (a) $\delta^{13}C$ of sedimentary alkenones (b) and (d) $\delta^{11}B$ of planktic foraminifera. (c) shows the $\delta^{11}B$ records from which the pCO_2 estimates in (d) are derived (Martinez-Boti *et al.*, 2015).

Pagani *et al.* (2010); Seki *et al.* (2010); Zhang *et al.* (2013a) and Badger *et al.* (2013) all use data from carbon isotope composition in sedimentary alkenones to produce mPWP CO_2 concentration estimates. Values of $\delta^{13}C$ (ratios of ^{13}C to ^{12}C) in the alkenones are used to calculate carbon isotope fractionation ($\varepsilon_{p37:2}$) from which aqueous CO_2 concentrations can be calculated (Seki *et al.*, 2010; Zhang *et al.*, 2013a). Atmospheric CO_2 estimate can then be calculated as with the Boron isotope method.

Estimates of approximately 240 ppm to 320 ppm were derived by Seki *et al.* (2010), based on carbon isotope composition from samples taken at ODP site 999. This technique was also used by Pagani *et al.* (2010), with data from six different sites (ODP sites 806, 882, 925, 982, 1012, 1208). Estimates gave a range of approximately 240 ppm to 450 ppm, with uncertainties of up to 100 ppm at some sites. A 40 million year pCO_2 record is produced by Zhang *et al.* (2013a) from ODP site 925, mid-Pliocene pCO_2 estimates are in the range 275 ppm to 400 ppm.

Badger *et al.* (2013) produce mid-Pliocene pCO_2 estimates of 250 to 300 ppm, at the lower end of the ranges produced by other studies. The results also indicate a more stable pCO_2 than the other studies suggest, with less than 55 ppm variability during the mPWP. A single site, ODP 999, was used in this study.

1.5 Reconstruction of mPWP temperatures

1.5.1 Sea surface temperatures

Figure 1.3 shows the locations of the PRISM marine sites. The level of coverage varies in different parts of the world. For example, there are over 20 marine sites in the North Atlantic, but only a single marine site in the entire Indian Ocean. The Pacific Ocean is well covered around its edges, particularly in the North-West of the ocean, but the coverage in the central Pacific is much sparser.

Faunal analysis was used to reconstruct mid-Pliocene SSTs up to PRISM2 (Dowsett, 2007). PRISM3 incorporated a multi-proxy approach to SST reconstruction - as well as faunal analysis, alkenone and Mg/Ca methods of SST estimation were also adopted (Dowsett, 2007).

The advantage of using a multi-proxy approach is that independent methods can be used to verify each other's results, as well as highlighting potential weakness or biases in certain proxy methods. It can take advantage of the strengths of individual proxies, whilst ideally minimising the limitations of a single-proxy approach. A multi-proxy approach should also improve spatial coverage, as it provides more options at any one given site.

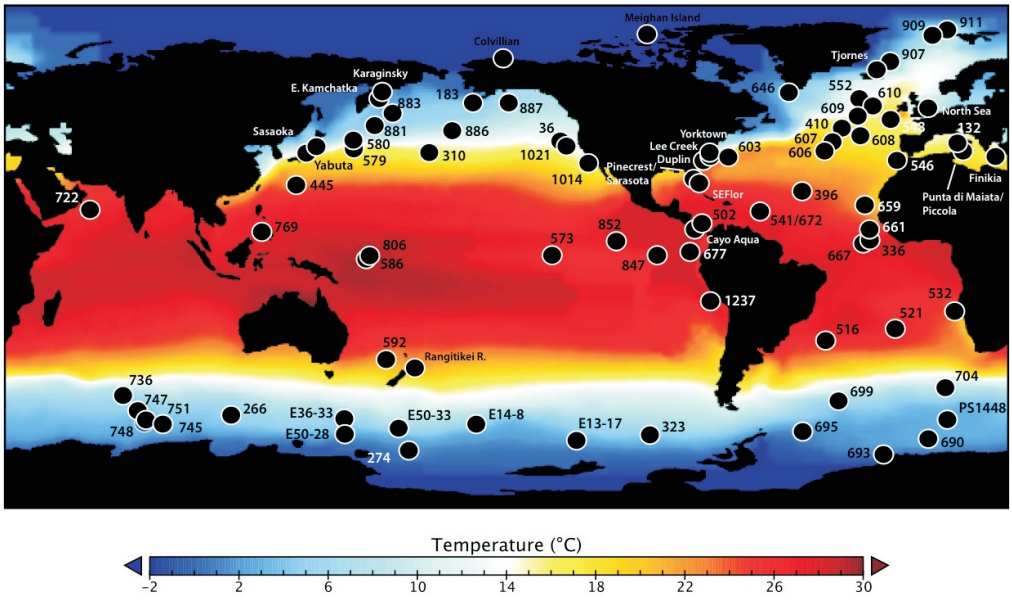

Figure 1.3: Location of the 86 PRISM marine data sites, on February SST reconstruction (Dowsett *et al.*, 2010).

A multi-proxy approach does come with challenges - combining several environmental signals into one single temperature estimate may require a sophisticated statistical evaluation. Calculating several different estimates for each site will also place greater demand on resources. Of the marine sites used to estimate PRISM3 SSTs, only 20% of them are derived using a multi-proxy approach (Dowsett *et al.*, 2012).

1.5.1.1 Faunal analysis

Planktic foraminifera were identified and picked from the PRISM interval section of the marine cores taken from the sites indicated in Figure 1.3. These were identified up to the species level, and counted to produce a profile of the numbers of each species present in that section of the marine core (Dowsett, 2007). This data was then used to produce an estimate for the SSTs, either by a transfer function, a modern analogue technique, or a semi-quantitative comparison to

modern fauna (e.g. Dowsett (2007); Dowsett & Poore (1990, 1991); Dowsett *et al.* (1996, 1999)).

Taxonomic grouping schemes were increased to simplify the taxonomic structure of the assemblages, with the assumption that the categories were the same in the mid-Pliocene as for modern day. The design of the categories was such to ensure that if the assumption produced any errors, the SSTs would be too cool rather than too warm (Dowsett, 2007).

This method relies upon the assumption that the taxonomic categories used to create the present and the mid-Pliocene assemblages had the same environmental preferences in the mid-Pliocene as in the present day. This is not a particularly unreasonable assumption, but nevertheless, the SST estimates from the faunal analysis depend in part on the environmental preferences of particular groups of planktic foraminifera not having changed significantly in 3 million years.

Imbrie & Kipp (1971) developed a transfer function to create equations which related data pertaining to the abundance of microfossils in core-top samples to SSTs. These methods can also be applied to down-core samples to produce palaeoecological estimates for past climates.

PRISM built on previous work to develop the transfer technique to be used in the Pliocene (Dowsett, 1991; Dowsett & Poore, 1990). A set of 18 counting categories, both for Pliocene and modern taxa were created, enabling the transfer function to be used for assemblages up to the mid-Pliocene. Analysis revealed that five planktic foraminifer assemblages accounted for approximately 95% of variance in the faunal data. Multiple regression techniques produced the equation

$$Y_{est} = B_{ct}^2 K + k_0 \tag{1.1}$$

where Y_{est} are the palaeoecological estimates, B_{ct} the cross-product matrix, K a vector of regression coefficients, and k_0 the equation intercept (Dowsett, 2007).

PRISM uses the squared chord distance (SCD) signal-to-noise measure:

$$d_{ij} = \sum k \left(p_{ik}^{1/2} - p_{jk}^{1/2} \right)^2 \tag{1.2}$$

d_{ij} is known as the squared chord distance between two multi-variate samples i and j. p_{ik} is the proportion of species k in sample i.

SCD ranges from 0 to 2. 0 indicates that i and j have identical proportions of each species that are being compared, and 2 indicates that the intersection of the two sets is empty. Values greater than 0.15 are considered non-analogue. The value indicates the faunal similarity between core samples, and is used to compare down-core samples to reference samples.

Mid-Pliocene diatoms from 6 North Pacific cores and 24 Southern Ocean sites were analysed in Barron (1996). SST estimates for the sites in the Southern Ocean were obtained by estimating the position of the Antarctic Polar front relative to the sites. North Pacific SSTs were obtained by using equations in Barron (1996) based on relative ratios of certain taxa.

1.5.1.2 Mg/Ca palaeothermometry

The ratio of Magnesium to Calcium (Mg/Ca) in foraminiferal tests from both laboratory culturing experiments and core-top samples has been observed to vary exponentially with temperature (e.g. (Lea *et al.*, 1999; Mashiotta *et al.*, 1999; Nrnberg *et al.*, 1996)). Culture-based calibrations are able to constrain temperature, reducing unknown factors which can complicate the calibrations. Whilst using core-top samples is disadvantaged due to the need for estimates of the environmental temperatures, there is uncertainty associated with culture calibrations concerning recreating realistic conditions to ensure natural chamber growth (Barker *et al.*, 2005).

Due to the relatively long oceanic residence times of both Mg and Ca, the Mg/Ca of seawater can be considered constant over glacial/interglacial timescales (Barker *et al.*, 2005). This means that a substantial amount of uncertainty (as seen with δ^{18}O, which is influenced by changes in isotopic composition of seawater as well as temperature), is removed when reconstructing palaeotemperatures. The equation

$$Mg/Ca = 0.474e^{0.107T} \tag{1.3}$$

where T is the temperature in °C, fits the data compiled in Mashiotta *et al.* (1999) with an R^2 value of 0.98. This equation was subsequently used to derive mid-Pliocene SST estimates for multiple species (Robinson *et al.*, 2008).

The calibration used to produce equation (1.3) in Mashiotta *et al.* (1999) is based on results whose temperature ranges from 10°C to 26°C, so any temperature estimate outside this range is derived from an extrapolation of an exponential. Furthermore, the temperatures used are clumped together into groups at 10, 12, 16, 22 and 26°C, meaning that there are large gaps within the calibration curve.

1.5.1.3 Biomarkers

Biomarker is a term used to describe an organic molecule found in sediments (Rosell-Melé & McClymont, 2007). One of the most commonly used biomarkers for palaeoclimate proxies, SSTs in particular, are C_{37} alkenones (alkenones consisting of 37 carbon atoms) (Rosell-Melé & McClymont, 2007).

$U_{37}^{k'}$ index The $U_{37}^{k'}$ index is used to estimate SSTs based on the ratios of the number of C_{37} molecules with 2, 3 or 4 double bonds (Brassell, 1993). Work by Brassell *et al.* (1986) and Marlowe (1984) established the formula

$$U_{37}^{k} = \frac{C_{37:2} - C_{37:4}}{C_{37:2} + C_{37:3} + C_{37:4}} \tag{1.4}$$

for unsaturated ketones with 37 carbon atoms. However, $C_{37:4}$ is not common away from high latitudes, and this led to an alternative index, developed by Prahl & Wakeham (1987):

$$U_{37}^{k'} = \frac{C_{37:2}}{C_{37:2} + C_{37:3}} \tag{1.5}$$

This index has been used by PRISM to estimate mid-Pliocene SSTs (Robinson *et al.*, 2008) using the calibration curve set out in Prahl *et al.* (1988). Further studies in Müller *et al.* (1998) and Conte *et al.* (2006) verify the global applicability of the Prahl *et al.* (1988) curve.

The temperature calibration used for $U_{37}^{k'}$ shown in Rosell-Melé & McClymont (2007) ranges from 0°C to 30°C. The coverage is higher for warmer temperatures, but lower ranges are reasonably well-represented as well. However, some studies

have suggested that there is an element of non-linearity in the SST-$U^{k'}_{37}$ relationship at temperatures below 8°C, and above 25°C (e.g. Conte *et al.* (2006); Pelejero & Calvo (2003); Rosell-Melé (1998); Sonzogni *et al.* (1997)).

1.5.1.4 TEX_{86}

TEX_{86} (tetraether index with 86 carbon atoms) is an SST proxy, based on the relative abundances of lipids known as isoprenoidal glycerol dialkyl glycerol tetraethers (GDGTs) in marine sediments, first proposed by Schouten *et al.* (2002). The TEX_{86} index is calculated using the formula

$$TEX_{86} = \frac{([GDGT-2]+[GDGT-3]+[Crenarchaeolregio-isomer])}{([GDGT-1]+[GDGT-2]+[GDGT-3]+[Crenarchaeolregio-isomer])} \tag{1.6}$$

with each term indicating the relative abundance of isoprenoidal GDGTs in the sample, classified by the number of cyclopentane rings contained in the molecule (Schouten *et al.*, 2002). Kim *et al.* (2008) calibrated the index with a global core top data set to the formula

$$SST = 56.2 \times TEX_{86} - 10.8 \tag{1.7}$$

with an r^2 of 0.935, based on a sample size of 223, for SSTs between 5 and 30°C. For temperatures lower than 5°C (typically occurring at high latitudes), changes in TEX_{86} were relatively minor, suggesting TEX_{86} to be a less suitable proxy for high latitude SSTs (Kim *et al.*, 2008; Schouten *et al.*, 2013).

1.5.1.5 Time-slab SST calculation

The PRISM reconstruction aims to produce a set of temperatures representative of a time-slab 300,000 years wide. To produce a single value representative of the range of results obtained from the core sample, a method known as 'peak averaging' is implemented (Dowsett & Poore, 1991; Dowsett & Robinson, 2006; Dowsett *et al.*, 2005). This approach aims to produce an estimate of the mean 'interglacial' climate during the time-slab, and reduces issues relating to specific point-to-point correlation between different core samples during the time-slab (Dowsett, 2007). The average is calculated by taking the mean of all the warm

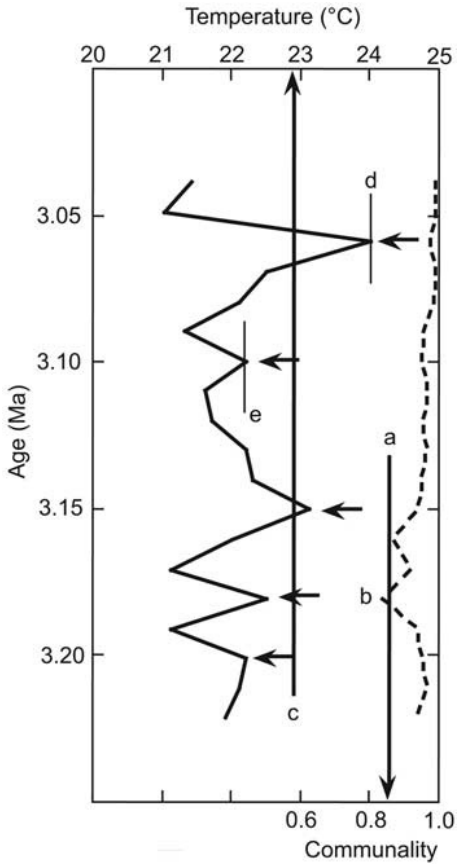

Figure 1.4: A hypothetical example of an SST record and the implementation of the warm peak averaging method from Dowsett (2007). The warm peaks are all indicated by arrows, with the maximum (**d**) and minimum (**e**) peaks labelled as well. The dotted line displays the communality values, and line **a** the communality cut-off, in this example 0.85. **b** indicates a warm peak whose communality is below the cut-off threshold. This peak is not included in the calculation of the mean warm peak value, which is indicated by line **c**.

peaks along the temperature profile for the time slab, where a warm peak is defined as a temperature estimate that is warmer than each of the estimates that sit above and below it, stratigraphically (Dowsett, 2007). There is a caveat to this method, however, as some warm peaks are not considered 'valid', and so not included in the warm peak average calculation (Dowsett *et al.*, 2005).

For SSTs calculated through a transfer function, the validity is gauged through

a communality cut-off calculation, using the formula:

$$h_k^2 = \sum_{i=1}^{k} s_i^2 \tag{1.8}$$

Here, s_i^2 refers to the correlation of factor i and variable k, and the square of this gives the part of the variance that is accounted for by that factor (Dowsett *et al.*, 2005). The value of h^2 will range between 0 and 1. For the PRISM reconstruction, a cut off point of $h^2 = 0.7$ is used, i.e. a warm peak with a communality less than 0.7 will not be included in the average (Dowsett *et al.*, 2005). For SSTs obtained using a Modern Analogue Technique, then samples with $d_{ij} > 0.15$ (from equation 1.2) are considered non-analogue and hence not included in the calculation (Dowsett & Robinson, 1998; Dowsett *et al.*, 1999).

Figure 1.4 illustrates a hypothetical example of warm peak averaging. The warm peaks are indicated by arrows, but the fourth one down has a communality below the cutoff point, so it is not included in the final average. As well as taking the average of the 'valid' warm peaks, the minimum and maximum warm peaks are also recorded (Dowsett *et al.*, 2005).

For each marine site, mid-Pliocene anomalies were produced for warm and cold seasons by subtracting modern SSTs. These were plotted on a $2° \times 2°$ grid, and a full map of mid-Pliocene SST anomalies was produced using modern SST contours as a template, under the assumption that the modern general pattern of ocean current systems also existed in the mid-Pliocene (Dowsett, 2007).

This mid-Pliocene anomaly map was applied to modern SSTs taken from Reynolds & Smith (1995) to produce February and August SSTs for the mid-Pliocene (Dowsett, 2007). Equation (1.9) is used to produce a set of monthly SST anomalies (where T_f is February SST, T_a is the August SST, and T_x is the SST for month x (with 1 for January through to 12 for December)).

$$T_x = T_f + \frac{T_a - T_f}{2}\left(1 + sin\left[\frac{2\pi(x-2)}{12} - \frac{\pi}{2}\right]\right) \tag{1.9}$$

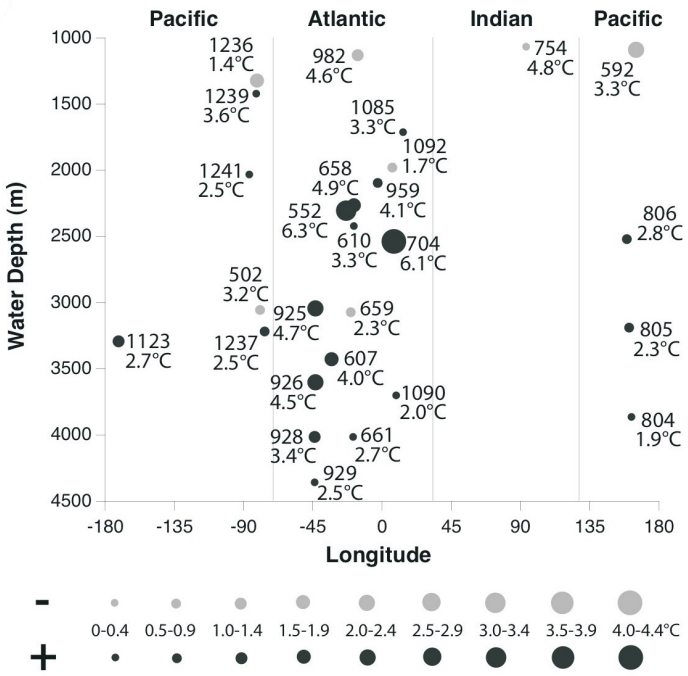

Figure 1.5: Mid-Pliocene deep ocean temperature estimates and anomalies (Dowsett *et al.*, 2010). Temperature estimates displayed are based on the mean of the warmest 10% of estimates from samples. Each point is labelled with the number of the site from which the samples were taken, and is plotted by water depth. The size of the symbol corresponds to the anomaly from modern.

1.5.2 Deep ocean temperatures and circulation

PRISM3 is the first time the PRISM project has attempted a deep-ocean temperature reconstruction to sit alongside the SST reconstruction (Dowsett *et al.*, 2010). Data is taken from 27 DSDP (Deep Sea Drilling Project) and ODP sites, representing depths ranging from 1000 m to 4500 m. Figure 1.5 indicates that the Atlantic has the best coverage, with 63% of the sites located there. The Pacific and Indian Ocean sites are primarily from the Southern Hemisphere (Dowsett *et al.*, 2009). The deep ocean temperature reconstruction is presented on a lattice with 33 depth layers, at a horizontal resolution of $4° \times 5°$ (latitude $\times$ longitude) (Dowsett *et al.*, 2009).

The bottom water temperature estimates are obtained from Mg/Ca palaeothermometry analysis. The Mg/Ca ratios relate to the shells of *Krithe*, a genus of deep-sea ostracodes (Dowsett *et al.*, 2009). The temperatures were calculated using the calibration of Dwyer *et al.* (1995), who used core-top *Krithe* Mg/Ca to create the following formula to relate these values to modern bottom water temperatures:

$$BWT = 0.854(Mg/Ca) - 5.75 \tag{1.10}$$

Here BWT refers to the bottom water temperature in °C. The associated error is ± 1°C (Cronin *et al.*, 2005; Dwyer, 2009). This was applied to Mg/Ca values from mid-Pliocene *Krithe*. A methodology similar to the warm peak averaging used for the SSTs is implemented to identify the warm phase of bottom water temperatures from the data set. Sites were ordered by temperature, and the warmest 10% were averaged to produce the bottom water temperature estimates (Dowsett *et al.*, 2010).

1.5.3 Surface air temperatures

Mean annual SAT estimates for the mPWP are obtained using palaeobotanical data of Pliocene vegetation from 45 sites, recorded in TEVIS (Tertiary Environmental Information System, Salzmann *et al.* (2008)). Due to poor age control and/or coarse temporal resolution in many Pliocene vegetation records, the palaeobotanical data covers 3.6 to 2.6 Ma, a wider temporal range than the mid-Pliocene (Salzmann *et al.*, 2008). At many of these sites, the Pliocene mean annual SATs are estimated using the coexistence approach (Mosbrugger & Utescher, 1997), which assumes that fossil taxa had similar climatic requirements, such as mean annual temperature or precipitation levels, to that of their closest living modern day taxa. By applying this to the taxa at each of the TEVIS sites used, estimates for the mean annual SAT at that site can be obtained.

At some sites, the Climate-Leaf Analysis Multivariate Program (CLAMP, Wolfe (1993)) is used. CLAMP generates a database incorporating up to 29 character states for each fossil leaf, such as size or length to width ratio. The

database also contains this data for modern plants along with corresponding meteorological data, such as annual precipitation, mean annual SAT and cold monthly mean SAT, from the region these plants are located. Multivariate correspondence analysis and polynomial regression are then used to estimate meteorological characteristics of the climate in which the fossilised plants existed. Mean annual SATs have standard errors of 0.7°C to 1.0°C associated.

1.6 Other PRISM boundary conditions

1.6.1 Sea level

PRISM sea level estimates have evolved along with the development of the PRISM project. The first estimate was 35 ± 18 m above present sea level, in Dowsett & Cronin (1990), based upon the altitude of a section of coastline in South Carolina. Based on this, and other work such as Haq *et al.* (1987a,b); Krantz (1991) and Shackleton *et al.* (1993), sea level was set at a 'conservative' +25 m in PRISM0 (Dowsett *et al.*, 1994). This was revised up to +35 m for PRISM1 (Dowsett *et al.*, 1996), and then reduced back to +25 m for PRISM2 (Dowsett *et al.*, 1999). PRISM3D has kept sea level at +25 m (Dowsett *et al.*, 2010).

The latest estimates of mid-Pliocene sea levels are documented in Miller *et al.* (2012). They used a combination of backstripping (from records in Virginia, New Zealand and Enewetak Atoll), benthic foraminiferal δ^{18}O records and some combined Mg/Ca and δ^{18}O records to produce a mid-Pliocene sea level estimate of 22 ± 10 m in comparison to present day. The upper estimates of this sea level change would imply a full deglaciation of the Greenland and West Antarctic Ice Sheets, and 25 - 45% deglaciation of the East Antarctic Ice Sheet (Miller *et al.*, 2012).

Sea level estimates from benthic foraminiferal δ^{18}O records were obtained by comparing the Pliocene records to modern, and attributing 67% of the changes due to changes in global ice volume, and 33% of the changes due to deep water temperature changes, resulting in a 0.1‰/10 m sea level δ^{18}O calibration. Error limits were produced where calculations were done with the ratios at 50:50 and

80:20 (ice:temperature). This resulted in a sea level change estimate of 21 ± 10 m in comparison to present day.

All methods used to estimate past sea levels have their limitations, and this results in there being large uncertainties in the final estimate. Even the latest in Miller *et al.* (2012) has uncertainties of 10 m either way, suggesting that the sea level could have been as low as 12 m above modern, or as high as 32 m above modern, which is a considerable difference. The uncertainties have a significant effect on the ice volume (i.e. the ice sheets in Greenland and Antarctica), as the estimates for their change in size is based on a sea level rise of 25 m (Sohl *et al.*, 2009). The IPCC AR5 gives a high confidence that global mean sea level was above present in the mPWP, and not higher than 20 m above present during the interglacials of the mPWP (Masson-Delmotte *et al.*, 2013).

1.6.2 Topography

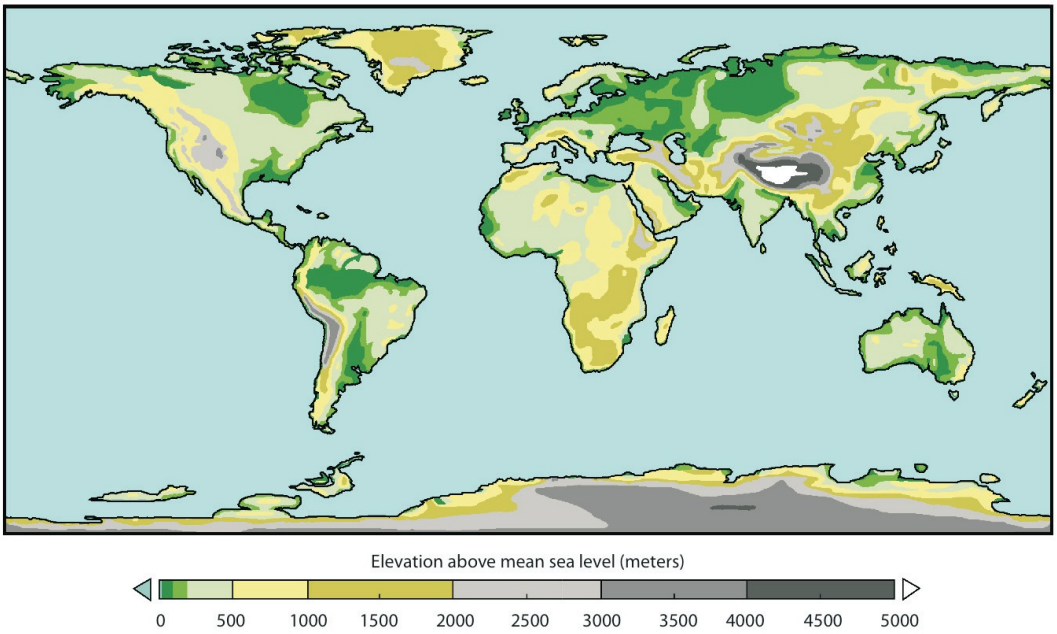

Figure 1.6: PRISM topographical reconstruction, coastline is altered from modern to take into account the estimated 25 m sea level increase in the mid-Pliocene (Sohl *et al.*, 2009). Pliocene elevation data based on Markwick (2007).

Figure 1.6 indicates the topographic reconstruction of PRISM3 (Sohl *et al.*, 2009). This reconstruction was created at the NASA Goddard Institute, as a development of the PRISM2 topography reconstruction, which used data from Thompson & Fleming (1996). The topographic reconstruction for the mid-Pliocene is largely similar to present day, with the key exceptions being that sea level is 25 m higher, Hudson Bay and the Great Lakes are filled in, and the West Antarctic ice sheet has disappeared, alongside reductions in the East Antarctic and Greenland ice sheets (Sohl *et al.*, 2009).

Sohl *et al.* (2009) uses the Pliocene palaeogeography of Markwick (2007) to aid in the topographical reconstruction, particularly in regions of poor detail in the previous PRISM reconstructions, often in lower elevation locations.

In PRISM2, Tibetan plateau elevations were left mostly the same as modern day, because there were substantial uncertainties over the exact timing of the uplift of the plateau. In the PRISM3 reconstructions, this was largely unaltered, as oxygen isotope data from Tibetan palaeosol carbonates suggested that the current elevations have existed since $\sim$ 10 Ma (Garzione *et al.*, 2000; Rowley *et al.*, 2001).

The elevation of the Northern Andes in South America was reduced to approximately half its modern height by Thompson & Fleming (1996), and hence this was included in the PRISM2 topography (Dowsett *et al.*, 1999). However, data from multiple proxies indicate that in fact these mountains had achieved most of their current height 6.8 Ma (Garzione *et al.*, 2006; Ghosh *et al.*, 2006). Small adjustments were made to the modern height for the Pliocene reconstruction, with a further 500 m elevation in regions of Peru and Chile, and the northern-most cordillera was set a few hundred metres lower than modern, due to results in Markwick (2007).

Data from Thompson & Fleming (1996) indicated that the elevation of the Rocky Mountains was approximately half the modern day value, and subsequently that height was used for the PRISM2 reconstruction (Dowsett *et al.*, 1999). However, McMillan *et al.* (2006) suggests that there has been little change in the elevation for approximately 35 million years, and Markwick (2007) gives a near modern topography for this region, which is also adopted by the PRISM3 reconstruction (Sohl *et al.*, 2009).

1.6.3 Vegetation

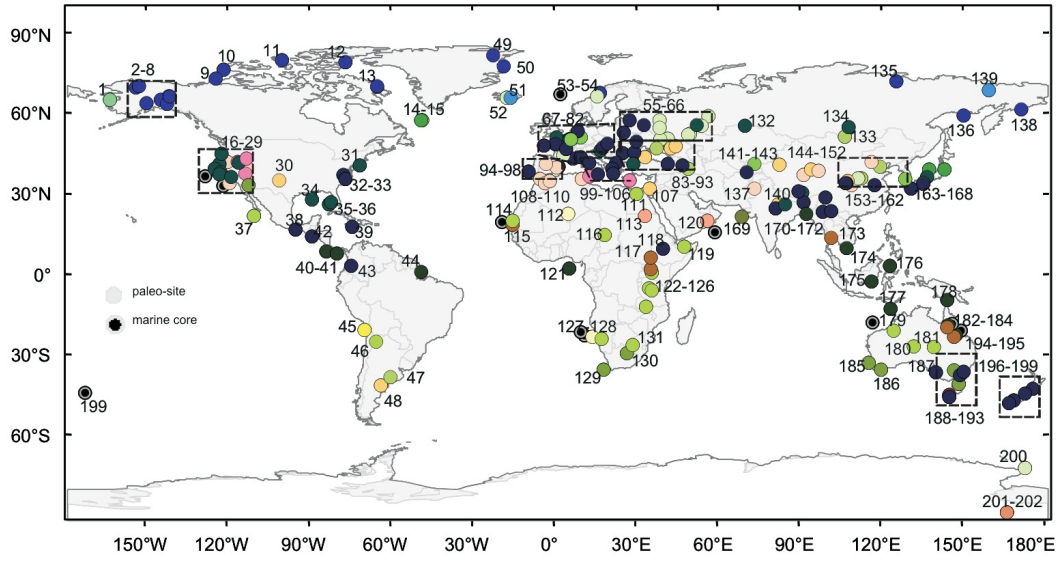

Figure 1.7: Location of the 202 PRISM terrestrial data sites (Salzmann *et al.*, 2008).

The vegetation reconstruction for the mid-Pliocene was based on a combination of data from 202 terrestrial sites (Figure 1.7) and results from BIOME4 (Kaplan, 2001), a vegetation model (Dowsett *et al.*, 2010; Salzmann *et al.*, 2008). Palaeobotanical data was compiled for the 202 sites based on existing literature and the extended data set of Thompson & Fleming (1996) (as described in section 1.5.3, the palaeobotanical data covers the period 3.6 to 2.6 Ma). This was then used to assign each data point to one of the 28 land cover classifications used in the BIOME4 model (see Figure 1.8) (Salzmann *et al.*, 2008).

Whilst the PRISM reconstruction covers the time slab of 3.29 - 2.97 Ma (Dowsett *et al.*, 2010), the data used for the vegetation covers the period from 3.6 to 2.6 Ma (Piacenzian Stage (Castradori *et al.*, 1998)), as the vegetation records have poor age control, and allowing a wider window enables a much greater geographical data coverage (Salzmann *et al.*, 2008). Thompson & Fleming (1996)

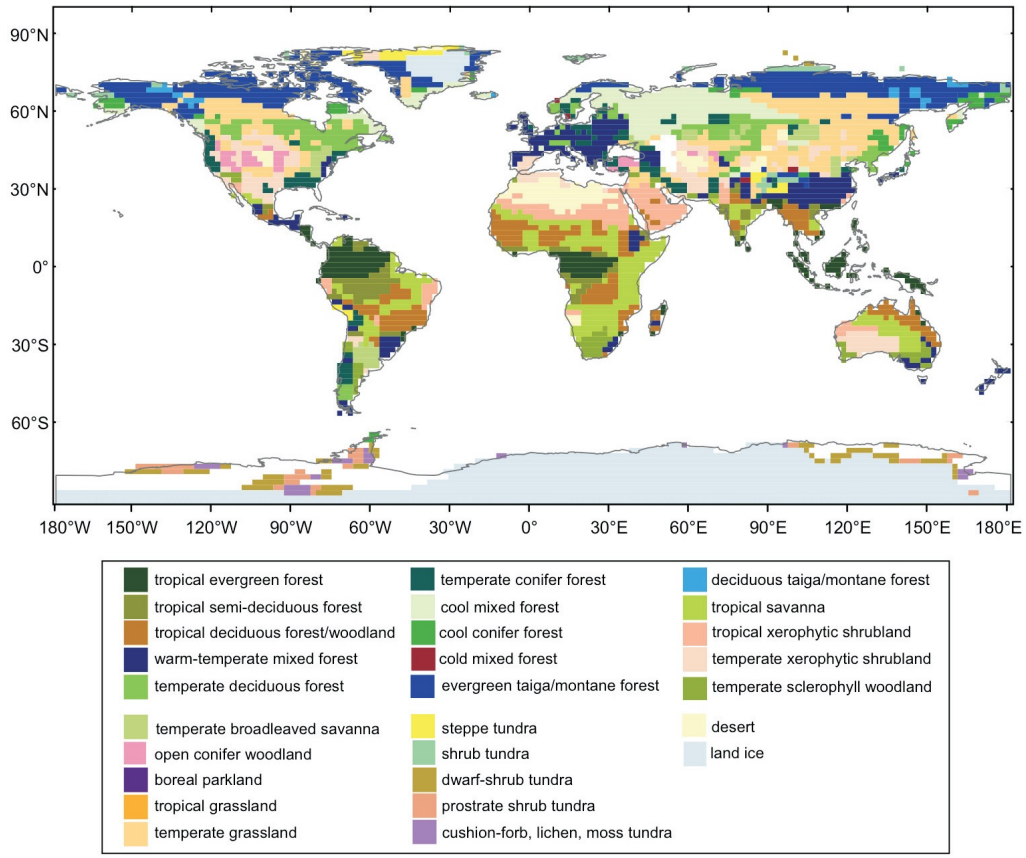

Figure 1.8: PRISM vegetation and land ice reconstruction based on the palaeodata from the sites in Figure 1.7 and BIOME4 results. Also shown is the key for the 28 BIOME4 land use classifications (Salzmann *et al.*, 2008).

suggest that any changes in vegetation from the PRISM time slab to the entire Piacenzian Stage were relatively small.

BIOME4 is a vegetation model which uses results from GCM simulations to create a prediction of the biome distribution for the simulated climate (Salzmann *et al.*, 2008). When used with HadAM3, the atmospheric component of HadCM3 (Pope *et al.*, 2000), each grid square on the $2.5° \times 3.75°$ resolution grid is assigned to one of 28 biome classifications, based upon the climate data for that particular area (Salzmann *et al.*, 2008).

To produce the vegetation reconstruction for PRISM, the results from the data are merged with those from the BIOME4 output. Each grid from the BIOME4 output was compared to the data results, and adjusted if the data disagreed with the model output (Salzmann *et al.*, 2008). This was done for any grid box which was 2 grid boxes or nearer to a data point. For the most part, areas with poor or no data coverage were left as the BIOME4 prediction indicated, unless evidence based on zonal biome distributions suggested that it was likely to be a different biome classification (Salzmann *et al.*, 2008). Areas with the highest levels of consistency between the models and the data were in Europe, China, Alaska and the western United States, all areas with a high frequency of data points (Salzmann *et al.*, 2008).

Figure 1.7 indicates the wide variation in spatial coverage across the globe for the data points used in the BIOME4 reconstructions. Adjustments were made to the model output for grid squares where nearby data suggested a different biome, but this could only be done for areas close to data points. Large areas, in particular in Africa, Siberia, and North and South America are not close to any data point, meaning it is difficult if not impossible to judge the validity of the model output. Given that changes have had to be made to some grid squares, it seems unlikely that these regions would all agree with the palaeobotanical data, were it to exist for those sites.

A consideration to make is that the data results may only be representative of a single point at the site, whereas the model results give a biome for an area representing an 86 km $\times$ 133 km grid (close to the equator, approaching the poles the grids will get narrower). In some regions of the world, particularly mountainous areas, there can be very drastic changes in vegetation over very short distances (Salzmann *et al.*, 2008).

1.6.4 Land ice

Two ice sheet distributions are produced for PRISM3 (Sohl *et al.*, 2009). The first of these is simply a minor adjustment to the ice sheets from PRISM2, where the West Antarctic ice sheet is completely removed, the Greenland ice sheet reduced

by 50%, and the East Antarctic ice sheet reduced by an amount which provides 15 m worth of sea level rise.

The second ice sheet reconstruction is generated by the British Antarctic Survey Ice Sheet Model (BASISM) (Hill *et al.*, 2007). This reconstruction is not significantly different from the first reconstructions, but there are slight differences in elevation in areas on the East Antarctic and Greenland ice sheets (Sohl *et al.*, 2009).

The ice sheet distributions are heavily dependent on the reconstructed sea level. Whilst several studies have put the sea level of the mid-Pliocene at around 25 m higher than present day, they are all accompanied by large uncertainties, suggesting the possibility of sea level as much as 35 m higher, or 12 m lower than present day, which would make a significant difference to the ice sheet distribution.

1.6.5 Sea ice

In the Northern Hemisphere, PRISM sea ice reconstruction is based on evidence from marine deposits along the Arctic Basin margins (Dowsett, 2007). Data from marine ostracodes from Greenland and Alaska imply that the sea ice extent was further north than present day (Brigham-Grette & Carter, 1992; Brouwers *et al.*, 1991; Cronin *et al.*, 1993). The SST estimates suggest that parts of the Arctic were substantially warmer than present day in some periods (Dowsett *et al.*, 1999, 2005), also implying a sea ice extent retreated in comparison to present day. In the Southern Hemisphere, PRISM sea ice extent estimates are based on the locations of sea ice related diatoms (Dowsett, 2007), as well as evidence from silicoflagellates (Whitehead & Bohaty, 2003) and opal sedimentation (Hillenbrand & Ehrmann, 2005).

The evidence points to a generally reduced sea ice extent in both hemispheres (Dowsett, 2007). For the PRISM reconstruction, the Northern Hemisphere is set to be ice-free in the summer, and the winter sea ice is set to be the same as modern summer sea ice extent (Dowsett *et al.*, 1994, 1996, 1999, 2005). For the Southern Hemisphere, barely any sea ice is present in the summer months, and winter sea ice extent is 4° - 6° latitude further south than the present day extent.

Sea ice extents for the intervening months are calculated using the relationship between SST and sea ice cover (Barron, 1996; Dowsett *et al.*, 1996, 1999, 2005).

1.7 Modelling the mPWP

The mid-Pliocene Warm Period has been the subject of many modelling studies (e.g. Ballantyne *et al.* (2013); Barreiro *et al.* (2005); Chandler *et al.* (1994); Dolan *et al.* (2011); Haywood & Valdes (2004, 2006); Haywood *et al.* (2005, 2007, 2009); Hill *et al.* (2007); Kamae & Ueda (2011); Kim & Crowley (2000); Krebs *et al.* (2011); Lunt *et al.* (2008a,b, 2009, 2010); Pope *et al.* (2011); Sloan *et al.* (1996); Zhang & Jiang (2014)).

Chandler *et al.* (1994) produced the first modelling study of the mPWP, using an atmosphere-only GCM developed by GISS, with a horizontal resolution of $8° \times 10°$, nine atmosphere layers and two ground layers. The simulation was restricted to the Northern Hemisphere, and results indicated a mean annual warming of 1.4°C compared to present day, with the highest levels of warming seen at high latitudes. Sloan *et al.* (1996) used an NCAR Genesis model (atmosphere only), with a $4.5° \times 7.5°$ resolution, snow and soil submodels, and boundary conditions provided by PRISM. The simulation covered the entire globe, and the results showed a global mean annual warming of 3.6°C, with warming greater at high latitudes, like Chandler *et al.* (1994). Kim & Crowley (2000) showed a decrease in Antarctic sea ice and lower Southern Ocean deep water outflow in the mid-Pliocene, using the Hamburg Ocean Primitive Equation (HOPE) model, an ocean-only GCM.

HadAM3, an atmosphere-only version of HadCM3, was used by Haywood *et al.* (2000b) to simulate the mid-Pliocene climate. Results indicated a 1.9°C increase in global mean annual temperature, with greater warming at higher latitudes, as with previous studies. Total precipitation was also observed to increase by 6%. Further HadAM3 simulation results demonstrated a warmer and wetter Europe and Mediterranean region in the mPWP (Haywood *et al.*, 2000a), and a warmer, wetter and less seasonal climate in North America (Haywood *et al.*, 2001). HadAM3 output was also used with BIOME4, a vegetation model

(Haywood *et al.*, 2002), which suggested reduced tundra and desert coverage in the mid-Pliocene, and an expansion of high-latitude forests.

Haywood & Valdes (2004) performed the first simulation of the mPWP with a fully-coupled atmosphere-ocean GCM. Using boundary conditions from PRISM2 (Dowsett *et al.*, 1999), the simulation showed an increase of 3°C in global mean annual temperatures in comparison to modern day, and as with previous studies, greater increases at high latitudes. Most regions indicated some level of warming, including the tropics. Mean annual SSTs increased, and Arctic sea ice was reduced. Using the HadCM3 output with TRIFFID, a dynamic vegetation model, suggests that the mPWP had greater forest cover and less bare soil in comparison to modern.

Barreiro *et al.* (2005) used two atmosphere only models (CAM3 and Speedy) to investigate the potential of a permanent El Niño in the mPWP, also investigated in Haywood *et al.* (2007). Results did not indicate a prediction of a permanent El Niño by the models, and concluded that it would have been unlikely to have been a major contributor to increased mid-Pliocene warmth. Haywood *et al.* (2005) showed warmer mid-Pliocene SSTs in the tropics and subtropics in comparison to modern, although the model results show disagreements with proxy-derived temperatures.

Lunt *et al.* (2008a) suggest decline in CO_2 following the mPWP was the most likely driver of Greenland glaciation. A further study also suggested that the closure of the Isthmus of Panama in the Pliocene was likely to have had only a small influence on the onset of Northern Hemisphere glaciation. Lunt *et al.* (2009) demonstrate, with HadCM3 and an ice sheet model, that the contribution of ice-sheet feedbacks and lower orography accounted for 42% of mid-Pliocene warming, compared to 35% due to increased CO_2 and 23% from vegetation changes. Lunt *et al.* (2010) indicated that earth system sensitivity (i.e. the effects of longer-term feedbacks) may be 30-50% greater than climate sensitivity from increased atmospheric CO_2.

Other recent modelling studies concerning the mPWP have demonstrated the sensitivity of Antarctic ice sheets to the orbital configuration (Dolan *et al.*, 2011), influence of changes in Indonesian throughflow on the aridification of Australia in

the Pliocene (Krebs *et al.*, 2011), and the effects on the model output of various adjustments to parameterisations in HadCM3 (Pope *et al.*, 2011).

A general pattern of increased temperatures in comparison to modern day is demonstrated in these studies, with mean annual SAT increases of around 2-4°C in comparison to present day. An increase in precipitation is also shown, along with reduction in sea ice and ice sheets, and a shift in the pattern of global vegetation cover. The warming observed in the model studies is typically not uniformly distributed, with greater temperature increases at higher latitudes (polar amplification, see section 2.2.2), resulting in a weakened equator-to-pole temperature gradient, matching the pattern in the increases in SSTs and SATs derived from proxy data (Dowsett *et al.*, 2011; Salzmann *et al.*, 2013).

1.8 High-latitude data-model mismatch

Output from the models has been compared to temperature estimates derived from proxies, for both SSTs and SATs. Both models and data demonstrate a rise in global SSTs and SATs (Dowsett *et al.*, 2011; Salzmann *et al.*, 2013), but whilst the warming is similar at low latitudes, at higher latitudes the model-simulated temperatures display lower levels of polar amplification than the proxy data temperatures (see Figures 1.9 and 1.10).

At ODP sites 907, 909 and 911 (located at 69.25°N, 12.70°W; 78.58°N, 3.07°W and 80.47°N, 8.23°W respectively, see Figure 1.9) the SST reconstruction is limited to Mg/Ca palaeothermometry and $U_{37}^{k'}$ indices, as planktic assesmblages in this region are unsuitable for faunal analysis, due to low foraminfera abundances, or the dominance of assemblages by extinct species with no extant descendants (Robinson *et al.*, 2008). At ODP 907, the mean annual SST estimate (11.7°C) is based solely on Mg/Ca paleothermometry from three samples (Robinson *et al.*, 2008). ODP 909 has greater data coverage, $U_{37}^{k'}$ indices are used at nine samples, with Mg/Ca palaeothermometry at a tenth, producing a mean annual SST estimate of 12.7°C. At ODP site 911, the mean annual SST estimate of 18.1°C is based on $U_{37}^{k'}$ indices from four samples (Robinson *et al.*, 2008). At Meighen Island (79.00°N, -99.00°W) and Colvillian (70.29°N, -150.42°W), mean annual

mid-Pliocene SST estimates of 1.71 and 1.22°C respectively are obtained through analysis of ostracode assemblages (Dowsett *et al.*, 1999).

Warmer SATs at high latitudes in the mid-Pliocene are indicated by palaeovegetation reconstructions (sites shown in Figure 1.7 indicating the presence of taiga forest over the majority of the areas that are covered by tundra in present day (Salzmann *et al.*, 2008). The forest-tundra boundary is shifted northwards in the mid-Pliocene, by approximately 250 km in Siberia, 500 km in Alaska and 2500 km in the Canadian Arctic Archipelago (Salzmann *et al.*, 2008).

Nine terrestrial sites used in the data-model comparison are at or north of 60°N (Salzmann *et al.*, 2013). Qualitative estimates based on modern analogues of the mid-Pliocene palaeobotanical assemblages are used for estimates of mid-Pliocene SATs at six of these sites (Salzmann *et al.*, 2013), whilst the coexistence approach (Mosbrugger & Utescher, 1997) is used at two. A multi-proxy approach, utilising the composition of palaeovegetation, analysis of bacterial composition in peat samples, and oxygen isotope ratios and annual ring widths in fossil wood is used for the mid-Pliocene SAT reconstruction at Beaver Pond (78.40°N, 82.00°W) (Ballantyne *et al.*, 2010).

GCMs have also not achieved the polar amplification indicated by proxies in simulations of other intervals of time. Heinemann *et al.* (2009) ran simulations of the Paleocene/Eocene climate ($\sim$ 55 Myr ago), in which the Arctic sea surface temperatures were approximately 11-13°C cooler than those indicated for the region by proxy data (e.g. Sluijs *et al.* (2006)). This followed several other modelling studies of the same interval, which all showed a large difference between proxy data reconstructions of Arctic SSTs, and those produced by models (e.g. Huber & Sloan (2001); Huber *et al.* (2003); Shellito *et al.* (2003, 2009); Sloan *et al.* (1995); Winguth *et al.* (2010)).

Lunt *et al.* (2012) describe the results of the Eocene Modelling Intercomparison Project (EoMIP), an ensemble of four models which have each run simulations of the early Eocene climate (55-50 Myr ago). At high northern latitudes, overlap between uncertainties in proxy-based SST estimates and simulated SSTs were seen only in runs with high CO_2 concentrations (8 or 16 times pre-industrial concentrations). Comparison of proxy data and model SATs revealed closer agree-

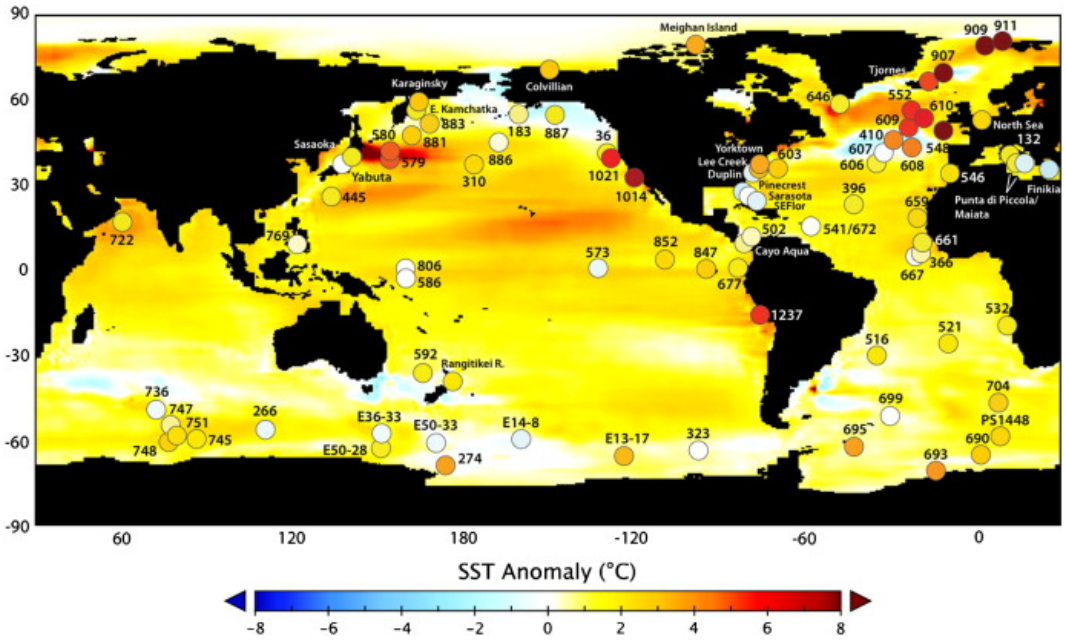

Figure 1.9: PRISM mean annual SST anomalies (compared to SSTs from Reynolds & Smith (1995)) superimposed on to mean annual SST anomalies from HadCM3 simulations (Dowsett *et al.*, 2011).

ment than SSTs, but the general pattern was for higher proxy SATs at high latitudes compared to model SATs.

Krapp & Jungclaus (2011) performed simulations of the mid-Miocene climatic optimum (MMCO, 17-14.5 Myr ago), with comparisons of high latitude temperatures with proxy estimates showing the proxies to be consistently warmer, for each of the three CO_2 concentrations used (360, 480 and 720 ppm). Similar simulations from Herold *et al.* (2011) and Goldner *et al.* (2014) revealed proxy reconstructed high latitude temperatures to be up to 15°C warmer than those produced by models.

The Pliocene Modelling Intercomparison Project (PlioMIP) compares GCM simulations of the mPWP from eight modelling groups (Haywood *et al.*, 2013b). Two experiments are performed - Experiment 1 uses atmosphere-only simulations (Haywood *et al.*, 2011a), with Experiment 2 focusing on simulations from fully-coupled atmosphere-ocean GCMs (Haywood *et al.*, 2011b). The multi-model

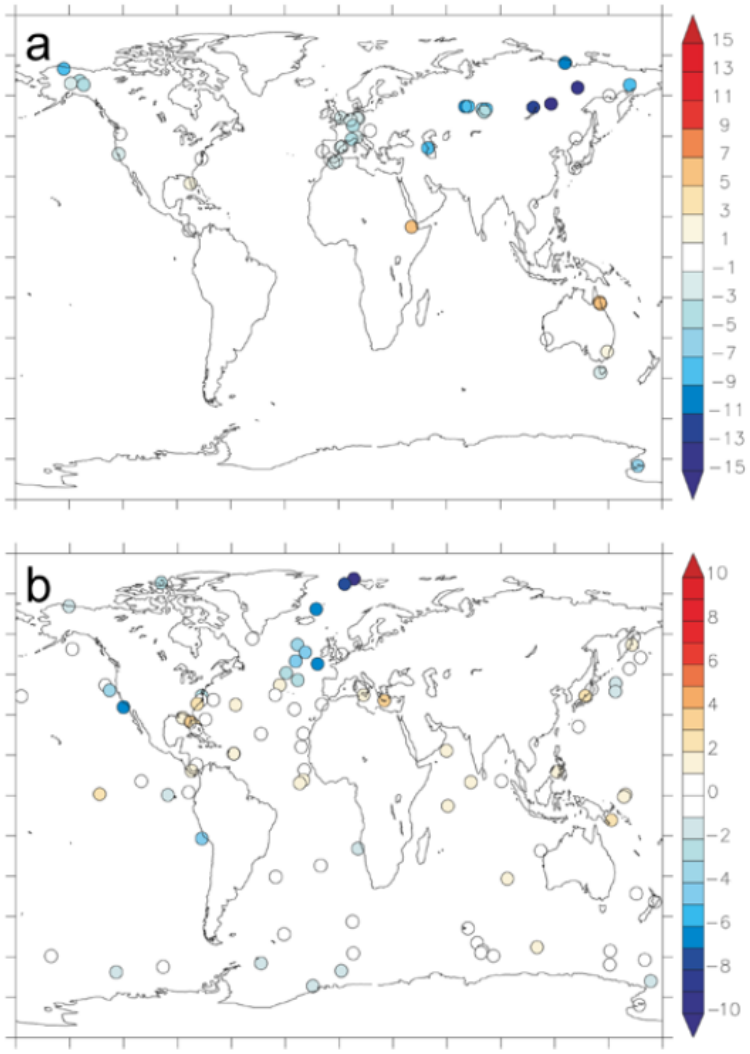

Figure 1.10: Point-based data-model comparison of (a) SAT and (b) SST anomalies (Pliocene model warming minus Pliocene proxy data warming) (Haywood *et al.*, 2013b). Model warming is the average of all the models in the PlioMIP ensemble (Haywood *et al.*, 2011b).

mean simulated temperatures also do not achieve the warming in high latitudes indicated by the proxy data, indicating that the lack of mid-Pliocene polar amplification is an issue faced by several GCMs.

It is important to attempt to understand why the discrepancy between high latitude proxy temperature estimates and model output exists. The discrepancy could be highlighting areas over the interpretation of the proxy data which are not yet sufficiently understood, and so are creating biases in the estimates of mid-Pliocene temperatures. It may be that the signals seen are seasonal, rather than annual. If summer temperatures are being interpreted as annual temperatures, this will bias the estimates to a warmer value.

There is a discord between the time interval from which the samples used for the data reconstruction represent, and the time interval represented by the simulations. The PRISM time slab interval is approximately 240,000 years long, whereas simulations generally represent a few hundred years. Over the duration of the PRISM interval, variations in the obliquity, eccentricity and precession of the Earth's orbit will affect both the total amount of solar radiation received, and its geographical and temporal distribution (Hays *et al.*, 1976; Milankovitch, 1941). The proxy data may be indicating mid-Pliocene temperatures during many different orbital configurations, but GCM simulations typically have a fixed orbit for the duration of their run, often the same as the modern day configuration. Haywood *et al.* (2013a) proposed constraining the PRISM time slab to a time slice, spanning a narrower period of time, to attempt to reduce uncertainties surrounding the data in relation to the orbital configuration. Prescott *et al.* (2014) showed, using the HadCM3 model, that changes in orbital forcings within a 40 kyr window of the mPWP were sufficient to produce regional differences of 2 to 3°C in simulated mean annual SATs, with seasonal regional changes exceeding 5°C.

The discrepancy may also be highlighting weaknesses in the model set up, in particular an inability to produce sufficient warming at high latitudes. There are numerous factors which may be affecting this, such as the model representation of poleward heat transport, or parameterisation of clouds at high latitudes. Chapter 2 discusses the influence of sea ice on high latitude climates, how it has been represented in models, and potential areas to explore and try to improve the models and reduce the data model mismatch.

1.9 Milankovitch theory

Milankovitch theory describes how cyclical changes in the earth's orbit influence the climate, in particular how variations in orbital eccentricity, axial tilt (obliquity) and precession influence both the quantity and spatial and temporal distribution of insolation (Hays *et al.*, 1976). The effect on the climate of these changes is known as orbital forcing.

1.9.1 Eccentricity

The eccentricity (e) of the earth's orbit describes the departure of the orbit from circularity, with $e = 0$ describing a circular orbit, and $0 < e < 1$ describing elliptical orbits ($e = 1$ gives a parabolic orbit, $e > 1$ a hyperbolic orbit). The eccentricity of earth's orbits ranges between 0.000055 and 0.0679 (Laskar *et al.*, 2011). Changes in e have periodicities of 95, 123 and 410 kyr. Eccentricity changes can produce small changes in mean annual insolation received by the earth, as well as having an effect on the length of the seasons, as the velocity of the earth's orbit changes with distance from the sun (Joussaume & Braconnot, 1997).

1.9.2 Obliquity

The obliquity (ϵ), or axial tilt of the earth gives the angle between the rotational and orbital axes. It oscillates between 22.1 and 24.5° (currently 23.4°) on a cycle of approximately 41 kyr. Obliquity changes do not affect the total insolation received by the earth, only the contrast between seasons, with increased obliquity resulting in greater seasonal contrasts. Lower obliquities result in conditions more favourable to ice ages, as cooler summers enable less melt of the winter precipitation (Imbrie *et al.*, 1992).

1.9.3 Precession

The precession describes the change in the orientation of the rotational axis over the earth on an approximately 26 kyr cycle, which affects the position of the

earth around the sun at solstices and equinoxes. Like obliquity changes, changes in precession do not affect the total insolation received by earth (Joussaume & Braconnot, 1997). Precession changes result in differences in seasonal contrasts between the northern and southern hemispheres. When the precessional cycle results in perihelion (time when earth is closest to the sun) occurring in the northern hemisphere summer (and consequently aphelion (furthest distance from sun) during winter), the difference between the northern hemisphere summer and winter will be larger than the difference between the southern hemisphere winter and summer (Hays *et al.*, 1976).

Chapter 2

Sea ice

2.1 Sea ice influence on climate

Sea ice exerts a strong influence on high latitude climates. It affects exchange of heat, moisture and momentum between the ocean and atmosphere by acting as an insulating barrier between the two (e.g. Dorn *et al.* (2007); Liu *et al.* (2009); Maykut (1978)), and in doing so influences atmospheric and oceanic circulations. It also has the ability to amplify initially small changes through feedback mechanisms (e.g. Curry *et al.* (1995); Gregory *et al.* (2002); Kellogg (1975)). Changes to sea ice extent or concentration will therefore have substantial local and remote effects. Figure 2.1 shows a simplified scheme demonstrating the influence of sea ice on the ocean and atmosphere.

Changes in sea ice concentration have been demonstrated to induce changes in Arctic surface air temperatures (e.g. Liu *et al.* (2009); Screen *et al.* (2012)), as a result of increased heat fluxes from the ocean to the atmosphere. Numerous studies have shown a negative correlation between Arctic sea ice extent and surface air temperatures (e.g. Gregory *et al.* (2002); Kumar *et al.* (2010); Mahajan *et al.* (2011); Ridley *et al.* (2007)). Lawrence *et al.* (2008) suggest that sea ice loss results in warming in Arctic terrestrial regions, which can cause the degradation of permafrost.

Early observations of remote responses to changes in Arctic sea ice cover are summarised in Herman & Johnson (1978). Brennecke (1904) and Meinardus (1906) indicated that colder temperatures observed at stations in Iceland were

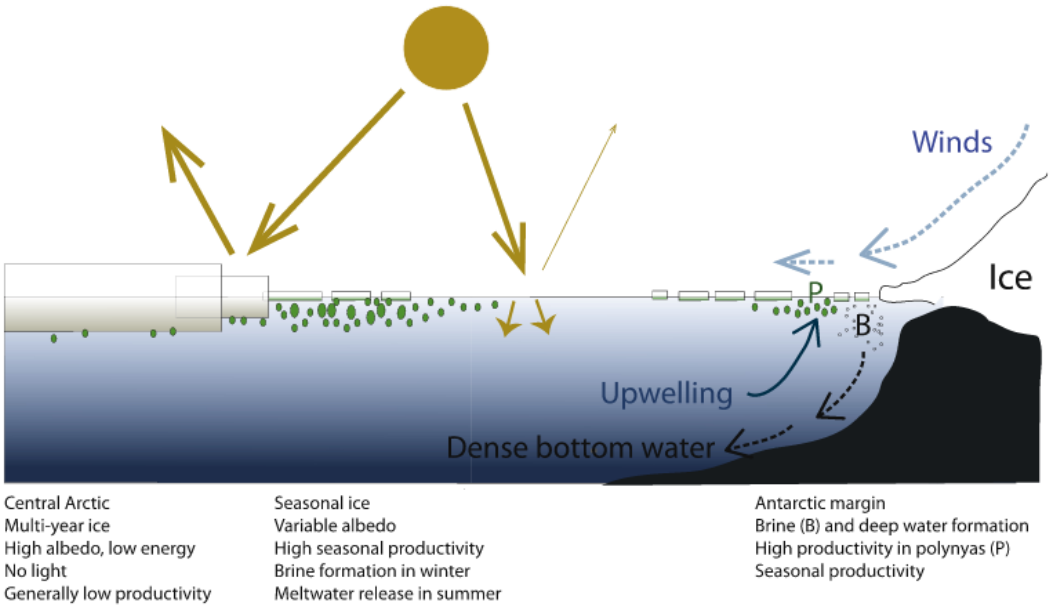

Figure 2.1: Simplified sea ice scheme from de Vernal *et al.* (2013a) showing the influence of sea ice on the climate in both the Arctic (left) and Antarctic (right). Yellow arrows indicate solar energy, dashed blue lines show katabatic winds. Green circles indicate primary production, with brine formation (B) and polynyas (P) both also indicated.

more likely to occur when the sea ice boundary extended further south, although they were unable to establish whether the cold temperatures were producing more extensive sea ice, or if the greater sea ice was inducing lower temperatures.

Subsequent studies attempted to establish the nature of the cause and effect. Hildebrandsson (1914) looked at late 19th century ice extent and meteorological data, and hypothesised that the nature of the summer sea ice in the East Greenland sea had an effect on Northern Hemisphere winter conditions. Wiese (1924) demonstrated evidence that the sea ice extent in the Greenland and Norwegian sea was associated with storm patterns in Europe. Scherhag (1936) suggested there was a relationship between the retreat of the East Greenland sea ice margin and warmer conditions observed in the North Atlantic in the early 1930s.

Walker (1947) concluded that correlations, albeit weak, existed between sea

ice extent in the North Atlantic and pressures over Iceland and Northern Europe, similarly Schell (1956, 1970) found connections between Arctic sea ice extents and temperatures and pressures over Europe. Defant (1961) concluded that there was a positive feedback between sea ice extent and atmospheric pressure in the Arctic.

Modelling studies have subsequently further demonstrated the effects of changes to the sea ice cover on global atmospheric circulation, surface air temperatures, precipitation and storm track activities (Budikova, 2009). Herman & Johnson (1978) demonstrated that large variations in sea ice extents in the Arctic had significant effects on the heights of geopotential surfaces, although the study was conducted with an atmosphere-only model, and so some of the observed effects may have occurred differently if factors such as ocean temperatures were allowed to vary in response to flux changes.

Murray & Simmonds (1995) used GCM simulations to explore the effects of variations in sea ice concentration, rather than the extent. They found that a decrease in sea ice concentration resulted in an increase in lower tropospheric temperatures in the Arctic, as well as a shallowing of the polar vortex and a decrease in the strengths of westerlies north of 45°N. The temperature response was demonstrated to be non-linear with respect to changes in the sea ice concentration.

Alexander *et al.* (2004) used an AGCM to look at the atmospheric response to changes in the winter Arctic sea ice cover. They demonstrate that reductions in sea ice result in surface heat flux anomalies greater than 100 W m^{-2}, although the spacial extent of these anomalies is only a few hundred kilometres. Locally, the effects of a reduction in sea ice are to cause near-surface warming, greater precipitation and evaporation, and a drop in sea level pressure over areas where ice has receded. Alexander *et al.* (2004) determine that the remote response to these changes in sea ice cover is determined by the interactions between the anomalous surface heat fluxes, and global atmospheric circulation. In the Atlantic sector, the reductions in sea ice cover cause the main branch of the North Atlantic storm track to weaken, whilst reductions in the Pacific sector excites stationary Rossby waves.

Dethloff *et al.* (2006) show, through AOGCM simulations, that changes in the energy balance of the Arctic as a result of changes in the sea ice cover alter

the strength of sub-polar westerlies and storm tracks, and so affect mid and high latitude climates.

As well as having a strong effect on the atmosphere, sea ice also influences ocean circulation. It affects the saltwater and freshwater budgets of the ocean - when sea ice is formed, a process known as brine rejection forces out salt into the surface layer of the ocean (Aagaard *et al.*, 1985). The cold and saline water that forms as a result sinks due to its density. In the Atlantic, the resultant water is called North Atlantic Deep Water (NADW). NADW is an important component of the thermohaline circulation (THC) of the ocean, particularly the Atlantic Meridional Overturning Circulation (AMOC) (Aagaard & Carmack, 1989). The overturning is sensitive to changes in sea surface temperature (SST) and salinity, and so can be affected by an outflow of fresh water as a result of melting sea ice (Broecker, 1997).

Most climate models predict a weakened THC as a result of a large melting of sea ice (Lemke & Ren, 2007), as the outflow of colder fresh water reduces the heat flux from the ocean to the atmosphere. Levermann *et al.* (2007) used a coupled climate model to investigate the effects of melting sea ice (as a result of a gradual increase in atmospheric CO_2 on simulated THC from CMIP models). They found that the models that simulated an initially stronger THC saw it weakened as a result of melting sea ice, but models with a weaker initial THC saw a strengthening. It was suggested that the reason for this effect was that those models with weaker THCs also had a more southerly Arctic sea ice margin, and as it melted more area was exposed to heat loss to the atmosphere, which helped to drive the THC. Those models with stronger THC saw it weaken due to the warming of atmospheric temperatures in the high latitude (as a result of the increased CO_2), which reduced the amount of heat lost from the ocean at higher latitudes.

2.1.1 The sea ice albedo effect

The sea ice-albedo effect is a positive feedback mechanism associated with changes to the surface albedo in regions with changing sea ice cover (Curry *et al.*, 1995) (see Figure 2.2). The albedo of snow-covered sea ice is very high at around 0.8 -

0.9 (Grenfell & Perovich, 2004; Lindsay & Rothrock, 1994; Perovich *et al.*, 1986), in contrast to open ocean, which has an albedo of ~ 0.07 (Grenfell & Perovich, 2004; Pegau & Paulson, 2001). When sea ice melts, the high-albedo snow and ice is replaced by low-albedo ocean, resulting in an increase in net downward shortwave radiation flux, due to a decrease in the upward shortwave flux. This will warm the upper ocean and melt more ice, leading to a further reduction in the overall albedo. The process can work in the opposite direction as well, where an increase in sea ice cover causes an overall albedo increase, reducing the absorbed shortwave radiation and thereby increasing the sea ice cover further. The sea-ice albedo effect is therefore a very important component of the climate, a fact which is cited by many studies (e.g. Björk *et al.* (2013); Curry *et al.* (1995); Grenfell & Perovich (2004); Hanesiak *et al.* (2001); Rind *et al.* (1995); Stroeve *et al.* (2012a)).

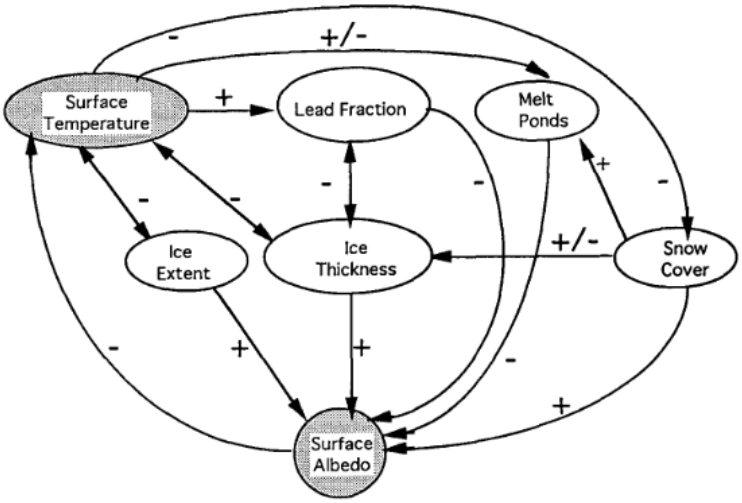

Figure 2.2: Schematic of sea ice-albedo feedback mechanism from Curry *et al.* (1995). Plus sign indicates a positive interaction (i.e. an increase in the first quantity leads to an increase in the second), and a minus sign indicates a negative interaction (i.e. an increase in the first quantity leads to a decrease in the second). A plus and minus indicate that there is uncertainty over the sign of the interaction, or that the sign changes over the annual cycle.

Early measurements by Perovich *et al.* (1986) showed sea ice albedo values ranging from 0.87, when the ice is covered with new snow, to 0.52 for bare, first year ice. Also measured are albedos for melt ponds (0.15 - 0.4), and open ocean (0.06). Lindsay & Rothrock (1994) measure area-averaged albedo of ice floes using the Advanced Very High Resolution Radiometer (AVHRR). Their measurements show albedo ranges within the ice pack of 0.18 to 0.91, with an overall mean of 0.58. Average albedo in spring is 0.7, dropping to between 0.4 and 0.5 in the summer.

Sea ice albedo has historically been a difficult quanitity to measure, as cloud cover can inhibit remote sensing (Perovich *et al.*, 2011), and field measurements can be hazardous, particularly on melting ice late in summer (Fetterer & Untersteiner, 1998). Measurements of first-year sea ice in the melt period in Hanesiak *et al.* (2001) range from 0.75, where sea ice is covered by moist snow, to 0.21, where dark melt ponds cover the surface. Perovich *et al.* (2002) measure the seasonal evolution of albedo on multiyear ice as part of the SHEBA field experiment (Uttal *et al.*, 2002). They note five distinct phases in seasonal evolution of sea ice albedo, measured from April to October. The sea ice albedo evolves from being high (0.8 to 0.9) and spatially uniform in April, when the ice is covered by snow, to highly variable (0.1 to 0.65) by late July, when the surface is a mixture of bare ice and melt ponds. Perovich & Polashenski (2012) conduct similar observations focusing on seasonal sea ice. Seasonal sea ice albedo evolution has two extra stages to the evolution of multiyear ice (open water and freezeup), and albedos as low as 0.2 are observed on heavily ponded sea ice in late summer (see Figure 2.3). Average albedo of seasonal sea ice is shown to decrease faster and to lower values than multiyear sea ice. Riihela *et al.* (2013) have observed a decline in Arctic sea ice albedo for the period from 1982-2009.

2.1.2 Factors affecting sea ice behaviour

The age and thickness of sea ice are important factors in influencing its overall behaviour. They are inherently linked, as younger ice is generally thinner than older ice as it has been growing for a shorter period (Comiso, 2002; Kwok, 2004). As a result, it melts more easily and thus increases the sensitivity of the climate

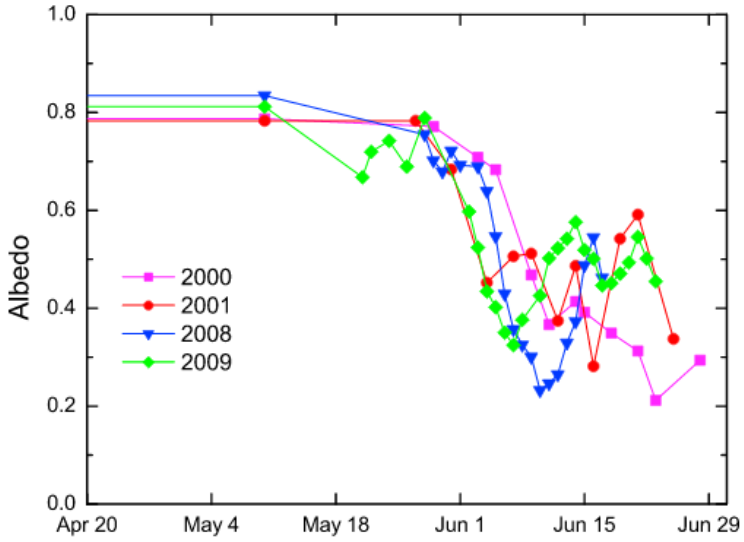

Figure 2.3: Timeseries of observations of sea ice albedo for Barrow, Alaska for four different campaigns (Perovich & Polashenski, 2012).

to warming (Holland & Bitz, 2003; Hunke, 2010; Rind *et al.*, 1995), although thinner ice does grow at a faster rate than thicker sea ice (Notz, 2009; Stranne & Bjork, 2012).

Warmer climates with a low sea ice extent, particularly with relation to the summer minimum, will have a sea ice cover that is likely to be dominated by first-year, or seasonal sea ice (sea ice that has grown since the end of the most recent melt season). Ice which has survived at least one summer melt season is known as multi-year ice. Modern sea ice cover is becoming increasingly dominated by first-year ice (Comiso, 2002; Kwok *et al.*, 2009; Stroeve *et al.*, 2012a), and it is likely that in warmer climates of the past, the percentage of first-year ice in the sea ice cover was greater than for the Arctic of the 20th century.

The thickness of sea ice is a substantial influence on many of its properties, such as surface temperature, salinity, compressive strength and growth rate (Maykut, 1978). The thickness distribution of sea ice at the beginning of the summer melt season has been cited as the most important factor affecting regional sea ice albedo distribution (Fetterer & Untersteiner, 1998), as it influences

the melt pond coverage.

Rind *et al.* (1995) demonstrate that the ease at which sea ice can be removed in models is just as important as the amount of sea ice, with respect to the sensitivity to warming. As thinner sea ice melts more easily than thicker ice, sensitivity of sea ice to warming is increased with thinner sea ice. Holland & Bitz (2003) show the importance of control sea ice thickness on simulated Arctic sea ice cover and surface air temperatures. Dorn *et al.* (2007) find that a correct distribution of ice thickness at the beginning of the melt season is crucial to reproducing the observed extent of summer sea ice. However, realistic sea ice thickness distributions are hard to achieve due to sparse observations.

First-year sea ice has been shown to have, on average, a lower albedo than multiyear ice (Kwok, 2004; Kwok & Untersteiner, 2011; Perovich & Polashenski, 2012; Perovich *et al.*, 2011), due to being thinner, less ridged, and prone to greater melt pond coverage. Maykut (1978) show that energy exchange over young, thin (less than 0.4 m) sea ice is between 1 to 2 orders of magnitude greater than over thick (greater than 1 m), multiyear ice. Above thicknesses of 1 m, very few changes in thermal properties are observed. Nicolaus *et al.* (2012) show that transmittance through first-year ice is almost three times larger than through multi-year ice, largely due to the higher melt pond coverage on first-year ice.

Hudson *et al.* (2013) suggest that due to the shift from multi-year to first-year ice, and the resultant increase in absorption and transmittance of the ice, the sea ice covered region in July and August will receive an additional 10^{20} J of solar input into the ice and ocean. This additional energy would be capable of melting 315 km^3 of ice, which would be a mean decrease in thickness of almost 13 cm in the region. They suggest that current understanding of sea ice behaviour is based largely on observations of multi-year ice, and this could have implications for how sea ice is represented in models of past or future climates with higher levels of first-year sea ice cover.

2.2 Observations of sea ice

2.2.1 History of observations

The Arctic is one of the least well observed areas of Earth, due largely to the extreme conditions and logistical difficulties in deploying instruments on sea ice (Uttal *et al.*, 2002). HadISST, the Hadley Centre's dataset of sea ice and sea surface temperatures, extends back to 1871 (Rayner *et al.*, 2003). Prior to the 1950s, the data set is primarily drawn from charts produced by the Danish Meteorological Institute (DMI) (Kelly, 1979; Walsh & Chapman, 2001). The charts were created based on a variety of observations, largely from ships, but shore-based observations are also included (Thomsen, 1947). Observations cover April to August, and coverage is largely dependent on location of ship traffic, if no observation exists at a certain location then data is extrapolated based on understanding of ice movement. September to March sea ice concentrations are interpolated based on the April-August record (Rayner *et al.*, 2003).

Walsh & Johnson (1979) combined several existing data sets to produce sea ice concentration data covering 1953 to 1977. Data was sourced from the UK Met Office, U.S. Naval Oceanographic Office, Canadian Meteorological Service, and the Icelandic Glaciological Society, as well as continuing to use the DMI charts (Table 1, Walsh & Johnson (1979)). Extra sources meant that the dataset was less vulnerable to errors in the observations, but data still did not exist for some months of the year, particularly in the early years of the study.

Satellite observations of the Arctic have been available from 1972 (Walsh & Chapman, 2001). The U.S. National Ice Center provided weekly sea ice concentration grids derived primarily from satellite data from 1972 to 1994. Since 1979, satellite passive-microwave data grids have also been obtained from the scanning multi-channel microwave radiometer (SMMR) (e.g. Parkinson *et al.* (1999)). Satellite data have provided a more extensive and comprehensive coverage of the Arctic than any previous observational record.

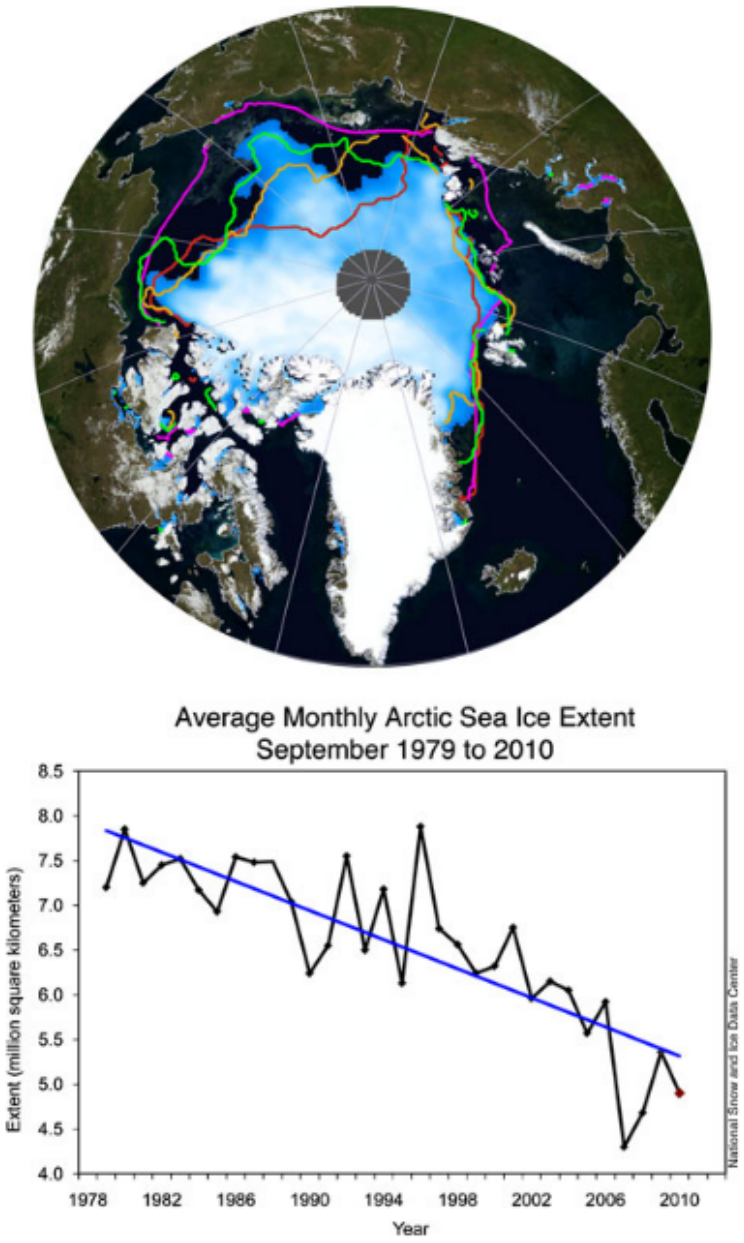

Figure 2.4: Above - September 2010 sea ice concentration, with extent boundaries for the same month in 2007 (red), 2008 (orange) and 2009 (green). The pink line indicates the mean September extent for 1979-2000. Below - Timeseries for September Arctic sea ice extent for 1979-2010, with linear trend line. Taken from Stroeve *et al.* (2012a).

Arctic sea ice extent, defined to be the total area where sea ice concentration exceeds 15% (Cavalieri *et al.*, 1999; Gregory *et al.*, 2002; Lemke & Ren, 2007) has declined dramatically over the last three decades (e.g. Comiso (2002); Serreze *et al.* (2003); Stroeve *et al.* (2007, 2012b); Zhang *et al.* (2013a)), (see Figures 2.4 and 2.5). A record minimum extent of 3.4×10^6 km^2 was observed on 13 September 2012 (Parkinson & Comiso, 2013). Arctic observations also demonstrate a large decrease in mean sea ice thickness (e.g. Comiso (2002); Giles *et al.* (2008); Maslanik *et al.* (2007); Rothrock *et al.* (1999); Sedláček *et al.* (2012)). The Arctic is predicted to be seasonally ice-free by the end of the 21st century (Boé *et al.*, 2009; IPCC, 2007), however some modelling studies suggest that summer sea ice may have vanished within 30 years (e.g. Holland *et al.* (2006); Stroeve *et al.* (2012b); Wang & Overland (2012)).

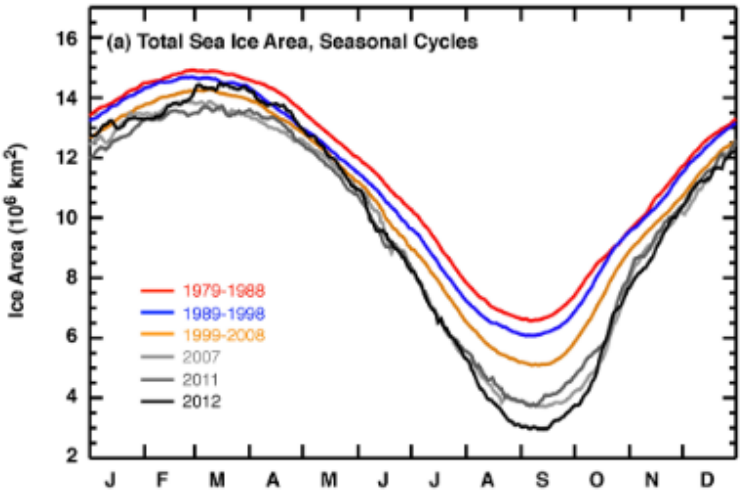

Figure 2.5: Annual cycle of daily sea ice area, showing three decadal averages (1979-1988, 1989-1998, 1999-2008) and three individual years (2007, 2011, 2012), from Parkinson & Comiso (2013)

2.2.2 Polar amplification

Observations of increased SATs show that the mean increase in the Arctic is greater than the global mean increase (e.g. ACIA (2005); Overland *et al.* (2004);

Rigor *et al.* (2000); Screen *et al.* (2012); Serreze & Francis (2006); Solomon *et al.* (2007)), a phenomenon which is known as Arctic or polar amplification (Serreze & Francis, 2006). Bekryaev *et al.* (2010) show that the mean annual SAT increases at high latitudes (i.e. North of 60°N) from 1875-2008 were 1.62 times the global mean annual SAT increases for the same period. Polar amplification is a phenomenon also observed in model predictions of future climate (e.g. Hansen *et al.* (1984); Holland & Bitz (2003); Manabe & Stouffer (1980); Meehl & Stocker (2007); Washington & Meehl (1996)), and there also exists palaeoclimate evidence of polar amplification (Brigham-Grette, 2009; Serreze & Barry, 2011). Serreze & Barry (2011) describes polar amplification as an 'inherent characteristic of Earth climate behaviour'.

The causes of polar amplification have been widely discussed. Surface albedo feedback is often attributed as a leading factor (Curry *et al.*, 1995; Holland & Bitz, 2003; Liu *et al.*, 2009; Serreze & Francis, 2006; Serreze *et al.*, 2009), as it leads to a diminished sea ice cover. Lower concentrations of sea ice result in a greater sensible heat content in the upper layer of the ocean in the summer months from increased absorption of downwelling shortwave radiation. Ice growth in autumn is delayed, and this results in an increase in upward heat fluxes from the ocean to the atmosphere, creating the polar amplification effect (Screen & Simmonds, 2010a,b; Serreze *et al.*, 2009). Several observational and modelling studies have attributed the cause of polar amplification to a reduction in sea ice (e.g. Kumar *et al.* (2010); Liu *et al.* (2009); Screen & Simmonds (2010b); Screen *et al.* (2012); Serreze *et al.* (2009))

However, some studies have indicated that sea ice albedo feedback cannot be the sole cause (e.g. Bekryaev *et al.* (2010); Serreze & Barry (2011)). High levels of polar amplification have been observed in modelling studies with no surface albedo feedback (e.g. Alexeev (2003); Alexeev *et al.* (2005); Flannery (1984); Graversen & Wang (2009); Langen & Alexeev (2005)). Other factors cited as potential causes or contributors to polar amplification include changes to cloud fraction (Hall, 2004), ocean heat transport (Winton, 2006), increased atmospheric heat transport (Alexeev & Jackson, 2013) and thermal surface inversion in winter (Bintanja *et al.*, 2011). Hall (2004) found that polar amplification levels were

higher in model simulations that included surface albedo feedbacks in comparison to simulations where these effects were suppressed.

The level of polar amplification seen in future projection varies between models (Holland & Bitz, 2003). One of the largest factors affecting the amount of polar amplification is the control sea ice conditions in the model (Dorn *et al.*, 2007; Holland & Bitz, 2003; Winton, 2006). Models which start with a greater sea ice extent exhibit higher levels of polar amplification, as there is more ice for the ice-albedo feedback to affect (Holland & Bitz, 2003), however greater polar amplification levels are observed in models with thinner control sea ice, as it is more vulnerable to melting and exposing open ocean (Winton, 2006). Control sea ice conditions exert a strong influence over future climate predictions in general (Dorn *et al.*, 2007; Walsh & Timlin, 2003; Winton, 2006).

Arctic SATs have been shown to have a high interannual variability (Polyakov & Johnson, 2000; Polyakov *et al.*, 2002; Schlesinger & Ramankutty, 1994), as well as low frequency variability (Polyakov *et al.*, 2002; Serreze & Barry, 2011; Serreze & Francis, 2006). Polyakov *et al.* (2002) claims that there is no significant polar amplification of SATs, and the trends observed are due to low frequency, high amplitude variability.

2.3 Sea ice modelling

In early energy balance climate models, such as Budyko (1969) and Sellers (1969), the treatment of the sea ice only extended as far as the albedo effect, which was parameterised as a function of the sea surface temperature. Bryan (1969) developed an early model of pack ice, expressed through an equation for the growth of ice, based on twelve parameters, including ice thickness, surface air temperature, snowfall and thermal conductivity of sea ice. As the thermodynamics of sea ice were much better understood than the dynamics, the model takes into account very little of the latter, focusing on the former. Simplifications were made to keep the computational requirements down, such as neglecting heat loss through cracks in the ice, making the sea ice conductivity uniformly equal (Bryan, 1969).

Maykut & Untersteiner (1971) developed a one-dimensional thermodynamic sea ice model, where the sea ice comprised of a snow layer and an ice layer. Heat

balance equations for the fluxes at the various boundaries between air, snow, ice and water, determine the thickness of the ice and snow layers, along with equations for heat conduction within snow and ice. A variety of input parameters are included, such as sea ice salinity, internal heating due to the penetration of solar radiation, and incoming and outgoing shortwave/longwave radiation fluxes. Snow cover accumulates linearly from August to May. Whilst the sea ice thicknesses produced by the model showed good agreement with observational values, the model has its limitations. It is unable to account for the effects of mechanical stresses on ice, unrealistic assumptions are made, and boundary conditions are oversimplified in some cases. Semtner (1976) simplified the model from Maykut & Untersteiner (1971) to enable it to be used more easily within a coupled atmosphere-ocean model, through the implementation of a 'streamlined numerical method'. However, the model continued to neglect the effects of sea ice dynamics.

The sea ice model described in Hibler (1979) attempts to include ice dynamics alongside thermodynamics. It incorporates a plastic rheology scheme, which is patterned after the model described in Coon *et al.* (1974). This models the motion of drifting pack ice, and enables the formation of leads and pressure ridges. The ice has an elastic mechanical response at low stress levels, and a plastic response for higher stresses. The model in Hibler (1979) also contains an ice concentration parameterisation. The model only considers two categories of sea ice ('thin' and 'thick'), and utilises an idealised thermodynamics scheme (Hibler, 1979).

Parkinson & Washington (1979) designed a sea ice model for use in a coupled ocean-atmosphere model which, unlike Maykut & Untersteiner (1971) and Semtner (1976), calculates some of the fluxes, such as incoming shortwave and longwave radiation, rather than specifying them all from observations. The model included a parameterisation of the effects of leads, as well as calculating ice movement and velocities, although there were limitations to these as the model used a uniform ice thickness, and several coefficient values were specified as constants. Other limitations of the model included unrealistic wind speeds in some regions, and no simulation of salinity in the oceans, which had a constant mixed layer depth. The use of monthly mean forcings for the specified fluxes also inhibited a proper simulation of interannual variabilities (Parkinson & Washington, 1979).

Flato & Hibler (1992) describe a sea ice model where the ice is modelled as a 'cavitating fluid', where the ice resists convergence (where the ice forms thicker, ridged ice from being pushed together), but does not resist divergence (where leads are formed from ice moving apart) or shear. They incorporate their numerical formulation of this rheology into a dynamic-thermodynamic sea ice model. Hakkinen & Mellor (1992) extended the model of Semtner (1976) to 3 levels, incorporating snow, thin ice and thick ice, and also introduce a parameterisation of the effect of leads.

Oberhuber (1993) developed a model similar to that of Hibler (1979), which solved similar equations but using a different numerical scheme, and used spherical, rather than Cartesian co-ordinates. Holland *et al.* (1993) used this model, with thermodynamics based on Parkinson & Washington (1979) and dynamics from the viscous plastic rheology scheme used in Hibler (1979). The model was demonstrated to produce a 'reasonable' simulation of the seasonal Arctic sea ice cycle (Holland *et al.*, 1993), reproducing all its known major features. The main limitation was that the model was not able to incorporate major feedback processes, due to not being incorporated into a fully coupled atmosphere-ocean-sea ice model (Holland *et al.*, 1993).

Ebert & Curry (1993) developed a one-dimensional intermediate thermodynamic sea ice model, based on the model described in Maykut & Untersteiner (1971). Effects of dynamics are partially accounted for through a prescribed sea ice divergence and a lead parameterisation adapted from Parkinson & Washington (1979). The parameterisation of leads enables the effects of absorption of solar radiation into the ocean to be included. A melt pond parameterisation is included, which allows for fractional areas of meltwater ponds of variable depth. A new surface albedo scheme is parameterised by considering five surface types, namely new snow, melting snow, bare ice, meltwater ponds and open water. The solar spectrum is partitioned into four, based on Curry & Ebert (1992). The surface albedo (α) is calculated through the equation

$$\alpha = \sum_{j=1}^{4} w_j \alpha_j \tag{2.1}$$

where α_j are the albedos for each spectrum, with w_j the relative weighting.

The thermodynamic/dynamic sea ice model that is used in HadCM2 and HadCM3 is described in Crossley & Roberts (1995). Thermodynamics are based on the zero-layer model of Semtner (1976), with parameterisation of leads based on Hibler (1979). The model uses the simple scheme set out in Bryan (1969) for sea ice dynamics, whereby sea ice advection is based on the mean speed of the currents in the first 100 m below the ocean surface.

To enable coupling with both the atmosphere and ocean components, the model is split into two parts, with one part interacting with the atmosphere component of the model, and the other interacting with the ocean component. The sea ice albedo parameterisation is a simple linear dependence on the surface air temperature (Crossley & Roberts, 1995).

Hunke & Dukowicz (1997) developed an elastic-viscous-plastic (EVP) model for sea ice dynamics, building on the non-linear viscous-plastic (VP) rheology set out in Hibler (1979), which had become established as the standard sea ice dynamics model. The model of Hibler (1979) treats the sea ice as a viscous fluid, and gives sea ice 'infinite viscosity' (Hunke & Dukowicz, 1997). This was countered by giving the sea ice a maximum viscosity bound, so that the sea ice 'creeps' slowly rather than being completely rigid. This however, proves computationally expensive due to viscosity ranging over several orders of magnitude. Lower maxima can ensure a less computationally expensive rheology, but at the cost of accuracy. The EVP scheme set out in Hunke & Dukowicz (1997) is a numerical approximation to the VP scheme of Hibler (1979). The computational efficiency of the model is greatly increased through the use of an elastic mechanism in regions of rigid ice.

The EVP scheme was implemented into HadCM3, with the results described in Connolley *et al.* (2006). The initial implementation produced increased winter sea ice extent in both the Arctic and Antarctic, where the standard HadCM3 model already produced extents greater than observations. The EVP scheme also worsened comparisons to observations for both hemispheres in summer, although there were some regional improvements. The EVP scheme was shown to increase ice velocities in both hemispheres, whilst not significantly affecting the broad scale patterns. Ice thicknesses showed improvements in comparison with observations in the eastern sector of Antarctica, but were demonstrated to be thinner than

observations in the western sector. Connolley *et al.* (2006) were able to improve the initial results of implementing the EVP scheme through tuning model parameters, leading to improved winter sea ice simulation in comparison to standard HadCM3 for both the Arctic and the Antarctic.

A relatively recent advance in sea ice model development is that of the representation of melt ponds. Melt pond effects were modelled implicitly in Maykut & Untersteiner (1971) through the selection of input parameters. In their ice-ocean coupled model, Mellor & Kantha (1989) included equations accounting for thermodynamic effects of melt ponds, but not a full parameterisation. Ebert & Curry (1993) include an explicit melt pond parameterisation in their model, which was based on a simple energy balance calculation due to the effects of ponds on absorption of solar radiation. A major limitation, however, was that the parameterisation did not take into account the effects of turbulent heat transport within the melt pond, and ignored time dependency of heat stored within the melt ponds (Taylor & Feltham, 2004).

Taylor & Feltham (2004) describe a one-dimensional thermodynamic melt pond model. The model is physically based, and uses a 'two-stream radiation model' to describe radiative transfer in sea ice, in contrast to previous models which used Beer's law for this purpose (e.g. Ebert & Curry (1993); Maykut & Untersteiner (1971)). This enables the albedo to be calculated within the model based upon the relative coverage of snow, bare ice and melt ponds produced, rather than being determined as an external parameter (Taylor & Feltham, 2004). Like the parameterisation in Ebert & Curry (1993), the total albedo is determined by the sum of the albedos at each wavelength, weighted accordingly.

Luthje *et al.* (2006) presents a melt pond model which describes horizontal and vertical evolution of summer sea ice cover, in contrast to the earlier version of Taylor & Feltham (2004), which operated only in one vertical dimension. Test simulations found that the topography of the ice was an important factor in determining the exact melt pond coverage, with lateral spread of meltwater dominating vertical drainage. The model still contained shortcomings, with the treatment of meltwater still crude in comparison to the complex nature of meltwater flow through ice, and the model does not consider snow cover or the hydrodynamic balance of the sea ice floe (Luthje *et al.*, 2006).

Flocco & Feltham (2007) aimed to develop a melt pond model suitable for incorporation into a GCM, which those of Taylor & Feltham (2004) and Luthje *et al.* (2006) were not. The model of Flocco & Feltham (2007) is based on the use of an ice thickness distribution function, which eases incorporation into a GCM. The model is unable to fully describe the topographical distribution of the sea ice cover, which prevents a detailed determination of the location and size of melt ponds, necessitating some assumptions. Nevertheless, test simulations indicated that the model produces a 'realistic' simulation of melt pond fraction on the sea ice (Flocco & Feltham, 2007).

2.4 Sea ice proxies

Sea ice can be defined by several metrics, including concentration, thickness and extent (area of at least 15% sea ice concentration), across both time and space. These can be difficult to measure for current sea ice, and so reconstructing past sea ice from proxies is very challenging (de Vernal *et al.*, 2013a). Nevertheless, several techniques exist, based on analysis of marine sediment, ice cores and terrestrial material (de Vernal *et al.*, 2008, 2013c; Polyak *et al.*, 2010).

Several proxies are based on the contents of marine sediments from regions that may have been covered by sea ice. Most core records come from sea ice margin zones, as the conditions make it easier to collect the cores than from seas with greater sea ice cover. Cores from the central Arctic are more likely to cover much longer periods of time, but due to low sedimentation rates may be of a low resolution, in contrast to Arctic continental margin cores, which can be very high resolution, but cover much shorter time intervals (Polyak *et al.*, 2010).

Organic biomarkers that are found in polar ocean floor sediment can be used to reconstruct past sea ice cover. In particular, a set of biomarkers known as highly branched isoprenoids (HBIs), which are biosynthesised by diatoms growing in sea ice, and released during melt, have been analysed (Collins *et al.*, 2013a). A proxy has been developed from an HBI known as IP_{25} (Ice Proxy with 25 carbon atoms) (Belt & Müller, 2013; Belt *et al.*, 2007; Brown & Belt, 2012; Müller *et al.*, 2011). IP_{25} is derived from diatoms at the base of spring sea ice, and its presence suggests seasonal sea ice, whilst convsersely the absence of IP_{25} is suggestive of either

perennial sea ice, or sea ice free conditions (Belt *et al.*, 2007). Understanding of IP_{25} and other HBIs from polar environments remains limited, due to the relative sparsity of observational data as a result of inherent challenges associated with collection in polar climates, combined with the difficulties of replicating Arctic conditions in the laboratory (Belt & Müller, 2013).

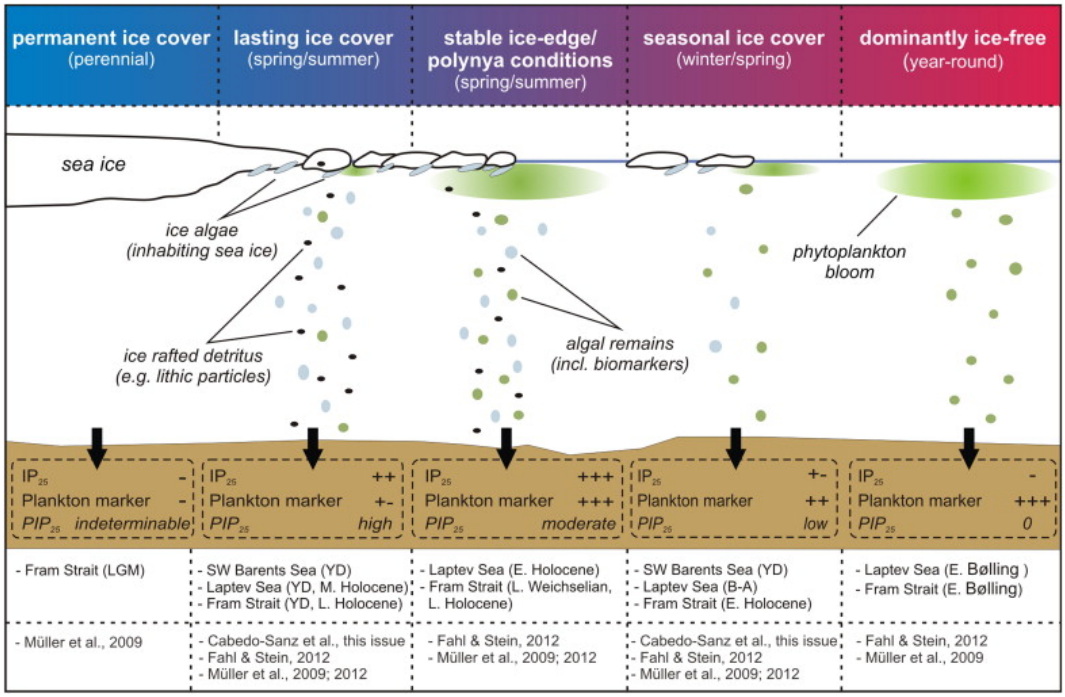

Figure 2.6: Schematic showing variation in IP_{25} and biomarker contents in the ocean in response to changing sea ice conditions (Belt & Müller, 2013).

IP_{25} has also been coupled with phytoplankton biomarkers to produce the index PIP_{25}, which aims to determine whether an absence of IP_{25} is indicative of perennial sea ice, or ice-free conditions (Müller *et al.*, 2011), although this index is still very new and requires further validation. Figure 2.6 shows a schematic demonstrating how IP_{25} and PIP_{25} vary under different sea ice conditions.

IP_{25} has been used to reconstruct sea ice cover over the Icelandic seas over the past 1200 years (Massé *et al.*, 2008) and the Canadian Arctic over the past 10,000 years (Vare *et al.*, 2009). It has been observed in sediment cores as far

back as 150 kya (Stein *et al.*, 2012), and 2.2 Ma (Stein & Fahl, 2013).

Knies *et al.* (2014) produce a record of IP_{25} at two sites (located at 80.16°N, 6.35°E and 80.28°N, 8.14°E) back over 5 million years ago. The results indicate that prior to 4 million years ago, the sea ice margin did not extend as far south as the location of the data sites, but has expanded since then to its modern position.

IP_{25} is not observed in the Southern Hemisphere, but other HBIs have been observed which can be used to reconstruct sea ice cover. Two particular HBIs, diene and triene, have been identified as possible Southern Ocean sea ice proxies (Collins *et al.*, 2013a). There are positive correlations seen between the presence of diene in Southern Ocean sediment cores and sea ice, based on reconstructions from other proxies. Similarly the presence of triene seems to indicate open waters in the past (Massé *et al.*, 2011). Reconstructions of Southern Ocean sea ice going back 60 ky based on HBI presence are available (Collins *et al.*, 2013a), although as diene and triene have so far only been validated against other proxies, further investigation is required in order to have more confidence in these results.

The presence of particular species of diatoms, which are known to live in sea ice, can be used for past sea ice reconstruction. Transfer functions are applied to abundance data (e.g. Justwan & Koc (2008)), which produce an estimate for spring sea ice concentration. Whilst some of the taxa used are very abundant in the sediment, other taxa associated with the presence of sea ice are small, and susceptible to dissolution, potentially distorting the diatom record in the sediment due to poor preservation (de Vernal *et al.*, 2013c). As the diatom flora differ between the North Atlantic and the Antarctic, different transfer functions are required to achieve the reconstruction.

Cronin *et al.* (2010) and Cronin *et al.* (2013) use the presence of the sea-ice dwelling ostracode *Acetabulastoma arcticum* to generate semi-quantitative reconstructions of sea ice in the Arctic, for the past 45 ky and 60 ky respectively. The presence of *Acetabulastoma arcticum* is shown to be associated with perennial sea ice, through comparison of an ostracode core-top database with observations of September sea ice concentrations from 1978-1991 (Cronin *et al.*, 2010). Due to low Arctic sedimentation rates and short-term sea ice variability, *Acetabulastoma arcticum* is not a perfect indicator of past perennial sea ice, instead the index

gives an indication of the likely proportion of the sampling interval over which the location was covered in perennial sea ice.

Distribution in Arctic sediment of cysts produced by dinoflagellates (dinocysts) have been used by several studies to reconstruct sea ice conditions during the Holocene and the Last Glacial Maximum (e.g. de Vernal *et al.* (2001, 2005, 2013b,c); Matthiessen *et al.* (2005); Rochon *et al.* (1999)). A modern analogue technique is applied to the dinocyst abundances, to produce a reconstruction of mean annual sea ice concentration, which when applied to modern observational data has a root mean square error of prediction of ±0.11 (de Vernal *et al.*, 2013c). Where perennial sea ice is present, primary productivity is very low, so resulting sediment is barren in dinocysts. Whilst the majority of taxa are associated with sea ice free regions, some are observed in areas of seasonal sea ice (de Vernal *et al.*, 2013b).

With the exception of *Islandinium minutum*, no dinoflagellate which produces a fossilisable cyst has been demonstrated to live in sea ice (de Vernal *et al.*, 2013c; Potvin *et al.*, 2013), and so the relationship between the dinocyst assemblages is indirect, and likely to be due to factors related to sea ice, such as temperature, salinity or density (de Vernal *et al.*, 2013c).

The sensitivity of benthic foraminifera to availability of food and oxygen has been cited to support the use of their presence in marine sediment as indication of past sea ice margins (e.g Schröder-Adams *et al.* (1990); Scott *et al.* (2009); Seidenkrantz (2013)). High benthic/planktic foraminifera ratios are also thought to be a potential indicator of perennial sea ice as the presence of planktic foraminifera is generally low under permanent sea ice conditions (Scott *et al.*, 1989). Whilst foraminifera can be used to provide information on past sea ice changes, it is emphasised that no species is a direct indicator of sea ice, and they must always be used in conjunction with other proxies in any reconstruction (Seidenkrantz, 2013).

As well as the abundance of particular species, the value of $\delta^{18}O$ in tests produced by foraminifera can be used to shed light on past sea ice growth rates (Hillaire-Marcel & de Vernal, 2008). Based on correlation with other proxies, light isotopic excursions of $\delta^{18}O$ in the shells of *Neogloboquadrina pachyderma* are thought to correspond to enhanced sea ice formation rates, with the suggestion

that the excursions are linked to 'low-salinity pulses' (Bauch *et al.*, 1997; Hillaire-Marcel *et al.*, 2004). This relationship is not equivocal or linear however, and must be used with other proxies to produce past sea ice production rates (Hillaire-Marcel & de Vernal, 2008).

Sediment originating from coastal margins too large to be transported by wind or ocean can also indicate the presence of sea ice in the past (e.g. de Vernal *et al.* (2008); Polyak *et al.* (2010)), although care has to be taken to distinguish between sediment transported by sea ice and those transported by icebergs (Lisitzin, 2002), or on the roots of trees uprooted and carried out to sea (Vogt & Parrish, 2012). Grains are entrained into sea ice during freeze-up, and released at melt onset, and sediment characteristics can be used to give an idea of past sea ice drift patterns (e.g. Andrews & Eberl (2007); Bischof & Darby (1997); Hebbeln & Wefer (1991); Pfirman *et al.* (1990)). Interpretation of the presence of such sediment is dependent on the location of the site. In the central Arctic, where perennial sea ice is more likely to have been present, increased ice-rafted sediment can indicate lower average concentrations, whereas at sites further from the pole it can suggest seasonal sea ice limits (e.g. (Darby *et al.*, 2001; Knudsen *et al.*, 2004)).

In addition to proxies found in marine sediment cores, polar ice cores yield proxies that can be used to glean information about the nature of sea ice in past climates (Abram *et al.*, 2013). There are two main proxies obtained from sea ice cores: sea salt aerosol and methanesulfonic acid.

Sea salt aerosol is generated from bubble bursting and sea spray over the ocean (de Leeuw *et al.*, 2011). Some smaller particles will be transported over terrestrial regions, and deposited inland (see Figure 2.7). Polar ice will indicate the changing levels of sea salt aerosol deposition in the past over these regions, and this can be used to infer past sea ice marginal zones, although this is largely limited to Southern Hemisphere sea ice (Abram *et al.*, 2013).

Sodium measurements are used to indicate sea salt aerosol levels, as other sources of sodium are relatively lower in comparison to other sea salt metals such as magnesium or calcium, and chloride can be subject to fractionation (Röthlisberger *et al.*, 2003). Any change in the sea ice margin will change the distance from a particular terrestrial site to the closest region of open water, and thus the nearest source of sea salt aerosol. As a result, a particular site should receive less

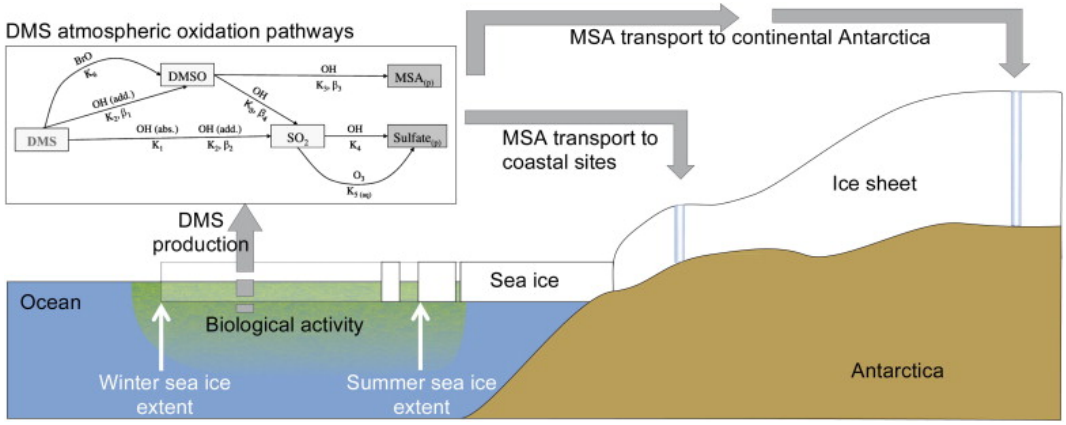

Figure 2.7: Schematic of MSA (methane sulphonic acid) showing the sea ice source, oxidation in the atmosphere (equations in inset), transportation over Antarctica and deposition over ice sheets (Abram *et al.*, 2013).

aerosol when sea ice extent is greater, and so the level of sodium in an ice core should in theory be negatively correlated with the sea ice extent (Abram *et al.*, 2013; Röthlisberger *et al.*, 2010). However, evidence suggests that on Antarctica, sea ice surface is the largest source of inland transported sea ice aerosol, with maximum concentrations observed in winter when the sea ice is at its largest extent (Rankin *et al.*, 2002; Wagenbach *et al.*, 1998; Wolff *et al.*, 2003).

Grumet *et al.* (2001) demonstrated a negative correlation between sea salt sodium in an ice core and spring sea ice extent in Baffin Bay, but further analysis demonstrated that only 7% of the sea salt variability was due to changes in the sea ice extent. Other studies have not been able to demonstrate inverse correlations between sea ice extent and sea salt aerosol in ice cores (Abram *et al.*, 2013). Ice core records of sea salt have been used in other studies to produce qualitative reconstructions of past sea ice extents based on a positive correlation between sea salt levels and sea ice extent (e.g. Fischer *et al.* (2007); Wolff *et al.* (2003, 2006)).

Due to the approximate radial symmetry of the Antarctic, the level of sea salt from a particular site can be seen as indicative for an average over a sector of the ocean, but this cannot be as easily applied to ice cores from Greenland, making

reconstructing Northern Hemisphere sea ice using the same methods much more difficult (Abram *et al.*, 2013).

The other major sea ice proxy obtained from ice core records is methanesulfonic acid (MSA, CH_3SO_3H), which is formed when dimethylsulphide (DMS, $(CH_3)_2S$), a biomarker produced by species of phytoplankton associated with sea ice, is oxidised when it is exchanged to the atmosphere. A sulphate (SO_4^{2-}) is also produced from this oxidation, but this can be produced from other sources, whereas MSA is only associated with marine biological activity, so this is used as an indicator for the production of DMS (Abram *et al.*, 2013). Increased levels of MSA observed in ice cores are expected to correlate positively with the extent of winter sea ice.

Whilst there have been quantitative reconstructions of Antarctic sea ice based on ice core records of MSA that show a strong positive relationship with winter sea ice extent (e.g. Abram *et al.* (2010); Curran *et al.* (2003)), Table 1 in Abram *et al.* (2013) summarised MSA signals from 22 Antarctic ice cores, and shows correlations between MSA records and sea ice extent are split between positive and negative, and the signal is reflecting a range of factors, including winter sea ice extent, absence of summer sea ice or atmospheric transport of MSA. Sea ice reconstructions based on MSA records currently only go back 160 years. While it does show potential, there still is a lot of work and development to be done to confidently reconstruct past sea ice conditions (Abram *et al.*, 2013).

Coastal and terrestrial records can also contain evidence that can be used for qualitative reconstructions of past sea ice conditions (Polyak *et al.*, 2010). Past changes in sea level have resulted in some formerly marine environments becoming terrestrial, although these sites are limited in geographic distribution and the time span over which they contain information. The presence of fossils of organisms known to be incapable of surviving in sea ice environments can be evidence of changing sea ice limits in the past (e.g. Brigham-Grette & Carter (1992); Carter *et al.* (1986); Kaufman & Brigham-Grette (1993)). Assemblages of fossils of bowhead whales, which are known to favour sea ice margin environments, can indicate its changes over the recent past (Polyak *et al.*, 2010). Similarly, pollen assemblages provide evidence of the northern treeline limit, which can indicate if past sea ice limits have receded or expanded (Brigham-Grette & Carter, 1992).

Driftwood logs of species such as spruce and larch have been found on Arctic coastlines, far from regions where the trees could have grown (e.g. Bennike (2004); England *et al.* (2008)). Their presence indicates transport of the driftwood, and in some cases the distances involved were too far for marine transport, suggesting that they must have been transported by ice instead (Haggblom, 1982; Tremblay *et al.*, 1997). This suggests the margins of sea ice have been further advanced at times in the past (Polyak *et al.*, 2010).

There is evidently a large variety of proxies which can be used for reconstructing past sea ice conditions. However, many of them are only qualitative or semi-quantitative, and can only be used if alongside at least one other sea ice proxy. Validating proxies against data has proved difficult, as satellite observations have only been available since 1979, and the rapid decline in sea ice cover over the past 50 years means it is difficult to validate against a system that is not in equilibrium. As a result, reconstructions of past sea ice are vague, contain large uncertainties, and typically date back only for tens of thousands of years.

There is very little proxy-based evidence regarding the nature of sea ice in the mid-Pliocene. As well as the IP_{25} analysis from Knies *et al.* (2014), Darby (2008) suggests that, based on the presence of iron oxide mineral grains in a sediment core taken from the Arctic Coring Expedition (ACEX) site (88°N, −138.3°E) that perennial sea ice was present in the Arctic during the past 14 million years. Based on estimates of sea ice drift and likely sources of the iron grains, it is determined that some of the material in every sample taken from the core must have taken more than a year to be transported to the location of the ACEX site. Due to the weight of the sediment, it can only have been transported in ice, indicating the presence of perennial sea ice at each of the sampled intervals.

The core was sampled approximately every 0.17 Ma, so it is possible that some seasonally ice free conditions occurred between the sampling intervals. However, whilst Darby (2008) concedes it is possible that this has occurred, it is considered unlikely that every sample missed a time of seasonal ice. So whilst we cannot say for certain that the mid-Pliocene did not see seasonally sea ice free conditions at any time, the evidence from Darby (2008) suggests that the probability of this is fairly low.

Chapter 3

Methods

3.1 HadCM3 model description

HadCM3 is the abbreviated name of the UK Met Office Hadley Centre Coupled Climate Model version 3. Results from HadCM3 have been used in the third, fourth and fifth assessment reports of the IPCC. HadCM3 consists of an atmosphere component and an ocean component, which can each be run as stand-alone atmosphere-only or ocean-only models (HadAM3 and HadOM3). It also contains vegetation and sea ice components (Gordon *et al.*, 2000). The model HadCM3 is described in detail in Gordon *et al.* (2000), a brief summation of the important details is included here.

3.1.1 Model components and coupling

3.1.1.1 Atmosphere component

The atmosphere component of HadCM3 has a horizontal resolution of $2.5° \times 3.75°$ (latitude $\times$ longitude), with 19 vertical levels, and a time step of 30 minutes. At the equator, a single grid box represents an area approximately 278 km by 419 km.

A full description of HadCM2, the predecessor to HadCM3, can be found in Johns *et al.* (1997). The following are major changes that have been made to the atmosphere component in HadCM3 (Pope *et al.* (2000) documents further minor changes that were made).

The model has a new radiation scheme, incorporating 6 spectral bands in the short wave, and 8 spectral bands in the long wave, as well as representing effects of greenhouse gases other than just CO_2, H_2O and O_3 (Edwards & Slingo, 1996). The model also incorporates a basic parameterisation of atmospheric aerosols, and the convection scheme has also been enhanced by parameterising its impact on momentum.

A new land surface scheme (Cox *et al.*, 1999) has been developed for the model, making use of MOSES (Met Office Surface Exchange System), a land surface model which is able to represent the freezing and melting of soil moisture. Additionally, the evaporation formulation has been modified to include the effect of CO_2, vapour pressure and temperature on stomatal resistance. The system also includes parameterisations of drag caused by mountain ranges (Milton & Wilson, 1996) and gravity waves (Gregory *et al.*, 1998).

Changes have been made to the partitioning of mixed phase clouds into ice and water, going from 0 to -15°C in the previous version, to 0 to -9° C in the current version (Gregory & Morris, 1996). This change is due to observational data based evidence from Moss & Johnson (1994). Several other parameterisations of factors affecting cloud formation have been added (Gordon *et al.*, 2000). There were also changes made to the boundary layer mixing in HadCM2, the most significant of which was to remove a non-local mixing scheme, which had been found to impair aerosol transportation and sinks.

3.1.1.2 Ocean component

The ocean component of the model has been modified and improved over a number of years, and the version that is detailed here is significantly different to other versions used in previous simulations. A description of this previous version can be found in Johns *et al.* (1997).

The horizontal grid spacing of the ocean component is $1.25° \times 1.25°$, compared to the previous version which had a spacing of $2.5° \times 3.75°$, the same horizontal spacing as seen in the atmosphere component of the model. This means that there are six ocean grid boxes for every atmosphere box. High latitude boxes can have partial sea ice cover. The component has 20 vertical levels, and is based

on the model in Cox (1984). The vertical levels are the same as in the previous version described in Johns *et al.* (1997), and are distributed so that they allow for greater resolution closer to the ocean surface.

For the topography in the model a dataset from ETOP05 (1988) was used, with a 1/12° resolution. Models such as these based on Bryan (1969) and Cox (1984) have a high sensitivity towards changes in the depths of channels along the Greenland-Iceland-Scotland ridge. These cannot all be represented as many are too small under the grid resolution, so three channels, each one grid point wide, are made through the ridge. These changes are described in Gordon *et al.* (2000). To avoid the potential problems of a singularity at the North Pole under the polar co-ordinate system, an island is placed here.

To parameterise horizontal eddy mixing of tracers, a version of the scheme in Gent & McWilliams (1990) by Visbeck *et al.* (1997) is used. Parameterisation of vertical mixing near to the surface uses a combination of a mixed layer sub-model from Kraus & Turner (1967) and a K-Theory scheme. Roberts *et al.* (1996) shows that simulations of the sub-polar gyre in the region of the Denmark Straits and the Iceland-Scotland ridge are particularly sensitive to details of the mixing of overflow water, so the convective adjustment is modified so that downslope mixing is represented more accurately. Similarly, a parameterisation is made of Mediterranean outflow water, where there is partial water mixing over the strait of Gibraltar.

Whilst the ocean component utilises a $1.25° \times 1.25°$ horizontal grid, for coast-line areas the atmospheric resolution of $2.5° \times 3.75°$ is used, to ease the coupling process (Gordon *et al.*, 2000).

3.1.1.3 Sea ice

The sea ice model utilised in HadCM3 uses a basic thermodynamic scheme, based on the zero-layer model described in Semtner (1976), which was developed from the one-dimensional sea ice model set out in Maykut & Untersteiner (1971). This model consists of four layers – ocean, ice, snow and atmosphere – with heat balance equations determining the fluxes at the boundaries between the layers, and equations describing heat conduction in the snow and ice layers. The ice heat

conduction equation includes a term for an internal heat source. Snow cover is affected by linear accumulations from August through to May. The model does not account for any mechanical stresses on ice.

Ice dynamics in HadCM3 are based on parameterisations set out in Bryan (1969). The advection of the sea ice is based on the mean speed of the currents in the first 100 m below the ocean surface. In HadCM3 the currents are based on the windstress, which is applied to the ocean below the ice (Gordon *et al.*, 2000).

Sea ice concentration parameterisation is based on Hibler (1979). The model creates sea ice when the sea surface temperature drops below -1.8°C, or from advection from the sea ice edge (Cattle & Crossley, 1995). New ice that is formed has thickness of 0.5 m, and enough sea ice is allowed to form to satisfy heat conservation. This enables fractional sea ice coverage in the model, and a parameterisation of leads. In the Arctic, sea ice can achieve a maximum concentration of 99.5%, with a maximum of 98% in the Antarctic (Gordon *et al.*, 2000).

The rate of change of the mean sea ice thickness (h_I) as a function of time, t, over a grid square changes according to equation (3.1), following Bryan *et al.* (1975). Here, $\boldsymbol{v}$ is the ocean current vector, A_H is ocean thermal diffusivity, and $\delta_h = 1$ when $h < 4$ m, and 0 when $h > 4$ m.

$$\partial h_I/\partial t = \nabla \cdot (\delta_h \boldsymbol{v} h_I) + A_H \nabla^2 h_I + \text{thermodynamic changes} \tag{3.1}$$

The effects of heat flux exchange over leads are divided into changes to the temperature of the upper layer of the ocean and the melting or formation of ice. The division of the effects is directly proportional to the concentration of sea ice over the given model grid square (Cattle & Crossley, 1995). The zero-layer model based on Semtner (1976) treats the ice-snow layer as a single slab, and the surface temperature of the ice is determined by equation (3.2):

$$C_* \partial T/\partial t = R_N + H + LE + k_S(T_S - T_F)/[h_S + (h_I k_S/k_I)] \tag{3.2}$$

where C_* is the effective surface thermal capacity, R_N is the net solar plus longwave radiation flux, H is the surface sensible heat flux, E is the surface evaporative flux and L is the latent heat of vaporisation (or sublimation of the surface if snow covered). k_S and k_I are thermal diffusivities of snow and ice,

h_S and h_I snow and ice layer thicknesses and T_S and T_F the ice/snow and ice bottom temperatures respectively. Both T_F and the surface temperature of leads are assumed to be -1.8°C (Cattle & Crossley, 1995).

In grid boxes containing sea ice above ocean surface layer temperatures higher than -1.8°C, the bottom heat flux from ocean to ice, H_o, is described by equation (3.3):

$$H_o = \rho c k (T_1 - T_F)/0.5\Delta z_1 \tag{3.3}$$

where ρ is the density of seawater, c the specific heat capacity of seawater, k a diffusivity parameter (set at 2.5×10^{-3} m^2 s^{-1}), with T_1 the temperature of the top ocean layer in the model, with depth Δz_1.

For surface air temperatures of -10°C or colder, the sea ice albedo is set at 0.8. For SATs between -10 and 0°C, the albedo decreases linearly to a minimum of 0.5. This temperature dependent evolution of sea ice albedo intends to capture the effects of the aging and melting of snow, and the presence of melt ponds on the sea ice albedo. Leads have a constant albedo of 0.06 (Gordon *et al.*, 2000). Sea ice is assumed to have a constant salinity of 0.6‰(Gordon *et al.*, 2000).

3.1.1.4 Atmosphere-ocean coupling

Coupling occurs once every day in the model run. First the atmosphere component runs for a day, with fixed SSTs. All the forcing fluxes accumulate every 30 minutes (time step of the model). Once a day has finished in the atmosphere component, the fluxes are passed to the ocean component, which then runs for one day as well. Once this has concluded, the updated SSTs and sea ice extents are passed to the atmospheric component of the model, and the next day's run begins with the new information. Because there are six ocean grid points for every atmosphere grid point, averaging and/or interpolation is required for the data transfer to take place.

3.1.2 Simulation of modern climate

3.1.2.1 Temperatures

Simulation of SSTs and sea ice extent by HadCM3 is discussed in Gordon *et al.* (2000), whilst Pope *et al.* (2000) analyses the SAT simulation using HadAM3, the atmosphere component of HadCM3. Sea surface temperatures are compared to GISST2.2 observations (Houghton *et al.*, 1996), sea ice extents to NSIDC satellite observations, and SATs to the climatology from Legates & Willmott (1990). Observations of SSTs and sea ice extents are compared to results from a 400 year HadCM3 simulation, with the averages calculated from the final 40 years of the run. Trace gases are set at pre-industrial levels (Gordon *et al.*, 2000).

Gordon *et al.* (2000) finds that all major observed SST features are reproduced by HadCM3, in particular abrupt horizontal SST gradients associated with major currents such as the North Atlantic Current, Antarctic Circumpolar Current and the Kuroshio Current. The higher resolution of the ocean component in comparison to HadCM2 is credited with being the major factor in the model ability to maintain these gradients (Gordon *et al.*, 2000).

Over most of the ocean, the SSTs are within 1°C of the observations, although there are some regions with greater differences, such as parts of the North Atlantic and North Pacific where simulated SSTs are more than 3°C cooler than observations. Temperatures with more than 1°C of warming compared to the observations are present south of the equator in the eastern tropics, off the coast of California and in the Southern Ocean (Gordon *et al.*, 2000). These error patterns are also observed in SST simulations from other models of a similar age, such as NCAR CSM1 (Boville & Gent, 1998) and ARPEGE T42/OPAICE (Barthelet *et al.*, 1998). Compared to the results from HadCM2, the HadCM3 SSTs represent a vast improvement (Gordon *et al.*, 2000).

HadCM3 is demonstrated to overestimate the extent of the sea ice maximum in the Arctic, with winter ice extending too far into the North Pacific, but the simulation of the minimum extent compares favourably with satellite observations. The failure of warm waters from the North Atlantic to reach the Barents sea is cited as a factor in the overestimation of winter sea ice extent (Gordon *et al.*, 2000). In the Southern Hemisphere, the seasonal variation and mean distribution

of the sea ice extent compares well to the observed climatology, but winter sea ice is too extensive.

The SATs simulated by HadAM3, as described in Pope *et al.* (2000), show a substantial reduction in temperature bias when compared to HadAM2, but the temperatures remain globally colder than the observed climatology (Legates & Willmott, 1990), with notable cold biases in the Northern Hemisphere in winter (Pope *et al.*, 2000).

The simulations that were performed and discussed in Gordon *et al.* (2000) and Pope *et al.* (2000) were set up with pre-industrial boundary conditions, but all the climatologies to which they are compared are from 20th century observations, when trace gases would have been higher, and the offset in some temperatures and sea ice extents may be reflecting this.

3.1.2.2 Sea ice

An analysis of the simulation of Arctic sea ice by HadCM3 in Gordon *et al.* (2000) shows that the simulated maximum sea ice extent exceeds the maximum extent from satellite observations, but the simulated minimum extent displays much better agreement. The high maximum extent is attributed to the winter sea ice extending further into the North Pacific than observations indicate would be realistic, as well as year round sea ice in the Barents sea. Gordon *et al.* (2000) attributes this partly to the model not representing Svalbard as an island, so warm North Atlantic currents are not diverted eastwards towards the Barents sea, leading to an oversimulation of ice. An important caveat to note is that Gordon *et al.* (2000) compared the results of a simulation intending to represent the climate of the pre-industrial era, whereas the satellite observations measure the sea ice extent of the late 20th century. Given the decline in sea ice that has been observed, it would be expected that the simulations should be more extensive than the observations. The close agreement of the minimum extent in observations and models may suggest that HadCM3 underestimates summer sea ice extent. HadCM3 was one of only two models in the CMIP2 ensemble to simulate ice-free conditions at the end of the 21st century (Hu *et al.*, 2004).

Gregory *et al.* (2002) compares the Arctic sea ice output from a transient simulation of the climate from 1860-2000 by HadCM3 with HadISST data (Rayner *et al.*, 2003), focusing on the comparison of the years 1970-1999. In addition to simulating a similar average mean annual extent over this period (13.4×10^6 km^2 in HadCM3, 13.3×10^6 km^2 in HadISST), the decadal trend over this period in HadCM3 ($-0.34 \times 10^6 \pm 0.07$ km^2 per decade, equating to -2.5 $\pm$0.5% per decade) is very close to the observational trend of -0.33×10^6 km^2 (-2.5%) per decade.

3.2 Experimental design

All the mPWP simulations used PRISM3D boundary conditions (Dowsett *et al.* (2010), section 1.3). The control simulation had an atmospheric CO_2 concentration of 400 ppm, and used an orbital configuration identical to modern. Minimum sea ice albedo was 0.5, with a maximum of 0.8.

The first ensemble of mPWP simulations looked at changes to the minimum and maximum sea ice albedo in HadCM3. In addition to the control, 23 simulations were run with changes to one or both of the minimum and maximum albedo, creating a 24-member ensemble. The maximum albedo values used ranged from 0.5 to 0.9, at intervals of 0.1, with minimum albedo values ranging from 0.2 to 0.7 at the same interval. Combinations where the minimum value was greater than or equal to the maximum value were not used. All combinations are shown in Figure 3.1. Analysis of the results in chapter 4 focuses on just 3 of the 23 simulations, with no change to the maximum albedo, but the minimum reduced to 0.2, 0.3 and 0.4. These are highlighted in Figure 3.1, with further details in Table 3.1. All these simulations were run for 200 model years, each spun off from a 500 year control run. Climatological averages were based on the final 30 years.

In addition to the mPWP simulations, four transient simulations were run, which started with pre-industrial boundary conditions, and increased greenhouse gas levels in line with historic rates up to the present day. The sea ice albedo limits in these runs were the same as the limits in the mPWP simulations whose results are analysed (see Table 3.1).

A second ensemble of mPWP is analysed in chapter 6. As in the first ensemble, PRISM3D boundary conditions are used, but changes are made in some

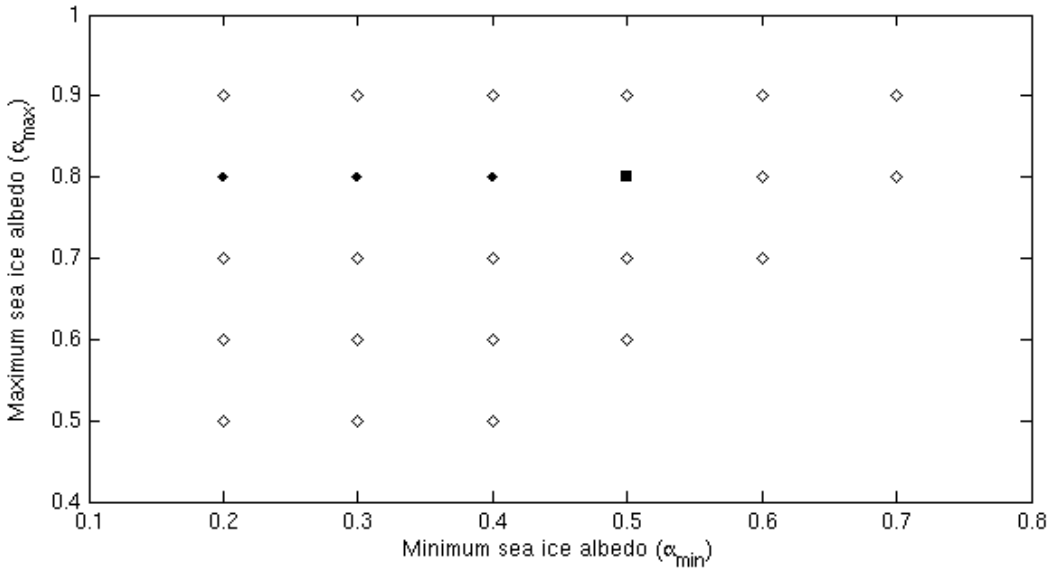

Figure 3.1: Minimum and maximum sea ice albedo combinations represented in the first ensemble of mPWP simulations run. Symbols filled in black represent simulations which are analysed in chapter 4 and from which the results are presented. The square icon indicates the albedo combinations of the control simulation.

simulations to orbital configuration and atmospheric CO_2 concentrations, as well as minimum sea ice albedo. Table 3.2 contains the details of all the ensemble members.

Five different orbital configurations are represented in the ensemble. In addition to the standard, identical to modern configuration, four configurations are selected, based on the astronomical solution of Laskar *et al.* (2004). These configurations have maximum insolation at 65°N in the mPWP during January, March, July and September. These months were selected as January and July are the middle months of the traditional definitions of winter (DJF) and summer (JJA), whilst March and September are the months when sea ice extent reaches its maximum and minimum respectively.

In addition to changes to the orbit, simulations were run with atmospheric CO_2 levels of 300 ppm and 500 ppm, to assess the sensitivity of changes in the

Table 3.1: Key details of the four mid-Pliocene simulations indicated in Figure 3.1 for which results are analysed in chapter 4, and details of the four modern transient simulations, also analysed in chapter 4.

Experiment type	Minimum sea ice albedo	Boundary conditions	Atmospheric CO_2 concentration (ppmv)
Mid-Pliocene	0.5 0.4 0.3 0.2	Mid-Pliocene (PRISM3D)	400 (constant)
Modern transient	0.5 0.4 0.3 0.2	Pre-industrial	Initial concentration of 280, followed by increase at historical observed rate

mid-Pliocene Arctic sea ice to variability in CO_2. Whilst some studies appear to suggest that 300 ppm is a plausible mid-Pliocene CO_2 value (e.g. Badger *et al.* (2013); Zhang *et al.* (2013a)), at least at some point, 500 ppm is above the upper estimates of mid-Pliocene CO_2. These simulations should therefore be viewed as an investigation of sea ice sensitivity, rather than a representation of what could have occurred in the mPWP.

The alternative minimum albedo of 0.2, studied in chapter 4, is also investigated in this ensemble. All combinations of the five orbital configurations, three atmospheric CO_2 concentrations and two minimum albedo values are used, giving a 30-member ensemble.

All simulations were run for 500 years, to ensure that all reached equilibrium once readjusting from the changes in orbit, although the timeseries demonstrated that all had reached equilibrium by 200 years. Climatological averages were based on the final 30 years. Like the first ensemble, all simulations were spun off from a 500 year control run.

The experiments analysed in chapter 5 are the results of the Pliocene Modelling Intercomparison Project (PlioMIP), for which eight different modelling groups conducted simulations of pre-industrial and mid-Pliocene climate, follow-

Table 3.2: Combinations of orbital configuration (with eccentricity, precession and obliquity values), pCO_2 and minimum sea ice albedo of the 30 simulations.

Experiment name	Orbital Equivalent (kyr BP)	Eccentricity/ Precession/ Obliquity	Global mean annual insolation (W/m^2)	Atmospheric CO_2 concentration (ppmv)	Minimum albedo
Mod_300_0.5				300	0.5
Mod_400_0.5		0.016702		400	0.5
Mod_500_0.5	Modern	0.01628	342.05	500	0.5
Mod_300_0.2		23.439		300	0.2
Mod_400_0.2				400	0.2
Mod_500_0.2				500	0.2
Jan_300_0.5				300	0.5
Jan_400_0.5		0.053487		400	0.5
Jan_500_0.5	3057	-0.02318	342.49	500	0.5
Jan_300_0.2		22.914		300	0.2
Jan_400_0.2				400	0.2
Jan_500_0.2				500	0.2
Mar_300_0.5				300	0.5
Mar_400_0.5		0.040574		400	0.5
Mar_500_0.5	3140	0.02343	342.28	500	0.5
Mar_300_0.2		22.719		300	0.2
Mar_400_0.2				400	0.2
Mar_500_0.2				500	0.2
Jul_300_0.5				300	0.5
Jul_400_0.5		0.051086		400	0.5
Jul_500_0.5	3037	-0.04239	342.45	500	0.5
Jul_300_0.2		23.642		300	0.2
Jul_400_0.2				400	0.2
Jul_500_0.2				500	0.2
Sep_300_0.5				300	0.5
Sep_400_0.5		0.054281		400	0.5
Sep_500_0.5	3053	0.03551	342.50	500	0.5
Sep_300_0.2		22.947		300	0.2
Sep_400_0.2				400	0.2
Sep_500_0.2				500	0.2

ing a consistent experimental design. Table 3.3 summarises the important details of the eight members of the PlioMIP ensemble. For details of the experimental design of PlioMIP, see chapter 5, in addition to Haywood *et al.* (2011a) and Haywood *et al.* (2011b).

Table 3.3: Technical details of the PlioMIP model ensemble: atmosphere and ocean resolutions, details of the sea ice component, and references for each of the eight PlioMIP Experiment 2 simulations.

Model	Atmosphere resolution (° lat × ° long)	Ocean resolution (° lat × ° long)	Length of run/ averaging period (years) Pre-industrial	mid-Pliocene	Sea Ice components and references	Reference
CCSM4	0.9 × 1.25	1 × 1	1300/100	550/100	EVP rheology, melt ponds Hunke & Dukowicz (1997); Hunke (2010); Holland *et al.* (2011)	Rosenbloom *et al.* (2013)
COSMOS	3.75 × 3.75	3 × 1.8	3000/30	1000/30	VP rheology, leads Marsland *et al.* (2003)	Stepanek & Lohmann (2012)
GISS-E2-R	2 × 2.5	1 × 1.25	950/30	950/30	VP rheology, leads Zhang & Rothrock (2000); Liu *et al.* (2003)	Chandler *et al.* (2013)
HadCM3	2.5 × 3.75	1.25 × 1.25	200/50	500/50	Free drift, leads Cattle & Crossley (1995)	Bragg *et al.* (2012)
IPSLCM5A	3.75 × 1.9	0.5 – 2 × 2	2800/100	730/30	VP rheology, leads Fichefet & Morales Maqueda (1999)	Contoux *et al.* (2012)
MIROC4m	2.8 × 2.8	0.5 – 1.4 × 1.4	3800/100	1400/100	EVP rheology, leads K-1 Model Developers (2004)	Chan *et al.* (2011)
MRI-CGCM	2.8 × 2.8	0.5 – 2 × 2.5	1000/50	500/50	Free drift, leads Mellor & Kantha (1989)	Kamae & Ueda (2012)
NorESM-L	3.75 × 3.75	3 × 3	1500/200	1500/200	Same as CCSM4	Zhang *et al.* (2012)

Chapter 4

Sensitivity of Pliocene Arctic climate to sea ice albedo

This chapter has been published in Geophysical Research Letters as:

Howell, F. W., Haywood, A. M., Dolan, A. M., Dowsett, H. J., Francis, J. E., Hill, D. J., Pickering, S. J., Pope, J. O., Salzmann, U., and Wade, B. S. "Can uncertainties in sea ice albedo reconcile patterns of data-model discord for the Pliocene and 20th/21st centuries?", *Geophys. Res. Lett.* (2014).

Abstract

General circulation model simulations of the mid-Pliocene warm period (mPWP, 3.264 to 3.025 million years ago) currently underestimate the level of warming that proxy data suggests existed at high latitudes, with discrepancies of up to 11°C for sea surface temperature estimates, and 17°C for surface air temperature estimates. Sea ice has a strong influence on high latitude climates, partly due to the albedo feedback. We present results demonstrating the effects of reductions in minimum sea ice albedo limits in GCM simulations of the mPWP. Whilst mean annual SAT increases of up to 6°C are observed in the Arctic, the maximum decrease in model-data discrepancies is just 0.81°C. Mean annual SSTs increase by up to 2°C, with a maximum model-data discrepancy improvement of 1.31°C.

It is also suggested that the simulation of observed 21st century sea ice decline could be influenced by the adjustment of the sea ice albedo parameterisation.

4.1 Introduction

The mid-Pliocene Warm Period (mPWP), covering the interval between 3.264 and 3.025 million years ago (Dowsett *et al.*, 2010), was a period of sustained global warmth, when global annual mean temperatures are estimated to have been 2 to 3°C warmer than present day (Haywood & Valdes, 2004), an increase within the warming range predicted by the IPCC for the end of the 21st century (IPCC, 2007). Estimates of pCO_2 fall in the range of 365-415ppm (Pagani *et al.*, 2010; Seki *et al.*, 2010). General circulation model (GCM) simulations of mid-Pliocene climates do not produce the level of high latitude warming, particularly in the North Atlantic and Arctic regions, implied by the proxy data (Dowsett *et al.*, 2011; Haywood *et al.*, 2013b; Salzmann *et al.*, 2013).

Sea ice exerts a strong influence over high latitude climates, particularly in the Arctic, through acting as an insulating cover between the ocean and the atmosphere, and its ability to amplify small changes through feedback mechanisms (Kellogg, 1975; Maykut, 1978), such as the albedo feedback, which can cause the amplification of an initial warming or cooling perturbation to the system (Curry *et al.*, 1995).

Sea ice albedo has often been used as a tuning mechanism in GCMs so that simulated sea ice extents and thicknesses have better agreement with modern observations (Eisenman *et al.*, 2008; Hunke, 2010). Since values in GCMs are tuned with respect to present day, they may not remain valid for simulating radically different climate states that existed in the past. This may also have implications for the validity of model predictions of global change. As proxy data indicates that high latitude surface air and sea surface temperatures (SATs and SSTs) were several degrees warmer in the mid-Pliocene (Dowsett *et al.*, 2011; Haywood *et al.*, 2013b; Salzmann *et al.*, 2013), it is likely that in comparison to present day, less winter ice cover would survive the summer. Data from ostracode assemblages and ice rafted debris sediments in the Arctic basin suggest the presence of seasonal,

rather than perennial sea ice in the Pliocene Arctic (Cronin *et al.*, 1993; Moran *et al.*, 2006; Polyak *et al.*, 2010).

Arctic summer sea ice extent has declined dramatically in the last 30 years (Comiso *et al.*, 2008; Stroeve *et al.*, 2007), resulting in a shift towards increasing levels of first-year sea ice (ice formed after the end of the most recent melt season). GCMs have not successfully reproduced this decline, and have generally overestimated Arctic sea ice extent, particularly for the recent rapid decline (Stroeve *et al.*, 2007, 2012b). This may have implications for forecast simulations of 21st century sea ice if the models have been tuned with respect to a climate with more multi-year Arctic sea ice (ice that has survived at least one summer melt season).

Perovich *et al.* (2007) and Perovich & Polashenski (2012) have provided observations demonstrating the evolution of multi-year and first-year sea ice albedo throughout the summer. Multi-year sea ice albedo is shown to fall from a maximum of 0.85 to a minimum of ~ 0.4 just before the onset of freeze-up. In contrast, first-year ice albedo can be as low as 0.2, and is less than multi-year ice albedo for most of the summer, never at any point exceeding it.

A large contribution to the difference in minimum albedo is the more extensive melt pond coverage on first-year ice (Perovich & Polashenski, 2012; Polashenski *et al.*, 2012). The difference between first-year and multi-year sea ice questions whether a minimum albedo value tuned for modern climate is appropriate for an Arctic with a higher proportion of first-year ice than present day.

This paper explores whether reducing the minimum sea ice albedo limit in the Hadley Centre Coupled Climate Model Version 3 (HadCM3), in accordance with that expected from a higher proportion of first-year ice, could improve model-data agreement at high latitudes for the mid-Pliocene warm period. We focus only on the sea ice albedo in order to better quantify the effects with regard to the observations in Perovich & Polashenski (2012). We also examine the response of September Arctic sea ice extent to albedo limit changes for modern transient simulations. If a lower minimum albedo can better reproduce the recent trend of sea ice decline, then as recent observations highlight a shift towards seasonal rather than perennial sea ice, this could reinforce the case for its use in simulations of warmer climates such as the mid-Pliocene.

4.2 Methods

4.2.1 Model Description

The model used in this study was HadCM3, a coupled atmosphere-ocean GCM produced by the UK Met Office Hadley Centre. In addition to the atmosphere and ocean, HadCM3 also contains vegetation and sea ice components (Gordon *et al.*, 2000).

The atmosphere component of HadCM3 has a horizontal resolution of 2.5° × 3.75° (latitude × longitude), which at the equator gives a grid box representing 278km × 419km, and comprises of 19 vertical levels (Gordon *et al.*, 2000). The horizontal grid resolution of the ocean component is 1.25° × 1.25°, giving six ocean grid boxes for every atmosphere box, with 20 vertical levels. Coupling occurs once per day in the model run, with the forcing fluxes accumulating every 30 minute model time step (Gordon *et al.*, 2000).

The sea ice model utilises parameterisations of ice drift and leads alongside a basic thermodynamic scheme (Cattle & Crossley, 1995). Semtner (1976) provides the basis for the thermodynamics of the model, and ice concentration parameterisation is based on Hibler (1979). The model also utilises a sea ice dynamics parameterisation, based on Bryan (1969). A more detailed description of the sea ice component can be found in Appendix A.

4.2.2 Experimental Set Up

In order to investigate the impacts of changes to the minimum sea ice albedo (α_{min}) on simulations of the mid-Pliocene, four simulations with mid-Pliocene boundary conditions were run with α_{min} values of 0.5 (control), 0.4, 0.3 and 0.2. All used the standard maximum albedo of 0.8. Each simulation was run for 200 years, spun off from an initial 500 year control run, with climatological averages based on the final 30 years. All simulations had achieved equilibrium before 200 years.

In addition to the Pliocene runs, we ran four transient simulations, which started with pre-industrial boundary conditions and increased greenhouse gas

levels in line with the historic rates up to the present day. Results were compared against historical observations from the Hadley Centre's HadISST data set (Rayner *et al.*, 2003). The alternative sea ice albedo limits used in the mid-Pliocene simulations were also applied to these runs.

The experimental design uses the template set out in Haywood *et al.* (2011b). All simulations use PRISM3D boundary conditions, at the time of writing the most recent version of the PRISM palaeoenvironmental reconstruction (Dowsett *et al.* (2010), see Appendix A for more details).

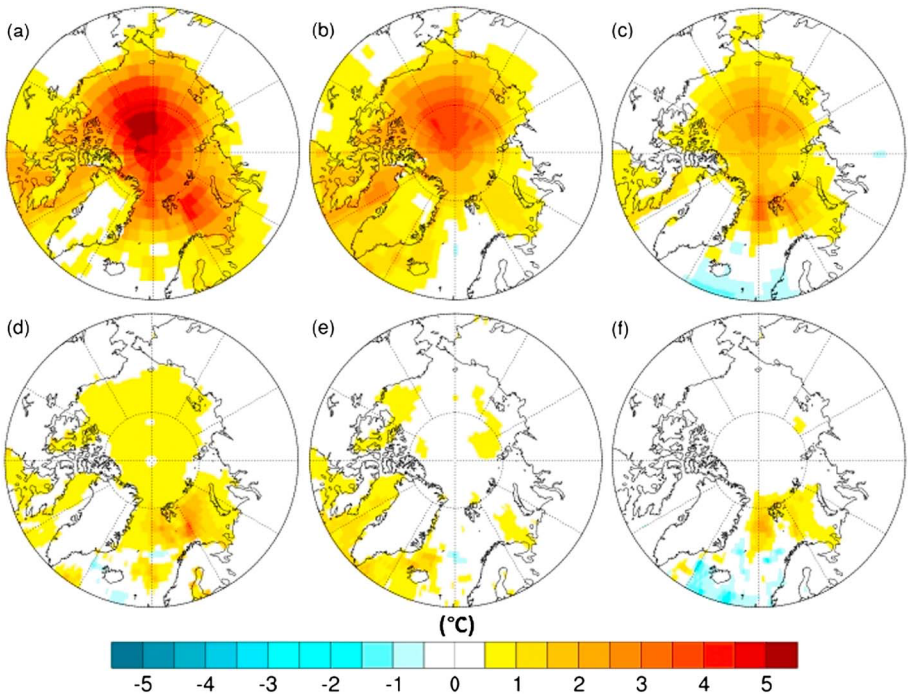

Figure 4.1: Mean annual temperature (°C) anomalies (alternative minus standard) for Pliocene simulations with α_{min} values: (a) & (d) 0.2, (b) & (e) 0.3, (c) & (f) 0.4. Standard α_{min} is 0.5 . (a) - (c) show the SAT anomalies, with (d) - (f) displaying SST anomalies. Locations of data sites from Tables 4.1 and 4.2 are also shown.

4.2.3 Model-Data Comparisons

To assess the effectiveness of the changes to the sea ice albedo limits on mid-Pliocene model-data mismatches, the model results were compared to mid-Pliocene SAT and SST proxy data temperature estimates. SAT estimates are based on palaeobotanical proxy data (Salzmann *et al.*, 2008, 2013), and SST estimates are achieved using multiple proxies, based on Mg/Ca and alkenone palaeothermometry, and planktonic foraminiferal assemblages (Dowsett *et al.*, 2013, 2010).

We focus on the region north of 60°N. Whilst several SAT and SST data sites outside of this region have large model-data differences, no significant warming is observed in the northern hemisphere south of 60°N in our simulations, so these sites display no change in the model-data mismatch. There are nine SAT and five SST data sites north of 60°N (Dowsett *et al.*, 2012; Salzmann *et al.*, 2013). For each site we identified the difference between the proxy data estimates and the control simulation temperatures. These are compared with the temperatures produced by the three simulations with reduced minimum albedo. Sites with a model-data mismatch reduction of greater than 0.5°C are presented in the main paper, with the full set shown in Appendix A.

4.3 Results

4.3.1 Pliocene Albedo Runs

4.3.1.1 Annual

Figure 4.1 shows the mean annual SAT and SST anomalies north of 60°N for the simulations with reduced minimum sea ice albedo. Each display an increase in SAT over the Arctic Ocean, and in most cases this warming spreads across some terrestrial regions. The SAT increase is in excess of 5°C in some areas in the simulation with $\alpha_{min} = 0.2$.

In comparison with the SAT response, the overall SST response is weaker (Figure 4.1). A small response is shown for the run with $\alpha_{min} = 0.2$, with an increase of around 1°C over most of the ocean north of 60°N, with the exception of a region east of Greenland and surrounding Iceland which shows largely no

change, as this region was already sea ice free in the standard Pliocene simulation. The simulations with α_{min} reduced to 0.3 and 0.4 show changes of a similar magnitude, but cover less area - in the case for $\alpha_{min} = 0.4$, the change is limited to a small region around the Barents Sea.

Table 4.1: Pliocene SAT anomalies (model simulated temperature minus proxy reconstructed temperature) at three palaeodata sites. Anomalies are displayed for the control and $\alpha_{min} = 0.2$ simulations.

Site	Latitude/Longitude	Control Anomaly	$\alpha_{min} = 0.2$ anomaly
Beaver Pond	78.40°/-82.00°	-14.51°C	-13.7°C
Ocean Point	70.00°/-153.00°	-8.92°C	-8.2°C
Lena River	72.20°/125.97°	-12.01°C	-11.4°C

At six of the nine SAT palaeodata sites north of 60°N, the temperature change between the control and the $\alpha_{min} = 0.2$ simulation was less than 0.25°. Table 4.1 shows the locations of the other three SAT data sites, which all displayed increases of at least 0.5°C in the $\alpha_{min} = 0.2$ simulation in comparison to the control, and the model minus data SAT anomalies for those two simulations at each site. Similarly, two of the five SST data sites north of 60°N displayed temperature differences of less than 0.25°C between the two discussed simulations. Table 4.2 summarises the same information for the three remaining SST sites as Table 4.1 does for the SAT sites. The locations of both the marine and terrestrial sites are displayed in Figures 4.1 and 4.2.

4.3.1.2 Seasonal

Figure 4.2 shows the four mean seasonal SAT anomalies for the run with $\alpha_{min} = 0.2$. The largest response is seen in northern hemisphere autumn (SON), where the SAT anomaly is as much as 10°C over some areas of the Arctic. Winter (DJF) also shows a strong response, with SAT increases over the Arctic basin of 4-6°C. DJF is the only season where any substantial terrestrial SAT increase is observed. In contrast to SON and DJF, the SAT anomalies in spring (MAM) and summer (JJA) are much weaker.

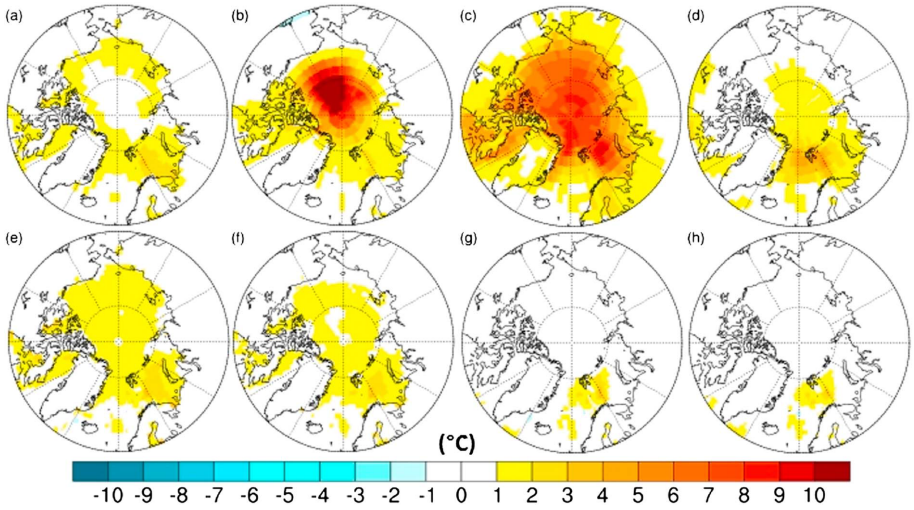

Figure 4.2: Mean seasonal temperature(°C) anomalies (alternative minus standard) for Pliocene simulation with $\alpha_{min} = 0.2$, showing (a) & (e) summer (JJA), (b) & (f) autumn (SON), (c) & (g) winter (DJF), (d) & (h) spring (MAM). (a) - (d) show the SAT anomalies, with (e) - (h) displaying SST anomalies. Locations of data sites from Tables 4.1 and 4.2 are also shown.

4.3.2 Transient Runs

Figure 4.3 shows the Arctic September sea ice extents (area where sea ice concentration is greater than 15%) for the four transient simulations for the historical period, alongside the HadISST sea ice extent observations (Rayner *et al.*, 2003). Generally, GCMs overestimate the simulation of sea ice extent (Stroeve *et al.*, 2007) in comparison to observations. However, Figure 4.3 indicates that HadCM3 is an exception, and for the majority of the observational period produces a lower September Arctic sea ice extent than observations. The HadCM3 standard simulated sea ice extent does not exceed the observations until into the 21st century, where large declines in September sea ice extent are observed, and not reproduced by HadCM3.

All three simulations with reduced minimum albedo produce lower extents than the control, and at all points are lower than the observations. Each shows a very rapid initial decline before settling in to a slower downward trend after less

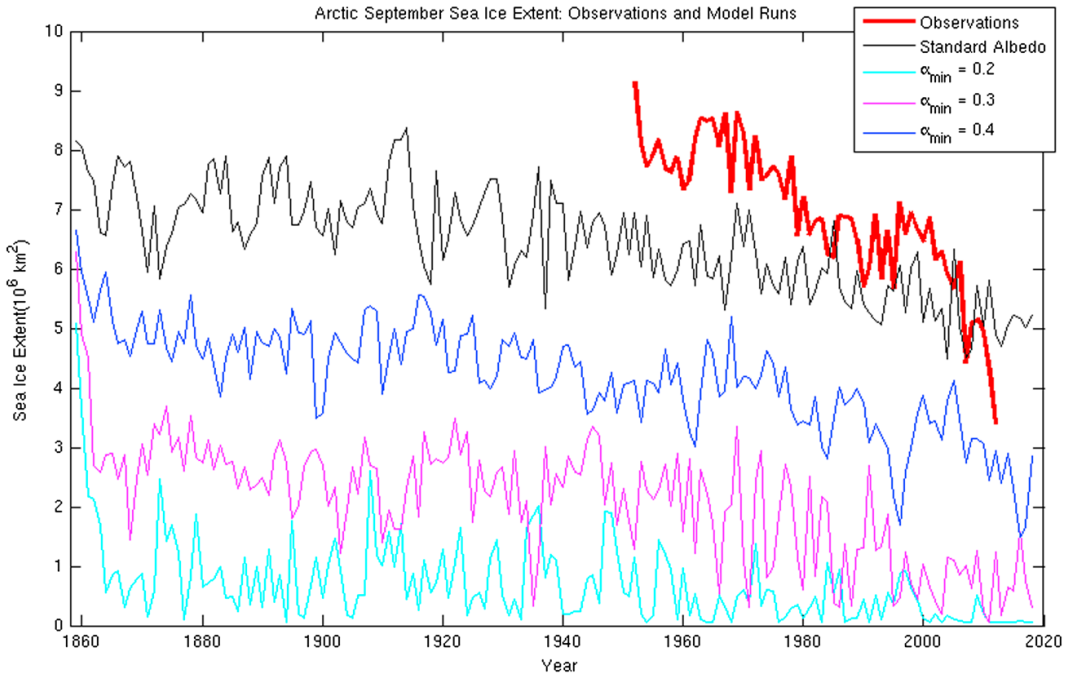

Figure 4.3: Arctic September sea ice extent (10^6 km^2) from observations (thick red line) and 4 HadCM3 transient simulations with varying minimum sea ice albedo.

than ten model years. The simulation with $\alpha_{min} = 0.2$ is intermittently sea ice free from approximately 20 years in to the simulation.

4.4 Discussion

4.4.1 Pliocene Albedo Runs

Tables 4.1 and 4.2 highlight that although the reduction in the minimum albedo limit has helped produced greater high latitude warming, it is having a limited effect on reducing the data-model mismatches. Substantial changes are only seen at six data sites, three marine and three terrestrial. Data for these sites are presented in Tables 4.1 and 4.2, with the data for all sites north of 60°N presented in Tables A.1 and A.2 in Appendix A.

Table 4.2: Pliocene SST anomalies (model simulated temperature minus proxy reconstructed temperature) at three palaeodata sites. Anomalies are displayed for the control and $\alpha_{min} = 0.2$ simulations.

Site	Latitude/Longitude	Control Anomaly	$\alpha_{min} = 0.2$ anomaly
Colvillian	70.29°/-150.42°	-2.26°C	-1.61°C
ODP 909	78.58°/-3.07°	-9.82°C	-8.51°C
ODP 911	80.47°/8.23°	-11.14°C	-10.21°C

The changes are mostly very small in comparison to the difference between the model and data temperature. For the SATs, the changes represent reductions in the model-data mismatch of just 5 to 8%. All increases are within the uncertainty ranges, when provided, for reconstructed SATs (Salzmann *et al.*, 2013). The largest increases in SAT over the Arctic have occurred over the ocean. In the terrestrial regions, where the Pliocene proxy data exists, temperature increases have been much lower.

Lawrence *et al.* (2008) demonstrate, using the CCSM3 model, that SAT increases as a result of sea ice loss can penetrate up to 1500km inland, covering a much larger area than shown in Figures 4.1 and 4.2. This suggests that CCSM3 has stronger inland atmospheric heat transport than HadCM3, and therefore there is an element of model dependency on the extent to which the SAT anomalies are reduced. A similar set of simulations performed with a model such as CCSM3 with stronger inland heat penetration may prove more effective at reducing the data-model discrepancies than HadCM3 has shown in this study.

The PRISM time slab covers a period of up to 300,000 years, during which the orbital configurations varied substantially. It is not clear whether the proxy data is representative of the orbital configuration used in the experiment (identical to modern), or whether they may be indicating temperatures from times with the warmest orbital configurations of the time slab.

Salzmann *et al.* (2013) ran a simulation under PlioMIP boundary conditions with orbital configurations adjusted to ensure maximum Pliocene top of the atmosphere incoming insolation 65°N in July, based on the astronomical solution of Laskar *et al.* (2004). Figure A.7 shows the SAT differences between this simula-

tion (Pliocene NH Max), and the simulation with $\alpha_{min} = 0.2$. The Pliocene NH Max simulation unsurprisingly produces higher SATs at mid-latitudes in spring and summer, as the orbit was picked to produce the maximum summer insolation at 65°N, and there is little warming produced at these latitudes by reducing α_{min}. However, the simulation with $\alpha_{min} = 0.2$ produces much higher SAT increases in autumn and winter over the region north of 60°N.

Figure A.8 demonstrates that, with the exception of part of the Bering Sea in winter and spring, the Pliocene NH Max simulation does not melt more sea ice than the $\alpha_{min} = 0.2$ simulation. The difference is particularly striking in the autumn months, where the Pliocene NH Max simulation does not produce the large sea ice reduction seen in the $\alpha_{min} = 0.2$ simulation. The effects of the combination of these two factors will be tested in a future study.

Whilst the overall SST response was weaker than the SAT response, the changes highlighted in Tables 4.1 and 4.2 show a slightly greater increase on average for the SST data sites. These changes resulted in reductions in the model-data mismatch of 8 to 29%, much higher than for the SATs, although this is partly due to the initial SAT differences being much larger. Similarly to the SATs, all SST changes are less than the errors associated to the techniques used to reconstruct the Pliocene temperatures (Dowsett *et al.*, 2009).

The counterintuitive seasonal SAT warming pattern, seen in Figure 4.2, has been previously observed in modelling and observational studies (Kumar *et al.*, 2010; Screen & Simmonds, 2010a,b), which look at the effects of declining Arctic sea ice cover. It is suggested that the pattern is caused when the increased heat absorbed by the ocean in summer due to sea ice loss is released over the autumn and winter as the sea ice recovers. The simulation with $\alpha_{min} = 0.2$ sees a 55% decrease in sea ice fraction in JJA, and an 89% decrease in SON, suggesting that the seasonal warming pattern of this simulation is also due to a large decrease in sea ice cover. Further discussion of this pattern is found in Appendix A.

4.4.2 Transient Runs

Whilst all simulations underestimated late 20th century sea ice extent, results for the 21st century show the observations declining faster than the HadCM3 stan-

dard simulation (Figure 4.3). The HadCM3 sea ice extent continues the same downward trend in the 21st century that it displays for the 20th, in comparison to the accelerated decline seen in the observations, implying that the two will continue to diverge. As the September sea ice extent declines further, an increasing proportion of the sea ice cover will be first-year ice, which has a lower albedo than multi-year ice (Perovich & Polashenski, 2012; Polashenski *et al.*, 2012). This may imply that a different sea ice albedo set up (with a lower minimum value) would be more appropriate for future simulations than one better suited to a climate with a greater proportion of multi-year ice.

Figure 4.3 demonstrates that there are problems using any fixed minimum sea ice albedo. Whilst the standard HadCM3 set up appears unsuitable for simulating 21st century sea ice, the simulations with reduced albedo produce sea ice extents substantially below observations. A more sophisticated parameterisation, allowing the minimum sea ice albedo to vary depending on the age of the ice, could enable the model to match the observations more closely. However, this would require the inclusion of a tracer for sea ice age into the model (e.g., Hunke & Bitz (2009)), a level of sophistication beyond the capabilities of HadCM3. More modern models, such as CCSM4, implement shortwave radiation parameterisations to simulate the surface albedo, rather than basing it on bulk sea ice properties such as surface temperatures (Holland *et al.*, 2011). The greater capabilities of these models highlights a disadvantage to using an older model such as HadCM3, although as Koenigk *et al.* (2013) demonstrates, CCSM4 still does not achieve the low albedos observed in Perovich & Polashenski (2012).

The divergence of the control HadCM3 simulated September sea ice extent and the observations in the 21st century shown in Figure 4.3 is a clear indication that the standard sea ice albedo settings are not suitable for simulating warmer climates with a higher proportion of first-year ice. As proxy data indicates that high latitude mid-Pliocene SSTs were warmer than present day (Dowsett *et al.*, 2010), then it is not unreasonable to infer that mid-Pliocene Arctic sea ice cover would have been diminished, with less sea ice surviving the summer. The sea ice would therefore have been dominated by first-year ice, and consequently a different albedo parameterisation, enabling a lower minimum, would be more suitable for mid-Pliocene simulations.

4.5 Conclusions

This paper has demonstrated the capabilities and limitations of the influence of the sea ice albedo feedback. The use of a lower sea ice albedo limit, one more suitable for a warmer than present day climate with almost certainly less multi-year ice, has led to mean annual SAT increases of up to 6°C over the Arctic ocean. However, the effect on mid-Pliocene model-data mismatches is much smaller. Any changes in these mismatches are small in comparison to the overall model-data temperature differences, and are within the uncertainty ranges of the temperature reconstruction for each site, when provided (Salzmann *et al.*, 2013). The maximum changes seen in data-model mismatches for SSTs are slightly higher than for SATs, despite the overall response being much weaker, however these changes are also less than the uncertainty ranges for the reconstructed temperatures (Dowsett *et al.*, 2009).

These results suggest that temperature increases large enough to eliminate the model-data mismatch, particularly for SATs, are unlikely to be solely driven by ocean based changes to the model, except in extreme scenarios such as the complete removal of Pliocene Arctic sea ice (e.g. Ballantyne *et al.* (2013)). The changes made to the minimum sea ice albedo can be considered a useful tool in helping to close this gap, but they can only be a small part of a larger effort.

The transient simulations highlight an area in which the albedo changes have had a particularly dramatic effect. There is a large sea ice reduction in autumn in the Pliocene simulations, and this is replicated in the transient runs, resulting in a large difference in the September sea ice extent minimum in comparison to the control. The failure of the HadCM3 standard parameterisation to reproduce the recent sea ice decline suggests it is not suited to simulating climates with higher proportions of first-year sea ice. Currently there is insufficient data to say with any certainty whether the alternative sea ice albedo minima will simulate 21st century Arctic sea ice better. However, these alternative albedo limits would appear to have a greater chance at replicating the rapid downward trend seen in the observations than the standard settings.

References

Ballantyne, A., Axford, Y., Miller, G., Otto-Bliesner, B., Rosenbloom, N. & White, J. (2013). The amplification of Arctic terrestrial surface temperatures by reduced sea-ice extent during the Pliocene. *Palaeogeography Palaeoclimatology Palaeoecology*, **386**, 59–67. 25, 84, 140, 162, 163, 166, 183

Bryan, K. (1969). Climate and the ocean circulation III: The ocean model. *Mon Weather Rev*, **97**, 806–827. 46, 49, 61, 62, 75, 142, 188

Cattle, H. & Crossley, J. (1995). Modeling Arctic climate change. *Philosophical Transactions of the Royal Society A-Mathematical, Physical and Engineering Sciences*, **352**, 201–213. 62, 63, 71, 75, 94, 117, 142, 188, 189

Comiso, J.C., Parkinson, C.L., Gersten, R. & Stock, L. (2008). Accelerated decline in the Arctic sea ice cover. *Geophysical Research Letters*, **35**, L01703. 74

Cronin, T.M., Whatley, R., Wood, A., Tsukagoshi, A., Ikeya, N., Brouwers, E.M. & Briggs, W.M. (1993). Microfaunal evidence for elevated Pliocene temperatures in the Arctic ocean. *Paleoceanography*, **8**, 161–173. 24, 74, 92, 124, 140, 181

Curry, J.A., Schramm, J.L. & Ebert, E.E. (1995). Sea ice-albedo climate feedback mechanism. *Journal of Climate*, **8**, 240–247. 34, 37, 38, 45, 73, 118, 140

Dowsett, H., Robinson, M. & Foley, K. (2009). Pliocene three-dimensional global ocean temperature reconstruction. *Climate of the Past*, **5**, 769–783. 16, 17, 82, 84, 166

Dowsett, H., Haywood, A., Valdes, P., Robinson, M., Lunt, D., Hill, D., Stoll, D. & Foley, K. (2011). Sea surface temperatures of the mid-Piacenzian Warm Period: A comparison of PRISM3 and HadCM3. *Palaeogeography Palaeoclimatology Palaeoecology*, **309**, 83–91. 1, 27, 29, 73, 140

Dowsett, H., Foley, K., Stoll, D., Chandler, M., Sohl, L., Bentsen, M., Otto-Bliesner, B., Bragg, F., Chan, W.L., Contoux, C., Dolan, A., Haywood, A., Jonas, J., Jost, A., Kamae, Y., Lohmann, G., Lunt, D., Nisancioglu, K., Abe-Ouchi, A., Ramstein, G., Riesselman, C., Robinson, M., Salzmann, U., Stepanek, C., Strother, S., Ueda, H., Yan, Q. & Zhang, Z. (2013). Sea Surface Temperature of the mid-Piacenzian Ocean: A Data-Model Comparison. *Sci. Rep.*, **3**, 149–163. 77, 144

Dowsett, H.J., Robinson, M.M., Haywood, A.M., Salzmann, U., Hill, D.J., Sohl, L., Chandler, M.A., Williams, M., Foley, K. & Stoll, D. (2010). The PRISM3D paleoenvironmental reconstruction. *Stratigraphy*, **7**, 123–139. 1, 3, 4, 5, 9, 16, 17, 18, 21, 66, 73, 76, 77, 83, 92, 95, 140, 143, 144, 190, 191

Dowsett, H.J., Robinson, M.M., Haywood, A.M., Hill, D.J., Dolan, A.M., Stoll, D.K., Chan, W.L., Abe-Ouchi, A., Chandler, M.A., Rosenbloom, N.A., Otto-Bliesner, B.L., Bragg, F.J., Lunt, D.J., Foley, K.M. & Riesselman, C.R. (2012). Assessing confidence in Pliocene sea surface temperatures to evaluate predictive models. *Nature Climate Change*, **2**, 365–371. 9, 77

Eisenman, I., Untersteiner, N. & Wettlaufer, J.S. (2008). Reply to comment by E. T. DeWeaver et al. on "On the reliability of simulated Arctic sea ice in global climate models". *Geophysical Research Letters*, **35**, L04502. 73, 119

Gordon, C., Cooper, C., Senior, C.A., Banks, H., Gregory, J.M., Johns, T.C., Mitchell, J.F.B. & Wood, R.A. (2000). The simulation of SST, sea ice extents and ocean heat transports in a version of the Hadley Centre

coupled model without flux adjustments. *Climate Dynamics*, **16**, 147–168. 2, 59, 60, 61, 62, 63, 64, 65, 75, 122, 141, 142, 188, 189

Haywood, A. & Valdes, P. (2004). Modelling Pliocene warmth: contribution of atmosphere, oceans and cryosphere. *Earth and Planetary Science Letters*, **218**, 363–377. 25, 26, 73, 140

Haywood, A.M., Dowsett, H.J., Robinson, M.M., Stoll, D.K., Dolan, A.M., Lunt, D.J., Otto-Bliesner, B.L. & Chandler, M.A. (2011). Pliocene Model Intercomparison Project (PlioMIP): experimental design and boundary conditions (Experiment 2). *Geosci. Model Dev.*, **4**, 571–577. 29, 30, 70, 76, 93, 95, 141, 143, 189

Haywood, A.M., Hill, D.J., Dolan, A.M., Otto-Bliesner, B.L., Bragg, F.J., Chan, W.L., Chandler, M.A., Contoux, C., Dowsett, H.J., Jost, A., Kamae, Y., Lohmann, G., Lunt, D.J., Abe-Ouchi, A., Pickering, S.J., Ramstein, G., Rosenbloom, N.A., Salzmann, U., Sohl, L., Stepanek, C., Ueda, H., Yan, Q. & Zhang, S.Z. (2013). Large-scale features of Pliocene climate: results from the Pliocene Model Intercomparison Project. *Clim. Past*, **9**, 191–209. 1, 3, 29, 30, 73, 92, 140, 141

Hibler, W.D. (1979). A dynamic-thermodynamic sea ice model. *Journal of Physical Oceanography*, **9**, 815–846. 47, 48, 49, 62, 75, 117, 142, 188

Holland, M.M., Bailey, D.A., Briegleb, B.P., Light, B. & Hunke, E.C. (2011). Improved sea ice shortwave radiation physics in CCSM4: The impact of melt ponds and aerosols on Arctic sea ice. *Journal of Climate*, **25**, 1413–1430. 71, 83, 94, 118

Hunke, E.C. (2010). Thickness sensitivities in the CICE sea ice model. *Ocean Modelling*, **34**, 137–149. 40, 71, 73, 94, 116, 119

Hunke, E.C. & Bitz, C.M. (2009). Age characteristics in a multidecadal arctic sea ice simulation. *Journal of Geophysical Research: Oceans*, **114**, C08013. 83

IPCC (2007). Climate Change 2007: The Physical Science Basis. Contribution of Working Group I to the Fourth Assessment Report of The Intergovernmental Panel on Climate Change. *Cambridge University Press, Cambridge, UK & New York*, 906pp. 44, 73

Kellogg, W. (1975). Climatic feedback mechanisms involving the polar regions. *Climate of the Arctic*, 111–116. 34, 73, 140

Koenigk, T., Devasthale, A. & Karlsson, K.G. (2013). Summer sea ice albedo in the Arctic in CMIP5 models. *Atmospheric Chemistry and Physics Discussions*, **13**, 25219–25251. 83

Kumar, A., Perlwitz, J., Eischeid, J., Quan, X., Xu, T., Zhang, T., Hoerling, M., Jha, B. & Wang, W. (2010). Contribution of sea ice loss to Arctic amplification. *Geophysical Research Letters*, **37**. 34, 45, 82, 151

Laskar, J., Robutel, P., Joutel, F., Gastineau, M., Correia, A. & Levrard, B. (2004). A long-term numerical solution for the insolation quantities of the Earth. *Astronomy and Astrophysics*, **428**, 261–285. 67, 81, 143, 189

Lawrence, D., Slater, A., Tomas, R., Holland, M. & Deser, C. (2008). Accelerated Arctic land warming and permafrost degradation during rapid sea ice loss. *Geophysical Research Letters*, **35**. 34, 81

Maykut, G. (1978). Energy exchange over young sea ice in the central Arctic. *Journal Of Geophysical Research - Oceans*, **83**, 3646–3658. 34, 40, 41, 73, 140

Moran, K., Backman, J., Brinkhuis, H., Clemens, S.C., Cronin, T., Dickens, G.R., Eynaud, F., Gattacceca, J., Jakobsson, M., Jordan, R.W., Kaminski, M., King, J., Koc, N., Krylov, A., Martinez, N., Matthiessen, J., McInroy, D., Moore, T.C., Onodera, J., O'Regan, M., Pälike, H., Rea, B., Rio, D., Sakamoto, T., Smith, D.C., Stein, R., St John, K., Suto, I., Suzuki, N., Takahashi, K., Watanabe, M., Yamamoto, M., Farrel, J., Frank, M., Kubik, P., Jokat, W. & Kristoffersen, Y. (2006). The Cenozoic palaeoenvironment of the Arctic Ocean. *Nature*, **441**, 601–605. 74, 92, 124, 140, 181

Pagani, M., Liu, Z., LaRiviere, J. & Ravelo, A.C. (2010). High Earth-system climate sensitivity determined from Pliocene carbon dioxide concentrations. *Nature Geoscience*, **3**, 27–30. 6, 8, 73, 92, 140, 189

Perovich, D. & Polashenski, C. (2012). Albedo evolution of seasonal Arctic sea ice. *Geophysical Research Letters*, **39**. 39, 40, 41, 74, 83, 144, 176, 177

Perovich, D.K., Nghiem, S.V., Markus, T. & Schweiger, A. (2007). Seasonal evolution and interannual variability of the local solar energy absorbed by the arctic sea iceocean system. *Journal of Geophysical Research: Oceans*, **112**, C03005. 74

Polashenski, C., Perovich, D. & Courville, Z. (2012). The mechanisms of sea ice melt pond formation and evolution. *Journal of Geophysical Research: Oceans*, **117**, C01001. 74, 83, 177

Polyak, L., Alley, R.B., Andrews, J.T., Brigham-Grette, J., Cronin, T.M., Darby, D.A., Dyke, A.S., Fitzpatrick, J.J., Funder, S., Holland, M.M., Jennings, A.E., Miller, G.H., O'Regan, M., Savelle, J., Serreze, M., St John, K., White, J.W.C. & Wolff, E. (2010). History of sea ice in the Arctic. *Quaternary Science Reviews*, **29**, 1757–1778. 51, 55, 57, 58, 74, 92, 124, 140, 166, 181

Rayner, N.A., Parker, D.E., Horton, E.B., Folland, C.K., Alexander, L.V., Rowell, D.P., Kent, E.C. & Kaplan, A. (2003). Global analyses of sea surface temperature, sea ice, and night marine air temperature since the late nineteenth century. *Journal of Geophysical Research-Atmospheres*, **108**, 4407, d14. 42, 66, 76, 79

Salzmann, U., Haywood, A., Lunt, D., Valdes, P. & Hill, D. (2008). A new global biome reconstruction and data-model comparison for the Middle Pliocene. *Global Ecology and Biogeography*, **17**, 432–447. 17, 21, 22, 23, 28, 77, 144, 191

Salzmann, U., Dolan, A., Haywood, A., Chan, W.L., Voss, J., Hill, D., Abe-Ouchi, A., Otto-Bliesner, B., Bragg, F., Chandler, M.,

Contoux, C., Dowsett, H., Jost, A., Kamae, Y., Lohmann, G., Lunt, D., Pickering, S., Pound, M., Ramstein, G., Rosenbloom, N., Sohl, L., Stepanek, C., Ueda, H. & Zhang, Z. (2013). Challenges in quantifying Pliocene terrestrial warming revealed by data-model discord. *Nature Climate Change*, **3**, 969–974. 1, 27, 28, 73, 77, 81, 84, 140, 144, 166

Screen, J. & Simmonds, I. (2010a). Increasing fall-winter energy loss from the Arctic Ocean and its role in Arctic temperature amplification. *Geophysical Research Letters*, **37**. 45, 82, 151

Screen, J. & Simmonds, I. (2010b). The central role of diminishing sea ice in recent Arctic temperature amplification. *Nature*, **464**, 1334–1337. 45, 82

Seki, O., Foster, G.L., Schmidt, D.N., Mackensen, A., Kawamura, K. & Pancost, R.D. (2010). Alkenone and boron-based Pliocene pCO_2 records. *Earth and Planetary Science Letters*, **292**, 201–211. 6, 7, 8, 73, 92, 140, 189

Semtner, A.J. (1976). A model for the thermodynamic growth of sea ice in numerical investigations of climate. *Journal of Physical Oceanography*, **6**, 379–389. 47, 48, 49, 61, 62, 75, 117, 142, 188

Stroeve, J., Holland, M.M., Meier, W., Scambos, T. & Serreze, M. (2007). Arctic sea ice decline: Faster than forecast. *Geophysical Research Letters*, **34**, L09501. 44, 74, 79, 93

Stroeve, J.C., Kattsov, V., Barrett, A., Serreze, M., Pavlova, T., Holland, M.M. & Meier, W.N. (2012). Trends in Arctic sea ice extent from CMIP5, CMIP3 and observations. *Geophysical Research Letters*, **39**, L16502. 1, 44, 74, 92, 93

Chapter 5

Assessment of simulations of Arctic sea ice in the PlioMIP models

This chapter is under review in Climate of the Past as:

Howell, F. W., Haywood, A. M., Otto-Bliesner, B. L., Bragg, F., Chan, W.-L., Chandler, M. A., Contoux, C., Kamae, Y., Abe-Ouchi, A., Rosenbloom, N. A., Stepanek, C. and Zhang, Z.. "Arctic sea ice simulation in the PlioMIP ensemble" (2015).

Abstract

Eight general circulation models have simulated the mid-Pliocene Warm Period (mid-Pliocene, 3.264 to 3.025 Ma) as part of the Pliocene Modelling Intercomparison Project (PlioMIP). Here, we analyse and compare their simulation of Arctic sea ice for both the pre-industrial and the mid-Pliocene. Mid-Pliocene sea ice thickness and extent is reduced, and the model spread of extent is more than twice the pre-industrial spread in some summer months. As for the proxy-record, the simulated predominant sea ice state is ambiguous; half of the models in the ensemble simulate ice-free conditions in the mid-Pliocene summer, in contrast to

proxy data evidence that suggests the possibility of perennial sea ice. Correlations between mid-Pliocene Arctic temperatures and sea ice extents are almost twice as strong as the equivalent correlations for the pre-industrial simulations. The need for more comprehensive sea ice proxy data is highlighted, in order to better compare model performances.

5.1 Introduction

The mid-Pliocene warm period (mid-Pliocene), spanning 3.264 to 3.025 Myr ago (Dowsett *et al.*, 2010) was a period exhibiting episodes of global warmth, with estimates of an increase of 2 to 3°C in global mean temperatures in comparison to the pre-industrial period (Haywood *et al.*, 2013b). The mid-Pliocene is the most recent period of earth history that is thought to have atmospheric CO_2 concentrations resembling those seen in the 21st century, with concentrations estimated to be between 365 and 415 ppm (e.g. Pagani *et al.* (2010); Seki *et al.* (2010)). Therefore, this time period is a useful interval in which to study the dynamics and characteristics of sea ice in a warmer world.

September 2012 saw Arctic sea ice fall to a minimum extent of 3.4×10^6 km^2, a reduction of 4.2×10^6 km^2 since the beginning of satellite observations in 1979 (Parkinson & Comiso, 2013; Zhang *et al.*, 2013a). The Arctic is widely predicted to become seasonally ice free before the end of the 21st century (under RCP 4.5) (e.g. Massonnet *et al.* (2012); Stroeve *et al.* (2012b)), with some projections suggesting an ice free Arctic by 2030 (Wang & Overland, 2012), whilst other studies (e.g. Boé *et al.* (2009)) suggest a later date for the disappearance of summer Arctic sea ice.

There is debate concerning whether the Arctic sea ice in the mid-Pliocene was seasonal or perennial. Darby (2008) suggests that the presence of iron grains in marine sediments extracted from the Arctic Coring Expedition (ACEX) core, located on the Lomonosov Ridge (87.5°N, 138.3°W), shows that there was year round coverage of sea ice at this location, whilst there are indications from ostracode assemblages and ice rafted debris sediments as far north as Meighen Island (approx. 80°N) that Pliocene Arctic sea ice was seasonal (Cronin *et al.*, 1993; Moran *et al.*, 2006; Polyak *et al.*, 2010). The prospect of the Arctic becoming

ice-free in summer in the future increases the importance of the investigation of past climates which may have had seasonal Arctic sea ice. Of particular interest is an understanding of the processes and sensitivities of Arctic sea ice under such conditions and of the general impact of reduced summer Arctic sea ice on climate.

Whilst many studies have focused on the simulation of Arctic sea ice for present and future climate by a variety of modelling groups (e.g. Arzel *et al.* (2006), Parkinson *et al.* (2006), Stroeve *et al.* (2007), Johnson *et al.* (2007), Holland & Stroeve (2011), Stroeve *et al.* (2012b), Johnson *et al.* (2012), Blanchard-Wrigglesworth & Bitz (2014), Stroeve *et al.* (2014), Shu *et al.* (2015)), there has been little focus on the simulation of past sea ice conditions by an ensemble of models, particularly for climates with warmer than modern temperatures and reduced Arctic sea ice cover. Berger *et al.* (2013) looks at the response of sea ice to insolation changes in simulations of mid-Holocene climate by PMIP2 and PMIP3 models, which shows that all the models simulate a modest reduction in summer sea ice extent in the mid-Holocene compared to the pre-industrial control (mean difference is lower than the difference in the mean observational Arctic sea ice extents for 1980-1989 and 2000-2009), but in the winter approximately half simulate a more extensive mid-Holocene sea ice cover.

The Pliocene Modelling Intercomparison Project (PlioMIP) is a multi-model experiment which compares the output of different models' simulations of the mid-Pliocene, as well as pre-industrial simulations, each following a standard experimental design, set out in Haywood *et al.* (2011a,b) (further details in section 5.2.1). In this study we analyse the simulation of Arctic sea ice in each of the participating models in PlioMIP Experiment 2 (see Table 5.1), focusing on both the pre-industrial and mid-Pliocene outputs. We quantify the variability of sea ice extent and thickness in both simulations, and present an overview of some of the important mechanisms influencing the simulation of sea ice.

Table 5.1: Technical details of the PlioMIP model ensemble: atmosphere and ocean resolutions, details of the sea ice component, and references for each of the eight PlioMIP Experiment 2 simulations.

Model	Atmosphere resolution (° lat × ° long)	Ocean resolution (° lat × ° long)	Length of run/ averaging period (years)		Sea Ice components and references	Reference
			Pre-industrial	mid-Pliocene		
CCSM4	0.9 × 1.25	1 × 1	1300/100	550/100	EVP rheology, melt ponds Hunke & Dukowicz (1997); Hunke (2010); Holland *et al.* (2011)	Rosenbloom *et al.* (2013)
COSMOS	3.75 × 3.75	3 × 1.8	3000/30	1000/30	VP rheology, leads Marsland *et al.* (2003)	Stepanek & Lohmann (2012)
GISS-E2-R	2 × 2.5	1 × 1.25	950/30	950/30	VP rheology, leads Zhang & Rothrock (2000); Liu *et al.* (2003)	Chandler *et al.* (2013)
HadCM3	2.5 × 3.75	1.25 × 1.25	200/50	500/50	Free drift, leads Cattle & Crossley (1995)	Bragg *et al.* (2012)
IPSLCM5A	3.75 × 1.9	0.5 − 2 × 2	2800/100	730/30	VP rheology, leads Fichefet and Morales Maqueda (1999)	Contoux *et al.* (2012)
MIROC4m	2.8 × 2.8	0.5 − 1.4 × 1.4	3800/100	1400/100	EVP rheology, leads K-1 Model Developers (2004)	Chan *et al.* (2011)
MRI-CGCM	2.8 × 2.8	0.5 − 2 × 2.5	1000/50	500/50	Free drift, leads Mellor & Kantha (1989)	Kamae & Ueda (2012)
NorESM-L	3.75 × 3.75	3 × 3	1500/200	1500/200	Same as CCSM4	Zhang *et al.* (2012)

5.2 Methods

5.2.1 PlioMIP experimental design

Two experimental designs for the PlioMIP simulations are described, Experiment 1 in Haywood *et al.* (2011a) and Experiment 2 Haywood *et al.* (2011b). Experiment 1 used atmosphere only GCMs (AGCMs), whilst Experiment 2 used coupled atmosphere-ocean GCMs (AOGCMs). Both experimental designs describe the model set-up for pre-industrial and mid-Pliocene simulations. The PRISM3D reconstruction provides the boundary conditions for the mid-Pliocene simulations, which in Experiment 1 also includes the prescribed SSTs and sea ice extents. SST reconstruction utilises a multi-proxy approach, based on faunal analysis, alkenone unsaturation index palaeothermometry, and foraminiferal Mg/Ca ratios Dowsett *et al.* (2010). Maximum sea ice extent in the mid-Pliocene is set as equal to modern sea ice extent minimum, with sea-ice free conditions for the mid-Pliocene minimum extent (Haywood *et al.*, 2011a). These boundary conditions are based on inferences from the SST reconstruction, and evidence from diatoms and sedimentological data (Dowsett *et al.*, 2010). In both Experiment 1 and Experiment 2, atmospheric CO_2 is 405 ppm, and a modern orbital configuration is used.

In Table 5.1, details of the eight models which ran PlioMIP Experiment 2 simulations are summarised. With the exception of GISS-E2-R, each model was also used for Experiment 1 simulations. Four of the models (CCSM4, GISS-E2-R, HadCM3 and IPSLCM5A) are also represented in the CMIP5 ensemble, the results for which are contrasted with the PlioMIP results. Higher resolution versions of MIROC4m and NorESM-L, and an updated version of MRI-CGCM also ran CMIP5 simulations. COSMOS was not represented in CMIP5, or any related version of it.

5.2.2 Analysis of results

We focus on the key sea ice metrics of extent (defined as the area of ocean where sea ice concentration is at least 15%), thickness, and volume. We follow the example of Berger *et al.* (2013) and examine the mean sea ice thickness

north of 80°N. To understand differences in the models' simulation of sea ice, we quantify correlations between the sea ice metrics and sea surface and surface air temperatures. We also compare the pre-industrial and mid-Pliocene sea ice extents to establish how closely correlated they are. This enables us to determine to which degree the mid-Pliocene sea ice cover is influenced by the temperatures and control simulations.

In our analysis, we define winter as the months February to April (FMA), and summer as the months August to October (ASO). The rationale is that in at least half of the models these are the three months with the highest and lowest mean sea ice extents respectively. This is in contrast to the typical seasonal definitions of winter (December to February) and summer (June to August).

5.3 Results

5.3.1 Pre-industrial sea ice simulations

5.3.1.1 Sea ice extent

Plots of the mean summer and winter pre-industrial Arctic sea ice concentrations are shown in Figure 5.1. Across the eight-member ensemble, the multi-model mean annual sea ice extent is 16.17 $\times 10^6$ km^2 (Table 2), with a winter (FMA) multi-model mean of 20.90 $\times 10^6$ km^2, and a summer (ASO) multi-model mean of 10.98 $\times 10^6$ km^2. The individual models' annual means range from 12.27 $\times 10^6$ km^2 (IPSLCM5A) to 19.85 $\times 10^6$ km^2 (MIROC4m) (Table 5.2), and monthly multi-model means range from a minimum of 10.01 $\times 10^6$ km^2 (September) to a maximum of 21.24 $\times 10^6$ km^2 (March, Figure 5.2). The lowest individual monthly extent is 7.00 $\times 10^6$ km^2 (HadCM3, September), with the highest monthly extent produced by MRI-CGCM (March), measuring 27.01 $\times 10^6$ km^2 (Figure 5.2).

Figure 5.2 reveals the differences in the annual sea ice extent cycles across the ensemble. The sea ice extent amplitudes of NorESM-L and IPSLCM5A are 6.39 and 7.36 $\times 10^6$ km^2 respectively (Table 5.2). These are the only models in the ensemble with seasonal amplitudes below 10 $\times 10^6$ km^2. Other models in the ensemble show a much larger seasonal cycle, in particular GISS-E2-R, MIROC4m and MRI-CGCM, which have sea ice extent amplitudes of 14.03, 14.05, and 15.91

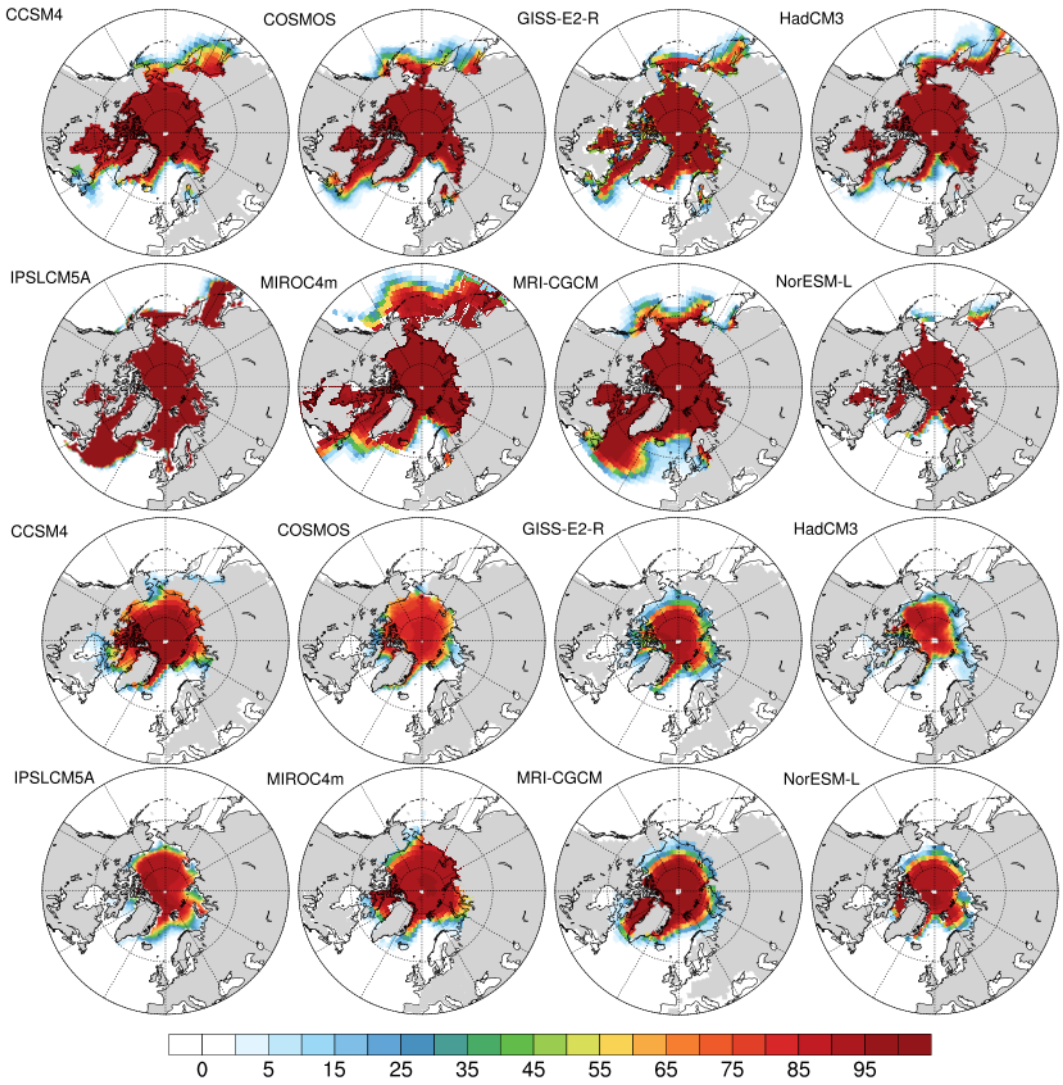

Figure 5.1: Mean sea ice concentrations (%) for winter (FMA, upper half) and summer (ASO, lower half) in the pre-industrial control simulations for each PlioMIP Experiment 2 model. Missing data at the poles is a plotting artefact (seen also in Figures 5.1, 5.3, 5.5, and 5.7).

$\times 10^6$ km^2 respectively (Table 2). The ensemble mean sea ice extent amplitude is

11.18×10^6 km^2.

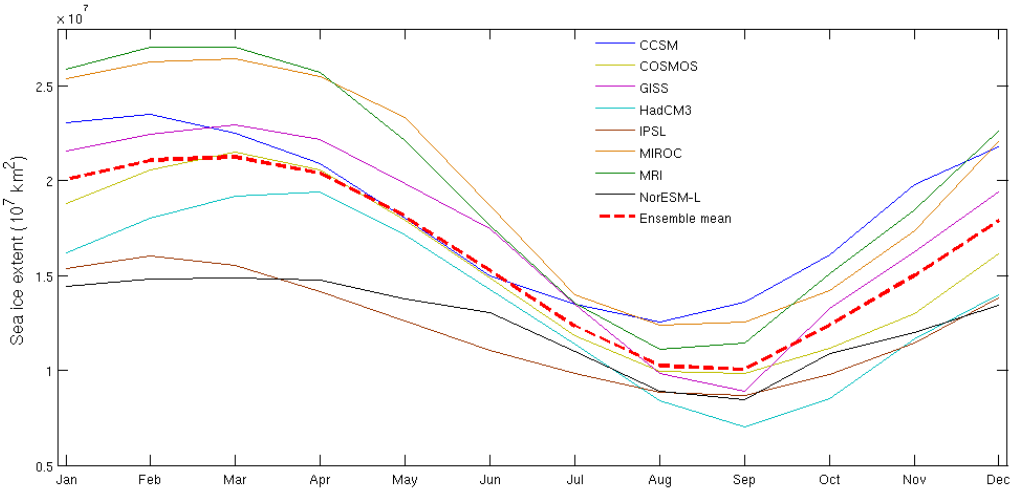

Figure 5.2: Annual cycle of total Arctic sea ice extent in the pre-industrial simulations for each participating model in PlioMIP Experiment 2, and the ensemble mean.

5.3.1.2 Sea ice thickness

North of 80°N, the multi-model mean annual thickness is 2.97 m, with a winter multi-model mean of 3.29 m and a summer multi-model mean of 2.52 m. Across the ensemble, the annual mean thickness varies from 2.27 m (HadCM3) to 3.81 m (CCSM4). The winter thicknesses range from 2.56 m (NorESM-L) to 4.01 m (CCSM4), with summer between 1.27 m (GISS-E2-R) and 3.60 m (CCSM4). Plots of mean winter and summer pre-industrial Arctic sea ice thicknesses are shown in Figure 5.3.

Root mean square errors (RMSE) and spatial pattern correlations for mean annual Arctic sea ice thickness are shown by Figure 5.4. MIROC4m has the highest spatial pattern correlation with the ensemble mean (0.93), despite the thickest ice in its simulation being located north of Eastern Siberia, opposite the region of thickest ice in many of the models (see Figure 5.3). It also has the lowest RMSE (0.55), marginally lower than COSMOS (0.56). MRI-CGCM displays the lowest spatial pattern correlation with the ensemble mean (0.76) and the highest

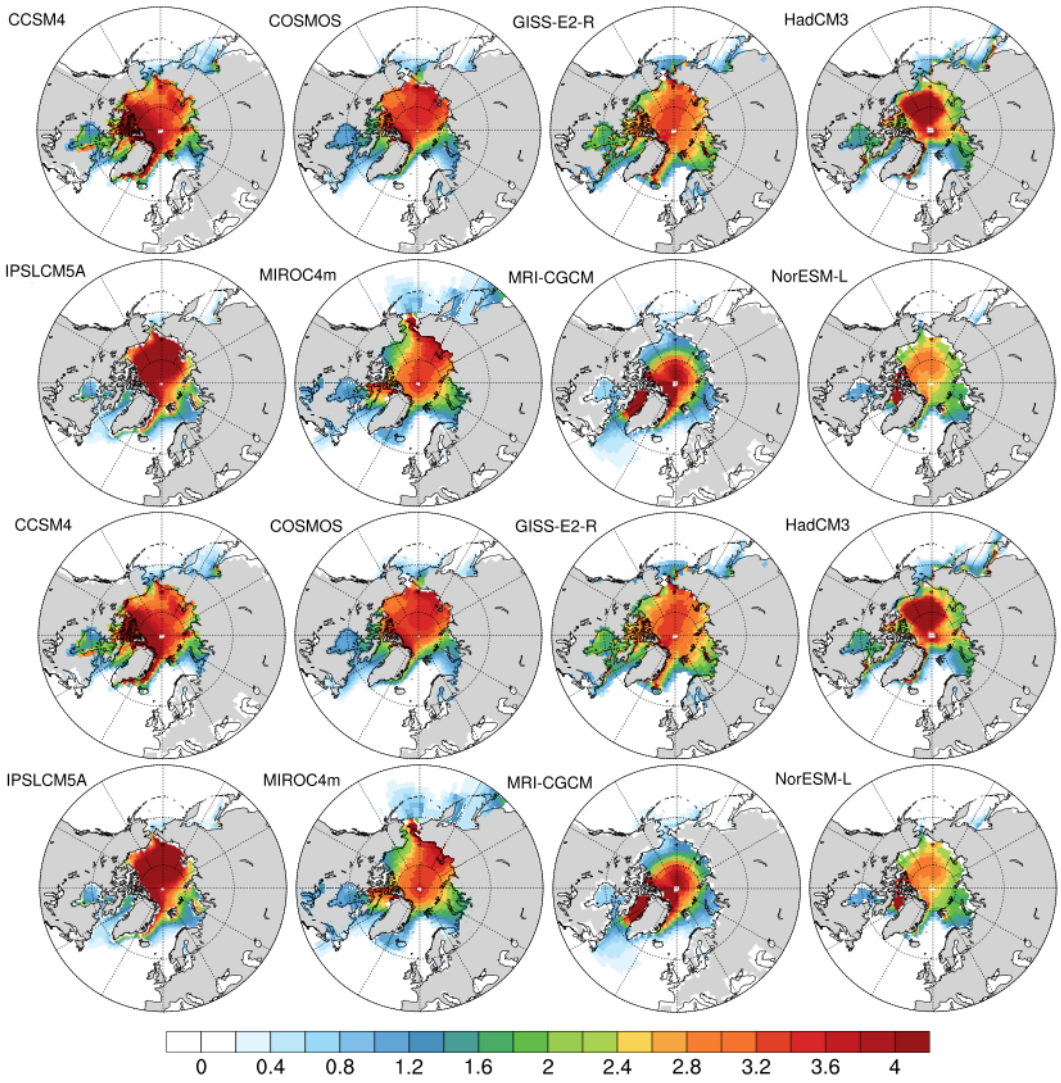

Figure 5.3: Mean sea ice thicknesses (m) for winter (FMA, upper half) and summer (ASO, lower half) in the pre-industrial control simulations for each PlioMIP Experiment 2 model.

RMSE (1.33). The lowest spatial pattern correlation between two models is 0.51 (HadCM3 and MRI-CGCM), which have a RMSE of 1.83, the highest of the ensemble. HadCM3 has a thickness spatial pattern which appears by eye very different to other PlioMIP models, with the thickest ice in a wedge bounded

approximately by the 70°N latitude line, and 120°W and 150°E (see Figure 5.3). However, it has a greater spatial pattern correlation with the ensemble mean than GISS-E2-R or MRI-CGCM, and the RMSE between the ensemble mean thickness and HadCM3 is lower than GISS-E2-R or MRI-CGCM when compared to the ensemble mean (Figure 5.4).

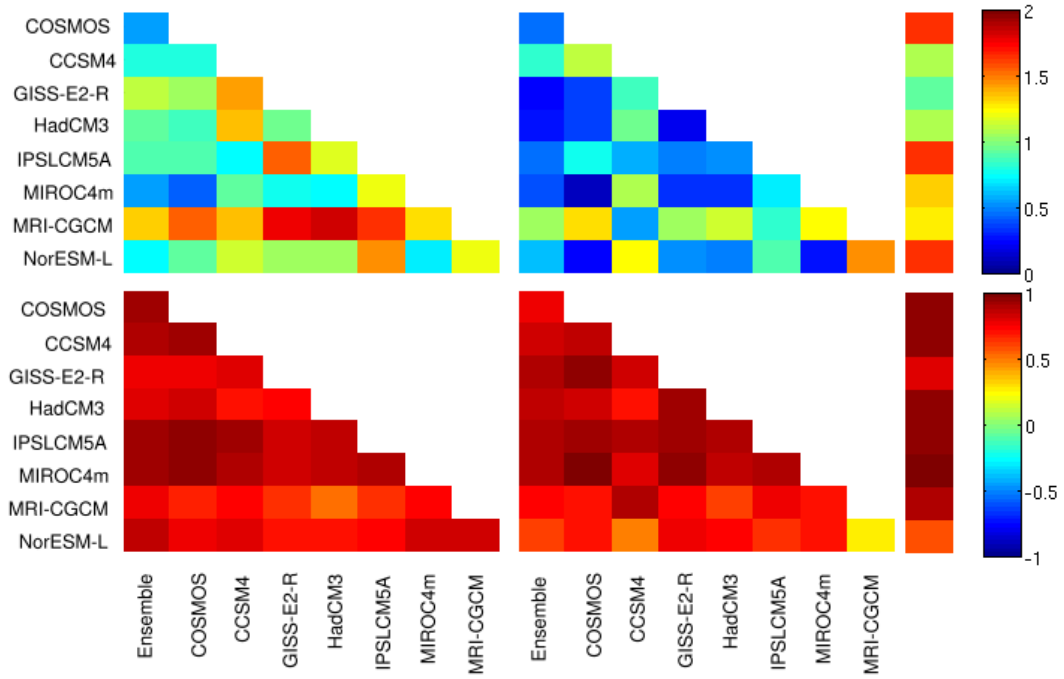

Figure 5.4: Root-mean-square error (RMSE) (top) and spatial pattern correlations (bottom) of Arctic ice thickness in the pre-industrial (left) and mid-Pliocene (right) simulations by the PlioMIP models and ensemble mean. The single columns to the right show the RMSE and spatial pattern correlations for between each model's pre-industrial and mid-Pliocene mean annual Arctic sea ice thickness.

5.3.2 Pliocene simulations

5.3.2.1 Sea ice extent

In agreement with enhanced greenhouse forcing each model in the ensemble simulates a smaller sea ice extent in the mid-Pliocene simulation in comparison to the pre-industrial (Figures 5.1 and 5.5). The multi-model mean annual extent for the mid-Pliocene simulations is 10.84 $\times 10^6$ km^2, a reduction of 5.33 $\times 10^6$ km^2 (33.0%) in comparison to the respective multi-model mean of the pre-industrial simulations. Annual means in the ensemble range from 7.60 $\times 10^6$ km^2 (NorESM-L), to 15.84 $\times 10^6$ km^2 (MRI-CGCM) (Table 5.1).

The lowest multi-model monthly mean extent is 3.15 $\times 10^6$ km^2 (September), and the highest is 16.59 $\times 10^6$ km^2 (March). In comparison to the pre-industrial simulation, the lowest multi-model monthly mean extent is reduced by 6.86 $\times 10^6$ km^2 (69%). The reduction for the highest monthly multi-model mean is 4.65 $\times 10^6$ km^2 (22%). The relative change in the lowest extent is therefore over three times greater than the relative change in the highest extent. Therefore, the mid-Pliocene is characterized by an enhanced seasonal cycle of sea ice extent, with severely reduced sea ice during boreal summer.

In four of the eight models (COSMOS, GISS-E2-R, MIROC4m and NorESM-L) the mid-Pliocene Arctic Ocean is ice-free at some time during the summer (August – September, Figure 5.6). In contrast to this, CCSM4 and MRI-CGCM simulate minimum sea ice extents of 8.90 $\times 10^6$ km^2 and 8.26 $\times 10^6$ km^2 respectively, which both exceed the pre-industrial minimum of HadCM3 (7.00 $\times 10^6$ km^2), with the CCSM4 minimum also exceeding the NorESM-L pre-industrial minimum (8.34 $\times 10^6$ km^2). Consequently, there is an overlap in sea ice extents between the mid-Pliocene and pre-industrial simulations.

MRI-CGCM, CCSM4 and MIROC4m simulate the highest maximum mid-Pliocene sea ice extents in the ensemble. Both CCSM4 and MRI-CGCM also provide the highest two minimum extents, but MIROC4m is one of the four models that simulates an ice-free Arctic summer. As a result, the sea ice extent amplitude in MIROC4m in the mid-Pliocene simulations is $\approx$ 64% greater than the pre-industrial simulation extent amplitude (Table 5.2). The ensemble mean extent amplitude of the mid-Pliocene simulations is by $\approx$ 20% greater than

Table 5.2: Mean annual sea ice extents and amplitude of sea ice extent (maximum annual sea ice extent minus minimum annual sea ice extent) for the pre-industrial (PI) and mid-Pliocene simulations from PlioMIP, and historical (1979-2005) simulations from CMIP5, for each participant model in PlioMIP Experiment 2 and for the ensemble mean. All values are in 10^6 km^2.

Model	PI mean annual extent	PI extent amplitude	mid-Pliocene mean annual extent	mid-Pliocene extent amplitude	CMIP5 mean annual extent	CMIP5 extent amplitude
CCSM4	18.35	10.94	14.99	10.26	12.33	8.56
COSMOS	15.52	11.66	7.72	12.75	–	–
GISS-E2-R	17.30	14.03	9.63	15.43	13.65	15.17
HadCM3	13.76	12.42	10.38	14.17	13.94	13.59
IPSLCM5A	12.27	7.36	9.06	7.05	12.72	10.07
MIROC4m	19.85	14.05	11.48	21.98	10.66	9.65
MRI-CGCM	19.80	15.91	15.84	13.69	15.01	15.27
NorESM-L	12.52	6.39	7.60	12.86	12.01	5.96
Ensemble mean	16.17	11.18	10.84	13.44	12.90	11.18

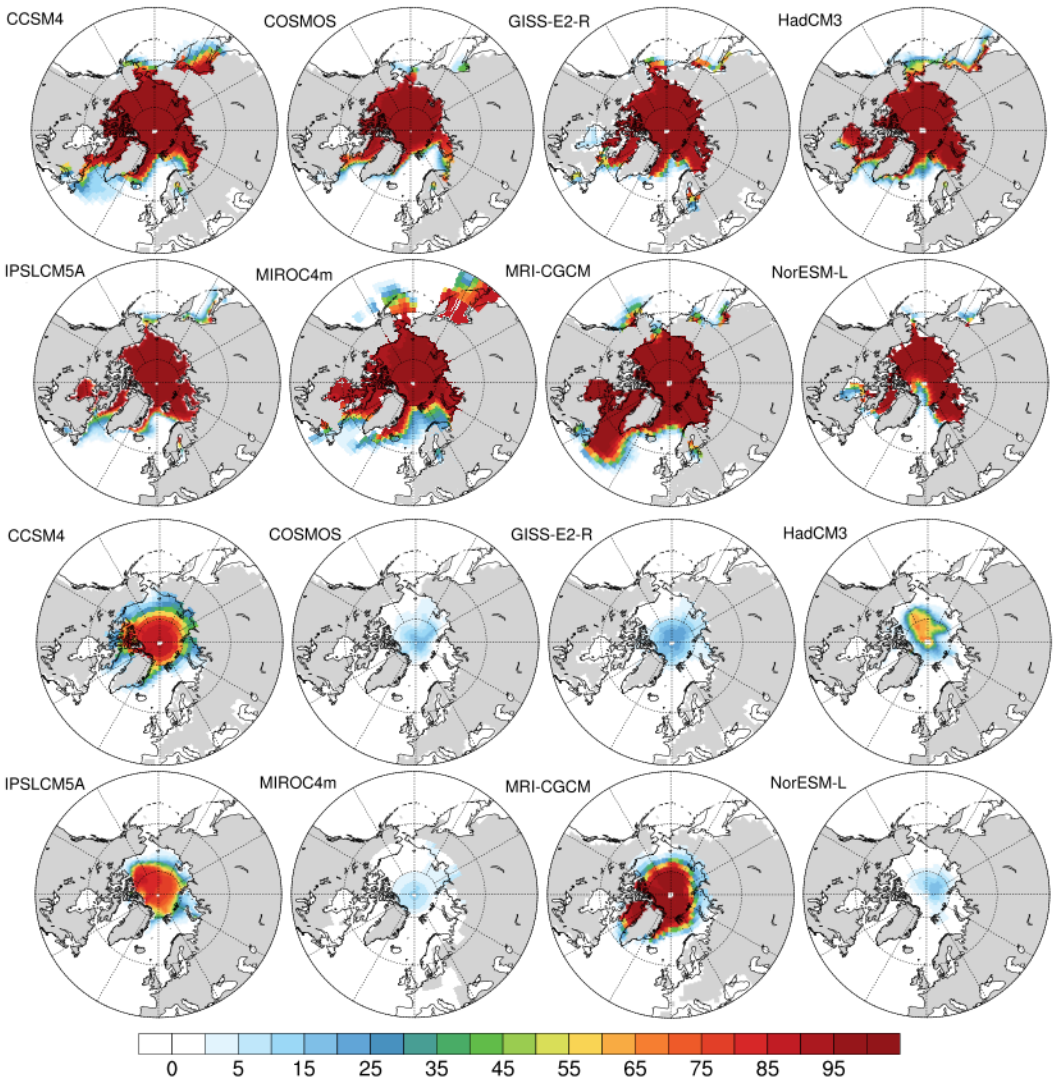

Figure 5.5: Mean sea ice concentrations (%) for winter (FMA, upper half) and summer (ASO, lower half) in the mid-Pliocene simulations for each PlioMIP Experiment 2 model.

the pre-industrial ensemble mean amplitude, further indication of the enhanced seasonal sea ice extent cycle in the mid-Pliocene simulations. Not all of the models, however, show this trend. Only five models (the four with ice-free summers and HadCM3) simulate a higher mid-Pliocene sea ice extent amplitude, the re-

maining three models simulate a (slightly) lower annual cycle in the mid-Pliocene simulations (Table 5.2).

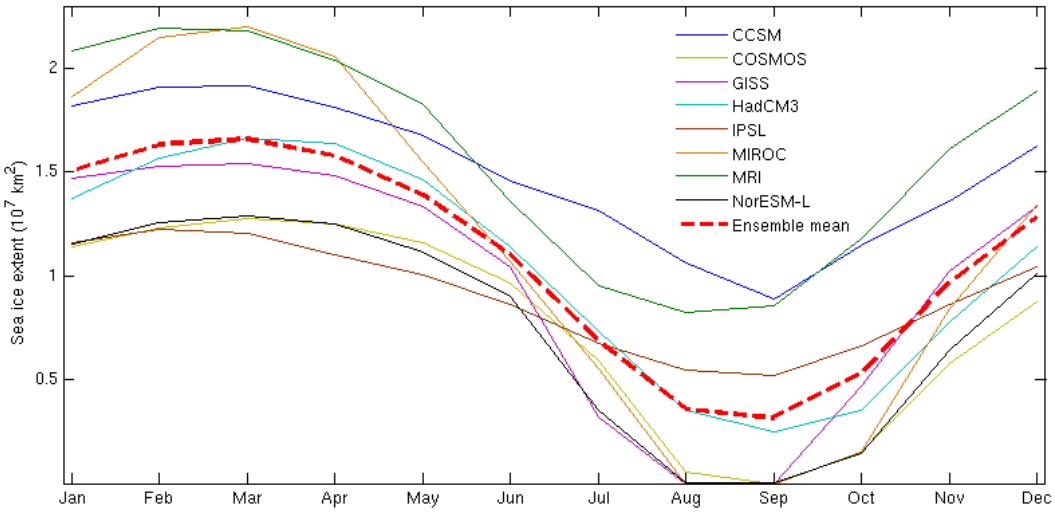

Figure 5.6: Annual cycle of sea ice extent in the mid-Pliocene simulations for each participating model in PlioMIP Experiment 2 and for the ensemble mean.

5.3.2.2 Sea ice thickness

Plots of the mean summer and winter mid-Pliocene Arctic sea ice thicknesses are shown in Figure 5.7. The multi-model mean annual sea ice thickness is 1.30 m, which, compared to the pre-industrial simulations, is a reduction of 1.7 m (56%). Across the ensemble, the annual mean thicknesses range from 0.44 m (NorESM-L) to 2.56 m (MRI-CGCM). The multi-model winter mean thickness is 1.77 m, 1.5 m (46%) less than the pre-industrial, whereas the summer multi-model mean thickness drops by 1.8 m (71%) to 0.74 m. Similarly to the sea ice extent, the summer sea ice thickness shows a greater relative decline with respect to pre-industrial than during the winter, although the contrast is not as stark for the thickness. The individual model winter sea ice thicknesses range from 0.79 m (NorESM-L) to 2.78 m (MRI-CGCM), with the summer sea ice thicknesses between 0.3 m (NorESM-L) and 2.24 m (MRI-CGCM).

Spatial pattern correlations and RMSEs between the pre-industrial and mid-Pliocene simulations are shown in Figure 5.4. All but five of the mid-Pliocene RMSEs are lower than the equivalent RMSE for the pre-industrial simulations. This trend is not seen in the spatial pattern correlations, where just over half (19 out of 36) of the mid-Pliocene correlations are higher than the corresponding pre-industrial correlation. These results show that the differences in thicknesses between the models are lower in the mid-Pliocene simulations, but the thickness patterns are overall no more or less similar. Lower overall RMSEs are likely to be at least part in due to the increase in the area of ice-free ocean, and lower mean thicknesses in the mid-Pliocene simulations compared to the pre-industrial.

GISS-E2-R has the highest correlation with the ensemble mean (0.90), with NorESM-L the lowest (0.60). NorESM-L has correlations of less than 0.5 with two models, CCSM4 (0.49) and MRI-CGCM (0.27). As with the pre-industrial results, MRI-CGCM has the highest RMSE compared to the ensemble of all the simulations (1.05), and the RMSE of 1.46 between MRI-CGCM and NorESM-L is the highest between any two models. The highest spatial pattern correlation between two models is 0.97, between COSMOS and MIROC4m, which also have the lowest RMSE, at 0.11.

Figure 5.4 also shows RMSEs and spatial pattern correlations between each model's pre-industrial and mid-Pliocene runs. All but two models had spatial pattern correlations exceeding 0.9 between the thicknesses of both simulations, with the exceptions being GISS-E2-R (0.81) and NorESM-L (0.56). The spatial pattern correlation between the ensemble means is 0.79.

5.3.3 Variability across the ensemble

The standard deviation (SD) of the monthly ensemble sea ice extents and thicknesses for both the pre-industrial and mid-Pliocene simulations is shown in Figure 5.8. In each month from December to June, the mid-Pliocene extent SD is lower than the pre-industrial extent SD. During these months, the maximum extent SD in both simulations occurs in February, and SD decreases each month from Feburary to June. In the pre-industrial simulation, extent SD is lowest in July,

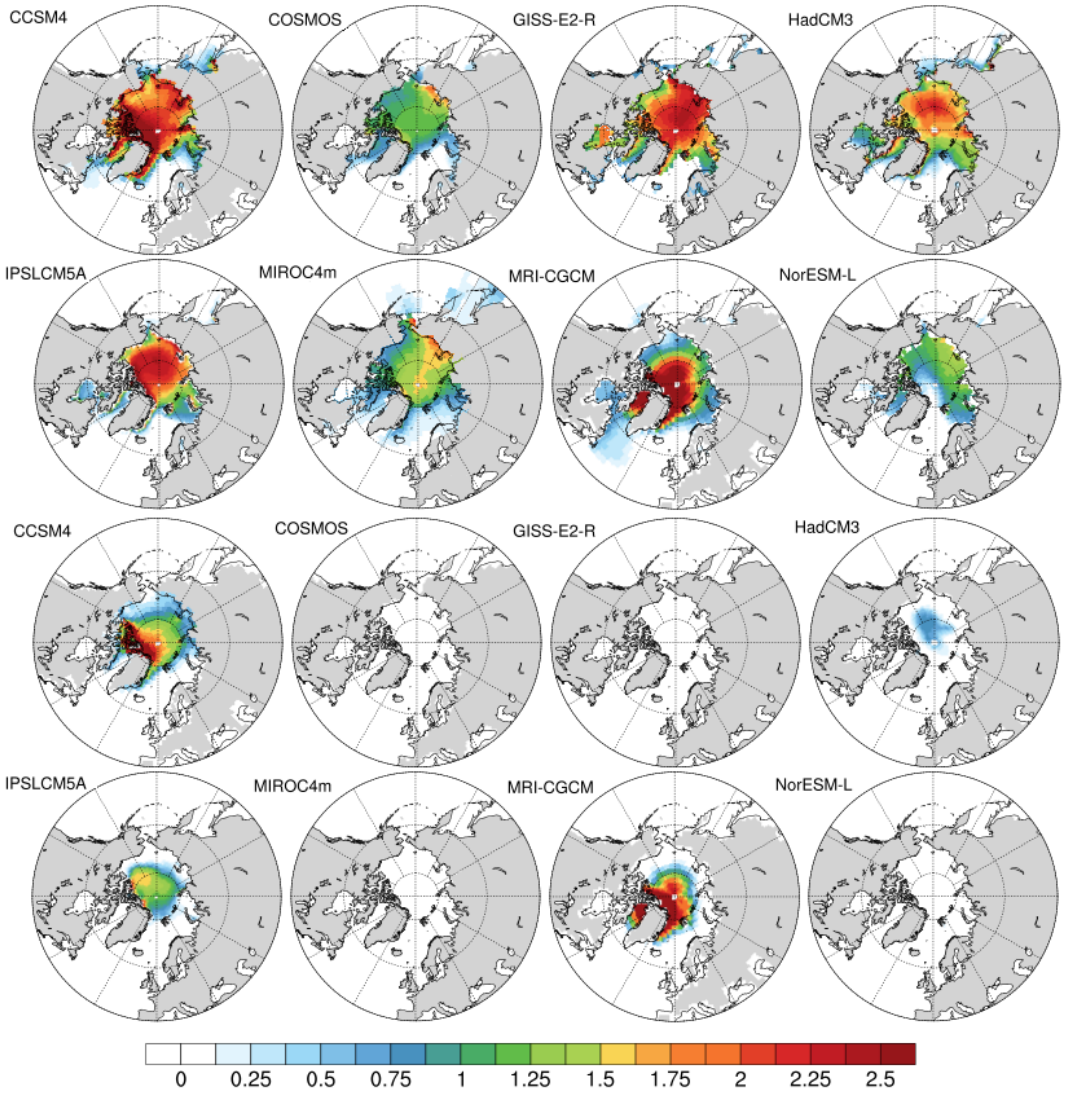

Figure 5.7: Mean sea ice thicknesses (m) for winter (FMA, upper half) and summer (ASO, lower half) in the mid-Pliocene simulations for each PlioMIP Experiment 2 model. Low sea ice concentrations in the summer plots for COSMOS, GISS-E2-R, MIROC4m and NorESM-L result in mean thicknesses very close to zero in each model grid cell.

following which it increases each month until to the February peak. In the mid-Pliocene simulations on the other hand, SD increases after June to July and then

August, and reaches maximum SD in October. SD in August and October are greater than in February/March in the mid-Pliocene extent. The annual cycle of of pre-industrial sea ice thickness SD has a minimum in May, and maximum in September. The mid-Pliocene sea ice thickness SD annual cycle follows a similar pattern, with the lowest SD in March, and maximum in July, both two months earlier than the equivalent pre-industrial extremes.

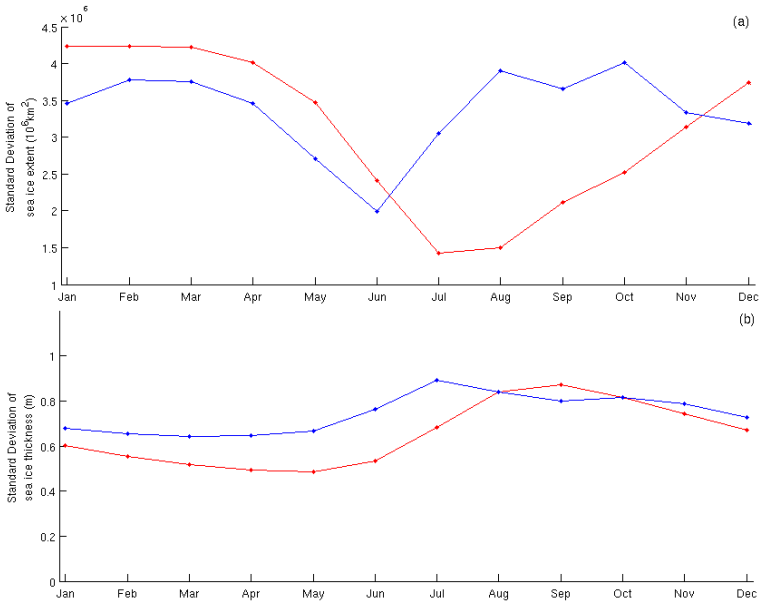

Figure 5.8: Annual cycle of the standard deviation (SD) of (a) sea ice extent and (b) sea ice thickness for the PlioMIP Experiment 2 ensemble. Red lines represent the pre-industrial annual cycle, blue lines represent the mid-Pliocene annual cycle.

5.3.4 Correlation of sea ice characteristics in the ensemble

The correlation coefficient between the mean summer sea ice extents of the pre-industrial and mid-Pliocene simulations is 0.47, compared to a correlation coefficient of 0.87 between the mean winter sea ice extents of both time slices (Figure 5.9 a,b). The models' annual mean sea ice extents for the two climate states show a correlation coefficient of 0.74 (not shown). Sea ice thicknesses simulated by the

pre-industrial and mid-Pliocene simulations are strongly correlated in both summer and winter, with correlation coefficients of 0.82 and 0.85 respectively (Figure 5.9 c,d). Whilst the winter pre-industrial sea ice thickness shows a weak relationship with the mid-Pliocene winter sea ice extent (Figure 5.9 f), with a correlation coefficient of just 0.30, the relationship between the summer values is stronger, with a correlation coefficient of 0.81 (Figure 5.9 e). It should be noted that with a sample size of just 8, only correlation coefficients greater than 0.70 are significant at the 95% level, and only those greater than 0.83 are significant at the 99% level.

The simulated mid-Pliocene sea ice extent and sea ice volume appear to show a stronger relationship with both surface air temperatures (SATs) and sea surface temperatures (SSTs) than the pre-industrial sea ice extent and sea ice volume (Figure 5.10). The correlation coefficient of the mid-Pliocene mean annual sea ice extent and the SAT, is -0.76, the correlation coefficient of the pre-industrial sea ice extent with SAT is -0.18. For SST the correlation with mid-Pliocene sea ice extents is -0.73, for pre-industrial sea ice extent the correlation coefficient is -0.26. For the summer, the mid-Pliocene sea ice extents have a correlation coefficient of -0.88 with both SAT and SST (not shown). In contrast, the pre-industrial sea ice extents have correlation coefficients of -0.27 (SAT) and -0.32 (SST) respectively (not shown). Mean annual pre-industrial SATs and SSTs have correlations with mean annual pre-industrial sea ice volume of -0.12 and -0.29 respectively. This contrasts to the respective mid-Pliocene correlation coefficients of -0.83 and -0.82. This confirms that the simulated mid-Pliocene sea ice extents and volumes have — independently from the season — a stronger negative correlation with temperatures than the simulated pre-industrial sea ice extents.

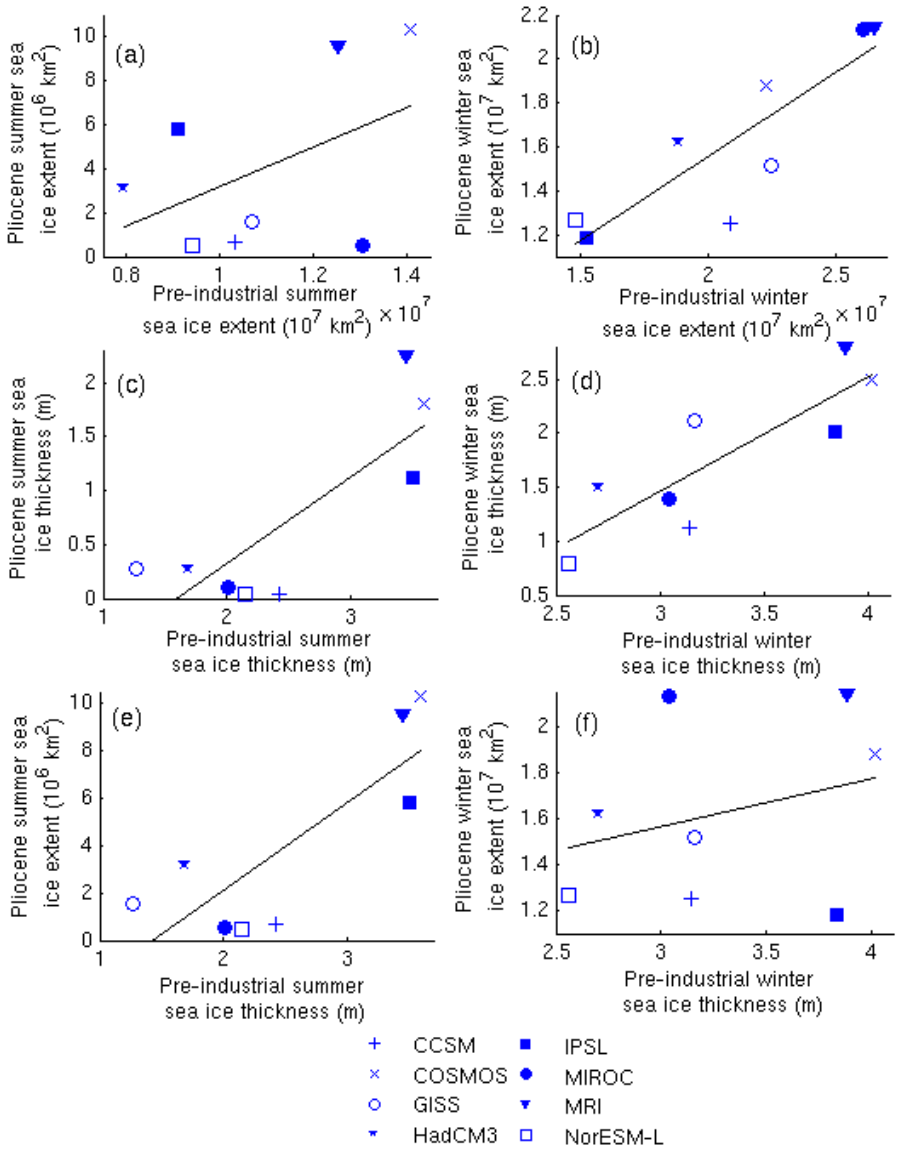

Figure 5.9: Relationship between various sea ice characteristics. Shown are pre-industrial values vs. mid-Pliocene values for (a) and (b) sea ice extent vs. sea ice extent, (c) and (d) sea ice thickness vs. sea ice thickness, (e) and (f) sea ice thickness vs. sea ice extent. (a), (c), and (e) illustrate summer conditions, (b), (d), and (f) illustrate winter conditions. Correlation coefficients for each plot are (a) 0.47, (b) 0.87, (c) 0.82, (d) 0.85, (e) 0.81, (f) 0.30.

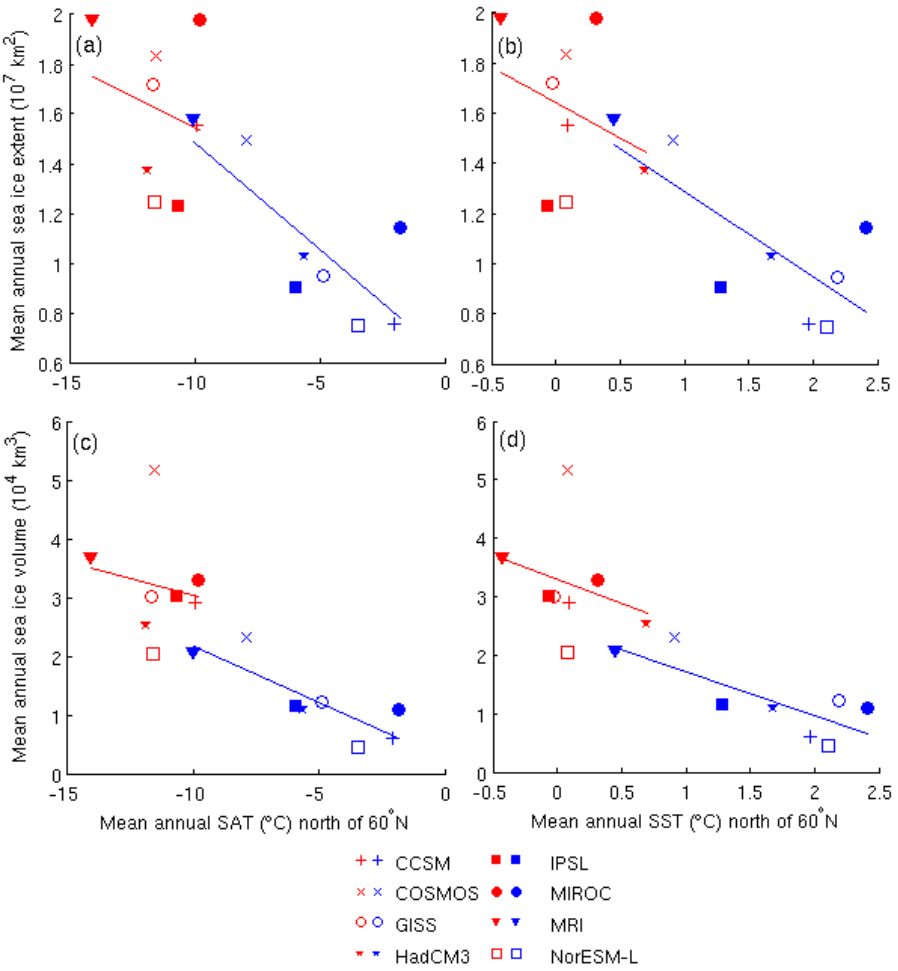

Figure 5.10: Mean annual surface temperatures north of 60°N vs. mean annual total Arctic sea ice extent (a,b), and mean annual surface temperatures north of 60°N vs. mean annual total Arctic sea ice volume (c,d) in both pre-industrial and mid-Pliocene simulations, for (a,c) SAT and (b,d) SST. Pre-industrial experiments are marked red, mid-Pliocene experiments are marked blue. Correlation coefficients for the pre-industrial simulations in each plot are (a) -0.18, (b) -0.26, (c) -0.12, (d) -0.29. Correlation coefficients for the mid-Pliocene simulations in each plot are (a) -0.76, (b) -0.73, (c) -0.83, (d) -0.82.

5.4 Discussion

5.4.1 Pre-industrial simulations

Before examining the simulations of Arctic sea ice for the mid-Pliocene, the simulations of pre-industrial sea ice cover by individual models are assessed. A comparison with observed sea ice characteristics is a suitable methodology. Ideally, we would have compared the output of the pre-industrial simulations to observations of sea ice from the same time period. However, the most spatially and temporally comprehensive observations of sea ice originate from satellites. Respective data sets date back only as far as 1979, which is more than 100 years after the time period that the pre-industrial simulations represent.

Whilst there are observations of sea ice characteristics available dating back to the early 20th century, that could have been used for the comparison, most, particularly the earliest, are ship-based observations of ice margins. These observations are only available for the spring and summer months (e.g. Thomsen (1947); Walsh & Chapman (2001)), and the sea ice extent in the remaining months must be estimated by extrapolation. Frequency and location of these observations are determined by shipping patterns, rather than by the scientific need for spatial and temporal coverage.

Due to the differences between the climate states represented by models and the chosen observations, we do not make any direct comparisons. However, all of the PlioMIP models, with the exception of COSMOS, are represented in the CMIP5 ensemble, for which historical simulations exist that can be directly compared to modern observations.

Shu *et al.* (2015) provides an assessment of the historical simulation of Arctic sea ice by the CMIP5 models for the period 1979-2005. Their results show that for the historical simulations by the 7 PlioMIP models represented in CMIP5, MRI-CGCM simulates the highest mean annual sea ice extent (15.01 $\times 10^6$ km^2), compared to the satellite observational mean of 12.02 $\times 10^6$ km^2 for the comparable period (1979-2005). MRI-CGCM simulates the second highest PlioMIP pre-industrial mean annual sea ice extent (just 0.05 $\times 10^6$ km^2 less than MIROC4m), and the highest mid-Pliocene mean annual sea ice extent. The CMIP5 historical

extent simulated by MRI-CGCM is almost 25% greater than the observational mean, showing MRI-CGCM consistently simulates Arctic sea ice extent larger than the ensemble mean.

In contrast, MIROC4m simulates a PlioMIP pre-industrial mean annual sea ice extent that is similar to the MRI-CGCM PlioMIP simulation, and represents the lowest historical mean annual sea ice extent of the CMIP5 models that are included in the PlioMIP ensemble (10.66 $\times 10^6$ km^2, Shu *et al.* (2015)). The NorESM-L, which simulates both the lowest PlioMIP pre-industrial and mid-Pliocene mean annual sea ice extents, is the CMIP5 model which simulates the closest historial mean annual sea ice extent to the observations (12.01 $\times 10^6$ km^2, just 0.01×10^6 km^2 lower than the observations). As with the PlioMIP pre-industrial simulations, NorESM-L simulates the lowest sea ice extent amplitude of the PlioMIP models in CMIP5 (Shu *et al.*, 2015).

In addition to the mean annual sea ice extent simulated by each model in the CMIP5 historical and PlioMIP simulations, Table 5.2 shows the ensemble mean annual extents for these sets of simulations. In both PlioMIP simulations, the ensemble mean annual extent is lower than the mean annual extent simulated by CCSM4, and higher than the mean annual extent simulated by HadCM3. However, in the CMIP5 historical simulations, the ensemble mean annual extent is greater than the CCSM4 mean annual extent, and lower than the mean annual extent simulated by HadCM3.

In the following, we also assess the simulated pre-industrial sea ice thickness. The simulation of Arctic sea ice thickness in the CMIP5 simulations is analysed in Stroeve *et al.* (2014). The correlations between the spatial patterns of Arctic sea ice thickness in the simulations (average over the years 1981-2010) and observations from Kwok *et al.* (2009) are less than 0.4 for all the considered PlioMIP models — with the exception of CCSM4, which has the highest spatial pattern correlation of the entire CMIP5 ensemble. For each PlioMIP model, the spatial patterns of sea ice thickness in the pre-industrial simulation resembles the thickness spatial pattern in that model's CMIP5 simulation, shown in Stroeve *et al.* (2014). It has been noted that the spatial pattern correlation between different ensemble simulations with the same model is significantly higher than the correlation between one model and the observations, which suggests that poor

correlations are more likely explained by biases within the models, rather than by natural variability.

5.4.2 Mid-Pliocene simulations

Four models out of the eight-member PlioMIP ensemble (COSMOS, GISS-E2-R, MIROC4m and NorESM-L) simulate almost ice-free conditions in the mid-Pliocene summer. For those models that simulate summer sea ice in the mid-Pliocene the summer sea ice conditions vary strongly. In summer sea ice in HadCM3 is confined to the Arctic basin, with concentrations that do not exceed 60%, and very low concentrations along all ice edges. The summer sea ice margin in MRI-CGCM, on the other hand, extends almost to the southern tip of Greenland, and a large proportion of the sea ice cover is characterized by concentrations greater than 90% (Figure 5.5).

Table 5.2 lists the seasonal extent amplitudes for each model's PlioMIP simulation, in addition to the mean annual sea ice extent. Three of the eight models (CCSM4, IPSLCM5A and MRI-CGCM) simulate mid-Pliocene sea ice extent amplitudes which are smaller than the pre-industrial extent amplitudes. For CCSM4 and IPSLCM5A, the differences in extent amplitude between pre-industrial and mid-Pliocene are less than 10^6 km^2, and represent changes of 4.1% and 6.1% respectively, and so there does not appear to have been a substantial change in the annual cycles of both simulations by CCSM4 and IPSLCM5A. The increase in MRI-CGCM on the other hand is larger (2.22×10^6 km^2, or 13.9%). The reduction in sea ice between the extent maxima in the MRI-CGCM simulation is largely due to the loss of lower concentration, thinner sea ice from regions further south than the pre-industrial maximum sea ice margins in other models (see Figures 5.1 and 5.5). Much of the pre-industrial sea ice in the summer months in MRI-CGCM is close to 100% concentration and greater than 4 m thick. Consequently, the maximum extent reduced by a greater amount than the minimum extent.

Four of the five models with larger mid-Pliocene extent amplitudes simulated ice-free conditions for part of the summer in the mid-Pliocene.The increase in

extent amplitude ranges from a 9.4 % increase in COSMOS to a 101.3% increase in NorESM-L. It might be expected that simulating a seasonally ice-free mid-Pliocene sea ice cover would lead to a decrease in extent amplitude, as the minimum extent has decreased as low as possible, however this is not the case. As Figure 5.3 shows, the four models with seasonally ice-free mid-Pliocene simulations have the thinnest pre-industrial summer ice, which disappears in the mid-Pliocene summer, whereas much of the winter sea ice has simply thinned, so there is less of a reduction in extent.

Given the pronounced disagreement within the ensemble with regard to the nature of mid-Pliocene sea ice particularly in summer, the comparison of the different models' sea ice simulation with a reconstruction of mid-Pliocene Arctic sea ice from proxy data could prove insightful. An independent data set, like a reconstructed palaeo sea ice characteristic, may indicate which models simulate the mid-Pliocene climate more realistically. A reasonable performance of a model in simulating mid-Pliocene sea ice may also improve confidence in its prediction of future sea ice, in particular if its simulation of present day sea ice matches observations closely. If a model simulation matches well with observations/proxy reconstructions for just one climate, this may not necessarily be due to a good model performance — rather, the model may be producing "the right answers for the wrong reasons", such as error compensation (Massonnet *et al.*, 2012). However, a greater degree of confidence could be held in the predictions from a model which produces sea ice simulations that closely match both modern observations in a modern simulation and proxy data-based reconstructions in a mid-Pliocene simulation, as the probability that the model compares well to the data by chance for both is reduced.

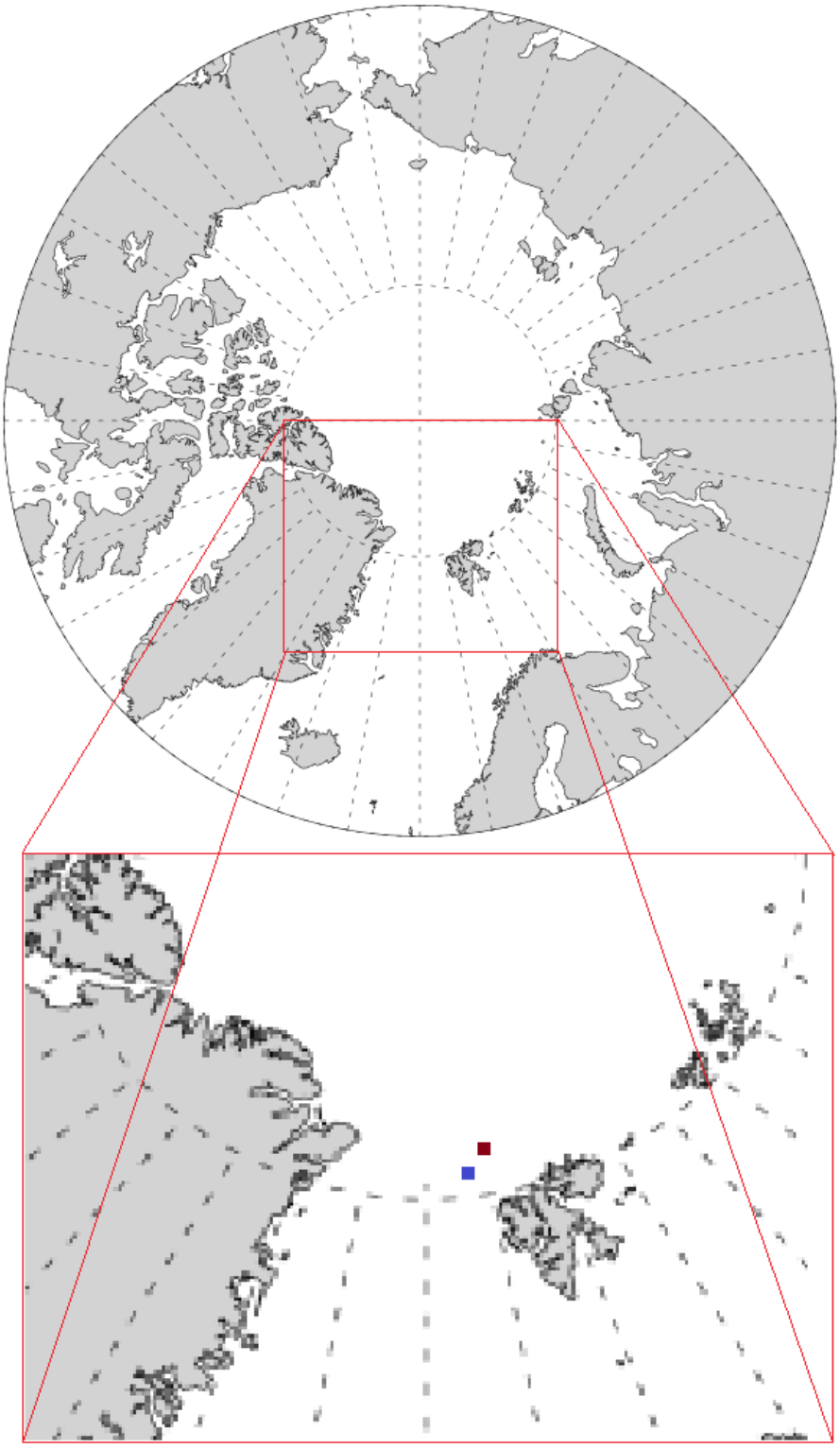

Figure 5.11: Location of Ocean Drilling Program (ODP) sites 911A (brown), and 910C (blue), used by Knies *et al.* (2014) for IP_{25} analysis.

Relating proxy data to mid-Pliocene sea ice is, however, subject to limitations due to uncertainty in the proxy itself. Darby (2008) demonstrates evidence for perennial Arctic sea ice in the mid-Pliocene, whilst the presence of IP_{25}, a biomarker proxy for sea ice coverage (Belt & Müller, 2013) in mid-Pliocene sediments, recovered from two boreholes in the Atlantic-Arctic gateway (located at 80.16°N, 6.35°E and 80.28°N, 8.17°E, see Figure 5.11), implies that the maximum sea ice margin during the mid-Pliocene extended southwards beyond these two sites, but the minimum margin did not (Knies *et al.*, 2014). The locations of these sites are within the maximum mid-Pliocene sea ice margins simulated by all of the PlioMIP models, but also within the minimum sea ice margins simulated by three of the models that simulate summer sea ice (CCSM4, IPSLCM5A and MRI-CGCM) — although the sea ice concentration at these sites is less than 50% in the CCSM4 and IPSLCM5A simulations. The extent of the sea ice minimum in HadCM3 does not reach the location of the sites analysed in Knies *et al.* (2014), and so is consistent with the conclusions drawn from proxy data in both the studies by Darby (2008) and Knies *et al.* (2014).

A greater spatial coverage of sea ice proxy data, such as that used in Knies *et al.* (2014), would improve the analysis of the simulation of sea ice by the PlioMIP models. At the moment, limited data availability does not allow for robust model-proxy comparisons. The sea ice simulated by HadCM3 has the closest agreement with the proxy data indications from Darby (2008) and Knies *et al.* (2014), but greater data coverage may provoke a different conclusion.

5.4.3 Causes of PlioMIP ensemble variability

5.4.3.1 Influence of the sea ice models

The sea ice components of each model differ in resolution, representation of sea ice dynamics and thermodynamics, and formulation of various parameterisations, such as sea ice albedo. The key details of each model's sea ice component are summarised in Table 5.1. The models CCSM4 and NorESM-L use the same sea ice component, based on CICE4 (Hunke, 2010), although NorESM-L has a coarser model grid in the atmosphere than CCSM4, and furthermore employs a completely different ocean component (Table 5.1).

The sea ice dynamics of the ensemble members can be categorised into three groups. First, CCSM4, NorESM-L, and MIROC4m, that all use the elastic-viscous-plastic (EVP) rheology of Hunke & Dukowicz (1997). Second, COSMOS, GISS-E2-R, and IPSLCM5A, that are based on viscous-plastic (VP) rheologies (Fichefet & Morales Maqueda, 1999; Marsland *et al.*, 2003; Zhang & Rothrock, 2000). Third, HadCM3 and MRI-CGCM, that do not consider any type of sea ice rheology, the sea ice following simple free drift dynamics (Cattle & Crossley, 1995; Mellor & Kantha, 1989). In PlioMIP, there does not appear to be any link between the type of dynamics of the sea ice components and the simulated sea ice extents — MRI-CGCM and MIROC4m produce the two highest annual means for pre-industrial whilst having very different sea ice dynamics. The three models that produce the lowest pre-industrial extents, i.e. NorESM-L, IPSLCM5A, and HadCM3, employ different rheologies — EVP, VP and no rheology respectively.

Most of the models use a leads parameterisation in their sea ice thermodynamics component, with only CCSM4 and NorESM-L employing explicit melt pond schemes. The models HadCM3 and COSMOS both use the leads parameterisation based on Hibler (1979). The models HadCM3, MIROC4m and MRI-CGCM all utilise the 'zero-layer' model developed by Semtner (1976). Similarly to the considered sea ice dynamics, there is no clear influence of the thermodynamics schemes used in the models on the simulated pre-industrial sea ice extent.

The simulation of Arctic sea ice by means of GCMs has been demonstrated to be very sensitive to the parameterisation of sea ice albedo. This has been observed in the case of variations of albedo in different models (Hodson *et al.*, 2013), and adjusting the parameterisation in one specific model (Howell *et al.*, 2014). Hill *et al.* (2014) show that clear sky albedo is the dominant factor in high latitude warming in the PlioMIP ensemble. The four models that display the highest warming effect from the clear sky albedo are those four models that simulate an ice-free mid-Pliocene summer (COSMOS, GISS-E2-R, MIROC4m, and NorESM-L). The NorESM-L shows the largest warming due to clear sky albedo, CCSM4 on the other hand shows the smallest clear sky albedo effect. Both NorESM-L and CCSM4 use the same sea ice component, based on CICE4 (Hunke & Lipscomb, 2008). This sea ice model employs a shortwave radiative

transfer scheme to internally simulate the sea ice albedo, and by that produce a more physically based parameterisation (Holland *et al.*, 2011).

Yet, it appears that the performance of this albedo scheme is very sensitive to differences in other components of the climate models: NorESM-L (that shows a large contribution of clear sky albedo) uses the same atmosphere component as CCSM4 (low contribution of clear sky albedo), albeit at a lower resolution version in the PlioMIP experiment, but it employs a different ocean component, that also has a lower resolution than the ocean component used in CCSM4. The contrast in the contribution of clear sky albedo to high latitude warming between NorESM-L and CCSM4 is reflected in the large difference in their simulations of summer mid-Pliocene sea ice. One cause is certainly the nature of the sea-ice albedo feedback mechanism (Curry *et al.*, 1995). Reduced albedo at high latitudes can be both a cause of and a result of a reduced sea ice extent. Models with parameterisations with a lower sea ice albedo minimum have therefore a greater potential to amplify the warming that originates from other sources in simulations of the mid-Pliocene, such as greenhouse gas emissivity. The low sea ice albedo assumed in NorESM-L is a likely explanation for the low sea ice extents it simulates (Figures 5.2 and 5.6), both in mid-Pliocene and pre-industrial simulations.

Second to NorESM-L, for MIROC4m clear sky albedo has the highest contribution to high latitude warming. In MIROC4m there is a fixed albedo of 0.5 for bare sea ice, with higher albedo for snow-covered sea ice, that furthermore varies according to ambient surface air temperature (K-1 Model Developers, 2004). Of the six models that do not use a radiative transfer scheme to internally simulate sea ice albedo (those except NorESM-L and CCSM4), only GISS-E2-R has an albedo minimum lower than 0.5. Yet, this model allows the albedo to vary between 0.44 and 0.84 (Schmidt *et al.*, 2006). All other models also allow the sea ice albedo to vary, and consequently MIROC4m has a lower overall albedo. This may help to explain the ability of MIROC4m to simulate an ice-free mid-Pliocene summer, despite simulating one of the highest winter sea ice extents for both pre-industrial and mid-Pliocene.

As the parameterisation of sea ice albedo is kept unchanged between pre-industrial and mid-Pliocene simulations, differences in the parameterisation between the models should have similar effects in both simulations. However, if

there is a temperature threshold above which the ice-albedo feedback becomes more dominant in some of the models, then this could explain the different influence of the sea ice parameterisation on pre-industrial and mid-Pliocene simulations.

General circulation models are tuned to best reproduce modern day climate conditions, and parameterisations are based on modern observations (Hunke, 2010; Mauritsen *et al.*, 2012). When simulating the climate of time periods with different climate states, such as the mid-Pliocene, models that are tuned towards present day conditions may be biased in some regions. However, it is disputed to which extent the adjustment of parameters, such as sea ice albedo, within the limits of observational uncertainties can affect the overall sea ice cover and compensate for other shortcomings in the model (DeWeaver *et al.*, 2008; Eisenman *et al.*, 2007, 2008).

5.4.3.2 Influence of the control simulation

Massonnet *et al.* (2012) describe the characteristics of Arctic sea ice simulated by the CMIP5 ensemble for the time period from 1979-2010 as being related in a 'complicated manner' to the simulated future change in September Arctic sea ice extent. Figure 5.9 demonstrates, based on correlation values, that some combinations of sea ice characteristics in the pre-industrial and mid-Pliocene simulations are much stronger related to each other than others. In section 5.4.1 it was highlighted that the differences in the PlioMIP models' simulation of sea ice for 1979-2005 in CMIP5 are not consistent with the differences in pre-industrial or mid-Pliocene simulations in the PlioMIP ensemble.

All of the models that simulate thinner pre-industrial summer sea ice than the ensemble mean also simulate ice-free conditions during the mid-Pliocene summer, with the exception of HadCM3. Holland & Bitz (2003) demonstrate that the thickness of sea ice in control simulations has a stronger influence on the climate state of the Northern Hemisphere polar region in simulations of future climates than sea ice extent. Massonnet *et al.* (2012) find that those CMIP5 models that predict an earlier disappearance of September Arctic sea ice generally have a smaller initial September sea ice extent. In PlioMIP, mean summer

pre-industrial sea ice thicknesses have correlation coefficients of 0.81 and 0.82 with mean summer mid-Pliocene sea ice extents and thicknesses, respectively. Mean summer pre-industrial sea ice extents on the other hand show weaker correlations with mean summer mid-Pliocene sea ice extents and thicknesses, with respective correlation coefficients of 0.47 and 0.51. The relatively thin pre-industrial summer sea ice simulated in PlioMIP by COSMOS, GISS-E2-R, MIROC4m and NorESM-L therefore appears to be an important factor for the ability of those models to simulate an ice-free mid-Pliocene summer. An exception is HadCM3, that simulates perennial sea ice in the mid-Pliocene, despite simulating relatively thin (within the PlioMIP ensemble) pre-industrial sea ice.

5.4.3.3 Influence of atmosphere and ocean on the sea ice simulation

In the mid-Pliocene simulations, the correlation coefficient between Arctic surface temperatures and simulated sea ice extent is much higher than the corresponding correlation coefficient in the pre-industrial simulations (Figure 5.10 a,b). Pre-industrial sea ice is thicker than mid-Pliocene sea ice, which could explain the lower sensitivity of the pre-industrial sea ice extent to surface temperatures. However, similar differences in correlation strength between the pre-industrial and mid-Pliocene simulations are also seen for mean sea ice volume (Figure 5.10, c,d), so there is no strong relationship between warmer pre-industrial simulations and those with less total ice.

In the pre-industrial simulations, much of the ocean north of 60°N is fully covered with sea ice, so all SSTs will be -1.8°C. The uniformity of the SSTs in this region could be a plausible explanation for the weak correlation between the overall Arctic sea ice extents and SSTs north of 60°N in the pre-industrial simulations of the PlioMIP ensemble. The reduced sea ice coverage in the mid-Pliocene simulations, particularly during the summer months, enables on the other hand a greater range of possible SST values. This is potentially the reason for a much stronger correlation with the simulated mid-Pliocene sea ice extents (Figure 5.10). In the models, the presence of ice in a grid box, even at low concentrations, restricts the warming in the ocean. Larger parts of the ocean are ice-free for longer periods in the year in the mid-Pliocene simulations than

in the pre-industrial simulations, meaning longer periods in the mid-Pliocene simulations where the ocean can warm. This will in turn affect the warming of the atmosphere in the models, and so is a possible reason for better correlation between sea ice extent and surface temperatures in the mid-Pliocene simulations.

In addition to SATs and SSTs, there are of course other atmospheric and oceanic influences on the simulation of Arctic sea ice. The Atlantic Meridional Overturning Circulation (AMOC) contributes significantly to poleward oceanic heat transport and has been shown to have a strong impact on Arctic sea ice (e.g. Day *et al.* (2012); Mahajan *et al.* (2011); Miles *et al.* (2014)). Zhang *et al.* (2013b) analyse the simulation of the AMOC in both pre-industrial and mid-Pliocene simulations of the PlioMIP ensemble and find that there is little difference between each model's pre-industrial and mid-Pliocene AMOC simulation. There is no consistent change in northward ocean heat transport, with half the models simulating a slight (less than 10%) increase, and half the models simulating a slight decrease (less than -15%). Of the models which simulate increased northward ocean heat transport (COSMOS, GISS-E2-R, IPSLCM5A and MRI-CGCM), only two (COSMOS and GISS-E2-R) simulate an ice-free mid-Pliocene summer. This suggests that the influence of AMOC and northward oceanic heat transport on the ensemble variability of sea ice in the mid-Pliocene simulation of PlioMIP is not the most important factor.

An analysis of multi-decadal variability influence on Arctic sea ice extent in selected CMIP3 simulations (covering 1953-2010) by Day *et al.* (2012) showed a significant correlation between Arctic sea ice extents and Atlantic Multi-decadal Oscillation (AMO) indices. Kwok (2000) and Parkinson (2008) demonstrate evidence of the North Atlantic Oscillation (NAO) on Arctic sea ice. Table 5.3 shows annual and decadal correlations between Arctic sea ice extent and AMO and NAO indices for simulations from three PlioMIP models (CCSM4, HadCM3 and NorESM-L), for which sufficiently long time series were available to perform the calculations.

All three models show a small but significant (at 90% level) correlation between the pre-industrial annual Arctic sea ice extents and the NAO indices. The correlation coefficients at the decadal time scale are increased for both HadCM3

and NorESM-L, but are not significant for any of the models. None of the correlations between mid-Pliocene Arctic sea ice extents and NAO indices are significant at the 90% level. The correlations between pre-industrial Arctic sea ice extents and AMO indices are all not significant at the 90% level. For the mid-Pliocene simulations, only the correlation between the annual Arctic sea ice extents and AMO indices from the CCSM4 simulations is significant at the 90% level.

There is no significant correlation between decadal sea ice extents and NAO/AMO indices in the three models shown, and so it is unlikely that differences in the mean sea ice extents (representing averages representing between 30 and 200 years worth of climatology) between different models and simulations can be explained by different influences of these variability indices. To more thoroughly investigate this would require much longer timeseries from all the modelling groups, which is not available. A comprehensive analysis of the relationships between variability indices and sea ice in the PlioMIP simulations is beyond the scope of this paper.

Patterns of ice thicknesses are strongly influenced by the motion of sea ice in the models. In each model, the equations used to determine sea ice motion account for stresses on the ice from surface winds and ocean currents, with the exceptions of HadCM3, which does not take surface winds into account (Gordon *et al.*, 2000), and MRI-CGCM, where the ocean currents are not taken into account in determining ice motion (Mellor & Kantha, 1989).

Figure 5.12 shows the mean annual 10 m surface winds for the COSMOS and MIROC4m mid-Pliocene simulations, where the dominant wind direction between 90°E and 180°E over the Arctic basin is towards the northern coast of Eastern Siberia, where a build up of thicker ice is present. Similarly, in the IPSLCM5A pre-industrial simulation (Figure 5.12), the dominant wind direction is towards the north of Greenland and the Canadian Arctic Archipelago where the thickest ice is. In the NorESM-L pre-industrial simulation (shown in Figure 5.12), the thickest ice is present between Greenland and the Canadian Arctic Archipelago. In the corresponding mid-Pliocene simulation, the mean annual 10 m surface winds over this region are weaker, and in a western direction, rather than north-west, towards the Canadian Arctic Archipelago, and so conditions are less conducive for a build up of thicker ice. Mean annual 10 m winds and sea ice

thicknesses for all simulations (excluding CCSM4, for which 10m winds are not an output) are included in the supplementary information.

In HadCM3, the ocean surface currents form a vortex in part of the Arctic basin, where the thickest sea ice is present in both simulations (see Figure 5.13). Given that the sea ice motion is entirely determined by the surface ocean current, its influence on the spatial pattern of sea ice thickness is clear. If sea ice motion were instead determined by surface wind stresses in addition to the ocean currents (which do not have the same patterns in HadCM3), this should result in a different configuration of sea ice in the Arctic basin, and would likely affect the location of the sea ice margins simulated by the model. Mean annual surface ocean currents and sea ice thicknesses for all simulations are included in the supplementary information.

Understanding the more precise influences of winds and ocean currents on the modelled sea ice, and the causes of differences between models, as well as different simulations with the same model, would require a far more extensive analysis. Differences in seasonal, as well as annual patterns, alongside atmospheric circulations at higher levels, may be explored in further work.

5.5 Conclusions

We have presented a detailed analysis of the simulation of Arctic sea ice in the PlioMIP model ensemble, for both pre-industrial control and mid-Pliocene simulations. The sea ice in the mid-Pliocene simulations is overall less extensive and thinner than the pre-industrial sea ice, with a 33% decrease in mean annual sea ice extent for the ensemble mean, and a 56% reduction in the ensemble mean annual sea ice thickness. The changes in the mid-Pliocene, relative to the pre-industrial, are largest during the summer months, both in absolute and relative terms, and for both sea ice extent and sea ice thickness.

The simulated mid-Pliocene sea ice extents are strongly negatively correlated with the Arctic temperatures. In contrast, there is only a weak correlation between pre-industrial sea ice extents and temperature. Hill *et al.* (2014) identified clear sky albedo as the dominant driver of high latitude warming in the mid-Pliocene simulations of PlioMIP, particularly in those models that simulate

an ice-free mid-Pliocene summer. Sea ice-albedo feedbacks may contribute to the stronger relationship between surface temperatures and sea ice in the mid-Pliocene simulations, as the feedback mechanism enhances the warming that originates from increased greenhouse gas concentrations. The effect of the sea ice-albedo feedback does not appear to be similarly pronounced in the pre-industrial simulations. If it is the case that some models see an enhanced ice-albedo feedback in warmer climates, then this is likely to affect those models' prediction of future Arctic sea ice change.

The HadCM3 is the only model that simulates both perennial mid-Pliocene Arctic sea ice and a minimum sea ice extent that is completely located north of the location of the two sites studied in Knies *et al.* (2014), located at 80.16°N, 6.35°E and 80.28°N, 8.17°E, where IP_{25} proxy data indicates the presence of a sea ice margin in the mid-Pliocene. HadCM3 therefore produces the mid-Pliocene simulation that is in best agreement with the proxy inferences from Darby (2008) and Knies *et al.* (2014), i.e. presence of perennial sea ice and a relatively northern location of summer sea ice during the mid-Pliocene. Yet, it should be noted that the proxy evidence is sparse, with available data originating from just two sites in the same region. Furthermore, the understanding of mid-Pliocene sea ice is still too low to have confidence in this simulation, particularly considering that the HadCM3 CMIP5 simulation is not closest to the observations, and the model simulates an unrealistic sea ice distribution, in part due to the sea ice motion having no influence from the surface winds. Of course, if the proxy studies indicating seasonal mid-Pliocene Arctic sea ice (e.g. Cronin *et al.* (1993); Moran *et al.* (2006); Polyak *et al.* (2010)) are correct, then the mid-Pliocene Arctic sea ice in COSMOS, GISS-E2-R, MIROC4m and NorESM-L models concur with the data indication.

Given the limited amount of suitable proxy data, we are currently not able to make firm judgements with respect to a selection of models that simulate a more accurate mid-Pliocene Arctic sea ice cover if compared to the geologic record. The availability of additional proxy data may enable such conclusion in the future, could help to identify strengths and weaknesses in the different models' simulations of sea ice, as well as gauge confidence in their predictions of future sea ice.

However, as discussed in section 5.4.3.3, there are numerous atmospheric and oceanic factors that influence the simulation of Arctic sea ice. As highlighted by Massonnet *et al.* (2012), a model can simulate the 'right' results for the wrong reasons, perhaps due to error compensation. This does not mean that the analysis of sea ice simulations for past climates, such as the mid-Pliocene, is not valuable and justified, but that it is important to highlight that the forcings behind the sea ice simulation have to be better understood. Variability modes, such as NAO or AMO, whilst shown to have influence on sea ice extent from an annual viewpoint, do not appear to exert significant influence over the mean sea ice state on a decadal time scale. The models' representation of sea ice motion, and by extension ocean currents and surface winds, are an important influence on the distribution of sea ice, and worthy of a more detailed study. Future studies must particularly aim at quantifying the contribution of the various forcings on the sea ice in warmer climates.

Table 5.3: Correlation between AMO and NAO indices, and mean annual and decadal Arctic sea ice extent for three PlioMIP models. Starred values are significant at the 90% level.

Model	Pre-industrial (annual)	Pre-industrial (decadal)	Mid-Pliocene (annual)	Mid-Pliocene (decadal)
	r(AMO,SIE)	r(AMO,SIE)	r(AMO,SIE)	r(AMO,SIE)
CCSM4	-0.036	-0.16	-0.23*	-0.27
HadCM3	-0.069	-0.17	-0.022	-0.22
NorESM-L	-0.10	-0.076	-0.035	0.12
	r(NAO,SIE)	r(NAO,SIE)	r(NAO,SIE)	r(NAO,SIE)
CCSM4	-0.18*	-0.099	-0.033	0.18
HadCM3	-0.24*	-0.33	-0.0063	-0.093
NorESM-L	-0.14*	-0.28	0.07	0.24

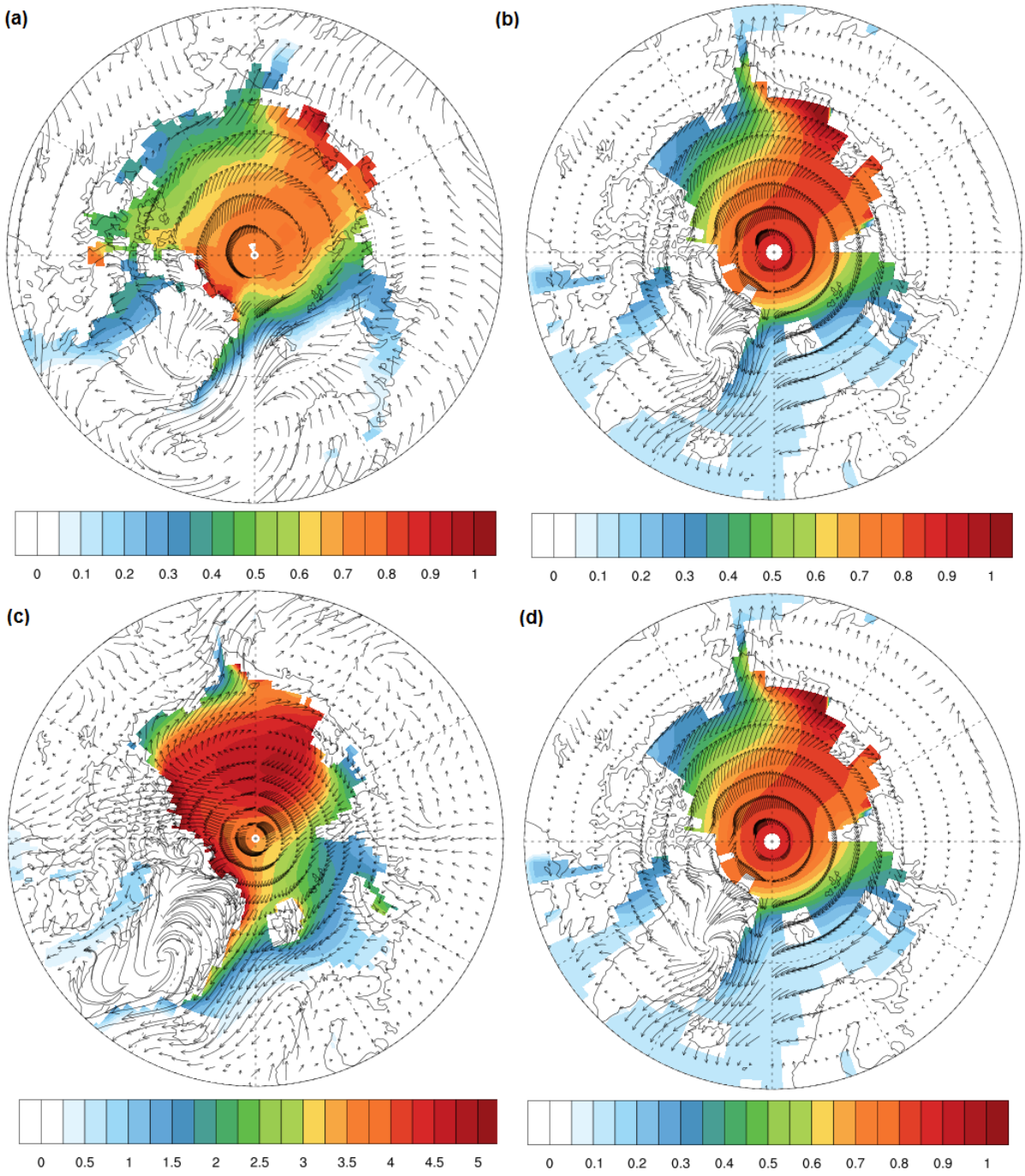

Figure 5.12: Mean annual 10 m winds and sea ice thicknesses (m) for (a) COSMOS mid-Pliocene, (b) MIROC4m mid-Pliocene, (c) IPSLCM5A pre-industrial and (d) NorESM-L pre-industrial. Vector length is proportional to wind speed.

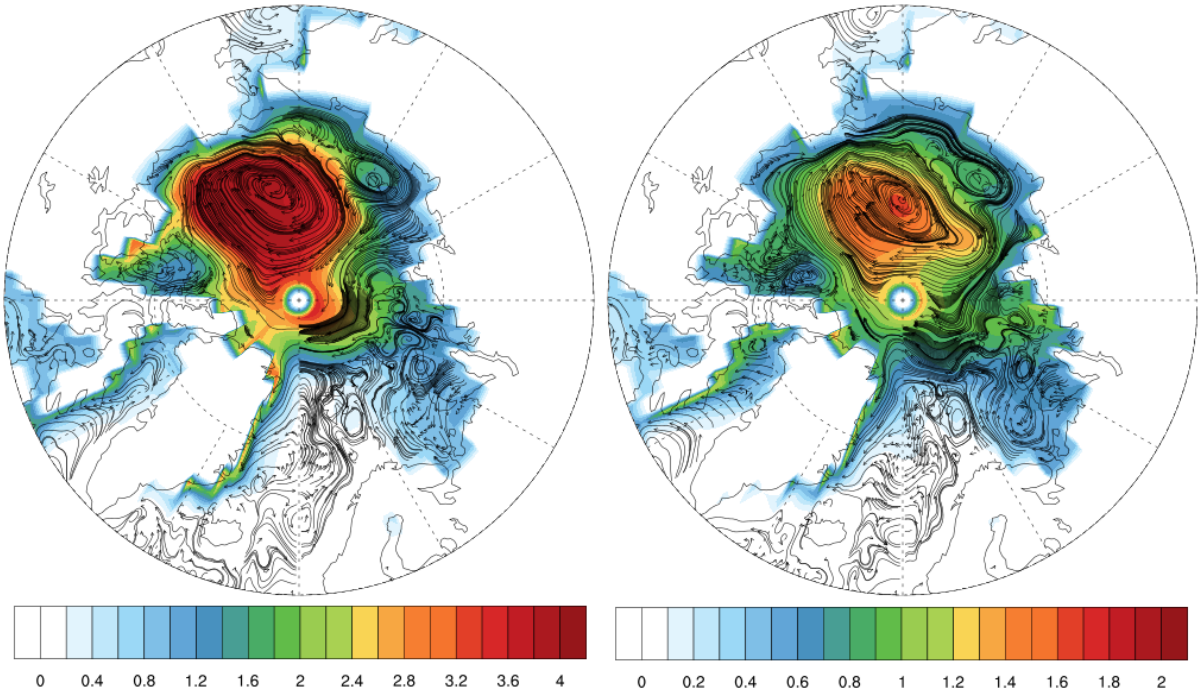

Figure 5.13: Mean annual ocean surface currents and sea ice thicknesses (m) for HadCM3 pre-industrial (left) and mid-Pliocene (right) simulations. Vector length is proportional to ocean current speed.

References

Arzel, O., Fichefet, T. & Goosse, H. (2006). Sea ice evolution over the 20th and 21st centuries as simulated by current AOGCMs. *Ocean Modelling*, **12**, 401 – 415. 93

Belt, S. & Müller, J. (2013). The Arctic sea ice biomarker IP_{25}: a review of current understanding, recommendations for future research and applications in palaeo sea ice reconstructions. *Quaternary Science Reviews*, **79**, 9–25. 51, 52, 116

Berger, M., Brandefelt, J. & Nilsson, J. (2013). The sensitivity of the Arctic sea ice to orbitally induced insolation changes: a study of the mid-Holocene Paleoclimate Modelling Intercomparison Project 2 and 3 simulations. *Clim. Past*, **9**, 969–982. 93, 95

Blanchard-Wrigglesworth, E. & Bitz, C. (2014). Characteristics of Arctic sea-ice thickness variability in GCMs. *J. Climate*, **27**, 8244–8258. 93

Boé, J.L., Hall, A. & Qu, X. (2009). September sea-ice cover in the Arctic Ocean projected to vanish by 2100. *Nature Geoscience*, **2**, 341–343. 44, 92

Bragg, F.J., Lunt, D.J. & Haywood, A.M. (2012). Mid-Pliocene climate modelled using the UK Hadley Centre Model: PlioMIP Experiments 1 and 2. *Geoscientific Model Development*, **5**, 1109–1125. 71, 94

Cattle, H. & Crossley, J. (1995). Modeling Arctic climate change. *Philosophical Transactions of the Royal Society A-Mathematical, Physical and Engineering Sciences*, **352**, 201–213. 62, 63, 71, 75, 94, 117, 142, 188, 189

Chan, W.L., Abe-Ouchi, A. & Ohgaito, R. (2011). Simulating the mid-Pliocene climate with the MIROC general circulation model: experimental design and initial results. *Geoscientific Model Development*, **4**, 1035–1049. 71, 94

Chandler, M.A., Sohl, L.E., Jonas, J.A., Dowsett, H.J. & Kelley, M. (2013). Simulations of the mid-Pliocene Warm Period using two versions of the NASA/GISS ModelE2-R Coupled Model. *Geoscientific Model Development*, **6**, 517–531. 71, 94

Contoux, C., Ramstein, G. & Jost, A. (2012). Modelling the mid-Pliocene Warm Period climate with the IPSL coupled model and its atmospheric component LMDZ5A. *Geoscientific Model Development*, **5**, 903–917. 71, 94

Cronin, T.M., Whatley, R., Wood, A., Tsukagoshi, A., Ikeya, N., Brouwers, E.M. & Briggs, W.M. (1993). Microfaunal evidence for elevated Pliocene temperatures in the Arctic ocean. *Paleoceanography*, **8**, 161–173. 24, 74, 92, 124, 140, 181

Curry, J.A., Schramm, J.L. & Ebert, E.E. (1995). Sea ice-albedo climate feedback mechanism. *Journal of Climate*, **8**, 240–247. 34, 37, 38, 45, 73, 118, 140

Darby, D.A. (2008). Arctic perennial ice cover over the last 14 million years. *Paleoceanography*, **23**, PA1S07. 58, 92, 116, 124, 140, 161, 166, 181

Day, J.J., Hargreaves, J.C., Annan, J.D. & Abe-Ouchi, A. (2012). Sources of multi-decadal variability in Arctic sea ice extent. *Environmental Research Letters*, **7**, 034011. 121

DeWeaver, E., Hunke, E. & Holland, M. (2008). Comment on "On the reliability of simulated Arctic sea ice in global climate models" by I. Eisenman, N. Untersteiner, and J. S. Wettlaufer. *Geophysical Research Letters*, **L04501**. 119

Dowsett, H.J., Robinson, M.M., Haywood, A.M., Salzmann, U., Hill, D.J., Sohl, L., Chandler, M.A., Williams, M., Foley, K. & Stoll, D. (2010). The PRISM3D paleoenvironmental reconstruction. *Stratigraphy*, **7**, 123–139. 1, 3, 4, 5, 9, 16, 17, 18, 21, 66, 73, 76, 77, 83, 92, 95, 140, 143, 144, 190, 191

Eisenman, I., Untersteiner, N. & Wettlaufer, J.S. (2007). On the reliability of simulated Arctic sea ice in global climate models. *Geophysical Research Letters*, **34**, L10501. 119

Eisenman, I., Untersteiner, N. & Wettlaufer, J.S. (2008). Reply to comment by E. T. DeWeaver et al. on "On the reliability of simulated Arctic sea ice in global climate models". *Geophysical Research Letters*, **35**, L04502. 73, 119

Fichefet, T. & Morales Maqueda, M.A. (1999). Modelling the influence of snow accumulation and snow-ice formation on the seasonal cycle of the Antarctic sea-ice cover. *Climate Dynamics*, **15**, 251–268. 117

Gordon, C., Cooper, C., Senior, C.A., Banks, H., Gregory, J.M., Johns, T.C., Mitchell, J.F.B. & Wood, R.A. (2000). The simulation of SST, sea ice extents and ocean heat transports in a version of the Hadley Centre coupled model without flux adjustments. *Climate Dynamics*, **16**, 147–168. 2, 59, 60, 61, 62, 63, 64, 65, 75, 122, 141, 142, 188, 189

Haywood, A.M., Dowsett, H.J., Otto-Bliesner, B., Chandler, M.A., Dolan, A.M., Hill, D.J., Lunt, D.J., Robinson, M.M., Rosenbloom, N., Salzmann, U. & Sohl, L.E. (2010). Pliocene Model Intercomparison Project (PlioMIP): experimental design and boundary conditions (Experiment 1). *Geoscientific Model Development*, **3**, 227–242. 29, 70, 93, 95

Haywood, A.M., Dowsett, H.J., Robinson, M.M., Stoll, D.K., Dolan, A.M., Lunt, D.J., Otto-Bliesner, B.L. & Chandler, M.A. (2011b). Pliocene Model Intercomparison Project (PlioMIP): experimental design and boundary conditions (Experiment 2). *Geosci. Model Dev.*, **4**, 571–577. 29, 30, 70, 76, 93, 95, 141, 143, 189

Haywood, A.M., Hill, D.J., Dolan, A.M., Otto-Bliesner, B.L., Bragg, F.J., Chan, W.L., Chandler, M.A., Contoux, C., Dowsett, H.J., Jost, A., Kamae, Y., Lohmann, G., Lunt, D.J., Abe-Ouchi, A., Pickering, S.J., Ramstein, G., Rosenbloom, N.A., Salzmann, U., Sohl, L., Stepanek, C., Ueda, H., Yan, Q. & Zhang, S.Z. (2013). Large-scale features of Pliocene climate: results from the Pliocene Model Intercomparison Project. *Clim. Past*, **9**, 191–209. 1, 3, 29, 30, 73, 92, 140, 141

Hibler, W.D. (1979). A dynamic-thermodynamic sea ice model. *Journal of Physical Oceanography*, **9**, 815–846. 47, 48, 49, 62, 75, 117, 142, 188

Hill, D.J., Haywood, A.M., Lunt, D.J., Hunter, S.J., Bragg, F.J., Contoux, C., Stepanek, C., Sohl, L., Rosenbloom, N.A., Chan, W.L., Kamae, Y., Zhang, Z., Abe-Ouchi, A., Chandler, M.A., Jost, A., Lohmann, G., Otto-Bliesner, B.L., Ramstein, G. & Ueda, H. (2014). Evaluating the dominant components of warming in Pliocene climate simulations. *Climate of the Past*, **10**, 79–90. 117, 123, 146, 153, 165

Hodson, D., Keeley, S., West, A., Ridley, J., Hawkins, E. & Hewitt, H. (2013). Identifying uncertainties in Arctic climate change projections. *Climate Dynamics*, **40**, 2849–2865. 117

Holland, M.M. & Bitz, C.M. (2003). Polar amplification of climate change in coupled models. *Climate Dynamics*, **21**, 221–232. 40, 41, 45, 46, 119

Holland, M.M. & Stroeve, J. (2011). Changing seasonal sea ice predictor relationships in a changing Arctic climate. *Geophysical Research Letters*, **38**, L18501. 93

Holland, M.M., Bailey, D.A., Briegleb, B.P., Light, B. & Hunke, E.C. (2011). Improved sea ice shortwave radiation physics in CCSM4: The impact of melt ponds and aerosols on Arctic sea ice. *Journal of Climate*, **25**, 1413–1430. 71, 83, 94, 118

Howell, F.W., Haywood, A.M., Dolan, A.M., Dowsett, H.J., Francis, J.E., Hill, D.J., Pickering, S.J., Pope, J.O., Salzmann, U. &

Wade, B.S. (2014). Can uncertainties in sea ice albedo reconcile patterns of data-model discord for the Pliocene and 20th/21st centuries? *Geophysical Research Letters*, **41**, 2011–2018. 117, 140, 144, 151, 154

Hunke, E.C. (2010). Thickness sensitivities in the CICE sea ice model. *Ocean Modelling*, **34**, 137–149. 40, 71, 73, 94, 116, 119

Hunke, E.C. & Dukowicz, J.K. (1997). An elastic-viscous-plastic model for sea ice dynamics. *Journal of Physical Oceanography*, **27**, 1849–1867. 49, 71, 94, 117

Hunke, E.C. & Lipscomb, W.H. (2008). CICE: The Los Alamos sea ice model user's manual, version 4.0. *Tech. Rep. LA-CC-06-012, Los Alamos, New Mexico.*, 76. 117

Johnson, M., Gaffigan, S., Hunke, E. & Gerdes, R. (2007). A comparison of Arctic Ocean sea ice concentration among the coordinated AOMIP model experiments. *Journal of Geophysical Research: Oceans*, **112**, C04S11. 93

Johnson, M., Proshutinsky, A., Aksenov, Y., Nguyen, A.T., Lindsay, R., Haas, C., Zhang, J., Diansky, N., Kwok, R., Maslowski, W., Häkkinen, S., Ashik, I. & de Cuevas, B. (2012). Evaluation of Arctic sea ice thickness simulated by Arctic Ocean Model Intercomparison Project models. *Journal of Geophysical Research: Oceans*, **117**, C00D13. 93

K-1 Model Developers (2004). K1 Coupled Model (MIROC) Description: K1 Technical Report 1, edited by: Hasumi, H. and Emori, S. *34 pp., Center for Climate System Research, University of Tokyo*. 71, 94, 118

Kamae, Y. & Ueda, H. (2012). Mid-Pliocene global climate simulation with MRI-CGCM2.3: set-up and initial results of PlioMIP Experiments 1 and 2. *Geoscientific Model Development*, **5**, 793–808. 71, 94

Knies, J., Cabedo-Sanz, P., Belt, S.T., Baranwal, S., Fietz, S. & Rosell-Melé, A. (2014). The emergence of modern sea ice cover in the Arctic Ocean. *Nat. Commun.*, **5:5608**. 53, 58, 115, 116, 124, 140, 166

Kwok, R. (2000). Recent changes in Arctic Ocean sea ice motion associated with the North Atlantic Oscillation. *Geophysical Research Letters*, **27**, 775–778. 121

Kwok, R., Cunningham, G.F., Wensnahan, M., Rigor, I., Zwally, H.J. & Yi, D. (2009). Thinning and volume loss of the Arctic Ocean sea ice cover: 2003-2008. *Journal of Geophysical Research*, **114**, C07005. 40, 112

Liu, J., Schmidt, G.A., Martinson, D., Rind, D.H., Russell, G.L. & Yuan, X. (2003). Sensitivity of sea ice to physical parameterizations in the GISS global climate model. *Journal of Geophysical Research*, **108**, 3053. 71, 94

Mahajan, S., Zhang, R. & Delworth, T. (2011). Impact of the Atlantic Meridional Overturning Circulation (AMOC) on Arctic surface air temperature and sea ice variability. *Journal of Climate*, **24**, 6573–6581. 34, 121

Marsland, S.J., Haak, H., Jungclaus, J.H., Latif, M. & Röske, F. (2003). The Max-Planck-Institute global ocean/sea ice model with orthogonal curvilinear coordinates. *Ocean Modelling*, **5**, 91–127. 71, 94, 117

Massonnet, F., Fichefet, T., Goosse, H., Bitz, C.M., Philippon-Berthier, G., Holland, M.M. & Barriat, P.Y. (2012). Constraining projections of summer Arctic sea ice. *The Cryosphere Discussions*, **6**, 2931–2959. 92, 114, 119, 125

Mauritsen, T., Stevens, B., Roeckner, E., Crueger, T., Esch, M., Giorgetta, M., Haak, H., Jungclaus, J., Klocke, D., Matei, D., Mikolajewicz, U., Notz, D., Pincus, R., Schmidt, H. & Tomassini, L. (2012). Tuning the climate of a global model. *Journal of Advances in Modeling Earth Systems*, **4**, M00A01. 119

Mellor, G.L. & Kantha, L. (1989). An ice-ocean coupled model. *Journal of Geophysical Research-Oceans*, **94**, 10937–10954. 50, 71, 94, 117, 122

Miles, M.W., Divine, D.V., Furevik, T., Jansen, E., Moros, M. & Ogilvie, A.E.J. (2014). A signal of persistent Atlantic multidecadal variability in Arctic sea ice. *Geophysical Research Letters*, **41**, 463–469, 2013GL058084. 121

Moran, K., Backman, J., Brinkhuis, H., Clemens, S.C., Cronin, T., Dickens, G.R., Eynaud, F., Gattacceca, J., Jakobsson, M., Jordan, R.W., Kaminski, M., King, J., Koc, N., Krylov, A., Martinez, N., Matthiessen, J., McInroy, D., Moore, T.C., Onodera, J., O'Regan, M., Pälike, H., Rea, B., Rio, D., Sakamoto, T., Smith, D.C., Stein, R., St John, K., Suto, I., Suzuki, N., Takahashi, K., Watanabe, M., Yamamoto, M., Farrel, J., Frank, M., Kubik, P., Jokat, W. & Kristoffersen, Y. (2006). The Cenozoic palaeoenvironment of the Arctic Ocean. *Nature*, **441**, 601–605. 74, 92, 124, 140, 181

Pagani, M., Liu, Z., LaRiviere, J. & Ravelo, A.C. (2010). High Earth-system climate sensitivity determined from Pliocene carbon dioxide concentrations. *Nature Geoscience*, **3**, 27–30. 6, 8, 73, 92, 140, 189

Parkinson, C.L., Vinnikov, K.Y. & Cavalieri, D.J. (2006). Evaluation of the simulation of the annual cycle of Arctic and Antarctic sea ice coverages by 11 major global climate models. *Journal of Geophysical Research: Oceans*, **111**, C07012. 93

Parkinson, C.L. (2008). Recent trend reversals in Arctic sea ice extents: possible connections to the North Atlantic Oscillation. *Polar Geography*, **31**, 3–14. 121

Parkinson, C.L. & Comiso, J.C. (2013). On the 2012 record low Arctic sea ice cover: Combined impact of preconditioning and an August storm. *Geophysical Research Letters*, **40**, 13561361. 44, 92

Polyak, L., Alley, R.B., Andrews, J.T., Brigham-Grette, J., Cronin, T.M., Darby, D.A., Dyke, A.S., Fitzpatrick, J.J., Funder, S., Holland, M.M., Jennings, A.E., Miller, G.H., O'Regan, M., Savelle, J., Serreze, M., St John, K., White, J.W.C. & Wolff, E. (2010).

History of sea ice in the Arctic. *Quaternary Science Reviews*, **29**, 1757–1778. 51, 55, 57, 58, 74, 92, 124, 140, 166, 181

Rosenbloom, N.A., Otto-Bliesner, B.L., Brady, E.C. & Lawrence, P.J. (2013). Simulating the mid-Pliocene Warm Period with the CCSM4 model. *Geoscientific Model Development*, **6**, 549–561. 71, 94

Schmidt, G.A., Reto, R., Hansen, J.E., Aleinov, I., Bell, N., Bauer, M., Bauer, S., Cairns, B., Canuto, V., Cheng, Y., Del Genio, A., Faluvegi, G., Friend, A.D., Hall, T.M., Hu, Y., Kelley, M., Kiang, N.Y., Koch, D., Lacis, A.A., Lerner, J., Lo, K.K., Miller, R.L., Nazarenko, L., Oinas, V., Perlwitz, J.P., Perlwitz, J., Rind, D., Romanou, A., Russell, G.L., Sato, M., Shindell, D.T., Stone, P.H., Sun, S., Tausnev, N., Thresher, D. & Yao, M.S. (2006). Present-day atmospheric simulations using GISS ModelE: Comparison to in situ, satellite, and reanalysis data. *Journal of Climate*, **19**, 153–192. 118

Seki, O., Foster, G.L., Schmidt, D.N., Mackensen, A., Kawamura, K. & Pancost, R.D. (2010). Alkenone and boron-based Pliocene pCO_2 records. *Earth and Planetary Science Letters*, **292**, 201–211. 6, 7, 8, 73, 92, 140, 189

Semtner, A.J. (1976). A model for the thermodynamic growth of sea ice in numerical investigations of climate. *Journal of Physical Oceanography*, **6**, 379–389. 47, 48, 49, 61, 62, 75, 117, 142, 188

Shu, Q., Song, Z. & Qiao, F. (2015). Assessment of sea ice simulations in the CMIP5 models. *The Cryosphere*, **9**, 399–409. 93, 111, 112, 162

Stepanek, C. & Lohmann, G. (2012). Modelling mid-Pliocene climate with COSMOS. *Geoscientific Model Development*, **5**, 1221–1243. 71, 94

Stroeve, J., Holland, M.M., Meier, W., Scambos, T. & Serreze, M. (2007). Arctic sea ice decline: Faster than forecast. *Geophysical Research Letters*, **34**, L09501. 44, 74, 79, 93

Stroeve, J., Barrett, A., Serreze, M. & Schweiger, A. (2014). Using records from submarine, aircraft and satellites to evaluate climate model simulations of Arctic sea ice thickness. *The Cryosphere*, **8**, 1839–1854. 93, 112

Stroeve, J.C., Kattsov, V., Barrett, A., Serreze, M., Pavlova, T., Holland, M.M. & Meier, W.N. (2012). Trends in Arctic sea ice extent from CMIP5, CMIP3 and observations. *Geophysical Research Letters*, **39**, L16502. 1, 44, 74, 92, 93

Thomsen, H. (1947). The annual aeports on the Arctic sea ice issued by the Danish Meteorological Institute. *Journal of Glaciology*, **1**, 140–141. 42, 111

Walsh, J.E. & Chapman, W.L. (2001). 20th-century sea-ice variations from observational data. *Annals of Glaciology*, **33**, 444–448. 42, 111

Wang, M. & Overland, J.E. (2012). A sea ice free summer Arctic within 30 years: An update from CMIP5 models. *Geophysical Research Letters*, **39**, L18501. 44, 92

Zhang, J. & Rothrock, D. (2000). Modeling Arctic sea ice with an efficient plastic solution. *Journal of Geophysical Research*, **105**, 3325–3338. 71, 94, 117

Zhang, J., Lindsay, R., Schweiger, A. & Steele, M. (2013a). The impact of an intense summer cyclone on 2012 Arctic sea ice retreat. *Geophysical Research Letters*, **40**, 720–726. 6, 7, 8, 44, 68, 92, 140, 143

Zhang, Z., Nisancioglu, K., Chandler, M., Haywood, A., Otto-Bliesner, B., Ramstein, G., Stepanek, C., Abe-Ouchi, A., Chan, W., Bragg, F., Contoux, C., Dolan, A., Hill, D., Jost, A., Kamae, Y., Lohmann, G., Lunt, D., Rosenbloom, N., Sohl, L. & Ueda, H. (2013b). Mid-Pliocene Atlantic Meridional Overturning Circulation not unlike modern. *Climate of the Past*, **9**, 1495–1504. 121, 183

Zhang, Z.S., Nisancioglu, K., Bentsen, M., Tjiputra, J., Bethke, I., Yan, Q., Risebrobrakken, B., Andersson, C. & Jansen, E. (2012). Pre-industrial and mid-Pliocene simulations with NorESM-L. *Geoscientific Model Development*, **5**, 523–533. 71, 94

Chapter 6

Sensitivity of Pliocene Arctic climate to orbital forcing, atmospheric CO_2 and sea ice albedo parameterisation

This chapter has been submitted to Earth and Planetary Science Letters as:

Howell, F. W., Haywood, A. M., and Pickering, S. J. "Sensitivity of Pliocene Arctic climate to orbital forcing, atmospheric CO_2 and sea ice albedo parameterisation", *Earth and Planetary Science Letters*.

Abstract

General circulation model (GCM) simulations of the mid-Pliocene Warm Period (mPWP, 3.264 to 3.025 Myr ago) do not reproduce the magnitude of Northern Hemisphere high latitude surface air and sea surface temperature (SAT and SST) warming that proxy data indicates. There is also large uncertainty regarding the state of sea ice cover in the mPWP. Evidence for both perennial and seasonal mPWP Arctic sea ice is found in analyses of marine sediments, whilst in a multi-model ensemble of mPWP climate simulations, half of the ensemble simulated ice-free summer Arctic conditions. Given the strong influence that sea ice exerts

on high latitude temperatures, a better understanding of the nature of mPWP Arctic sea ice would be highly beneficial in understanding proxy derived estimates of high latitude surface temperature change, and the ability of climate models to reproduce this.

In GCM simulations, the mPWP is typically represented with fixed orbital forcing, usually identical to modern, and atmospheric CO_2 concentrations of $\sim$ 400 ppm. However, orbital forcing varied over the $\sim$ 240,000 years of the mPWP, and it is likely that atmospheric CO_2 varied as well. A previous study has suggested that the parameterisation of sea ice albedo in the HadCM3 GCM may not reflect the sea ice albedo for a warmer climate, where seasonal sea ice constitutes a greater proportion of the Arctic sea ice cover. These three factors, in isolation and combined, can greatly influence the simulation of Arctic sea ice cover and the degree of high latitude surface temperature warming.

This paper explores the impact of various combinations of potential mPWP orbital forcing, atmospheric CO_2 concentrations and minimum sea ice albedo on sea ice extent and high latitude warming. The focus is on the Northern Hemisphere, due to availability of proxy data, and the large data-model discrepancies in this region. Changes in orbital forcings are demonstrated to be sufficient to alter the Arctic sea ice simulated by HadCM3 from perennial to seasonal, although only when atmospheric CO_2 concentrations exceed 300 ppm. Reduction of the minimum sea ice albedo from 0.5 to 0.2 is also sufficient to simulate seasonal sea ice, with any of the combinations of atmospheric CO_2 and orbital forcing. Compared to a mPWP control simulation, monthly mean increases north of 60°N of up to 4.2°C (SST) and 9.8°C (SAT) are simulated. However, data-model comparisons show the model temperatures still fail to match the proxy data temperatures. It is suggested that further high latitude warming may be achieved through adjustments to cloud parameterisation, although the gap between model and data temperature in simulations, even with significantly reduced sea ice cover compared to the control, suggests that agreement may still be difficult to achieve.

6.1 Introduction

The mid-Pliocene Warm Period (mPWP, 3.264 to 3.025 Myr ago (Dowsett *et al.*, 2010)) is widely characterised as a period of sustained warmth in Earth's history (e.g. Haywood & Valdes (2004); Haywood *et al.* (2013b)), with mean annual temperatures thought to be 2-3°C higher than the pre-industrial era. Estimates of mid-Pliocene pCO_2 have typically been within the range of 365-415 ppm (Pagani *et al.*, 2010; Seki *et al.*, 2010), but other studies have suggested that it may have been lower, around 270-300 ppm (e.g. Badger *et al.* (2013); Zhang *et al.* (2013a)). GCM simulations of the mPWP have not reproduced the magnitude of high-latitude warming of sea surface and surface air temperatures (SSTs and SATs) indicated by proxy data (e.g. Dowsett *et al.* (2011); Salzmann *et al.* (2013)). A detailed understanding of forcings which have a strong effect on high latitude climates is therefore important, as their representation in models may have a strong impact on the simulated climates of the past, present and future.

The representation of sea ice in models is one such example, as sea ice can enhance perturbations to the climate via feedback processes such as albedo, in addition to acting as an insulator between the ocean and the atmosphere (Curry *et al.*, 1995; Kellogg, 1975; Maykut, 1978). Previous studies have attempted to reduce the discrepancy between mid-Pliocene high latitude temperature estimates derived from proxy data and model simulated temperatures through reduced sea ice cover, either by artificially removing it year-round in an atmosphere-only simulation (Ballantyne *et al.*, 2013), or by changes to the parameterisation of some sea ice processes (Howell *et al.*, 2014).

Understanding of the state of Arctic sea ice from proxy data in the mid-Pliocene remains limited. Based on the presence of iron grains in marine sediments (located at 87.5°N, 138.3°W), Darby (2008) concludes that the Arctic has had perennial sea ice for the past 14 million years. Analysis of IP_{25}, a sea ice proxy biomarker (Belt *et al.*, 2007; Brown *et al.*, 2014), in two cores (located at 80.2°N, 6.4°E and 80.3°N, 8.1°E) by Knies *et al.* (2014) shows that the mid-Pliocene minimum sea ice margin was located to the north of these two sites. Cronin *et al.* (1993), Moran *et al.* (2006) and Polyak *et al.* (2010) show evidence

from ostracode assemblages and ice rafted debris that appear to suggest that the mid-Pliocene Arctic sea ice cover was seasonal in nature.

The Pliocene Modelling Intercomparison Project (PlioMIP) has compared the output of the simulation of the mPWP by GCMs from eight different modelling groups (Haywood *et al.*, 2013b). Howell *et al.* (2015) showed that variability in the ensemble simulation of mid-Pliocene Arctic sea ice is high in the summer months, where four of the models simulate ice-free summers, and the other four, including HadCM3, maintain at least some sea ice coverage year-round.

Model simulations of the mPWP, such as those performed for PlioMIP, typically represent the mid-Pliocene through a fixed atmospheric CO_2 concentration, usually $\sim$ 400 ppm, and orbital configuration typically identical to modern (Haywood *et al.*, 2011b). However, the mPWP time slab is $\sim 240,000$ years long, across which there may have been variations in pCO_2, as well as changes in orbital forcing, which will have affected the state of the Arctic sea ice cover.

This paper focuses on two main issues. It explores the sensitivity of modelled mid-Pliocene Arctic sea ice in HadCM3 to variations in orbital configuration, atmospheric CO_2 concentration and sea ice albedo parameterisation, in isolation as well as in combinations of these factors. In addition, through focusing on those simulations where there is the most extreme reductions in sea ice, this paper investigates the extent to which such large changes can influence the outcomes of data-model comparison, and if they are capable of bringing model and data results into closer agreement.

6.2 Methods

6.2.1 Model description

The simulations carried out in this paper were run using HadCM3 (Hadley Centre Coupled Climate Model version 3), a coupled atmosphere-ocean GCM from the UK Met Office, incorporating sea ice and vegetation components in addition to the atmosphere and ocean components (Gordon *et al.*, 2000).

The ocean component contains 20 vertical levels, and has a horizontal resolution of $1.25° \times 1.25°$, which gives a grid box at the equator of approximately 139

km × 139 km. Vertical levels are distributed to allow greater resolution closer to the surface (Gordon *et al.*, 2000). The atmosphere component of the model contains 19 vertical levels with a horizontal resolution of 2.5° × 3.75° (latitude × longitude), giving six ocean boxes for every atmosphere grid box. Schemes incorporated in the atmosphere component include a radiation scheme representing effects of minor trace gases (Edwards & Slingo, 1996), a land surface scheme capable of representing the effects of soil moisture melting and freezing (Cox *et al.*, 1999) and a gravity wave drag parameterisation (Gregory *et al.*, 1998).

Parameterisations of ice drift and leads, combined with a basic thermodynamic scheme, are the basis of the sea ice model in HadCM3 (Cattle & Crossley, 1995; Gordon *et al.*, 2000). The thermodynamic scheme is based on the zero-layer model from Semtner (1976), developed from the one-dimensional sea ice model described in Maykut & Untersteiner (1971). Ice dynamics are based on parameterisations described by Bryan (1969), whilst sea ice advection is derived from the mean current speeds in the top 100 m of the ocean, which are based on windstress in HadCM3 (Gordon *et al.*, 2000). The parameterisation of sea ice concentration is based on Hibler (1979). For SATs between -10°C and 0°C, sea ice albedo is a linear function of the temperature. Albedo is 0.8 at -10°C and colder, and 0.5 at 0°C. Salinity of sea ice is constant, at 0.6‰.

6.2.2 Experimental design

This paper investigates the sensitivity of simulated mPWP Arctic sea ice to changes in orbital configuration, atmospheric CO_2 concentrations, and reduced minimum albedo, as well as combinations of these changes. Including the control values, five different orbital configurations are used, three different atmospheric CO_2 concentrations, and two minimum albedo values. All combinations of these are run, giving 30 simulations in total, summarised in Table 6.1, which also describes the notation used to identify individual simulations. Each simulation was run for 500 years, spun off from the same 500 year control run. Climatological averages are based on the last 30 years, and the boundary conditions used are derived from PRISM3D, a reconstruction of mPWP sea surface and deep ocean

temperatures, in addition to sea level, topography, vegetation and ice sheet reconstructions (Dowsett *et al.*, 2010), following the PlioMIP alternate experimental design outlined in Haywood *et al.* (2011b).

6.2.2.1 Orbital configurations

In addition to the control, simulations of the mPWP were run with four alternative orbital configurations selected to test the sensitivity of simulated Arctic sea ice in the mPWP to increased insolation at different times of the year. The four orbits selected were those that, according to the astronomical solution of Laskar *et al.* (2004), gave the greatest insolation at 65°N in the mPWP during January, March, July and September. January and July were selected due to being the middle months of the traditional definitions of winter (DJF) and summer (JJA) respectively. March and September were selected as Arctic sea ice reaches its maximum and minimum extents respectively in these months. Eccentricity, precession and obliquity values for each orbital configuration, including the control, are summarised in Table 6.1.

6.2.2.2 Atmospheric CO_2 concentrations

Simulations with atmospheric CO_2 concentrations of 300 ppm and 500 ppm are run in addition to the control level of 400 ppm. Whilst some studies have suggested that 300 ppm is a plausible pCO_2 value for the mPWP, or at least for some part of the period (e.g. (Badger *et al.*, 2013; Zhang *et al.*, 2013a)), 500 ppm is greater than the maximum values that have normally been suggested for the mid-Pliocene. The 500 ppm solutions are intended to provide a guide to the sensitivity of the Arctic sea ice to changes in pCO_2, and the state of the Arctic climate under extreme forcings to the sea ice, rather than a simulation of a mid-Pliocene climate that is likely to have necessarily existed. CO_2 is only one greenhouse gas, and others such as CH_4 have traditionally been omitted in mid-Pliocene experiments, allowing some room for manoeuvre in terms of greenhouse gas radiative forcing.

6.2.2.3 Minimum sea ice albedo

Recent observations have demonstrated that sea ice albedos are generally lower on seasonal sea ice in comparison to multi-year sea ice (Perovich & Polashenski, 2012; Riihela *et al.*, 2013). Howell *et al.* (2014) suggested that the standard parameterisation of sea ice albedo in HadCM3, with a fixed lower limit of 0.5, may not be appropriate for the mPWP, as with a warmer than present climate the Arctic sea ice cover is likely to have consisted of a greater proportion of seasonal sea ice compared to present day. Howell *et al.* (2014) used parameterisations with alternative lower limits of 0.2, 0.3 and 0.4. The lowest limit of 0.2 is used in the ensemble in this study, along with the standard lower limit of 0.5.

6.2.3 Data analysis techniques

6.2.3.1 Data-model comparison

This paper uses the same methods as Howell *et al.* (2014) for the data-model comparison. Proxy data temperature estimates for SATs are based on palaeobotanical data (Salzmann *et al.*, 2008, 2013) and for SSTs from planktonic foraminiferal assemblages, and Mg/Ca and alkenone palaeothermometry (Dowsett *et al.*, 2013, 2010).

Data sites north of 60°N provide the focus for this paper, as this is where the significant warming is observed in model simulations. Howell *et al.* (2014) focuses on just six data sites, three marine and three terrestrial, as temperature changes are small at all other sites. This paper extends the focus of the DMC to all data sites north of 60°N where the proxy data temperature estimate exceeds the mean annual temperature from the control simulation (see Table 6.2 and Figure 6.1).

The data-model comparison will focus on the difference between the proxy data estimates and the highest mean annual temperature in the ensemble at each data site. In addition to the mean annual temperature, the highest monthly temperature increase in the ensemble at each data site will be shown.

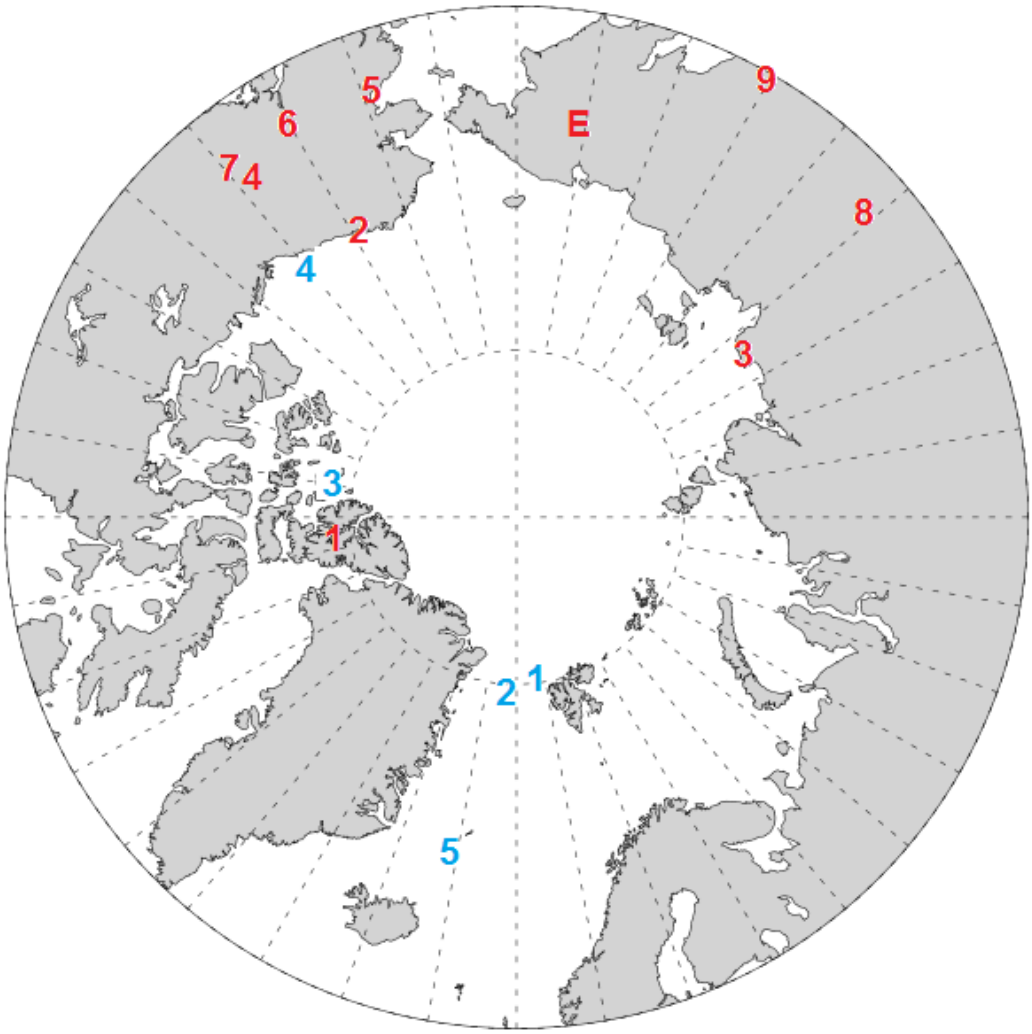

Figure 6.1: Location of marine (blue) and terrestrial (red) data sites.
Marine data sites: 1. ODP 911, 2. ODP 909, 3. Meighen Island, 4. Colvillian, 5. ODP 907.
Terrestrial data sites: 1. Beaver Pond, 2. Ocean Point, 3. Lena River, 4. Alaska Circle, 5. Blizkiy, 6. Nenana Valley, 7. Lost Chicken Mine, 8. Delyankir, 9. Magadan District, E. Lake El'gygytgyn.

6.2.3.2 Energy balance analysis

This paper uses the methods set out in Hill *et al.* (2014) to determine the breakdown of contribution to high latitude SAT changes in selected simulations, enabling an analysis of the differences in patterns of temperature and sea ice changes resulting from the different forcing changes.

6.3 Results

6.3.1 Sea Ice

6.3.1.1 Sea ice extent

Twenty-three of the simulations produce a lower mean annual sea ice extent than the control simulation (10.61×10^6 km^2), with 6 producing higher mean annual extents (all 5 simulations with 300 ppm pCO_2 and standard albedo, and Mar_400_0.5). The annual sea ice extent cycles for each of the 30 simulations are displayed in Figure 6.2. Each panel represents six different boundary condition scenarios, with the only difference between simulations in any given panel being the orbital configuration used.

The effects of just changing the orbital configurations from the PlioMIP experimental design are shown in Figure 6.2(c), which includes the control simulation. Mar_400_0.5 produces a higher mean annual sea ice extent than the control, whilst the other three altered orbital simulations produce lower mean annual extents, the lowest being Jul_400_0.5 with a mean annual extent of 8.92×10^6 km^2, a decrease of 15.90% compared to the control. A striking feature of Figure 6.2(c) is the difference in summer sea ice in the Jul_400_0.5 simulation compared to the other orbital configurations. The Jul_400_0.5 summer sea ice extent is 2.34×10^6 km^2 (70.0%) lower than the control summer sea ice extent, and in September measures just 0.37×10^6 km^2, classified as 'sea ice-free' as it is less than 10^6 km^2 (e.g. Wang & Overland (2009)). This demonstrates the importance of the orbital configuration on the simulation of mid-Pliocene Arctic sea ice.

Raising the atmospheric CO_2 levels to 500 ppm results in a decline in sea ice in every month for all five orbital configurations, with the largest reduction in

Table 6.1: Combinations of orbital configuration (with eccentricity, precession and obliquity values), pCO_2 and minimum sea ice albedo of the 30 simulations.

Experiment name	Orbital Equivalent (kyr BP)	Eccentricity/ Precession/ Obliquity	Global mean annual insolation (W/m^2)	Atmospheric CO_2 concentration (ppmv)	Minimum albedo
Mod_300_0.5				300	0.5
Mod_400_0.5		0.016702		400	0.5
Mod_500_0.5	Modern	0.01628	342.05	500	0.5
Mod_300_0.2		23.439		300	0.2
Mod_400_0.2				400	0.2
Mod_500_0.2				500	0.2
Jan_300_0.5				300	0.5
Jan_400_0.5		0.053487		400	0.5
Jan_500_0.5	3057	-0.02318	342.49	500	0.5
Jan_300_0.2		22.914		300	0.2
Jan_400_0.2				400	0.2
Jan_500_0.2				500	0.2
Mar_300_0.5				300	0.5
Mar_400_0.5		0.040574		400	0.5
Mar_500_0.5	3140	0.02343	342.28	500	0.5
Mar_300_0.2		22.719		300	0.2
Mar_400_0.2				400	0.2
Mar_500_0.2				500	0.2
Jul_300_0.5				300	0.5
Jul_400_0.5		0.051086		400	0.5
Jul_500_0.5	3037	-0.04239	342.45	500	0.5
Jul_300_0.2		23.642		300	0.2
Jul_400_0.2				400	0.2
Jul_500_0.2				500	0.2
Sep_300_0.5				300	0.5
Sep_400_0.5		0.054281		400	0.5
Sep_500_0.5	3053	0.03551	342.50	500	0.5
Sep_300_0.2		22.947		300	0.2
Sep_400_0.2				400	0.2
Sep_500_0.2				500	0.2

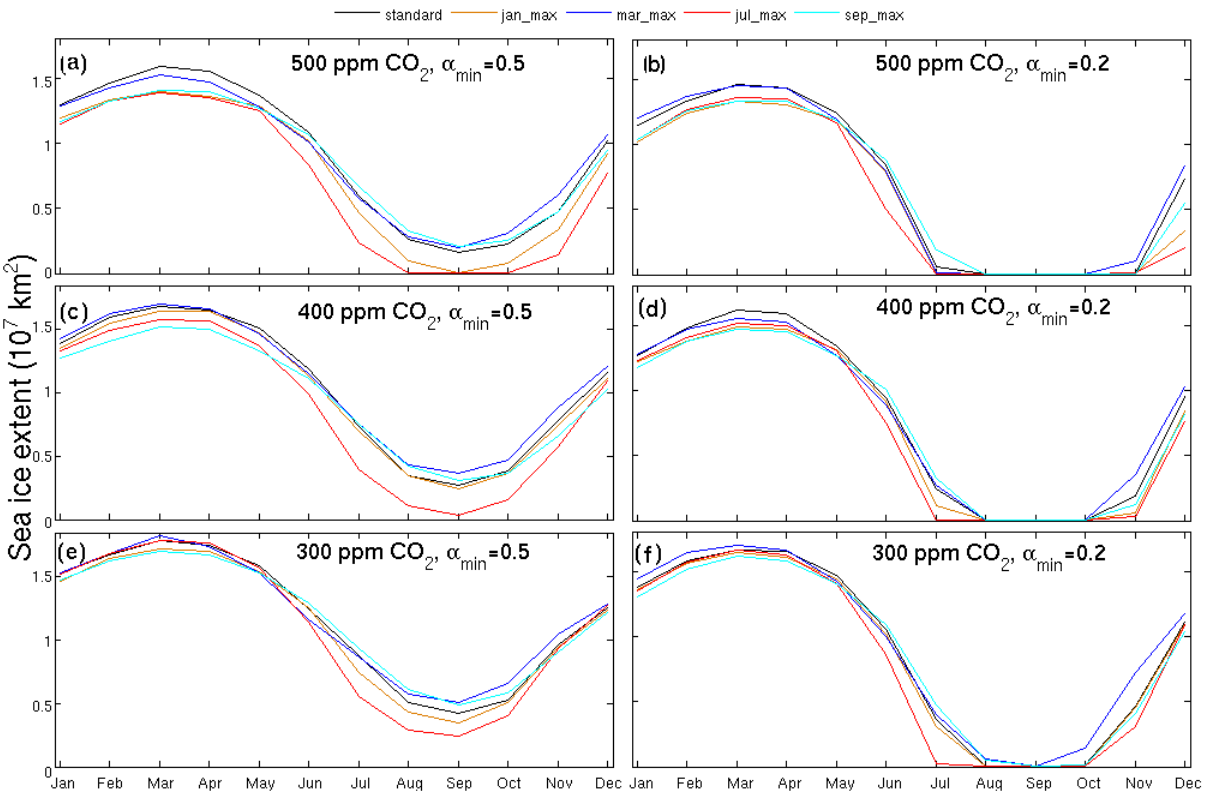

Figure 6.2: Annual sea ice extent (10^7 km^2) cycle for all 30 ensemble members. Each panel shows the five orbital simulations with the same pCO_2 and minimum albedo combinations.

November in each simulation. From August to September, both the Jan_500_0.5 and Jul_500_0.5 simulations produce a sea ice free Arctic, but the extent in the Mod_500_0.5 simulation does not fall below 1.62×10^6 km^2. Reduction of the atmospheric CO_2 concentration to 300 ppm has the effect of an increase in sea ice extent in every month, with none of the simulations in this scenario producing sea ice-free months.

Reducing minimum albedo to 0.2 also causes a decrease in sea ice extent in each month of every orbital simulation, compared to the same orbit under standard conditions. All five simulations produce no sea ice from August to

October, with the Jul_400_0.2 simulation also producing no sea ice in July. With atmospheric CO_2 levels at 300 ppm and reduced minimum albedo, all simulations produce months with an ice-free Arctic, but have a more rapid sea ice growth in November and December compared to the 400 ppm simulation. Increasing the atmospheric CO_2 to 500 ppm with reduced minimum albedo results in a longer ice-free Arctic period in most of the simulations, and a slower recovery in November and December.

The mean annual change in sea ice extent is 2.11×10^6 km^2 (19.9%). The main driver of this is summer sea ice extent, which sees a mean change of 2.35×10^6 km^2 (69.4%), contrasting to a mean winter change of just 1.46×10^6 km^2 (8.88%).

6.3.1.2 Sea ice thickness

Twenty-three simulations produce a thinner mean annual sea ice cover (north of 80°N) in comparison to the control simulation, the same number of simulations that showed a decline in mean annual extent. Mean annual thickness anomalies for eight of the simulations are shown in Figure 6.3. The Sep_400_0.5 simulation simulates a thicker ice cover, despite also simulating a reduced extent. The Jul_300_0.5 simulation simulates thinner than control sea ice, in addition to a greater extent. In all other simulations, the change in mean annual thickness is the same sign as the change in mean annual extent.

The change in mean annual sea ice thickness north of 80°N across the ensemble is 0.73 m (34.3%). The mean change in winter is 0.71 m (20.1%), and 0.65 m (72.6%) in summer. The seasonal changes in thickness are far closer in value in comparison to the extent seasonal changes, although the change of 0.65 m in summer represents a proportionally much greater change from the control than the winter change of 0.71 m.

The simulations with increased atmospheric CO_2 produced less extensive, but thicker winter sea ice in comparison to the simulations with reduced minimum albedo. The mean sea ice thickness north of 80°N thins by an average of 0.54 m in comparison to the control in the increased pCO_2 simulations, whilst the decreased minimum albedo simulations show an average thinning of 0.97 m.

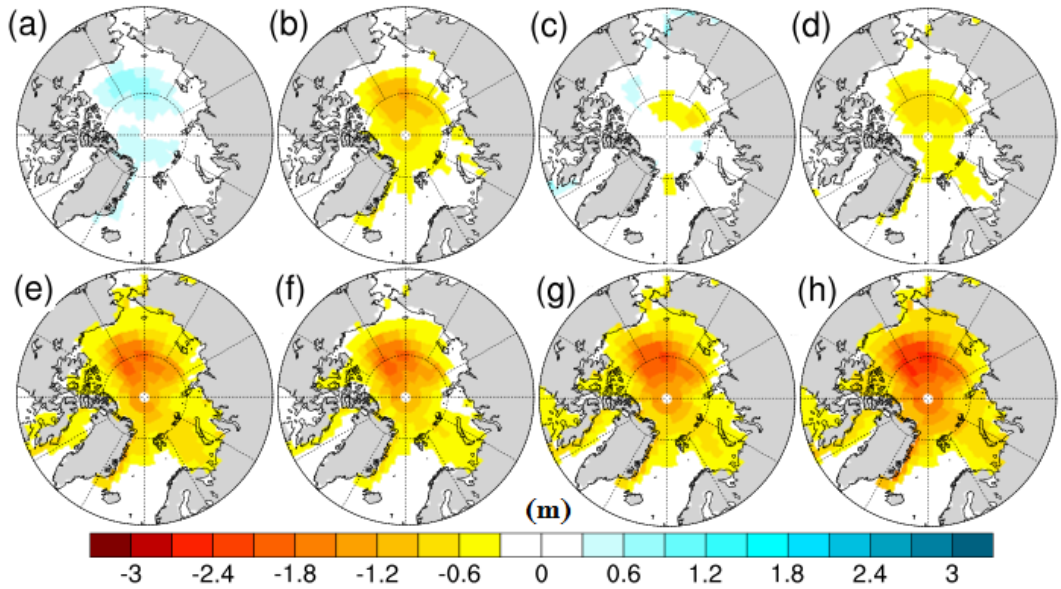

Figure 6.3: Mean annual sea ice thickness (m) anomaly (alternative minus control) for simulations: (a) Mar_400_0.5 (b) Jul_400_0.5 (c) Jul_300_0.5 (d) Mod_500_0.5 (e) Jul_500_0.5 (f) Mod_400_0.2 (g) Mod_500_0.2 (h) Jul_500_0.2.

6.3.2 Temperature changes

6.3.2.1 Annual and seasonal changes

The large reduction in sea ice seen in many of the simulations has substantial effects on SATs and SSTs predicted by the model. Feedback processes mean that reduced sea ice will likely be both a cause of and result of increased temperatures. All simulations where the mean annual sea ice extent was reduced in comparison to the control had increases in the mean annual SATs and SSTs north of 60°N, with the exception of the Mar_300_0.2 simulation, where the mean annual SAT and SST are reduced, in comparison to the control, by 0.18°C and 0.03°C respectively. Figures 6.4 and 6.5 show mean annual SAT and SST anomalies for eight of the ensemble members, whilst Figures 6.6 and 6.7 show the seasonal anomalies for the Jul_500_0.2 simulation, for SAT and SST respectively.

Changes in SAT are on average greater than changes in SST. For example, as a result of increasing pCO_2 to 500 ppm, the mean annual increase in SST north of

60°N compared to the control in those five simulations is 0.85°C, the equivalent increase in SAT is 2.90°C. The patterns of warming are also different, the largest increases in SST typically occur in July and August, whereas the larger SAT increases are observed in November and December. The SST increase is greatest in summer due to the increase in open water, which would previously have been covered by sea ice. This heat is then released into the atmosphere during the autumn as the sea ice refreezes, producing the large SAT autumn increase. As water has a greater specific heat capacity than air, the overall SST response is smaller than the SAT response. This delayed warming effect and lower SST response have been observed and discussed in previous studies (e.g. Howell *et al.* (2014); Kumar *et al.* (2010); Screen & Simmonds (2010a)).

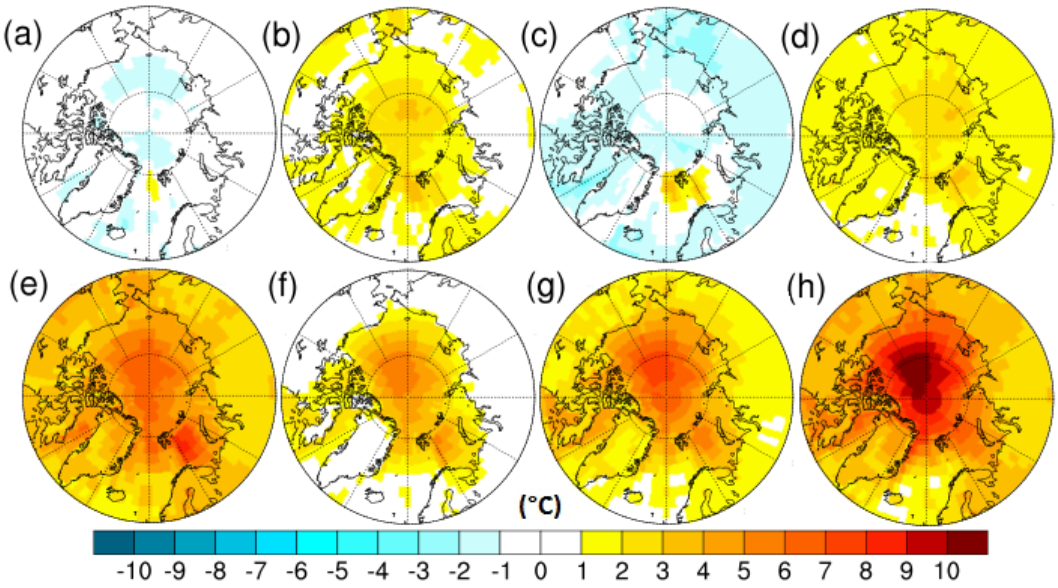

Figure 6.4: Mean annual SAT (°C) anomaly (alternative minus control) for simulations: (a) Mar_400_0.5 (b) Jul_400_0.5 (c) Jul_300_0.5 (d) Mod_500_0.5 (e) Jul_500_0.5 (f) Mod_400_0.2 (g) Mod_500_0.2 (h) Jul_500_0.2.

The largest increases occur in the simulations with both reduced minimum albedo and increased pCO_2. The mean annual increase in SST north of 60°N in these simulations is 1.26°C, with a maximum of 1.78°C in the Jul_500_0.2

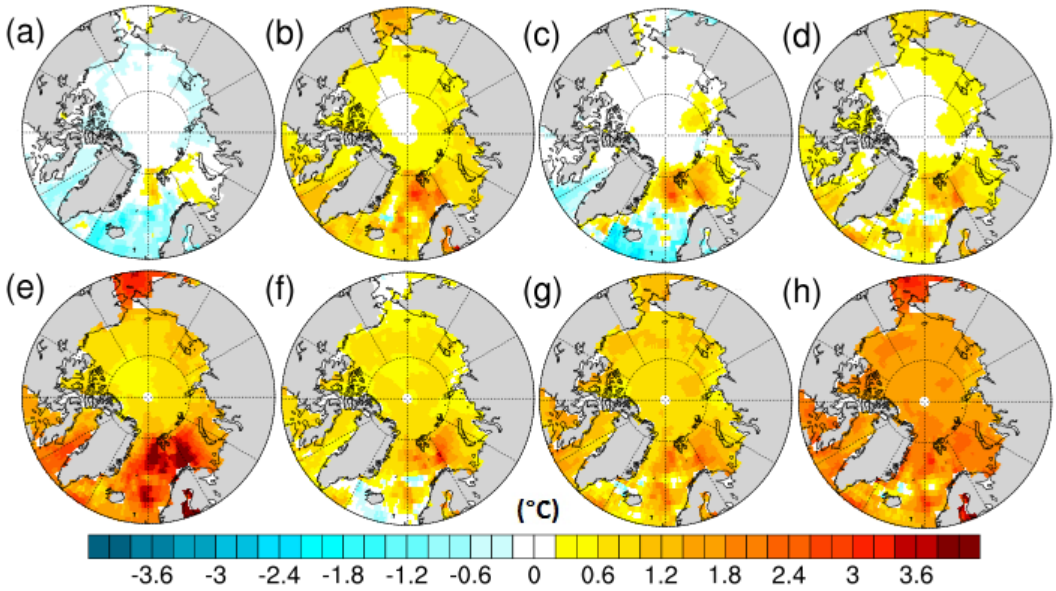

Figure 6.5: Mean annual SST (°C) anomaly (alternative minus control) for simulations: (a) Mar_400_0.5 (b) Jul_400_0.5 (c) Jul_300_0.5 (d) Mod_500_0.5 (e) Jul_500_0.5 (f) Mod_400_0.2 (g) Mod_500_0.2 (h) Jul_500_0.2.

simulation. The highest mean monthly SST increase is 4.19°C in August in Jul_500_0.2. The mean annual SAT increase north of 60°N in the same five simulations is 3.99°C. Jul_500_0.2 also shows the greatest increase in mean annual SAT, with a rise of 4.82°C, whilst the 9.84°C rise in January in the Jan_500_0.2 simulation is the largest rise in any single month.

Focusing north of 80°N, the SAT changes are even greater, the Jul_500_0.2 mean annual increase is 8.25°C, and the increase in December of the same simulation is 19.83°C. SST increases north of 80°N, however, do not show uniformly higher increases compared to north of 60°N. The mean increase in mean annual SST across the five simulations is 1.08°C, the highest single mean annual change being 1.73°C in Jul_500_0.2. The greatest monthly change is higher, however, with August in Jul_500_0.2 showing an SST increase of 5.01°C compared to the control.

Figure 6.8 indicates that the warming north of 60°N from increased pCO_2

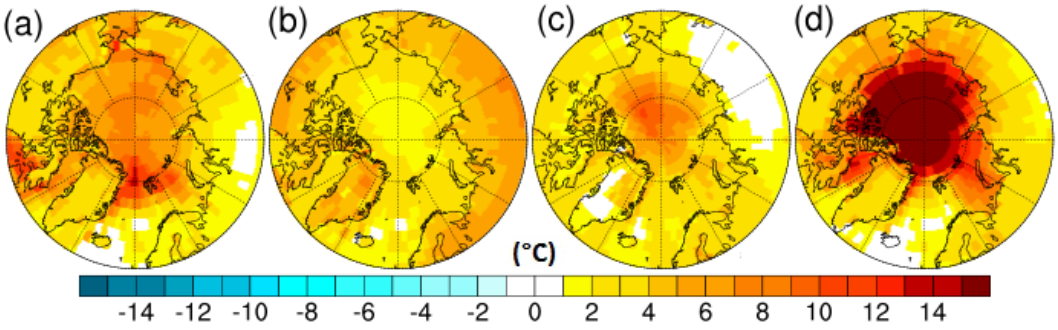

Figure 6.6: Seasonal SAT (°C) anomalies (compared to control) for the Jul_500_0.2 simulation for (a) FMA (b) MJJ (c) ASO (d) NDJ.

is greater than the warming seen in the reduced albedo (400 ppm) simulations (comparing the same orbit), despite there being a smaller reduction in sea ice extent. Whilst this is not also true in all cases when looking at the SST changes, the Jan_500_0.5, Jul_500_0.5 and Sep_500_0.5 simulations with 500 ppm pCO_2 all have higher mean annual SSTs north of 60°N than the same orbital simulations with $\alpha_{min} = 0.2$.

6.3.2.2 Energy balance

Using the methods of Hill *et al.* (2014), energy balance calculations have quantified the contributions of the different components of the SAT warming (compared to the mid-Pliocene control simulation) for the Mod_400_0.2 and Mod_500_0.5 simulations (Figure 6.9). The zonal warming varies more in Mod_400_0.2, with very little temperature change at latitudes south of 60°N, and more than 4°C of warming close to 90°N. The Mod_500_0.5 simulation shows similar levels of warming at all latitudes north of 60°N, between 0.5 and 2°C.

North of 60°N, the largest contribution to SAT warming in Mod_500_0.5 is greenhouse gas emissivity, marginally ahead of clear sky albedo. Cloud emissivity and meridional heat transport have a small warming contribution, whilst there is a small cooling contribution due to cloud albedo. All the individual contributions are less than 1°C. In contrast, in the Mod_400_0.2 simulation, the contribution

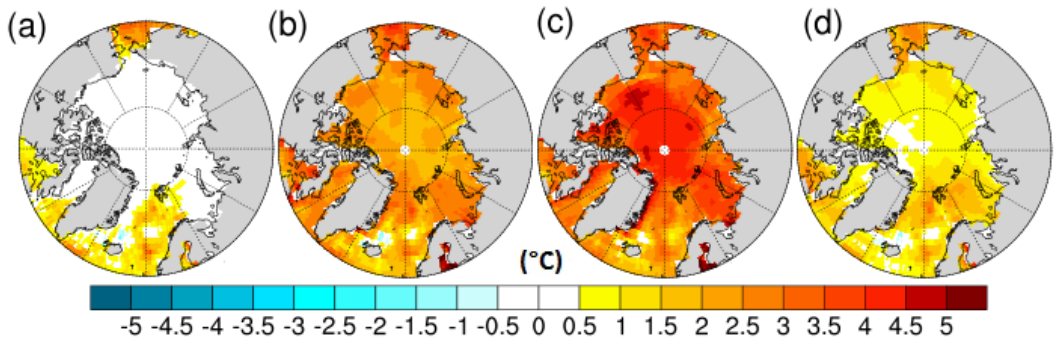

Figure 6.7: Seasonal SST (°C) anomalies (compared to control) for the Jul_500_0.2 simulation for (a) FMA (b) MJJ (c) ASO (d) NDJ.

from clear sky albedo is up to 6°C at high northern latitudes, and makes by far the largest contribution to the warming north of 60°N. Greenhouse gas and cloud emissivity also contribute to the warming, whilst there are cooling contributions of up to 2°C from meridional heat transport, and 3.5°C from cloud albedo.

6.3.2.3 Data-model comparison

Tables 6.2 and 6.3 show the data-model comparison for data sites north of 60°N where the proxy temperature estimate exceeds the control simulation temperature (analysed previously in Howell *et al.* (2014)), showing the greatest temperature increase in the ensemble for each particular site. For all of the SAT sites, and two of the SST sites, the greatest increase relative to the control simulation is seen in the Jul_500_0.2 simulation. The largest increases at the remaining three SST sites come from the Jul_500_0.5 simulation.

The discrepancy between proxy data and model mean annual SSTs has been reduced to less than 0.5°C at two sites, Meighen Island and Colvillian. For the remaining three sites, the gap between the model temperatures and proxy estimates is greater than 3°C, the largest gap at just under 9°C.

At each of the nine SAT data sites north of 60°N, there is an increase in mean annual SAT of at least 3°C in comparison to the control simulation. The highest change in mean annual SAT is seen at Beaver Pond, with an increase of 5.11°C.

Table 6.2: Name and location of terrestrial proxy data sites (see also Figure 6.1), and the differences in SAT at the sites for (from left to right): proxy data minus modern observations, mid-Pliocene model control (mPWP^c) minus pre-industrial (PI) model, mid-Pliocene model control minus proxy data, mid-Pliocene model alternative (mPWP^a) minus proxy data. At each site, the alternative simulation used is the one showing the greatest warming. The percentage change in the differences between the proxy data and the mid-Pliocene simulations is also shown.

Site	Latitude/Longitude	ΔMAT (proxy – observation)	ΔMAT (mPWP^c – PI)	ΔMAT (mPWP^c – proxy)	ΔMAT (mPWP^a – proxy)	Percentage Change
Beaver Pond	78.40°/-82.00°	14.25°C	11.69°C	-14.51°C	-9.40°C	35.2%
Ocean Point	70.00°/-153.00°	13.18°C	7.07°C	-8.92°C	-4.40°C	50.7%
Lena River	72.20°/125.97°	16.25°C	9.26°C	-12.01°C	-8.50°C	29.2%
Alaska Circle	65.50°/-144.08°	8.74°C	5.60°C	-5.26°C	-1.38°C	73.8%
Blizkiy	64.00°/-162.00°	12.62°C	10.44°C	-10.5°C	-7.24°C	31.1%
Nenana Valley	64.53°/-149.08°	6.67°C	3.36°C	-7.01°C	-3.33°C	52.5%
Lost Chicken Mine	64.06°/-141.95°	7.81°C	5.91°C	-4.39°C	-0.43°C	90.2%
Delyankir	63.00°/133.00°	17.82°C	3.53°C	-16.98°C	-13.64°C	19.7%
Magadan District	59.98°/150.65°	6.13°C	6.66°C	-7.05°C	-4.02°C	43.0%

Table 6.3: As Table 6.2, but for marine sites and SSTs.

Site	Latitude/Longitude	ΔMAT (proxy – observation)	ΔMAT (mPWP[c] – PI)	ΔMAT (mPWP[c] – proxy)	ΔMAT (mPWP[a] – proxy)	Percentage Change
Colvillian	70.29°/-150.42°	3.01°C	0.53°C	-2.26°C	-0.42°C	81.4%
ODP 909	78.58°/-3.07°	11.47°C	-1.12°C	-9.82°C	-6.62°C	32.6%
ODP 911	80.47°/8.23°	13.88°C	-1.14°C	-11.14°C	-8.85°C	20.6%
Meighen Island	79.00°/-99.00°	3.50°C	1.30°C	-1.84°C	-0.43°C	76.5%
ODP 907	69.25°/-12.7°	3.32°C	1.71°C	-6.16°C	-3.46°C	45.5%

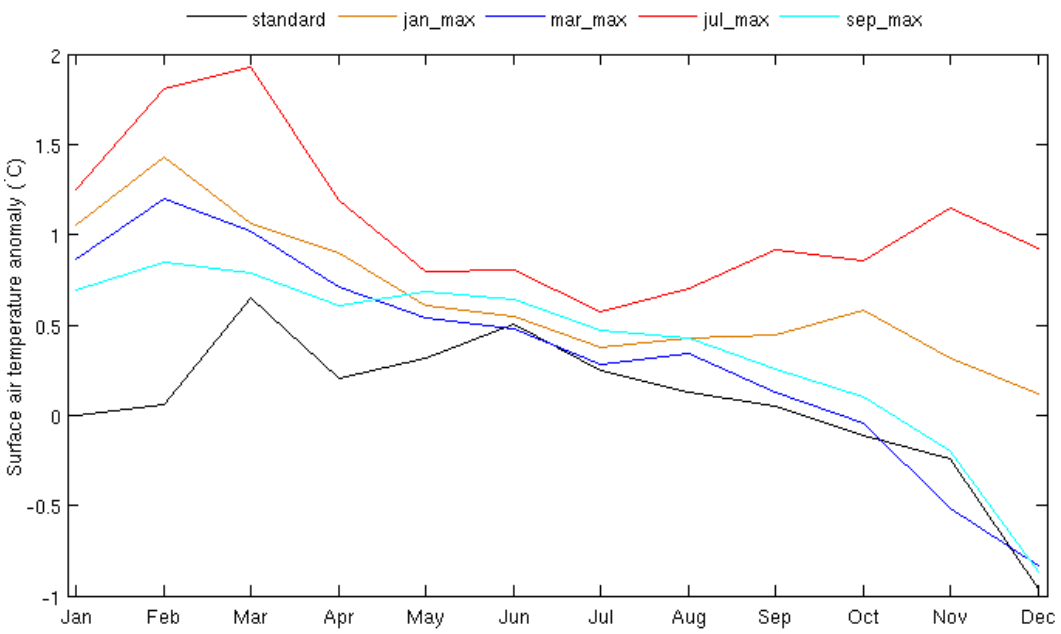

Figure 6.8: Mean annual cycle of the difference in mean SAT north of 60°N between the 5 simulations with 500 ppm pCO_2 and $\alpha_{min} = 0.5$, and the 5 with 400 ppm pCO_2 and $\alpha_{min} = 0.2$. Difference shown is 500_0.5 minus 400_0.2, for the same orbital configurations.

The model temperatures all remain cooler than the proxy estimate, the smallest difference being 0.43°C at Lost Chicken Mine. In the control simulation, the discrepancy was 4.39°C at this site. At only one other site, Alaska Circle, is the model-data difference less than 2°C, at the remaining seven the difference is at least 3°C, the largest difference being 13.64°C at Delyankir.

Analysis of pollen assemblages extracted from sediment at Lake El'gygytgyn (67.30°N, 172.05°E, see Figure 6.1) suggests that warmest monthly SATs at this site in the mid-Pliocene were approximately 16-17°C (Andreev *et al.*, 2014; Brigham-Grette *et al.*, 2013) (not shown in Tables 6.2 or 6.4, as these show mean annual and December SATs). The warmest monthly temperature in the control simulation shows a temperature of 14.36°C at the location of Lake El'gygytgyn, 1.6 - 2.6°C cooler than the indications from proxy data. The model fails to

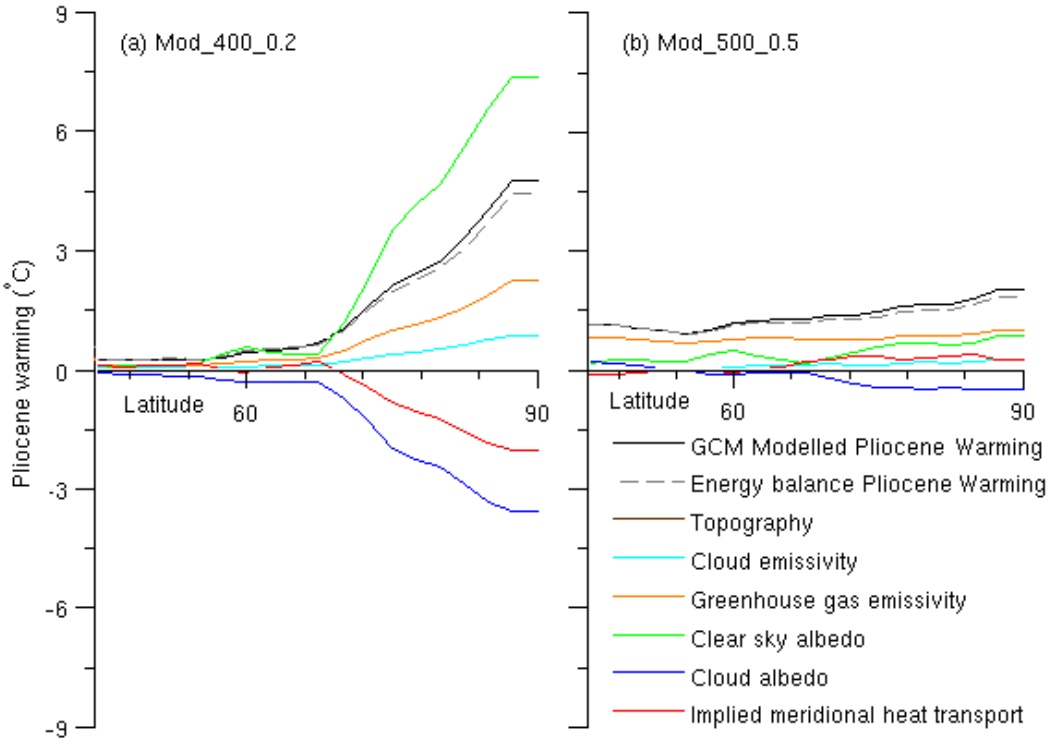

Figure 6.9: Energy balance analysis north of 30°N for (a) Mod_400_0.2 (b) Mod_500_0.2. Plots show zonal mean warming for each of the energy balance components, along with the zonal mean SAT increase compared to the mid-Pliocene control, and the approximated zonal mean SAT increase from the energy balance contributions.

achieve the level of warming indicated by the data, as with the mean annual SATs shown in Table 6.2, but with a smaller temperature discrepancy. Out of the rest of the ensemble, four simulations (Jan_400_0.2, Jul_400_0.2, Jul_300_0.5 and Jul_300_0.2) produced maximum monthly SAT values within the 16-17°C range, with a further four (Jul_400_0.5, Jan_500_0.5, Jul_500_0.5 and Jul_500_0.2) exceeding this range for warmest monthly mean.

Tables 6.2 and 6.3 also shows the mid-Pliocene warming at each site for data and models (using differences between the proxy data temperatures and modern observations, (from Legates & Willmott (1990) and Thompson & Flem-

ing (1996)), and the differences between the simulated mid-Pliocene and pre-industrial temperatures). The model warming exceeds the data warming only at the Magadan District terrestrial site (by 0.53°C). The greatest SAT difference is at Blizkiy (14.29°C), whilst the largest SST difference is at ODP911 (15.02°C). At ODP sites 909 and 911, the pre-industrial SSTs are actually warmer than those from the mid-Pliocene simulation. An important caveat to note is that the observations are from the 20th century, so are likely to be warmer than temperatures from the pre-industrial, for which the model simulation comparisons are run.

At six of the terrestrial sites, and one marine site, the largest increase in the ensemble (compared to the mid-Pliocene control) is greater than the difference between the data and model warming. Under these conditions therefore, the models show a similar, or larger, increase in temperature from the pre-industrial simulation as the proxy data with comparison to modern observations, showing a degree of agreement between the proxies and simulations.

Table 6.4 shows the greatest increase in December SAT (consistently largest SAT increase of all months) in the ensemble from the control, at each terrestrial data site. Out of the nine data sites, the largest monthly change at six of them is smaller than the difference between the mean annual temperature estimates from the proxy data and control simulation, although at Ocean Point, the December increase is just 0.24°C smaller than the data-model mismatch. Table 6.5 shows the greatest increase in August SST (consistently largest SST increase of all months) in the ensemble for each data site. At two sites, Colvillian and Meighen Island, the maximum monthly increase exceeds the model-data mean annual anomaly for the control, but at the three ODP sites, the maximum monthly increase would not be enough to close the data-model disparity, even if it was sustained year-round.

The Jul_500_0.2 simulation provides the greatest increase in mean annual SAT at each terrestrial data site. The sum of the SAT increases at each site from the three simulations with just one change from the control sums to less than the warming produced by the combined simulation. This is in contrast to the mean annual warming over a larger region, such as north of 60°N, where the sum of the mean annual increases of 1.32°C, 1.86°C and 1.79°C are less than the 4.82°C increase of the combined simulation.

Table 6.4: December SAT (°C) increase (compared to mid-Pliocene control) in the ensemble at palaeodata sites at or north of 60°N.

Site	Latitude/Longitude	ΔMAT (mPWP^c – proxy)	ΔT (December) (mPWP^a – mPWP^c)
Beaver Pond	78.40°/-82.00°	-14.51°C	6.97°C
Ocean Point	70.00°/-153.00°	-8.92°C	8.68°C
Lena River	72.20°/125.97°	-12.01°C	6.21°C
Circle, Alaska	65.50°/-144.08°	-5.26°C	6.57°C
Blizkiy	64.00°/-162.00°	-10.5°C	4.81°C
Nenana Valley	64.53°/-149.08°	-7.01°C	7.16°C
Lost Chicken Mine	64.06°/-141.95°	-4.39°C	6.28°C
Delyankir	63.00°/133.00°	-16.98°C	1.89°C
Magadan District	59.98°/150.65°	-7.05°C	2.95°C

Table 6.5: August SST (°C) increase (compared to mid-Pliocene control) in the ensemble at palaeodata sites at or north of 60°N.

Site	Latitude/Longitude	ΔMAT (mPWP^c – proxy)	ΔT (August) (mPWP^a – mPWP^c)
Colvillian	70.29°/-150.42°	-2.26°C	5.39°C
ODP 909	78.58°/-3.07°	-9.82°C	3.79°C
ODP 911	80.47°/8.23°	-11.14°C	3.39°C
Meighen Island	79.00°/-99.00°	-1.84°C	3.64°C
ODP 907	69.25°/-12.7°	-6.16°C	4.00°C

6.4 Discussion

6.4.1 Sea ice

Figure 6.2(c) indicates that a change in orbital forcing is sufficient to cause the mid-Pliocene Arctic to become ice-free at some point during the summer in HadCM3. In the Jul_400_0.5 simulation, sea ice extent dropped to 0.37×10^6 km^2 in September. However, when the atmospheric CO_2 concentration was also lowered to 300 ppm, no simulation was ice-free at any point. This implies that knowing the atmospheric CO_2 concentration to within 100 ppm is important to ascertaining whether the mid-Pliocene Arctic saw sea ice-free conditions (using HadCM3).

The Jan_500_0.5 simulation achieves ice-free conditions in addition to the Jul_500_0.5, but other orbital simulations, notably the standard orbital configuration, do not. This is an important result as it appears to suggest that the Arctic sea ice in the mid-Pliocene is more sensitive to changes that result due to the different orbital configurations than an increase in 100 ppm pCO_2.

The difference between some simulations producing ice-free conditions under 400 ppm but not under 300 ppm is also an important result. Atmospheric CO_2 during the mPWP is likely to have varied during the period, and so, based on the results of these simulations, the coinciding of particular orbital configurations with variations in pCO_2 is crucial to whether the Arctic becomes ice-free or not in HadCM3. This suggests that much tighter age control on proxy data will be required in order to make a consistent data-model comparison.

Sea ice-free conditions in the mid-Pliocene Arctic would contradict Darby (2008), who show evidence from iron grains in the ACEX core (located at 87.5°N, -138.3°E) implying that perennial sea ice was present in the Arctic at least as far back as 14 Myr ago. The samples from the core represent approximately 1 ka, sampled at an average rate through the core of 0.17 Ma (± 0.35). It is possible that there were sea ice-free events during the mid-Pliocene which were missed by the sampling, although Darby (2008) asserts that the probability of each of the 155 ACEX samples missing a time where seasonal ice was present is low.

When minimum albedo is reduced to 0.2, the orbital configuration is less significant, as the sea ice disappears completely in each simulation from August to October, implying that if this is an appropriate parameterisation within HadCM3 for the mPWP, then the orbital configuration is less relevant in relation to the issue of the Arctic being ice-free, although it still makes a difference to the timing and duration of the ice-free conditions. The Jan_400_0.2 and Jul_400_0.2 simulations have faster declines from June to July, and slower recoveries after October, which is likely to have an effect on the surface temperatures. Even under 300 ppm pCO_2, all simulations produce ice-free conditions, with the main effect of the lower pCO_2 appearing to be facilitating a faster sea ice recovery in the winter. Increasing to 500 ppm pCO_2 extends the period time over which the ice-free summer conditions exist, and slows down the winter recovery.

An important caveat in any assessment of the sensitivity of simulated Arctic sea ice is that conclusions are based on the assumption that HadCM3 is able to simulate mid-Pliocene sea ice well. Howell *et al.* (2015) suggested that, based on the limited proxy data evidence regarding Pliocene Arctic sea ice, that HadCM3 had the best agreement with the conclusions of the data in its mPWP simulation of all the PlioMIP models, although other models' CMIP5 sea ice simulations matched modern observations more closely (Shu *et al.*, 2015).

Within the PlioMIP ensemble, HadCM3 was not one of the four models which simulated an ice-free Arctic summer, but did have the lowest summer extent of the four simulations which maintained ice year-round. In light of the sensitivity which HadCM3 displays with regard to orbit, atmospheric CO_2 and albedo parameterisation, similar assessments of other models, both with summer sea ice and without, would provide interesting insights.

6.4.2 Temperatures

Using CAM3, an atmosphere-only model, Ballantyne *et al.* (2013) ran a simulation of the mPWP where Arctic sea ice is absent year round, and showed warming of 10°C to 15°C extending into the continental interior, and subsequently a much closer, although not complete, agreement with proxy data SAT estimates than the control simulation. However, as stated in Ballantyne *et al.* (2013), a complete

absence of sea ice is not likely to be a realistic mid-Pliocene boundary condition. The ensemble simulations with the highest sea ice reduction (Figure 6.2(b)) produce sea ice-free conditions for almost half the year, but by March the extent has recovered to 82.4% of the control value, albeit with a 38.2% drop in mean thickness.

A fully coupled GCM cannot maintain the latent heat transfer from ocean to atmosphere throughout the year that is seen in the atmosphere only simulation of Ballantyne *et al.* (2013), which appears to be required to provide a consistent level of temperature increase in order to close the data-model mismatch. Even if the temperature increases at each site in December were replicated in all other months, this would not be sufficient to produce agreement between models and proxy data temperatures at more than half the terrestrial sites (Table 6.4).

Closer agreement appears to have been achieved at some SST sites, where the model-data anomaly is less than 0.5°C at two sites (Meighen Island and Colvillian). At the other sites north of 60°N however, the situation is similar to the terrestrial mismatch, where if the largest monthly increase (in August for SSTs) were maintained year-round, there would not be agreement between model and proxy data temperatures.

The discrepancy is lower when comparing the temperature increases for models and data, as opposed to just the temperatures, and at some sites the model warming in some ensemble members is close to or exceeds the data warming. However, at three terrestrial and four marine sites, the model warming is still lower than the data warming, even in the warmest simulations.

The simulations with atmospheric CO_2 increased to 500 ppm have higher SATs than the simulations with α_{min} reduced to 0.2 in most months, but larger sea ice extents (Figures 6.2, 6.8). The breakdown of the different contributions to high latitude warming is shown in Figure 6.9. Clear sky albedo is the dominant contributor in the $\alpha_{min} = 0.2$ simulations, coming as a result of the change to the albedo parameterisation and subsequent exposure of greater areas of open water as more ice melts, which will then lead to temperature increases.

Greenhouse gas emissivity is, marginally ahead of clear sky albedo, the largest contributor to warming in the 500 ppm simulations. In these runs, the higher

atmospheric CO_2 concentrations lead to higher temperatures, which leads to melting sea ice. Feedbacks will enhance both sea ice melt and warming in both sets of simulations, but in the $\alpha_{min} = 0.2$ runs, it is initial reductions in sea ice which then drive temperature increases, whilst the reverse is the case in the 500 ppm pCO_2 simulations.

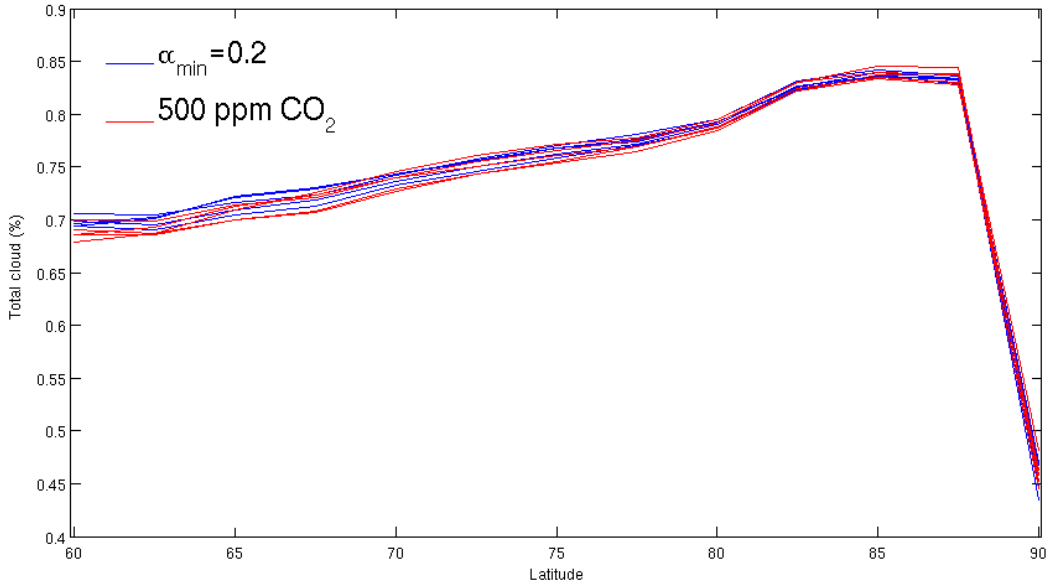

Figure 6.10: Zonal mean total cloud north of 60°N for April-September for the five simulations with $\alpha_{min} = 0.2$ and pCO_2= 400ppm (blue lines), and the five simulations with $\alpha_{min} = 0.2$ and pCO_2= 400ppm (red lines).

In the Mod_400_0.2 simulation, cloud albedo contributed up to 4°C of cooling at high latitudes compared to the control simulation (Figure 6.9). The Mod_500_0.5 simulation showed a much lower cooling contribution due to cloud albedo effects at high latitudes in Mod_400_0.2, and other simulations with reduced minimum albedo. As demonstrated in Figure 6.10, there is little difference between mean zonal total cloud north of 60°N for April-September (months of highest insolation in the Arctic) in the $\alpha_{min} = 0.2$ simulations compared to the 500 ppm simulations, in both annual and monthly means. The energy balance differences may be due to changes in the type of cloud simulated (e.g. different

proportions of low, medium and high cloud), or it may be a reflection of changes to the overall surface albedo at high latitudes (Hill *et al.*, 2014).

However, as the results shown in Figure 6.8 indicate, changes to the model that directly reduce sea ice, such as the changes made to sea ice albedo, do result in greater high latitude temperatures, but do not appear to be as effective as changes which have a more direct impact on temperature changes, such as atmospheric CO_2 increases. This suggests it may be difficult to achieve the large temperature increases necessary to significantly reduce the data-model disagreements through model adjustments which only indirectly lead to higher temperatures. Alternatively, if models cannot simulate sufficiently warm mean annual temperatures at the proxy data locations, even with significant forcings at high latitudes, then the possibility that the temperatures inferred from proxy data relate to maximum or growing season temperatures, as opposed to mean annual seems more likely.

6.5 Conclusions

This results in this paper emphasise the uncertainty with regards to the state of sea ice in the mid-Pliocene Arctic. Howell *et al.* (2015) demonstrated the range of summer sea ice extents from various models, whilst these results show that forcing uncertainties are sufficient, in the simulation of HadCM3, to make a difference between seasonal and perennial sea ice coverage. Results seen in this paper and Howell *et al.* (2015) give a wide range of potential states of mid-Pliocene Arctic sea ice cover derived from multiple climate models. This demonstrates the need for greater coverage of sea ice proxy data for the mid-Pliocene, which can help to identify the most suitable model and forcing combination which reflects the state of sea ice best. Orbital sensitivity to sea ice cover suggests that it may be difficult. If the sea ice cover in the mid-Pliocene moved between seasonal and perennial coverage depending on the orbital configuration, then the proxy information would have to be highly constrained in time to identify these changes.

Given the effect on the SATs and SSTs which are associated with the variations in sea ice cover, the ability to more accurately constrain the sea ice conditions in the mid-Pliocene may also help constrain the resulting high latitude temperature changes. However, it is likely to be difficult to distinguish between

the various ice-free scenarios which are seen in the ensemble. Proxy data would need to indicate the timing of the disappearance and freeze-up of the sea ice, or give an indication to other metrics, such as winter thickness, for which no proxy indicator currently exists.

With the exception of the Meighen Island and Colvillian marine sites, and Lost Chicken Mine and Alaska Circle terrestrial sites, no simulation was able to reduce the data-model discrepancies for mean annual temperature estimates at any of the data sites to less than 3°C, with some discrepancies still exceeding 8°C. Uncertainties associated with the temperature reconstructions are specified for some terrestrial data sites (Salzmann *et al.*, 2013), but none of the alternative anomalies in Table 6.2 are less than any of the given uncertainties. Errors associated with the SST reconstruction methods are less than 2°C (Dowsett *et al.*, 2009), so the alternative anomalies at Meighen Island and Colvillian are within the uncertainties, but not at the other sites (Table 6.3). The percentage change at more than half of the sites is less than 50%, with only one terrestrial and one marine site seeing a reduction exceeding 80%. The effect of even a very dramatic reduction in the total sea ice cover is not capable of producing agreement at most sites, and even if the highest monthly temperature increase compared to the control were replicated year-round, the gap would not be closed at most sites.

As a number of simulations lose summer sea ice the potential impacts of sea ice parameterisation is reduced. However, as the next biggest component in the energy balance, cloud parameterisation could have a significant impact.

As suggested in Ballantyne *et al.* (2013), a year-round absence of sea ice is perhaps the only way that such high temperature increases can be maintained throughout the year in order to get close agreement between models and data. However, there is evidence for the presence of mid-Pliocene Arctic sea ice (e.g. Darby (2008); Knies *et al.* (2014); Polyak *et al.* (2010)), and maintaining ice-free conditions in a coupled AOGCM would require a source of heat into the Arctic during the winter months to prevent freeze-up until the spring. A severely depleted, but not absent, winter sea ice cover might allow for sufficient temperature increase to reduce the data-model mismatch, but it is clear from the results of this study that if there is to be closer agreement between proxy and model temperatures, then even the dramatic reductions in sea ice seen in this study will not

be sufficient on their own, although they can play an important part in reducing the differences between proxy data and model results.

References

Andreev, A.A., Tarasov, P.E., Wennrich, V., Raschke, E., Herzschuh, U., Nowaczyk, N.R., Brigham-Grette, J. & Melles, M. (2014). Late Pliocene and early Pleistocene vegetation history of Northeastern Russian Arctic inferred from the Lake El'gygytgyn pollen record. *Climate of the Past*, **10**, 1017–1039. 157

Badger, M., Schmidt, D., Mackensen, A. & Pancost, R. (2013). High-resolution alkenone palaeobarometry indicates relatively stable pCO_2 during the Pliocene (3.3-2.8 Ma). *Philos. Trans. R. Soc. A*, **68**, 20130094. 6, 7, 8, 68, 140, 143

Ballantyne, A., Axford, Y., Miller, G., Otto-Bliesner, B., Rosenbloom, N. & White, J. (2013). The amplification of Arctic terrestrial surface temperatures by reduced sea-ice extent during the Pliocene. *Palaeogeography Palaeoclimatology Palaeoecology*, **386**, 59–67. 25, 84, 140, 162, 163, 166, 183

Belt, S., Masse, G., Rowland, S., Poulin, M., Michel, C. & LeBlanc, B. (2007). A novel chemical fossil of palaeo sea ice: IP_{25}. *Organic Geochemistry*, **38**, 16–27. 51, 52, 140

Brigham-Grette, J., Melles, M., Minyuk, P., Andreev, A., Tarasov, P., DeConto, R., Koenig, S., Nowaczyk, N., Wennrich, V., Rosn, P., Haltia, E., Cook, T., Gebhardt, C., Meyer-Jacob, C., Snyder, J. & Herzschuh, U. (2013). Pliocene warmth, polar amplification, and stepped Pleistocene cooling recorded in NE Arctic Russia. *Science*, **340**, 1421–1427. 157

Brown, T., Belt, S., Tatarek, A. & Mundy, C. (2014). Source identification of the Arctic sea ice proxy IP_{25}. *Nature Communications*, **5**. 140

Bryan, K. (1969). Climate and the ocean circulation III: The ocean model. *Mon Weather Rev*, **97**, 806–827. 46, 49, 61, 62, 75, 142, 188

Cattle, H. & Crossley, J. (1995). Modeling Arctic climate change. *Philosophical Transactions of the Royal Society A-Mathematical, Physical and Engineering Sciences*, **352**, 201–213. 62, 63, 71, 75, 94, 117, 142, 188, 189

Cox, P., Betts, R., Bunton, C., Essery, R., Rowntree, P. & Smith, J. (1999). The impact of new land surface physics on the GCM simulation of climate and climate sensitivity. *Climate Dynamics*, **15**, 183–203. 60, 142

Cronin, T.M., Whatley, R., Wood, A., Tsukagoshi, A., Ikeya, N., Brouwers, E.M. & Briggs, W.M. (1993). Microfaunal evidence for elevated Pliocene temperatures in the Arctic ocean. *Paleoceanography*, **8**, 161–173. 24, 74, 92, 124, 140, 181

Curry, J.A., Schramm, J.L. & Ebert, E.E. (1995). Sea ice-albedo climate feedback mechanism. *Journal of Climate*, **8**, 240–247. 34, 37, 38, 45, 73, 118, 140

Darby, D.A. (2008). Arctic perennial ice cover over the last 14 million years. *Paleoceanography*, **23**, PA1S07. 58, 92, 116, 124, 140, 161, 166, 181

Dowsett, H., Robinson, M. & Foley, K. (2009). Pliocene three-dimensional global ocean temperature reconstruction. *Climate of the Past*, **5**, 769–783. 16, 17, 82, 84, 166

Dowsett, H., Haywood, A., Valdes, P., Robinson, M., Lunt, D., Hill, D., Stoll, D. & Foley, K. (2011). Sea surface temperatures of the mid-Piacenzian Warm Period: A comparison of PRISM3 and HadCM3. *Palaeogeography Palaeoclimatology Palaeoecology*, **309**, 83–91. 1, 27, 29, 73, 140

Dowsett, H., Foley, K., Stoll, D., Chandler, M., Sohl, L., Bentsen, M., Otto-Bliesner, B., Bragg, F., Chan, W.L., Contoux, C., Dolan, A., Haywood, A., Jonas, J., Jost, A., Kamae, Y., Lohmann, G., Lunt, D., Nisancioglu, K., Abe-Ouchi, A., Ramstein, G., Riesselman, C., Robinson, M., Salzmann, U., Stepanek, C., Strother, S., Ueda, H., Yan, Q. & Zhang, Z. (2013). Sea Surface Temperature of the mid-Piacenzian Ocean: A Data-Model Comparison. *Sci. Rep.*, **3**, 149–163. 77, 144

Dowsett, H.J., Robinson, M.M., Haywood, A.M., Salzmann, U., Hill, D.J., Sohl, L., Chandler, M.A., Williams, M., Foley, K. & Stoll, D. (2010). The PRISM3D paleoenvironmental reconstruction. *Stratigraphy*, **7**, 123–139. 1, 3, 4, 5, 9, 16, 17, 18, 21, 66, 73, 76, 77, 83, 92, 95, 140, 143, 144, 190, 191

Edwards, J. & Slingo, A. (1996). Studies with a flexible new radiation code. 1: Choosing a configuration for a large-scale model. *Quarterly Journal of the Royal Meteorological Society*, **122**, 689–719. 60, 142

Gordon, C., Cooper, C., Senior, C.A., Banks, H., Gregory, J.M., Johns, T.C., Mitchell, J.F.B. & Wood, R.A. (2000). The simulation of SST, sea ice extents and ocean heat transports in a version of the Hadley Centre coupled model without flux adjustments. *Climate Dynamics*, **16**, 147–168. 2, 59, 60, 61, 62, 63, 64, 65, 75, 122, 141, 142, 188, 189

Gregory, D., Shutts, G. & Mitchell, J. (1998). A new gravity-wave-drag scheme incorporating anisotropic orography and low-level wave breaking: Impact upon the climate of the UK Meteorological Office Unified Model. *Quarterly Journal of the Royal Meteorological Society*, **124**, 463–493. 60, 142

Haywood, A. & Valdes, P. (2004). Modelling Pliocene warmth: contribution of atmosphere, oceans and cryosphere. *Earth and Planetary Science Letters*, **218**, 363–377. 25, 26, 73, 140

Haywood, A.M., Dowsett, H.J., Robinson, M.M., Stoll, D.K., Dolan, A.M., Lunt, D.J., Otto-Bliesner, B.L. & Chandler, M.A. (2011).

Pliocene Model Intercomparison Project (PlioMIP): experimental design and boundary conditions (Experiment 2). *Geosci. Model Dev.*, **4**, 571–577. 29, 30, 70, 76, 93, 95, 141, 143, 189

Haywood, A.M., Hill, D.J., Dolan, A.M., Otto-Bliesner, B.L., Bragg, F.J., Chan, W.L., Chandler, M.A., Contoux, C., Dowsett, H.J., Jost, A., Kamae, Y., Lohmann, G., Lunt, D.J., Abe-Ouchi, A., Pickering, S.J., Ramstein, G., Rosenbloom, N.A., Salzmann, U., Sohl, L., Stepanek, C., Ueda, H., Yan, Q. & Zhang, S.Z. (2013). Large-scale features of Pliocene climate: results from the Pliocene Model Intercomparison Project. *Clim. Past*, **9**, 191–209. 1, 3, 29, 30, 73, 92, 140, 141

Hibler, W.D. (1979). A dynamic-thermodynamic sea ice model. *Journal of Physical Oceanography*, **9**, 815–846. 47, 48, 49, 62, 75, 117, 142, 188

Hill, D.J., Haywood, A.M., Lunt, D.J., Hunter, S.J., Bragg, F.J., Contoux, C., Stepanek, C., Sohl, L., Rosenbloom, N.A., Chan, W.L., Kamae, Y., Zhang, Z., Abe-Ouchi, A., Chandler, M.A., Jost, A., Lohmann, G., Otto-Bliesner, B.L., Ramstein, G. & Ueda, H. (2014). Evaluating the dominant components of warming in Pliocene climate simulations. *Climate of the Past*, **10**, 79–90. 117, 123, 146, 153, 165

Howell, F.W., Haywood, A.M., Dolan, A.M., Dowsett, H.J., Francis, J.E., Hill, D.J., Pickering, S.J., Pope, J.O., Salzmann, U. & Wade, B.S. (2014). Can uncertainties in sea ice albedo reconcile patterns of data-model discord for the Pliocene and 20th/21st centuries? *Geophysical Research Letters*, **41**, 2011–2018. 117, 140, 144, 151, 154

Howell, F.W., Haywood, A.M., Otto-Bliesner, B.L., Bragg, F., Chan, W.L., Chandler, M.A., Contoux, C., Kamae, Y., Abe-Ouchi, A., Rosenbloom, N.A., Stepanek, C. & Zhang, Z. (2015). Arctic sea ice in the PlioMIP ensemble: is model performance for modern climates a reliable guide to performance for the past or the future? *Climate of the Past Discussions*, **11**, 1263–1312. 141, 162, 165

Kellogg, W. (1975). Climatic feedback mechanisms involving the polar regions. *Climate of the Arctic*, 111–116. 34, 73, 140

Knies, J., Cabedo-Sanz, P., Belt, S.T., Baranwal, S., Fietz, S. & Rosell-Melé, A. (2014). The emergence of modern sea ice cover in the Arctic Ocean. *Nat. Commun.*, **5:5608**. 53, 58, 115, 116, 124, 140, 166

Kumar, A., Perlwitz, J., Eischeid, J., Quan, X., Xu, T., Zhang, T., Hoerling, M., Jha, B. & Wang, W. (2010). Contribution of sea ice loss to Arctic amplification. *Geophysical Research Letters*, **37**. 34, 45, 82, 151

Laskar, J., Robutel, P., Joutel, F., Gastineau, M., Correia, A. & Levrard, B. (2004). A long-term numerical solution for the insolation quantities of the Earth. *Astronomy and Astrophysics*, **428**, 261–285. 67, 81, 143, 189

Legates, D. & Willmott, C. (1990). Mean seasonal and spatial variability in global surface air temperature. *Theor. Appl. Climatol.*, **41**, 11–21. 64, 65, 158

Maykut, G. (1978). Energy exchange over young sea ice in the central Arctic. *Journal Of Geophysical Research - Oceans*, **83**, 3646–3658. 34, 40, 41, 73, 140

Maykut, G. & Untersteiner, N. (1971). Some results from a time-dependent thermodynamic model of sea ice. *Journal of Geophysical Research*, **76**, 1550–1575. 46, 47, 48, 50, 61, 142, 188

Moran, K., Backman, J., Brinkhuis, H., Clemens, S.C., Cronin, T., Dickens, G.R., Eynaud, F., Gattacceca, J., Jakobsson, M., Jordan, R.W., Kaminski, M., King, J., Koc, N., Krylov, A., Martinez, N., Matthiessen, J., McInroy, D., Moore, T.C., Onodera, J., O'Regan, M., Pälike, H., Rea, B., Rio, D., Sakamoto, T., Smith, D.C., Stein, R., St John, K., Suto, I., Suzuki, N., Takahashi, K., Watanabe, M., Yamamoto, M., Farrel, J., Frank, M., Kubik, P., Jokat, W. & Kristoffersen, Y. (2006). The Cenozoic palaeoenvironment of the Arctic Ocean. *Nature*, **441**, 601–605. 74, 92, 124, 140, 181

Pagani, M., Liu, Z., LaRiviere, J. & Ravelo, A.C. (2010). High Earth-system climate sensitivity determined from Pliocene carbon dioxide concentrations. *Nature Geoscience*, **3**, 27–30. 6, 8, 73, 92, 140, 189

Perovich, D. & Polashenski, C. (2012). Albedo evolution of seasonal Arctic sea ice. *Geophysical Research Letters*, **39**. 39, 40, 41, 74, 83, 144, 176, 177

Polyak, L., Alley, R.B., Andrews, J.T., Brigham-Grette, J., Cronin, T.M., Darby, D.A., Dyke, A.S., Fitzpatrick, J.J., Funder, S., Holland, M.M., Jennings, A.E., Miller, G.H., O'Regan, M., Savelle, J., Serreze, M., St John, K., White, J.W.C. & Wolff, E. (2010). History of sea ice in the Arctic. *Quaternary Science Reviews*, **29**, 1757–1778. 51, 55, 57, 58, 74, 92, 124, 140, 166, 181

Riihela, A., Mannien, T. & Laine, V. (2013). Observed changes in the albedo of the Arctic sea-ice zone for the period 1982-2009. *Nature Climate Change*, **3**, 895–898. 39, 144, 176

Salzmann, U., Haywood, A., Lunt, D., Valdes, P. & Hill, D. (2008). A new global biome reconstruction and data-model comparison for the Middle Pliocene. *Global Ecology and Biogeography*, **17**, 432–447. 17, 21, 22, 23, 28, 77, 144, 191

Salzmann, U., Dolan, A., Haywood, A., Chan, W.L., Voss, J., Hill, D., Abe-Ouchi, A., Otto-Bliesner, B., Bragg, F., Chandler, M., Contoux, C., Dowsett, H., Jost, A., Kamae, Y., Lohmann, G., Lunt, D., Pickering, S., Pound, M., Ramstein, G., Rosenbloom, N., Sohl, L., Stepanek, C., Ueda, H. & Zhang, Z. (2013). Challenges in quantifying Pliocene terrestrial warming revealed by data-model discord. *Nature Climate Change*, **3**, 969–974. 1, 27, 28, 73, 77, 81, 84, 140, 144, 166

Screen, J. & Simmonds, I. (2010). Increasing fall-winter energy loss from the Arctic Ocean and its role in Arctic temperature amplification. *Geophysical Research Letters*, **37**. 45, 82, 151

Seki, O., Foster, G.L., Schmidt, D.N., Mackensen, A., Kawamura, K. & Pancost, R.D. (2010). Alkenone and boron-based Pliocene pCO_2 records. *Earth and Planetary Science Letters*, **292**, 201–211. 6, 7, 8, 73, 92, 140, 189

Semtner, A.J. (1976). A model for the thermodynamic growth of sea ice in numerical investigations of climate. *Journal of Physical Oceanography*, **6**, 379–389. 47, 48, 49, 61, 62, 75, 117, 142, 188

Shu, Q., Song, Z. & Qiao, F. (2015). Assessment of sea ice simulations in the CMIP5 models. *The Cryosphere*, **9**, 399–409. 93, 111, 112, 162

Thompson, R. & Fleming, R. (1996). Middle Pliocene vegetation: Reconstructions, paleoclimatic inferences, and boundary conditions for climate modeling. *Marine Micropaleontology*, **27**, 27–49. 20, 21, 158, 191

Wang, M. & Overland, J. (2009). A sea ice free summer Arctic within 30 years? *Geophysical Research Letters*, **36**. 146, 178

Zhang, J., Lindsay, R., Schweiger, A. & Steele, M. (2013). The impact of an intense summer cyclone on 2012 Arctic sea ice retreat. *Geophysical Research Letters*, **40**, 720–726. 6, 7, 8, 44, 68, 92, 140, 143

Chapter 7

Discussion and conclusions

The aim of this research was to investigate the nature of sea ice in the mid-Pliocene Warm Period, and its effects on the climate of northern high latitudes. This thesis has suggested alternative parameterisations of sea ice albedo in the HadCM3 model, and demonstrated how these change the simulation of the climate of the mid-Pliocene Arctic. The response of sea ice and wider climatic impacts is explored further by applying increased orbital and CO_2 forcings, and combining these with alternative albedo parameterisations. Model dependency of mPWP Arctic sea ice simulation is explored in analysis of the output from the Pliocene Modelling Intercomparison Project.

7.1 Summary

After outlining the project rationale, and identifying the aims and objectives for this thesis, chapter 1 reviewed the current literature regarding the climate of the mPWP, previous modelling studies concerning the period, and data-model comparisons. Chapter 2 provided a review of current literature concerning sea ice, discussing the impact of sea ice on climate, the history of sea ice observations, how sea ice modelling has progressed, and the development of proxies for past sea ice cover. Chapter 3 outlined the methodology for chapters 4-6 of the thesis, and included a description of HadCM3, the model which performed the majority of simulations analysed in this thesis. Chapter 4 presented the results of simulations of the mPWP and modern climate where the minimum sea ice albedo was

adjusted. This included a data-model comparison for high-latitude sites, as well as a comparison of simulated minimum Arctic sea ice extent with observations. Chapter 5 analysed the simulation of Arctic sea ice for both pre-industrial and mid-Pliocene climates by eight different GCMs. Chapter 6 focused on the impact of uncertainties in orbital forcing, atmospheric CO_2 concentrations and minimum sea ice albedo, in isolation and combination, on mid-Pliocene Arctic sea ice and temperatures. A data-model comparison, similar to that seen in chapter 4, is presented.

7.2 Research questions

In section 1.1, three research questions were outlined. The next section reviews how these were answered by the results presented in chapters 4-6.

7.2.1

1. Is it appropriate to use the same parameterisation of sea ice albedo for simulations of different climate states? Are there alternative parameterisations for the mid-Pliocene that can substantially improve data-model disagreements?

Recent observations have demonstrated how the albedo of Arctic sea ice has changed as the proportion of first year sea ice increases (e.g. Perovich & Polashenski (2012); Riihela *et al.* (2013)). The control simulation of the mPWP by HadCM3 does not simulate an ice-free Arctic in the summer, but the minimum extent is much reduced in comparison to the pre-industrial simulation. The difference between the maximum and minimum extent is greater in the mid-Pliocene simulation, and so the maximum sea ice extent in March contains more first year sea ice than the pre-industrial simulation. With the standard sea ice albedo parameterisation, the sea ice albedo can not be lower than 0.5, yet as the observations of Perovich & Polashenski (2012) demonstrate, the albedo can be lower than this, with albedo measurements of 0.2 observed.

In HadCM3, the sea ice albedo is dependent only on the surface temperature. This means that when the minimum is reduced to 0.2, the sea ice albedo will take that value, or close to it, when the SAT is at or near 0°C. This might overrepresent lower albedo values, which were only observed by Perovich & Polashenski (2012) amongst times of large melt pond coverage, which is variable through the melting season (Polashenski *et al.*, 2012). Lowering the minimum albedo to 0.2 might therefore mean that low albedo values are represented at the expense of the average albedo in the model less accurately representing the actual sea ice albedo. As there is large uncertainty concerning the nature of Arctic sea ice in the mid-Pliocene, it is difficult to assess what the average albedo of the sea ice cover would have been.

Minor adjustments to relatively simplistic parameterisations such as the representation of sea ice albedo in HadCM3 may be able to closer reflect sea ice albedo for a different climate state, but larger improvements would likely be achieved by implementing a more sophisticated parameterisation that was able to simulate an albedo based on factors such as sea ice age, ridging and melt pond coverage, in addition to temperature. Such a parameterisation may also be suitable for use when simulating different climate states, as opposed to the HadCM3 parameterisation, where manual adjustments may be necessary.

To determine for certain whether or not it is appropriate to use the same parameterisation of sea ice albedo for different climate states would require sufficiently comprehensive observations or proxy reconstructions of the climate states being simulated. Currently proxy reconstructions are not detailed enough, and modern satellite observations only began in 1979, although other less comprehensive observations exist prior to then. Figure 4.3 in chapter 4 shows that although the HadCM3 control mean September Arctic sea ice extent is lower than the observational means, there are individual years when the observations are lower, so there is overlap, and potentially could be closer agreement depending on the natural variability. The trend in September sea ice extent from 1979 is -0.793×10^6 km^2/decade for observations, and -0.329×10^6 km^2/decade for the models for the same time period. However, for the most recent ten years of observations, the observational trend increases to -1.31×10^6 km^2/decade, whereas there is much less change in the modelled trend over this period (-0.351×10^6 km^2/decade).

It should be noted that this difference in trend is only based on a ten-year period, and so any conclusions from this should be treated with caution. Over a longer period, the model and observed trends may be very similar. However, the fact that the models have not simulated this increased downward trend seen in the observations could be a sign that, as the nature of the sea ice cover is changing and becoming more dominated by first year ice, the standard model set up is no longer best reflecting the overall state of the Arctic sea ice albedo. This evidence, albeit very limited, may be indicating that the use of the same parameterisation of sea ice albedo, at least a simplistic one as used in HadCM3, cannot reflect changes in sea ice albedo that occur even in relatively small shifts in climate state. Analysis based on longer time periods are necessary for greater confidence in any conclusions. It should be noted that forcings other than from CO_2 emissions (e.g. from other greenhouse gases, aerosols, volcanoes) are not accounted for in the historical simulations, and this may affect the comparison of the simulations against the observations.

In the mid-Pliocene simulations, reduction of the minimum albedo caused a shift in the simulated sea ice cover from perennial to seasonal. With the minimum albedo at 0.2 or 0.3, no sea ice was simulated from August to October. With a minimum albedo value of 0.4, HadCM3 simulates a September sea ice extent of 0.77×10^6 km^2, less than 1.00×10^6 km^2, so also meets the definition of a sea ice free Arctic (e.g. Wang & Overland (2009)). As discussed previously, proxy data evidence concerning whether mid-Pliocene sea ice was seasonal or perennial is conflicted. Without knowing what the nature of mid-Pliocene Arctic sea ice may have been, it is difficult to judge if any of the alternative parameterisations of sea ice albedo are more suitable or not.

Whilst the simulations of mid-Pliocene Arctic sea ice have very limited proxy data to compare to, there is greater coverage of temperature proxy data. As detailed in chapter 4, whilst the reduction of the minimum albedo to 0.2 results in some large increases in Arctic temperatures, particularly SAT in the autumn, the data-model disagreement shows only a small reduction.

As discussed in chapter 4, the strength of inland heat transfer in HadCM3 may be a factor in the much smaller temperature changes at the terrestrial data sites compared to over the central Arctic. However, though annual increases of

over 5°C are seen in the Arctic, it is only over a relatively small area, so even if some of this heat increase moved further inland, it is still not likely to create a particularly large increase in SAT to result in much closer agreement with the data.

The results from chapter 4 show that even if the lower albedo minimum of 0.2 is more appropriate for the mid-Pliocene simulation, whilst the increase in warming reduces the data-model disagreement slightly, is not close to achieving agreement between the two.

7.2.2

2. What is the spread between different models simulation of the mid-Pliocene sea ice? How does the ensemble variability compare to the same models simulation of the pre-industrial climate?

In terms of spread between the PlioMIP ensemble members' simulation of mid-Pliocene sea ice, one of the most key findings of the analysis in chapter 5 is that four of the eight ensemble members simulate ice-free conditions in the Arctic in summer. As discussed previously, understanding of mid-Pliocene Arctic sea ice is low, but the discussion surrounding whether the ice was perennial or seasonal is a key issue around which there is uncertainty.

There is also variation within the four models that simulated year-round sea ice in the Arctic, from HadCM3 which simulates a small amount of lower concentration sea ice, all contained within the Arctic basin, to MRI where a substantial proportion of the summer sea ice is at 100% concentration. The PlioMIP ensemble provides several quite different realisations of Arctic sea ice cover in the mid-Pliocene summer.

Whilst there are differences in the winter sea ice simulated by the ensemble, the overall spread is lower, which is evidenced by the coefficient of variation calculations, indicating a large increase in the summer months. In winter, 100% concentration sea ice covers everywhere north of 80°N, and the region north of the Bering strait between the latitudes of 90°E and 90°W (through 180°E) in all

models, with the exception of NorESM, where there is some open ocean north of 80°N.

There is greater variation in the ensemble thickness simulation, although a similar pattern to the extent is seen, with the greatest variation in the summer months. Thickness is a factor that is likely to vary more than extent - as discussed, there are large regions where all the models will simulate 100% coverage in the winter, and therefore the models will be in complete agreement with regards to the extent, whereas the thickness of the ice across the region has the potential to vary much more. The higher variability of thickness in summer is likely to be strongly influenced by the four models which simulate ice-free summers.

Figure 5.10 appears to offer a simple explanation of model differences in simulated sea ice, as there is a strong correlation between surface temperatures and sea ice extent and volume. However, these strong correlations are not observed in the pre-industrial simulations, and given that there is a positive feedback between sea ice reduction and temperature increase, it is difficult to ascribe any certainty to whether the increased temperature is the cause of sea ice reduction in the mid-Pliocene, or whether some of the increased temperature is due to the reduction in sea ice.

The influence of multi-decadal oscillations, such as the North Atlantic Oscillation (NAO) or Atlantic multi-decadal oscillation (AMO) on Arctic sea ice is discussed in chapter 5, but their effects on the PlioMIP ensemble sea ice simulation was not explored, due to the differences in run length and averaging periods of the simulations. It is possible that in the pre-industrial simulations, there was a stronger influence on the simulated sea ice during the averaging periods compared to the mid-Pliocene simulations, which could explain why the influence of the surface temperatures appears to be weaker in the pre-industrial ensemble.

7.2.3

3. To what extent can atmospheric CO_2 uncertainty and orbital variations influence the nature of simulated Pliocene sea ice, and thereby high latitude temperatures? What is the optimal combination of these

factors in the model?

Both atmospheric CO_2 and orbital forcing were demonstrated to have a strong influence on the simulation of the Arctic sea ice cover by HadCM3. In particular, it was shown that changes in either one of these factors could have a significant impact on whether HadCM3 simulated ice-free conditions in the mid-Pliocene summer.

As discussed previously in chapters 5 and 6, there is evidence from marine sediment in the Arctic for both perennial and seasonal Arctic sea ice conditions in the mid-Pliocene. As chapter 6 shows, a difference in orbital forcing can be enough to change the summer sea ice from perennial to seasonal, so if the HadCM3 simulation is representing mid-Pliocene conditions accurately enough, then it is likely that the Arctic was characterised by intervals of both year-round sea ice coverage, and periods of sea ice free summers. This is perhaps why Darby (2008) finds evidence for perennial sea ice, and Cronin *et al.* (1993), Moran *et al.* (2006) and Polyak *et al.* (2010) find evidence for seasonal sea ice.

The influence of atmospheric CO_2 must be considered, particularly as the results show that at 300 ppm pCO_2, perennial sea ice was simulated under all orbital forcings (only for standard minimum albedo), indicating that not only is it important to have a good understanding of the atmospheric CO_2 concentrations in the mid-Pliocene, but if there were variations of over 100 ppm across the time slab, then understanding when these occurred is just as important.

The winter sea ice is also affected by the orbital forcing and atmospheric CO_2 changes, although the reductions in extent are not as large as for the summer months, and a northward shift of the maximum extent margin is not as dramatic a change as the disappearance of summer sea ice, so the winter changes do not have as striking an impact. In simulations with reduced ice extent, the winter sea ice is also thinner, and recovers more slowly in the freeze-up months, due to the increased ocean heat, which is transferred to the air in the summer.

One of the most important conclusions to be drawn from the results concerns how much high latitude warming can be achieved from severe reductions in Arctic sea ice. The data-model discrepancy is still considerable at many sites, particularly terrestrial sites, despite dramatic reductions made to the sea ice. The

simulations with the highest reductions in sea ice produce sea ice which is less extensive than our current understanding of the mid-Pliocene suggests is realistic. Given that even under these conditions the data-model discrepancy is still large at many sites, the following possibilities should be considered as further ways to tackle the data-model mismatch:

- Stronger inland transport of SAT
- Effects of cloud albedo cooling at high latitudes need to be reduced
- Greater heat transport (either SST or SAT) from lower latitudes
- Re-evaluation of proxy data and consideration of what the data represents

Greater inland SAT transport was discussed as a possible mechanism for generating warming at terrestrial sites when analysing the results from chapter 4. The results in chapter 6 further emphasise this, as the greatest SAT warming remains over the Arctic basin, largely as a result of delayed regrowth of sea ice due to warmer oceans. However, despite the large warming seen here, there are no proxy data sites in these locations, so this warming does can not contribute directly to any reduction in the model-data discrepancy. It was discussed with regards to the chapter 4 results that even if the extra heat over the Arctic basin was dispersed further inland it would likely make only a small difference to the data-model discrepancy. In the simulations with greatest warming (e.g. Jul_500_0.2) there is greater SAT increase over the Arctic basin compared to the Mod_400_0.2 simulation which was analysed in chapter 6, as well as greater warming at the terrestrial data sites. A further dispersal of the heat over the Arctic basin may not be sufficient to produce complete agreement, given that the discrepancy exceeds 9°C at some sites, but it could make a significant difference.

One potential side effect to consider is that if inland heat transport in the model were stronger, then the ocean would likely release heat faster, compensating for heat loss inland, and so the sea ice would start to recover sooner. This could lead to a thicker and more extensive sea ice maximum, which would take longer and require greater heat to melt, meaning less additional warming in the ocean

over the summer. This could potentially negate any effect that a stronger inland heat transport would have.

Unlike the SAT warming, the average increase in SST does not get higher when looking at regions closer to the pole in every simulation. In many simulations the strongest regions of warming occur between 70 and 80°N, as a result of a more northerly maximum sea ice extent margin, leaving some regions ice-free year round. As these areas of greater warming are at lower latitudes than the greater SAT warming, and thus closer to the data sites, then the mismatches in the SST data-model comparisons are smaller than in the SAT comparisons.

The energy balance analysis reveals that some of the warming at high latitudes as a result of the reduction in sea ice albedo is offset by a cooling from an increase in overall cloud albedo. However, the total cloud output at high latitudes from the simulations with reduced minimum albedo and no change to CO_2 showed little difference compared to simulations with 500 ppm CO_2, but standard sea ice albedo. This suggests that changes may have occurred in the type of cloud (e.g. low, medium or high cloud) or characteristics of the cloud affecting the albedo.

This suggests there is potential to reduce the cooling effect at high latitudes by analysing the parameterisation of clouds at high latitude. There are no observations of the effects of an ice-free Arctic ocean on cloud formation, which gives a broad scope for plausible simulation of cloud at high latitudes. Given the cooling effect indicated by the energy balance analysis, it is only likely to have a small effect on the overall data-model comparison, but it could make an important contribution.

Chapter 6 demonstrated the limitations of the effect of reduction in sea ice on warming effectively. Without a further severe reduction in sea ice, or complete removal, like in Ballantyne *et al.* (2013), there is a limit to the level of warming that can be achieved. This means that additional heat is likely to be required from more southerly latitudes. This can be in the form of stronger ocean heat transport, which will lead to warmer SSTs, and then an increase in SATs in the autumn and winter months, or a stronger atmospheric heat transport, which will increase the SATs and result in a slower release of heat from the oceans in autumn and winter, and thus lead to an increase in overall SST.

Zhang *et al.* (2013b) showed that the simulation of AMOC by the PlioMIP models was similar in the mid-Pliocene and pre-industrial simulations, which either suggests that an increased ocean heat transport is not realistic, or that all the models are failing to represent some mechanism leading to an AMOC strengthening, and potential greater northward heat transport.

Data-model comparisons are generally much closer at lower latitudes, so an increase in the transport of heat from these regions further north could weaken those close agreements. If this were combined with a change in forcing that resulted in warming at lower latitudes as well as higher, such as an increase in atmospheric CO_2, then this could perhaps enable greater high-latitude warming without being at the expense of poorer representations of lower latitudes. It is important in general to ensure that any changes made to try and improve model performance in one region do not do so by worsening it in another.

If achieving agreement between proxies and models appears to be beyond the capabilities of the models, then a reevaluation of the interpretation of the proxy data ought to be condidered. It is assumed that the proxy data indicate mean annual temperatures, but the signal may be seasonal, perhaps growing season or maximum temperature. Arctic growing season is short but intense, as the days when temperatures are sufficiently warm are also very long, and so there is high light availability. Present day Arctic growing season is estimated to be 69-99 days long (Courtin & Labine, 1977), but may have been longer in the warmer mid-Pliocene. Csank *et al.* (2011) estimates mid-Pliocene Arctic growing season temperatures of 12.7 ± 1.9°C, based on mollusc shell analysis. This represents an increase of 14.3 ± 2.2°C in comparison to modern.

The mean annual SAT proxy data estimates are lower than the maximum temperatures in the control simulation, and are close in value to the control simulation temperatures in May and August/September. For the SSTs, the three mean annual temperature estimates for the ODP sites exceed even the maximum SST simulated by the control simulation, so even if they were reflective of the maximum temperature there would not be agreement with the control. The highest maximum temperature in the ensemble from chapter 6 at ODP907, where the mean annual temperature estimate is 11.7°C, is 11.67°C. If the proxy data were indicating maximum temperature, then this one simulation would be displaying

agreement. At ODP sites 909 and 911 however, the highest maximum simulated temperatures were more than 3°C lower than the proxy estimated mean annual temperature. At the other two sites, Colvillian and Meighen Island, the control maximum is just 1°C less at Colvillian, and exceeds the Meighen Island proxy estimate, so if these were showing maximum temperatures then there could be agreement, even with the control simulation.

Further work and consideration of what the proxy data is representing could reveal that the models are not as far off simulating the climate of the mid-Pliocene Arctic as initially it seems. However, if proxies were re-interpreted this could have implications for estimates at lower latitudes, where the models and data are generally considered in much better agreement, although as seasonality decreases with latitude the effects on low-latitude data-model comparisons may not be very large.

7.3 Overall conclusions

The two main areas the work in this thesis aimed to explore related to understanding the nature of mid-Pliocene Arctic sea ice, and in particular considering whether the Arctic was likely characterised by seasonal or perennial sea ice, and how much effect changes in sea ice cover have on the simulated mid-Pliocene climate.

Results analysed in chapter 4 show that changes to sea ice albedo parameterisation to accommodate potential physical changes in the sea ice as a result of a shift to a greater dominance of the sea ice cover by first year sea ice can result in a change from simulated perennial sea ice to seasonal sea ice. Whilst some large seasonal temperature changes are observed as a result of the large reduction in Arctic sea ice, this is restricted largely to the ocean region of the Arctic, and the changes at palaeodata sites are much smaller, and generally within the uncertainties associated with the proxy reconstructions. Chapter 6 extends the work of chapter 4 further, and adds additional forcings that can further reduce the sea ice and increase warming. The key conclusions to take from chapter 6 relate to the fact that a reduction in sea ice does not appear to be as effective in increasing temperatures as more direct forcings, such as increased CO_2, and

there are still large data-model discrepancies even when providing conditions conducive to large sea ice melt. Additionally, the results show that the Arctic may have alternated between perennial and seasonal sea ice phases, dependent on the orbit and CO_2, and assuming the standard albedo parameterisation is suitable for these conditions.

The analysis of results in chapter 5 shows that care must be taken when making conclusions about mid-Pliocene sea ice based on one model's simulation, as there is model dependency with regards to the results, particularly relating to whether the Arctic saw sea ice free conditions. Sea ice albedo feedback was identified as a key influence on the simulation of sea ice, reinforcing the need for models to be able to reflect as accurately as possible how sea ice albedo changes along with properties of the sea ice. It was also highlighted that the oceanic and atmospheric forcings have a very strong influence on the simulation of sea ice, and so it is vital that this aspect of the climate is being well represented in the model, in addition to a sea ice model with a good representation of processes affecting sea ice.

7.4 Future work

Sea ice in the mid-Pliocene remains an area around which little is currently understood. The results in this thesis show the wide uncertainty range over the nature of the sea ice cover in the mid-Pliocene. Future work on model simulation of mid-Pliocene climate ideally needs to be coupled with a much greater quantity of proxy data information relating to Arctic sea ice in the mid-Pliocene. The results of chapter 6 indicate that the sea ice is highly sensitive to changes in orbit and CO_2, and so could identify narrower slices of time within the mid-Pliocene where greater information about the sea ice cover and likely atmospheric CO_2 concentrations could indicate whether the models' simulation of the Arctic sea ice is a realistic reflection of the sea ice cover of the time.

As was highlighted in chapter 6, high latitude clouds have a cooling effect on the climate when sea ice is removed. This appears to be as a result of changes in the type or property of clouds, rather than the total cloud amount. Further work looking more precisely at the changes to the simulated clouds would prove

insightful, in addition to an investigation into the parameterisation of clouds in the model, looking to see whether there are reasonable adjustments that could be made in order to facilitate further high latitude warming.

Chapter 5 briefly highlighted the influence that multi-decadal oscillations have on sea ice. These have been analysed in simulations of future sea ice conditions, but the effect in simulations of past climates has not been explored. In particular, it should be investigated whether using differing averaging periods significantly changes the model output with regard to Arctic sea ice, due to how much effect from multi-decadal oscillations may be seen in an average of 30 years, compared to a 50 or 100 year average. This could help explain some of the differences in the influences on the pre-industrial and mid-Pliocene sea ice simulated by the PlioMIP models.

In terms of the general pattern with the data-model comparison, and the insufficient high-latitude warming the models are producing, then in addition to exploring further methods to try to increase the high latitude warming, a reconsideration the model-data comparison techniques would also prove worthwhile. In addition, more numerous proxy studies, with finer temporal resolution, if possible, and greater global coverage would enhance comparisons with models. In this thesis, the data-model comparison used have been very basic, with the uncertainty associated with the data techniques discussed, but not incorporated into any comparison technique. Using more advanced statistical methods, for example, that incorporate modelling and data uncertainties into a comparison may provide a different outlook.

Appendix A

Appendix

This appendix consists of the supplementary information accompanying the paper in which the material from chapter 4 was published.

A.1 Sea Ice Model Description

The sea ice model utilised in HadCM3 uses a basic thermodynamic scheme, based on the zero-layer model described in Semtner (1976), which was developed from the one-dimensional sea ice model set out in Maykut & Untersteiner (1971). This model consists of four layers, ocean, ice, snow and atmosphere, with heat balance equations determining the fluxes at the boundaries between the layers, and equations describing heat conduction in the snow and ice layers. The ice heat conduction equation includes a term for an internal heat source. Snow cover is affected by linear accumulations from August through to May. The model does not account for any mechanical stresses on ice.

Ice dynamics in HadCM3 are based on parameterisations set out in Bryan (1969). The advection of the sea ice is based on the mean speed of the currents in the first 100 m below the ocean surface. In HadCM3 the currents are based on the windstress, which is applied to the ocean below the ice (Gordon *et al.*, 2000).

Sea ice concentration parameterisation is based on Hibler (1979). The model creates sea ice when the sea surface temperature drops below -1.8°C, or from advection from the sea ice edge Cattle & Crossley (1995). New ice that is formed has thickness of 0.5 m, and enough sea ice is allowed to form to satisfy heat

conservation. This enables fractional sea ice coverage in the model and a parameterisation of leads. In the Arctic, sea ice can achieve a maximum concentration of 99.5%, with a maximum of 98% in the Antarctic (Gordon *et al.*, 2000).

The effects of heat flux exchange over leads are divided into changes to the temperature of the upper layer of the ocean and the melting or formation of ice. The division of the effects is directly proportional to the concentration of sea ice over the given model grid square (Cattle & Crossley, 1995).

For surface air temperatures of $-10°C$ or colder, the sea ice albedo is set at 0.8. For SATs between -10 and 0°C, the albedo increases linearly to a minimum of 0.5. This temperature dependent evolution of sea ice albedo intends to capture the effects of the aging and melting of snow, and the presence of melt ponds on the sea ice albedo. Leads have a constant albedo of 0.06 (Gordon *et al.*, 2000). Sea ice is assumed to have a constant salinity of 0.6‰(Gordon *et al.*, 2000).

A.2 Experimental Set Up

A.2.1 Experimental Design

The experimental design in this study uses the PlioMIP Experiment 2 template set out in Haywood *et al.* (2011b). Atmospheric CO_2 concentration in the atmosphere was set to 405 ppmv, based on proxies derived from stomatal indices, boron and carbon isotope analyses and alkenones (Kürschner *et al.*, 1996; Pagani *et al.*, 2010; Raymo *et al.*, 1996; Seki *et al.*, 2010). These various reconstructions give a range of mid-Pliocene CO_2 of 350 to 415 ppmv. All other trace gas concentrations are set to pre-industrial levels.

Solar constant and orbital configuration are both specified to be the same as those used in pre-industrial simulations. Based on astronomical solutions such as Laskar *et al.* (2004), a modern orbit may not best represent the mean orbital forcing for the mid-Pliocene. However, as the PRISM data is representative of an average of warm peaks during a time slab covering approximately 300,000 years, it is very difficult to produce an orbital configuration which best represents the mid-Pliocene warm period.

24 Pliocene simulations were run in total (including the control simulation), each with different combinations of minimum and maximum sea ice albedo limits, which are shown in Figure A.1. These were run in order to assess the overall effects of any general change to either the minimum or maximum albedo limit. However, this paper focuses solely on the three runs where the minimum albedo is lowered, and no change is made to the maximum albedo, which are indicated by the black diamonds in Figure A.1.

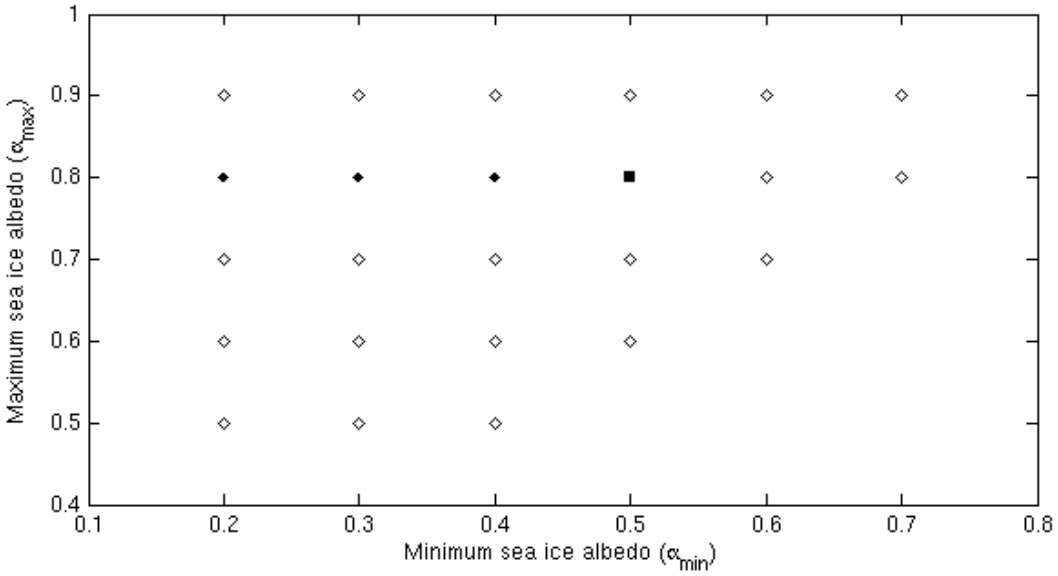

Figure A.1: 24 combinations of minimum and maximum sea ice albedo used for the Pliocene simulations. The black sqaure indicates the control run, and the black diamonds indicate the three runs which the paper focuses on.

A.2.2 Boundary Conditions

The PRISM (Pliocene Research, Interpretation and Synoptic Mapping) project is an 'internally consistent and comprehensive global synthesis of a past interval of relatively warm and stable climate', developed by the United States Geological Survey (Dowsett *et al.*, 2010). The reconstruction ranges over the interval from 3.264 Ma to 3.025 Ma (Dowsett *et al.*, 2010), and consists of reconstructions of

mid-Pliocene sea surface and deep ocean temperatures, in addition to sea level, topgraphy, vegetation and ice sheets.

PRISM uses a multi-proxy approach for the reconstruction of mid-Pliocene SSTs - as well as faunal analysis, alkenone and Mg/Ca methods of SST estimation are also adopted (Dowsett, 2007). The reconstructions are based on samples taken from 86 Deep Sea Drilling Project (DSDP) and Ocean Drilling Program (ODP) sites (Dowsett *et al.*, 2010). Deep ocean temperatures are estimated from 27 DSDP and ODP sites, representing depths ranging from 1000 m to 4500 m.

The topographic reconstruction for the mid-Pliocene is largely similar to present day, with the key exceptions being that sea level is 25 m higher, Hudson Bay and the Great Lakes are filled in, and the West Antarctic ice sheet has disappeared, alongside reductions in the East Antarctic and Greenland ice sheets (Dowsett *et al.*, 2010; Sohl *et al.*, 2009).

The vegetation reconstruction for the mid-Pliocene was based on a combination of data from 202 terrestrial sites and results from BIOME4, a vegetation model (Dowsett *et al.*, 2010; Salzmann *et al.*, 2008). Palaeobotanical data was compiled for the 202 sites based on existing literature and the extended data set of Thompson & Fleming (1996). This was then used to assign each data point to one of the 28 land cover classifications used in the BIOME4 model (Salzmann *et al.*, 2008).

A.3 Delayed Warming Effect

The direct effect of an overall reduction in sea ice albedo is to increase in the net downward shortwave (SW) radiation over regions of sea ice coverage, as less getss reflected from the surface. Figure A.2 shows this increase in the spring and summer months for the simulation with $\alpha_{min} = 0.2$. Autumn and winter have very low levels of incoming SW radiation at high latitudes, so a change in albedo makes a much smaller difference. The effects of this increase are divided between the melting of sea ice and the heating of the upper layer of the ocean. This effect is demonstrated in Figure A.3, which shows a 55% reduction in summer sea ice. Figure 4.2 in Chapter 4 shows the mean increase in SST of 1.2°C in the region north of 60°N in the summer. These changes are not observed to this extent

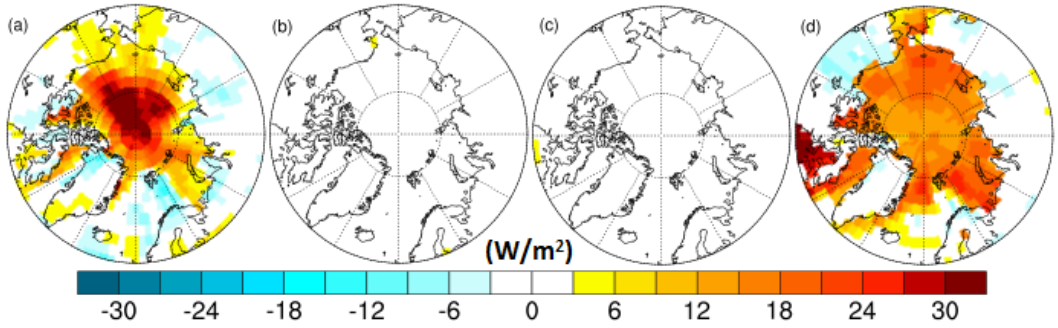

Figure A.2: Mean seasonal net downward shortwave radiation flux (W/m^2) anomalies (alternative minus standard) for Pliocene simulation with minimum sea ice albedo reduced to 0.2, showing (a) summer (JJA), (b) autumn (SON), (c) winter (DJF), (d) spring (MAM).

in the spring months, however the sea ice thickness is shown to decrease by an average of 0.64 m (26.6%, Figure A.4).

The autumn months experience higher SSTs, and a loss in sea ice concentration of 89% (Figures 4.2 and A.3). Owing to this large loss of the insulating sea ice cover, there is a large increase in net upward longwave (LW) flux and sensible heat flux from ocean to atmosphere (Figures A.5 and A.6), resulting in the increase in SATs shown in Figure 4.2. This remains the case, to a lesser extent, for the winter months (SSTs show little change, but the sea ice cover is still reduced, and the mean thickness is reduced by 34.7%), and so SATs are also seen to increase in winter, but not by the amount as seen in autumn (Figure 4.2). Warming is also seen over land in winter, in contrast to the other three seasons, suggesting inland transport of some of the heat initially emitted into the atmosphere in the autumn.

Figure A.3 shows that the sea ice coverage has mostly recovered by the spring, as a result it retains the insulating cap on the ocean surface and so there is little increase in surface air temperature at this time of year.

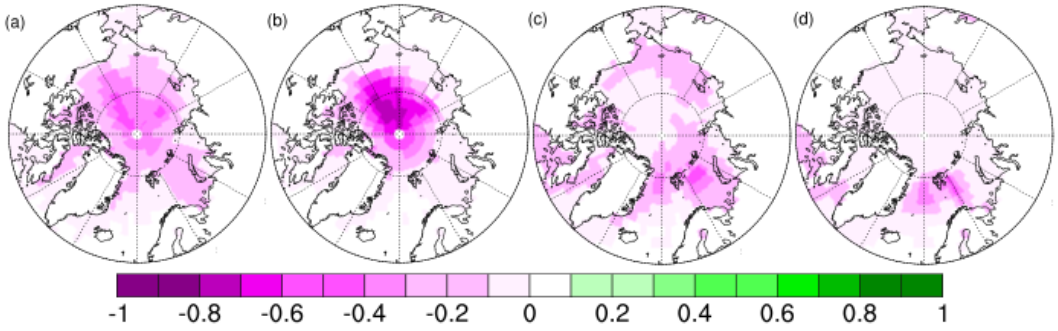

Figure A.3: Mean seasonal sea ice fraction anomalies (alternative minus standard) for Pliocene simulation with minimum sea ice albedo reduced to 0.2, showing (a) summer (JJA), (b) autumn (SON), (c) winter (DJF), (d) spring (MAM).

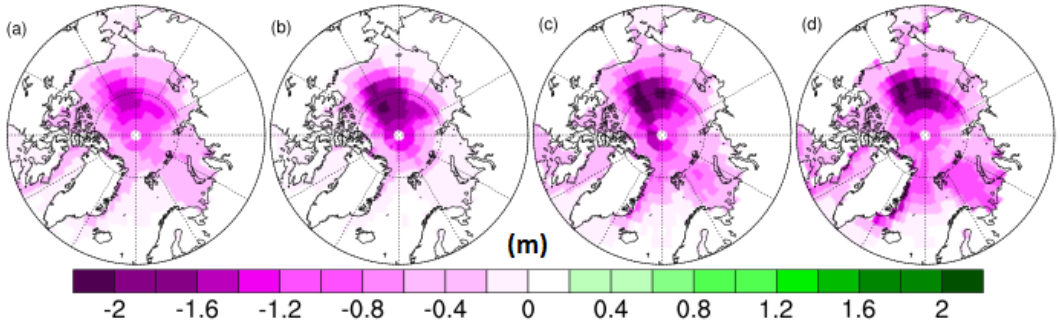

Figure A.4: Mean seasonal sea ice thickness (m) anomalies (alternative minus standard) for Pliocene simulation with minimum sea ice albedo reduced to 0.2, showing (a) summer (JJA), (b) autumn (SON), (c) winter (DJF), (d) spring (MAM).

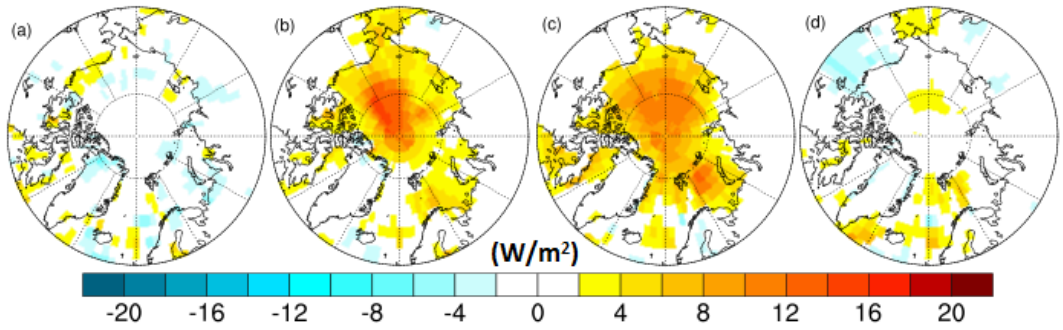

Figure A.5: Mean seasonal net upward longwave radiation flux (W/m^2) anomalies (alternative minus standard) for Pliocene simulation with minimum sea ice albedo reduced to 0.2, showing (a) summer (JJA), (b) autumn (SON), (c) winter (DJF), (d) spring (MAM).

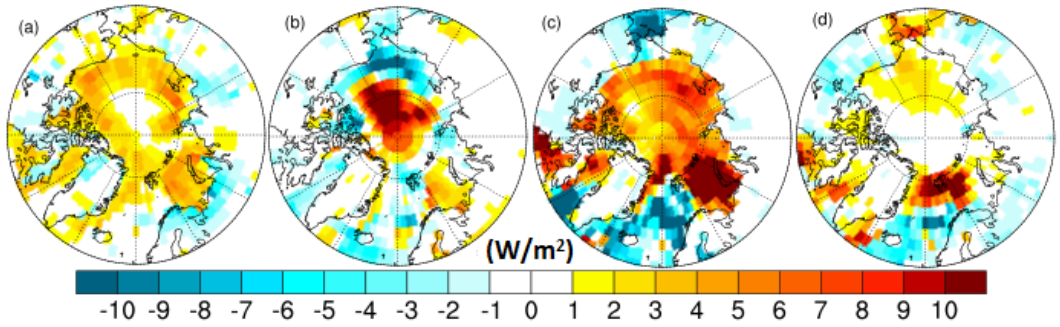

Figure A.6: Mean seasonal sensible heat flux (W/m^2) anomalies (alternative minus standard) for Pliocene simulation with minimum sea ice albedo reduced to 0.2, showing (a) summer (JJA), (b) autumn (SON), (c) winter (DJF), (d) spring (MAM).

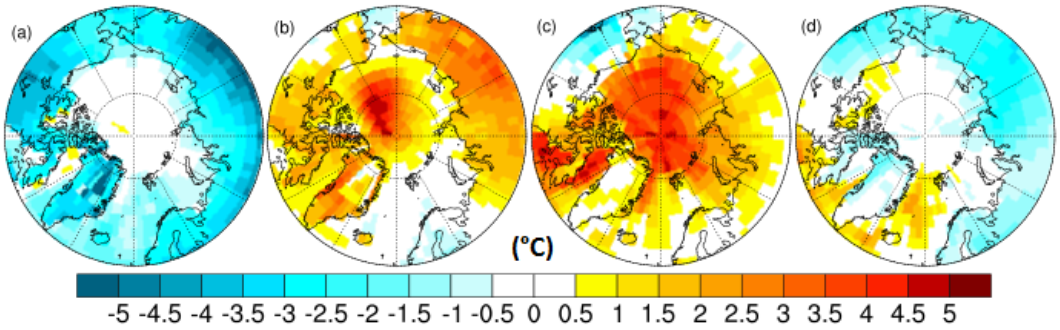

Figure A.7: Mean seasonal SAT (°C) anomalies (α_{min} = 0.2 minus Pliocene NH Max) comparing effects of changes in minimum albedo to changes in orbit, showing (a) summer (JJA), (b) autumn (SON), (c) winter (DJF), (d) spring (MAM).

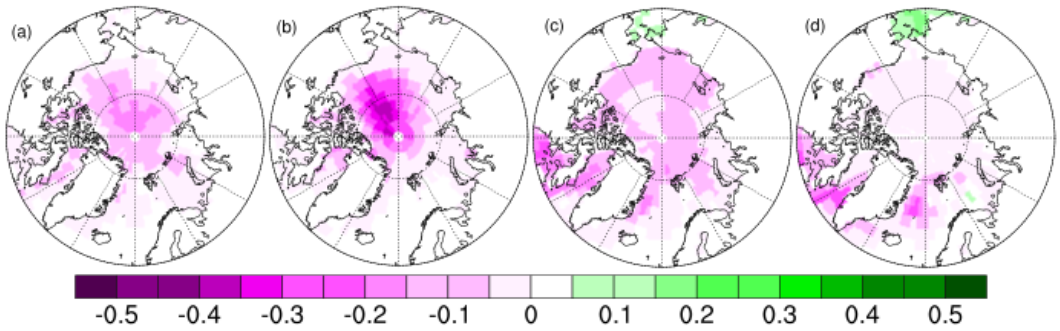

Figure A.8: Mean seasonal sea ice concentration anomalies (α_{min} = 0.2 minus Pliocene NH Max) comparing effects of changes in minimum albedo to changes in orbit, showing (a) summer (JJA), (b) autumn (SON), (c) winter (DJF), (d) spring (MAM).

A. APPENDIX

Table A.1: SAT anomalies (model simulated temperature minus proxy reconstructed temperature) for all palaeodata sites at or north of 60°N. Anomalies are displayed for the control and $\alpha_{min} = 0.2$ simulations.

Site	Latitude/Longitude	Control Anomaly	$\alpha_{min} = 0.2$ anomaly
Beaver Pond	78.40°/-82.00°	-14.51°C	-13.7°C
Ocean Point	70.00°/-153.00°	-8.92°C	-8.2°C
Lena River	72.20°/125.97°	-12.01°C	-11.4°C
Circle, Alaska	65.50°/-144.08°	-5.26°C	-5.23°C
Blizkiy	64.00°/-162.00°	-10.5°C	-10.1°C
Nenana Valley, Alaska	64.53°/-149.08°	-7.01°C	-7.01°C
Lost Chicken Mine	64.06°/-141.95°	-4.39°C	-4.35°C
Delyankir	63.00°/133.00°	-16.98°C	-16.80°C
Magadan District	59.98°/150.65°	-7.05°C	-6.76°C

Table A.2: SST anomalies (model simulated temperature minus proxy reconstructed temperature) for all palaeodata sites at or north of 60°N. Anomalies are displayed for the control and $\alpha_{min} = 0.2$ simulations.

Site	Latitude/Longitude	Control Anomaly	$\alpha_{min} = 0.2$ anomaly
Colvillian	70.29°/-150.42°	-2.26°C	-1.61°C
ODP 909	78.58°/-3.07°	-9.82°C	-8.51°C
ODP 911	80.47°/8.23°	-11.14°C	-10.21°C
Meighen Island	79.00°/-99.00°	-1.84°C	-1.63°C
ODP 907	69.25°/-12.7°	-6.16°C	-6.09°C
Tjornes	66.16°/-17.25°	0.94°C	0.90°C

References

Bryan, K. (1969). Climate and the ocean circulation III: The ocean model. *Mon Weather Rev*, **97**, 806–827. 46, 49, 61, 62, 75, 142, 188

Cattle, H. & Crossley, J. (1995). Modeling Arctic climate change. *Philosophical Transactions of the Royal Society A-Mathematical, Physical and Engineering Sciences*, **352**, 201–213. 62, 63, 71, 75, 94, 117, 142, 188, 189

Dowsett, H. (2007). The PRISM palaeoclimate reconstruction and Pliocene sea-surface temperature. *Deep-Time Perspectives on Climate Change: Marrying the Signal from Computer Models and Biological Proxies*, 459–480. 8, 9, 10, 13, 14, 15, 24, 191

Dowsett, H.J., Robinson, M.M., Haywood, A.M., Salzmann, U., Hill, D.J., Sohl, L., Chandler, M.A., Williams, M., Foley, K. & Stoll, D. (2010). The PRISM3D paleoenvironmental reconstruction. *Stratigraphy*, **7**, 123–139. 1, 3, 4, 5, 9, 16, 17, 18, 21, 66, 73, 76, 77, 83, 92, 95, 140, 143, 144, 190, 191

Gordon, C., Cooper, C., Senior, C.A., Banks, H., Gregory, J.M., Johns, T.C., Mitchell, J.F.B. & Wood, R.A. (2000). The simulation of SST, sea ice extents and ocean heat transports in a version of the Hadley Centre coupled model without flux adjustments. *Climate Dynamics*, **16**, 147–168. 2, 59, 60, 61, 62, 63, 64, 65, 75, 122, 141, 142, 188, 189

Haywood, A.M., Dowsett, H.J., Robinson, M.M., Stoll, D.K., Dolan, A.M., Lunt, D.J., Otto-Bliesner, B.L. & Chandler, M.A. (2011). Pliocene Model Intercomparison Project (PlioMIP): experimental design and

boundary conditions (Experiment 2). *Geosci. Model Dev.*, **4**, 571–577. 29, 30, 70, 76, 93, 95, 141, 143, 189

Hibler, W.D. (1979). A dynamic-thermodynamic sea ice model. *Journal of Physical Oceanography*, **9**, 815–846. 47, 48, 49, 62, 75, 117, 142, 188

Kürschner, W., van der Burgh, J., Visscher, H. & Dilcher, D. (1996). Oak leaves as biosensors of late neogene and early pleistocene paleoatmospheric CO2 concentrations. *Marine Micropaleontology*, **27**, 299–312. 6, 189

Laskar, J., Robutel, P., Joutel, F., Gastineau, M., Correia, A. & Levrard, B. (2004). A long-term numerical solution for the insolation quantities of the Earth. *Astronomy and Astrophysics*, **428**, 261–285. 67, 81, 143, 189

Maykut, G. & Untersteiner, N. (1971). Some results from a time-dependent thermodynamic model of sea ice. *Journal of Geophysical Research*, **76**, 1550–1575. 46, 47, 48, 50, 61, 142, 188

Pagani, M., Liu, Z., LaRiviere, J. & Ravelo, A.C. (2010). High Earth-system climate sensitivity determined from Pliocene carbon dioxide concentrations. *Nature Geoscience*, **3**, 27–30. 6, 8, 73, 92, 140, 189

Raymo, M., Grant, B., Horowitz, M. & Rau, G. (1996). Mid-Pliocene warmth: Stronger greenhouse and stronger conveyor. *Marine Micropaleontology*, **27**, 313–326. 189

Salzmann, U., Haywood, A., Lunt, D., Valdes, P. & Hill, D. (2008). A new global biome reconstruction and data-model comparison for the Middle Pliocene. *Global Ecology and Biogeography*, **17**, 432–447. 17, 21, 22, 23, 28, 77, 144, 191

Seki, O., Foster, G.L., Schmidt, D.N., Mackensen, A., Kawamura, K. & Pancost, R.D. (2010). Alkenone and boron-based Pliocene pCO_2 records. *Earth and Planetary Science Letters*, **292**, 201–211. 6, 7, 8, 73, 92, 140, 189

Semtner, A.J. (1976). A model for the thermodynamic growth of sea ice in numerical investigations of climate. *Journal of Physical Oceanography*, **6**, 379–389. 47, 48, 49, 61, 62, 75, 117, 142, 188

Sohl, L., Chandler, M., Schmunk, R., Mankoff, K., Jonas, J., Foley, K. & Dowsett, H. (2009). PRISM3/GISS topographic reconstruction. *U.S. Geological Survey Data Series*, **419**, 6pp. 19, 20, 23, 24, 191

Thompson, R. & Fleming, R. (1996). Middle Pliocene vegetation: Reconstructions, paleoclimatic inferences, and boundary conditions for climate modeling. *Marine Micropaleontology*, **27**, 27–49. 20, 21, 158, 191

Appendix B

Appendix

This appendix consists of the supplementary information accompanying the paper in which the material from chapter 5 was submitted.

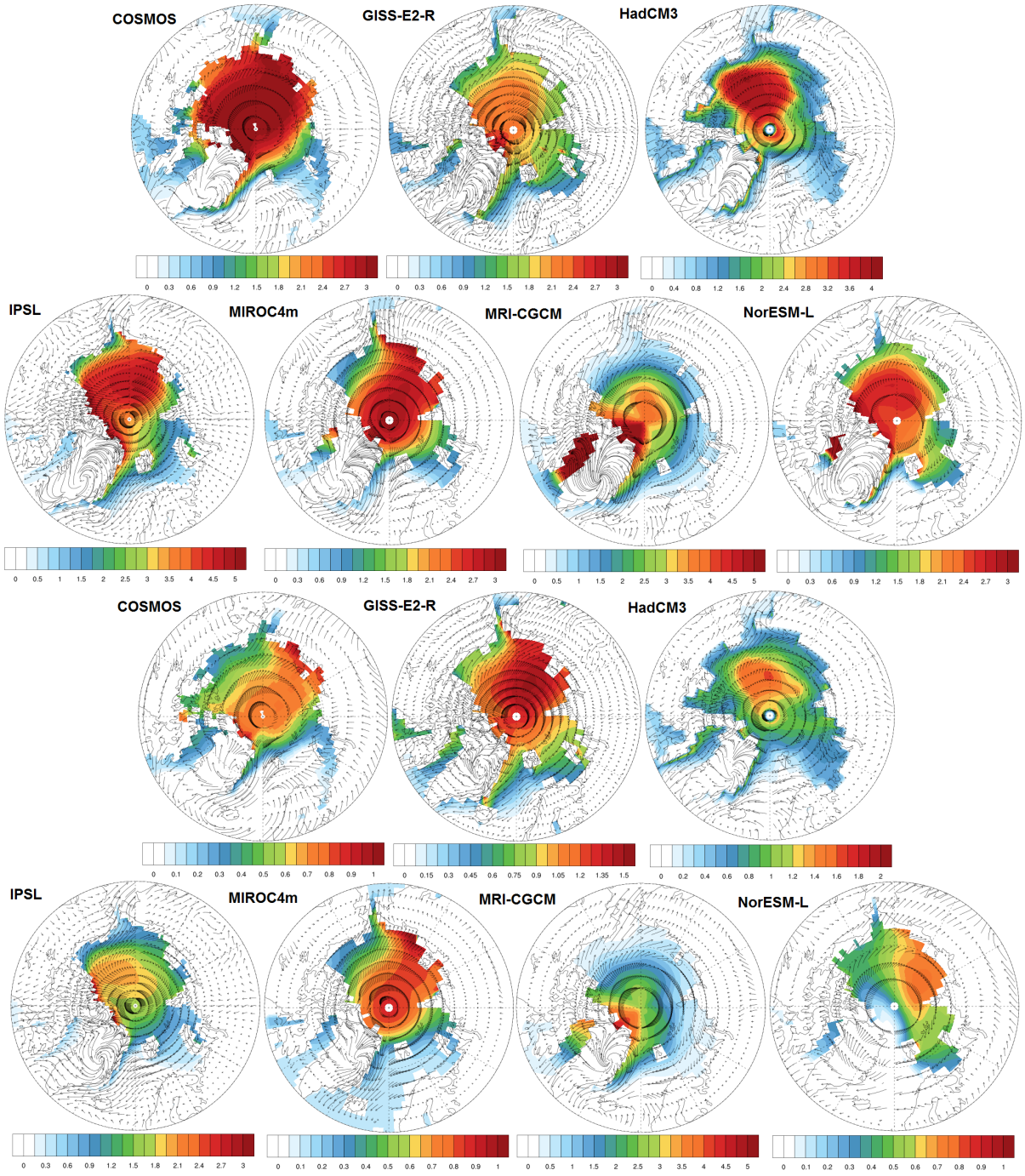

Figure B.1: Mean annual 10 m winds and mean annual sea ice thickness (m) in pre-industrial (upper half) and mid-Pliocene (lower half) for each PlioMIP Experiment 2 model (excluding CCSM4). Vector length is proportional to wind speed.

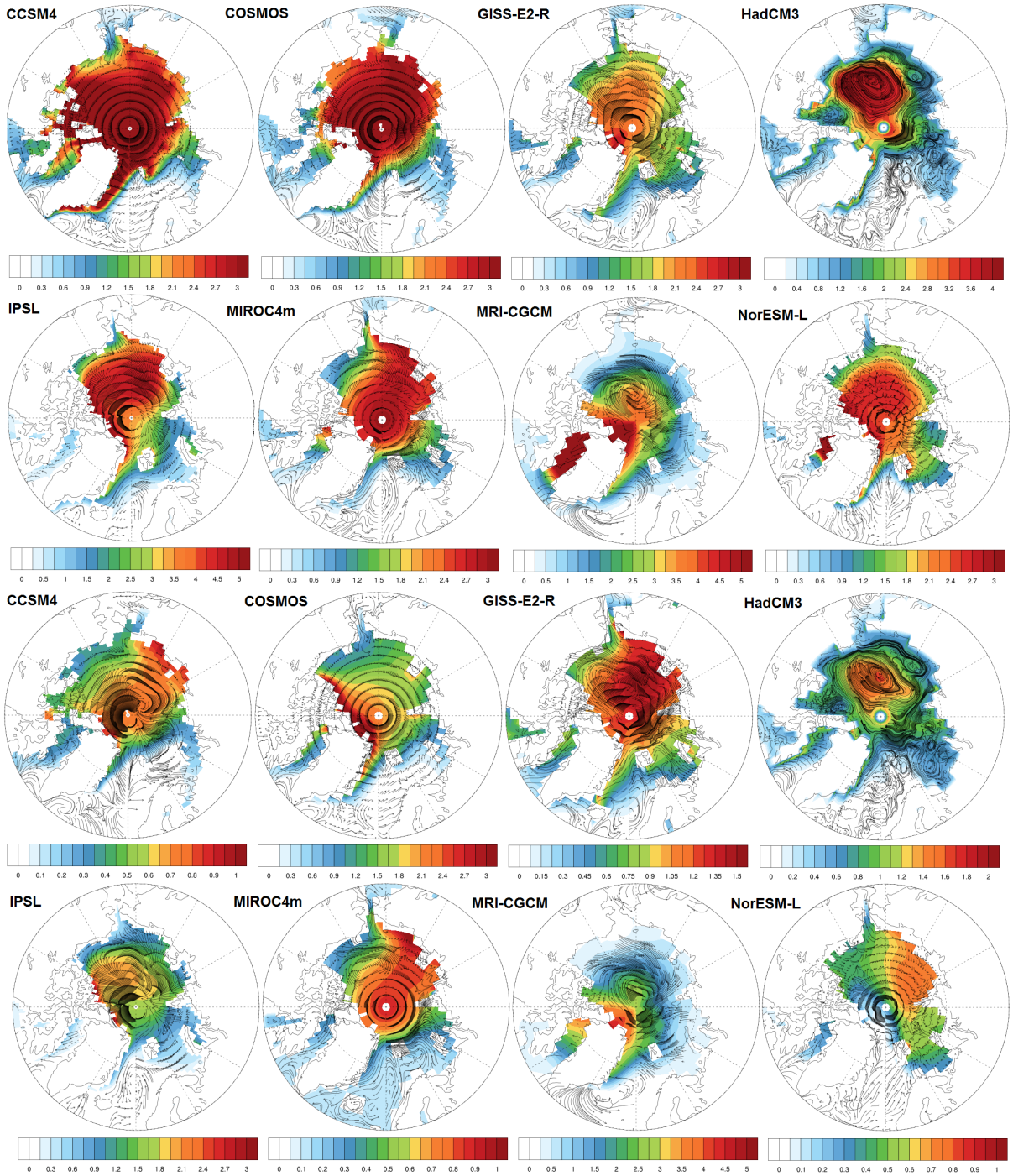

Figure B.2: Mean annual surface ocean currents and sea ice thicknesses (m) in pre-industrial (upper half) and mid-Pliocene (lower half) for each PlioMIP Experiment 2 model. Vector length is proportional to ocean current speed.

References

Aagaard, K. & Carmack, E.C. (1989). The role of sea ice and other fresh water in the Arctic circulation. *Journal of Geophysical Research - Oceans*, **94**, 14485–14498. 37

Aagaard, K., Swift, J. & Carmack, E. (1985). Thermohaline circulation in the Arctic mediterranean seas. *Journal of Geophysical Research - Oceans*, **90**, 4833–4846. 37

Abram, N., Thomas, E., McConnell, J., Mulvaney, R., Bracegirdle, T., Sime, L. & Aristarain, A. (2010). Ice core evidence for a 20th century decline of sea ice in the Bellingshausen Sea, Antarctica. *Journal of Geophysical Research-Atmospheres*, **115**. 57

Abram, N., Wolff, E. & Curran, M. (2013). A review of sea ice proxy information from polar ice cores. *Quaternary Science Reviews*, **79**, 168–183. 55, 56, 57

ACIA (2005). Arctic Climate Impact Assessment. *Cambridge University Press*, 1042p. 44

Alexander, M., Bhatt, U., Walsh, J., Timlin, M., J.S., M. & Scott, J. (2004). The atmospheric response to realistic Arctic sea ice anomalies in an AGCM during winter. *Journal of Climate*, **17**, 890–905. 36

Alexeev, V. (2003). Sensitivity to CO_2 doubling of an atmospheric GCM coupled to an oceanic mixed layer: a linear analysis. *Climate Dynamics*, **20**, 775–787. 45

REFERENCES

Alexeev, V. & Jackson, C. (2013). Polar amplification: is atmospheric heat transport important? *Climate Dynamics*, **41**, 533–547. 45

Alexeev, V., Langen, P. & Bates, J. (2005). Polar amplification of surface warming on an aquaplanet in "ghost forcing" experiments without sea ice feedbacks. *Climate Dynamics*, **24**, 655–666. 45

Andreev, A.A., Tarasov, P.E., Wennrich, V., Raschke, E., Herzschuh, U., Nowaczyk, N.R., Brigham-Grette, J. & Melles, M. (2014). Late Pliocene and Early Pleistocene vegetation history of northeastern Russian Arctic inferred from the Lake El'gygytgyn pollen record. *Climate of the Past*, **10**, 1017–1039. 157

Andrews, J. & Eberl, D. (2007). Quantitative mineralogy of surface sediments on the Iceland shelf, and application to down-core studies of Holocene ice-rafted sediments. *Journal of Sedimentary Research*, **77**, 469–479. 55

Arzel, O., Fichefet, T. & Goosse, H. (2006). Sea ice evolution over the 20th and 21st centuries as simulated by current AOGCMs. *Ocean Modelling*, **12**, 401 – 415. 93

Badger, M., Schmidt, D., Mackensen, A. & Pancost, R. (2013). High-resolution alkenone palaeobarometry indicates relatively stable pCO_2 during the Pliocene (3.3-2.8 Ma). *Philos. Trans. R. Soc. A*, **68**, 20130094. 6, 7, 8, 68, 140, 143

Ballantyne, A., Greenwood, D., Damste, J., Csank, A., Eberle, J. & Rybczynski, N. (2010). Significantly warmer Arctic surface temperatures during the Pliocene indicated by multiple independent proxies. *Geology*, **38**, 603–606. 28

Ballantyne, A., Axford, Y., Miller, G., Otto-Bliesner, B., Rosenbloom, N. & White, J. (2013). The amplification of Arctic terrestrial surface temperatures by reduced sea-ice extent during the Pliocene. *Palaeogeography Palaeoclimatology Palaeoecology*, **386**, 59–67. 25, 84, 140, 162, 163, 166, 183

Barker, S., Cacho, I., Benway, H. & Tachikawa, K. (2005). Planktonic foraminiferal Mg/Ca as a proxy for past oceanic temperatures: a methodological overview and data compilation for the Last Glacial Maximum. *Quaternary Science Reviews*, **24**, 821–834. 11

Barreiro, M., Philander, G., Pacanowski, R. & Fedorov, A. (2005). Simulations of warm tropical conditions with application to middle Pliocene atmospheres. *Climate Dynamics*, **26**, 349–365. 25, 26

Barron, J. (1996). Diatom constraints on the position of the Antarctic Polar Front in the middle part of the Pliocene. *Marine Micropaleontology*, **27**, 195–213. 11, 25

Barthelet, P., Terray, L. & Valcke, S. (1998). Transient CO_2 Experiment using the ARPEGE/OPAICE non flux corrected coupled model. *Geophysical Research Letters*, **25**, 149–163. 64

Bartoli, G., Hönish, B. & Zeebe, R. (2009). Atmospheric CO_2 decline during the Pliocene intensification of Northern Hemisphere glaciations. *Paleoceanography*, **PA4213**, 149–163. 6

Bauch, D., Carstens, J. & Wefer, G. (1997). Oxygen isotope composition of living *Neogloboquadrina pachyderma* (sin.) in the Arctic Ocean. *Earth and Planetary Science Letters*, **146**, 47–58. 55

Bekryaev, R., Polyakov, I. & Alexeev, V. (2010). Role of polar amplification in long-term surface air temperature variations and modern Arctic warming. *Journal of Climate*, **23**, 3888–3906. 45

Belt, S. & Müller, J. (2013). The Arctic sea ice biomarker IP_{25}: a review of current understanding, recommendations for future research and applications in palaeo sea ice reconstructions. *Quaternary Science Reviews*, **79**, 9–25. 51, 52, 116

Belt, S., Masse, G., Rowland, S., Poulin, M., Michel, C. & LeBlanc, B. (2007). A novel chemical fossil of palaeo sea ice: IP_{25}. *Organic Geochemistry*, **38**, 16–27. 51, 52, 140

Bennike, O. (2004). Holocene sea-ice variations in Greenland: onshore evidence. *Holocene*, **14**, 607–613. 58

Bentsen, M., Bethke, I., Debernard, J.B., Iversen, T., Kirkevåg, A., Seland, Ø., Drange, H., Roelandt, C., Seierstad, I.A., Hoose, C. & Kristjánsson, J.E. (2013). The Norwegian Earth System Model, NorESM1-M - Part 1: Description and basic evaluation of the physical climate. *Geoscientific Model Development*, **6**, 687–720.

Berger, M., Brandefelt, J. & Nilsson, J. (2013). The sensitivity of the Arctic sea ice to orbitally induced insolation changes: a study of the mid-Holocene Paleoclimate Modelling Intercomparison Project 2 and 3 simulations. *Clim. Past*, **9**, 969–982. 93, 95

Berggren, W., Kent, D., Swisheri, C. & Aubry, M. (1995). A revised Cenozoic geochronology and chronostratigraphy, In: Berggren, W. A., Kent, D. V., Aubry, M. P., Hardenbol, J., Eds. *Geochronology, time scales and global stratigraphic correlation*, **Tulsa, OK: Society for Sedimentary Geology Special Publication, 29**, 129–212. 4

Bintanja, R., Graversen, R. & Hazeleger, W. (2011). Arctic winter warming amplified by the thermal inversion and consequent low infrared cooling to space. *Nature Geoscience*, **4**, 758–761. 45

Bischof, J. & Darby, D. (1997). Mid to Late Pleistocene ice drift in the western Arctic Ocean: Evidence for a different circulation in the past. *Science*, **277**, 74–78. 55

Björk, G., Stranne, C. & Borenas, K. (2013). The sensitivity of the Arctic Ocean sea ice thickness and its dependence on the surface albedo parameterisation. *Journal of Climate*, **26**, 1355–1370. 38

Blanchard-Wrigglesworth, E. & Bitz, C. (2014). Characteristics of Arctic sea-ice thickness variability in GCMs. *J. Climate*, **27**, 8244–8258. 93

Boé, J.L., Hall, A. & Qu, X. (2009). September sea-ice cover in the Arctic Ocean projected to vanish by 2100. *Nature Geoscience*, **2**, 341–343. 44, 92

Boville, B. & Gent, P. (1998). The NCAR Climate System Model, version one. *Journal of Climate*, **11**, 1115–1130. 64

Bragg, F.J., Lunt, D.J. & Haywood, A.M. (2012). Mid-Pliocene climate modelled using the UK Hadley Centre Model: PlioMIP Experiments 1 and 2. *Geoscientific Model Development*, **5**, 1109–1125. 71, 94

Brassell, S. (1993). Applications of biomarkers for delineating marine palaeoclimatic fluctuations during the Pleistocene. *Organic geochemistry principles and applications*, 699–738. 12

Brassell, S., Eglinton, G., Marlowe, I., Pflaumann, U. & Sarnthein, M. (1986). Molecular stratigraphy - A new tool for climatic assessment. *Nature*, **320**, 129–133. 12

Brennecke, W. (1904). Beziehungen zwischen der Luftdruck verteilung und den Eisverhaltnissen des Ostgrönlandischen Meeres. *Ann. Hydrograph. Marit. Meteorol*, **32**, 49–62. 34

Brigham-Grette, J. (2009). Contemporary Arctic change: A paleoclimate déjà vu? *Proceedings of the National Academy of Sciences*, **106**, 18431–18432. 45

Brigham-Grette, J. & Carter, L. (1992). Pliocene marine transgressions of Northern Alaska: Circumarctic correlations and paleoclimatic interpretations. *Arctic*, **45**, 74–89. 24, 57

Brigham-Grette, J., Melles, M., Minyuk, P., Andreev, A., Tarasov, P., DeConto, R., Koenig, S., Nowaczyk, N., Wennrich, V., Rosn, P., Haltia, E., Cook, T., Gebhardt, C., Meyer-Jacob, C., Snyder, J. & Herzschuh, U. (2013). Pliocene warmth, polar amplification, and stepped Pleistocene cooling recorded in NE Arctic Russia. *Science*, **340**, 1421–1427. 157

Broecker, W. (1997). Thermohaline circulation, the Achilles heel of our climate system: Will man-made CO_2 upset the current balance? *Science*, **278**, 1582–1588. 37

Brouwers, E., Jorgensen, N. & Cronin, T. (1991). Climatic significance of the ostracode fauna from the Pliocene Kap Kobenhavn Formation, North Greenland. *Micropaleontology*, **37**, 245–267. 24

Brown, T. & Belt, S. (2012). Identification of the sea ice diatom biomarker IP_{25} in Arctic benthic macrofauna: direct evidence for a sea ice diatom diet in Arctic heterotrophs. *Polar Biology*, **35**, 131–137. 51

Brown, T., Belt, S., Tatarek, A. & Mundy, C. (2014). Source identification of the Arctic sea ice proxy IP_{25}. *Nature Communications*, **5**. 140

Bryan, K. (1969). Climate and the ocean circulation III: The ocean model. *Mon Weather Rev*, **97**, 806–827. 46, 49, 61, 62, 75, 142, 188

Bryan, K., Manabe, S. & Pacanowski, R.C. (1975). A global ocean-atmosphere climate model. Part II. The oceanic circulation. *Journal of Physical Oceanography*, **5**, 30–46. 62

Budikova, D. (2009). Role of Arctic sea ice in global atmospheric circulation: A review. *Global and Planetary Change*, **68**, 149–163. 36

Budyko, M. (1969). Effect of solar radiation variations on the climate of the earth. *Tellus*, **21**, 611–619. 46

Carter, L., Brighamgrette, J., Marincovich, L., Pease, V. & Hillhouse, J. (1986). Late Cenozoic Arctic Ocean sea ice and terrestrial paleoclimate. *Geology*, **14**, 675–678. 57

Castradori, D., Rio, D., Hilgen, F. & Lourens, L. (1998). The Global Standard Stratotype-section and Point (GSSP) of the Piacenzian Stage (Middle Pliocene). *Episodes*, **21**, 88–93. 21

Cattle, H. & Crossley, J. (1995). Modeling Arctic climate change. *Philosophical Transactions of the Royal Society A-Mathematical, Physical and Engineering Sciences*, **352**, 201–213. 62, 63, 71, 75, 94, 117, 142, 188, 189

Cavalieri, D., Parkinson, C., Gloersen, P., Comiso, J. & Zwally, H. (1999). Deriving long-term time series of sea ice cover from satellite passive-microwave multisensor data sets. *Journal of Geophysical Research-Oceans*, **104**, 15803–15814. 44

Chan, W.L., Abe-Ouchi, A. & Ohgaito, R. (2011). Simulating the mid-Pliocene climate with the MIROC general circulation model: experimental design and initial results. *Geoscientific Model Development*, **4**, 1035–1049. 71, 94

Chandler, M., Rind, D. & Thompson, R. (1994). Joint investigations of the middle Pliocene climate II: GISS GCM Northern Hemisphere results. *Global and Planetary Change*, **9**, 197–219. 25

Chandler, M.A., Sohl, L.E., Jonas, J.A., Dowsett, H.J. & Kelley, M. (2013). Simulations of the mid-Pliocene Warm Period using two versions of the NASA/GISS ModelE2-R Coupled Model. *Geoscientific Model Development*, **6**, 517–531. 71, 94

Collins, L., Allen, C., Pike, J., Hodgson, D., Weckström, K. & Massé, G. (2013a). Evaluating highly branched isoprenoid (HBI) biomarkers as a novel Antarctic sea-ice proxy in deep ocean glacial age sediments. *Quaternary Science Reviews*, **79**, 87–98. 51, 53

Collins, M., Knutti, R., Arblaster, J., Dufresne, J.L., Fichefet, T., Friedlingstein, P., Gao, X., Gutowski, W., Johns, T., Krinner, G., Shongwe, M., Tebaldi, C., Weaver, A. & Wehner, M. (2013b). Observations: Atmosphere and Surface. In: *Climate Change 2013: The Physical Science Basis. Contribution of Working Group I to the Fifth Assessment Report of the Intergovernmental Panel on Climate Change* [Stocker, T.F., D. Qin, G.-K. Plattner, M. Tignor, S.K. Allen, J. Boschung, A. Nauels, Y. Xia, V. Bex and P.M. Midgley (eds.)]. Cambridge University Press, Cambridge, United Kingdom and New York, NY, USA. 4

Comiso, J. (2002). A rapidly declining perennial sea ice cover in the Arctic. *Geophysical Research Letters*, **29**. 39, 40, 44

Comiso, J.C., Parkinson, C.L., Gersten, R. & Stock, L. (2008). Accelerated decline in the Arctic sea ice cover. *Geophysical Research Letters*, **35**, L01703. 74

Connolley, W., Keen, A. & McLaren, A. (2006). Results from the implementation of the Elastic Viscous Plastic sea ice rheology in HadCM3. *Ocean Science*, **2**, 201–211. 49, 50

Conte, M., Sicre, M., Ruhlemann, C., Weber, J., Schulte, S., Schulz-Bull, D. & Blanz, T. (2006). Global temperature calibration of the alkenone unsaturation index $U_{37}^{k'}$ in surface waters and comparison with surface sediments. *Geochemistry Geophysics Geosystems*, **7**. 12, 13

Contoux, C., Ramstein, G. & Jost, A. (2012). Modelling the mid-Pliocene Warm Period climate with the IPSL coupled model and its atmospheric component LMDZ5A. *Geoscientific Model Development*, **5**, 903–917. 71, 94

Coon, M., Maykut, G., Pritchard, R., Rothrock, D. & Thorndike, A. (1974). Modeling the pack ice as an elastic-plastic material. *AIDJEX Bulletin Numerical Modeling Report*, **24**, 1–106. 47

Courtin, G. & Labine, C. (1977). Microclimatological studies on truelove lowland. *BLISS, L.C., ed., Truelove Lowland, Devon Island, Canada: A High Arctic Ecosystem: University of Alberta Press, Edmonton*, 73–106. 184

Cox, M. (1984). A primitive equation, 3 dimensional model of the ocean. *GDFL Ocean Group Technical Rep 1, Princeton, NJ, USA*, 143pp. 61

Cox, P., Betts, R., Bunton, C., Essery, R., Rowntree, P. & Smith, J. (1999). The impact of new land surface physics on the GCM simulation of climate and climate sensitivity. *Climate Dynamics*, **15**, 183–203. 60, 142

Cronin, T., Dowsett, H., Dwyer, G., Baker, P. & Chandler, M. (2005). Mid-Pliocene deep sea bottom water temperatures based on ostracode Mg/Ca ratios. *Marine Micropaleontology*, **54**, 249–261. 17

Cronin, T., Gemery, L., Briggs Jr., W., Jakobsson, M., Polyak, L. & Brouwers, E. (2010). Quaternary sea-ice history in the Arctic Ocean based on a new ostracode sea-ice proxy. *Quaternary Science Reviews*, **29**, 3415–3429. 53

Cronin, T., Polyak, L., Reed, D., Kandiano, E., Marzen, R. & Council, E. (2013). A 600-ka Arctic sea-ice record from Mendeleev Ridge based on ostracodes. *Quaternary Science Reviews*, **79**, 157–167. 53

Cronin, T.M., Whatley, R., Wood, A., Tsukagoshi, A., Ikeya, N., Brouwers, E.M. & Briggs, W.M. (1993). Microfaunal evidence for elevated Pliocene temperatures in the Arctic Ocean. *Paleoceanography*, **8**, 161–173. 24, 74, 92, 124, 140, 181

Crossley, J. & Roberts, D. (1995). The thermodynamic/dynamic sea ice model. *Unified Model Documentation*, **45**, 1–29. 49

Csank, A.Z., Tripati, A.K., Patterson, W.P., Eagle, R.A., Rybczynski, N., Ballantyne, A.P. & Eiler, J.M. (2011). Estimates of Arctic land surface temperatures during the Early Pliocene from two novel proxies. *Earth and Planetary Science Letters*, **304**, 291 – 299. 184

Curran, M., van Ommen, T., Morgan, V., Phillips, K. & Palmer, A. (2003). Ice core evidence for Antarctic sea ice decline since the 1950s. *Science*, **302**, 1203–1206. 57

Curry, J. & Ebert, E. (1992). Annual cycle of radiation fluxes over the Arctic Ocean - sensitivity to cloud optical properties. *Journal of Climate*, **5**, 1267–1280. 48

Curry, J.A., Schramm, J.L. & Ebert, E.E. (1995). Sea ice-albedo climate feedback mechanism. *Journal of Climate*, **8**, 240–247. 34, 37, 38, 45, 73, 118, 140

Darby, D., Bischof, J., Cutter, G., de Vernal, A., Hillaire-Mercal, C., Dwyer, G., McManus, J., Osterman, L., Polyak, L. & Poore,

R. (2001). New record shows pronounced changes in Arctic Ocean circulation and climate. *Eos Transactions, AGU*, **82**, 601. 55

Darby, D.A. (2008). Arctic perennial ice cover over the last 14 million years. *Paleoceanography*, **23**, PA1S07. 58, 92, 116, 124, 140, 161, 166, 181

Day, J.J., Hargreaves, J.C., Annan, J.D. & Abe-Ouchi, A. (2012). Sources of multi-decadal variability in Arctic sea ice extent. *Environmental Research Letters*, **7**, 034011. 121

de Leeuw, G., Andreas, E., Anguelova, M., Fairall, C., Lewis, E., O'Dowd, C., Schulz, M. & Schwartz, S. (2011). Production flux of sea spray aerosol. *Rev. Geophys.*, **49**. 55

de Vernal, A., Henry, M., Matthiessen, J., Mudie, P., Rochon, A., Boessenkool, K., Eynaud, F., Grøsfjeld, K., Guiot, J., Hamel, D., Harland, R., Head, M., Kunz-Pirrung, M., Levac, E., Loucheur, V., Peyron, O., Pospelova, V., Radi, T., Turon, J. & Voronina, E. (2001). Dinoflagellate cyst assemblages as tracers of sea-surface conditions in the northern North Atlantic, Arctic and sub-Arctic seas: the new 'n=677' data base and its application for quantitative palaeoceanographic reconstruction. *Journal of Quaternary Science*, **16**, 681–698. 54

de Vernal, A., Eynaud, F., Henry, M., Hillaire-Marcel, C., Londeix, L., Mangin, S., Matthiessen, J., Marret, F., Radi, T., Rochon, A., Solignac, S. & Turon, J. (2005). Reconstruction of sea-surface conditions at middle to high latitudes of the Northern Hemisphere during the Last Glacial Maximum (LGM) based on dinoflagellate cyst assemblages. *Quaternary Science Reviews*, **24**, 897–924. 54

de Vernal, A., Hillaire-Marcel, C., Solignac, S., Radi, T. & Rochon, A. (2008). Reconstructing sea ice conditions in the Arctic and sub-Arctic prior to human observations. *Arctic sea ice decline: Observations, projections, mechanisms, and implications*, 27–45. 51, 55

de Vernal, A., Gersonde, R., Goosse, H., Seidenkrantz, M.S. & Wolff, E. (2013a). Sea ice in the paleoclimate system: the challenge of reconstructing sea ice from proxies - an introduction. *Quaternary Science Reviews*, **79**, 1–8. 35, 51

de Vernal, A., Hillaire-Marcel, C., Rochon, A., Fréchette, B., Henry, M., Solignac, S. & Bonnet, S. (2013b). Dinocyst-based reconstructions of sea ice cover concentration during the Holocene in the Arctic ocean, the northern North Atlantic ocean and its adjacent seas. *Quaternary Science Reviews*, **79**, 111–121. 54

de Vernal, A., Rochon, A., Fréchette, B., Henry, M., Radi, T. & Solignac, S. (2013c). Reconstructing past sea ice cover of the Northern Hemisphere from dinocyst assemblages: status of the approach. *Quaternary Science Reviews*, **79**, 122–134. 51, 53, 54

Defant, A. (1961). Physical Oceanography, Vol. I. MacMillan. **728 pp**. 36

Dethloff, K., Rinke, A., Benkel, A., Køltzow, M., Sokolova, E., Saha, S., Handorf, D., Dorn, W., Rockel, B., von Storch, H., Haugen, J., Roed, L., Roeckner, E., Christensen, J. & Stendel, M. (2006). A dynamical link between the Arctic and the global climate system. *Geophysical Research Letters*, **33**. 36

DeWeaver, E., Hunke, E. & Holland, M. (2008). Comment on "On the reliability of simulated Arctic sea ice in global climate models" by I. Eisenman, N. Untersteiner, and J. S. Wettlaufer. *Geophysical Research Letters*, **L04501**. 119

Dolan, A., Haywood, A., Hill, D., Dowsett, H., Hunter, S., Lunt, D. & Pickering, S. (2011). Sensitivity of Pliocene ice sheets to orbital forcing. *Palaeogeography Palaeoclimatology Palaeoecology*, **309**, 98–110. 25, 26

Dorn, W., Dethloff, K., Rinke, A., Frickenhaus, S., Gerdes, R., Karcher, M. & Kauker, F. (2007). Sensitivities and uncertainties in a coupled regional atmosphere-ocean-ice model with respect to the simulation of

Arctic sea ice. *Journal of Geophysical Research-Atmospheres*, **112**. 1, 34, 41, 46

Dowsett, H. (1989). Application of the graphic correlation method to Pliocene marine sequences. *Marine Micropaleontology*, **14**, 3–32. 4

Dowsett, H. (1991). The development of a long-range foraminifer transfer function and application to late Pleistocene North Atlantic climatic extremes. *Paleoceanography*, **6**, 259–273. 10

Dowsett, H. (2007). The PRISM palaeoclimate reconstruction and Pliocene sea-surface temperature. *Deep-Time Perspectives on Climate Change: Marrying the Signal from Computer Models and Biological Proxies*, 459–480. 8, 9, 10, 13, 14, 15, 24, 191

Dowsett, H. & Cronin, T. (1990). High eustatic sea level during the middle Pliocene - evidence from the Southeastern United States Atlantic coastal plain. *Geology*, **18**, 435–438. 18

Dowsett, H. & Poore, R. (1990). A new planktic foraminifer transfer function for estimating Pliocene-Holocene paleoceanographic conditions in the North Atlantic. *Marine Micropaleontology*, **16**, 1–23. 10

Dowsett, H. & Poore, R. (1991). Pliocene sea surface temperatures of the North Atlantic Ocean at 3.0 Ma. *Quaternary Science Reviews*, **10**, 189–204. 10, 13

Dowsett, H. & Robinson, M. (1998). Application of the modern analogue technique (MAT) of sea surface temperature estimation to middle Pliocene North Pacific planktic foraminifer assemblages. *Palaeontologia Electronica*, **1**. 15

Dowsett, H. & Robinson, M. (2006). Stratigraphic framework for Pliocene paleoclimate reconstruction: The correlation conundrum. *Stratigraphy*, **3**, 53–64. 4, 13

Dowsett, H., Thompson, R., Barron, J., Cronin, T., Fleming, F., Ishman, S., Poore, R., Willard, D. & Holtz, T. (1994). Joint Investigations of the Middle Pliocene Climate I: PRISM Paleoenvironmental Reconstructions. *Global and Planetary Change*, **9**, 169–195. 5, 18, 24

Dowsett, H., Barron, J. & Poore, R. (1996). Middle Pliocene sea surface temperatures: A global reconstruction. *Marine Micropaleontology*, **27**, 13–25. 5, 10, 18, 24, 25

Dowsett, H., Barron, J., Poore, R., Thompson, R., Cronin, T., Ishman, S. & Willard, D. (1999). Middle Pliocene paleoenvironmental reconstruction: PRISM 2. *US Geological Survey Open File Report 99-535*. 5, 10, 15, 18, 20, 24, 25, 26, 28

Dowsett, H., Chandler, M., Cronin, T. & Dwyer, G. (2005). Middle Pliocene sea surface temperature variability. *Paleoceanography*, **20**. 5, 13, 14, 15, 24, 25

Dowsett, H., Robinson, M. & Foley, K. (2009). Pliocene three-dimensional global ocean temperature reconstruction. *Climate of the Past*, **5**, 769–783. 16, 17, 82, 84, 166

Dowsett, H., Haywood, A., Valdes, P., Robinson, M., Lunt, D., Hill, D., Stoll, D. & Foley, K. (2011). Sea surface temperatures of the mid-Piacenzian Warm Period: A comparison of PRISM3 and HadCM3. *Palaeogeography Palaeoclimatology Palaeoecology*, **309**, 83–91. 1, 27, 29, 73, 140

Dowsett, H., Foley, K., Stoll, D., Chandler, M., Sohl, L., Bentsen, M., Otto-Bliesner, B., Bragg, F., Chan, W.L., Contoux, C., Dolan, A., Haywood, A., Jonas, J., Jost, A., Kamae, Y., Lohmann, G., Lunt, D., Nisancioglu, K., Abe-Ouchi, A., Ramstein, G., Riesselman, C., Robinson, M., Salzmann, U., Stepanek, C., Strother, S., Ueda, H., Yan, Q. & Zhang, Z. (2013). Sea Surface Temperature of the mid-Piacenzian Ocean: A Data-Model Comparison. *Sci. Rep.*, **3**, 149–163. 77, 144

Dowsett, H.J., Robinson, M.M., Haywood, A.M., Salzmann, U., Hill, D.J., Sohl, L., Chandler, M.A., Williams, M., Foley, K. & Stoll, D. (2010). The PRISM3D paleoenvironmental reconstruction. *Stratigraphy*, **7**, 123–139. 1, 3, 4, 5, 9, 16, 17, 18, 21, 66, 73, 76, 77, 83, 92, 95, 140, 143, 144, 190, 191

Dowsett, H.J., Robinson, M.M., Haywood, A.M., Hill, D.J., Dolan, A.M., Stoll, D.K., Chan, W.L., Abe-Ouchi, A., Chandler, M.A., Rosenbloom, N.A., Otto-Bliesner, B.L., Bragg, F.J., Lunt, D.J., Foley, K.M. & Riesselman, C.R. (2012). Assessing confidence in Pliocene sea surface temperatures to evaluate predictive models. *Nature Climate Change*, **2**, 365–371. 9, 77

Draut, A., Raymo, M., McManus, J. & Oppo, D. (2003). Climate stability during the Pliocene warm period. *Paleoceanography*, **18**. 5

Dwyer, G. (2009). DSDP 592 and ODP 754, 804, 805, 806, 928, 929, 982, 1085, 1090, 1092, 1123, 1236, 1237, 1239 and 1241 ostracode Mg/Ca data. *IGBP PAGES/World Data Centre for Paleoclimatology*. 17

Dwyer, G., Cronin, T., Baker, P., Raymo, M., Buzas, J. & Correge, T. (1995). North Atlantic deep water temperature change during late Pliocene and late Quaternary climatic cycles. *Science*, **270**, 1347–1351. 17

Ebert, E. & Curry, J. (1993). An intermediate one-dimensional thermodynamic sea ice model for investigating ice atmosphere interactions. *Journal of Geophysical Research-Oceans*, **98**, 10085–10109. 48, 50

Edwards, J. & Slingo, A. (1996). Studies with a flexible new radiation code. 1: Choosing a configuration for a large-scale model. *Quarterly Journal of the Royal Meteorological Society*, **122**, 689–719. 60, 142

Eisenman, I., Untersteiner, N. & Wettlaufer, J.S. (2007). On the reliability of simulated Arctic sea ice in global climate models. *Geophysical Research Letters*, **34**, L10501. 119

Eisenman, I., Untersteiner, N. & Wettlaufer, J.S. (2008). Reply to comment by E. T. DeWeaver et al. on "On the reliability of simulated Arctic sea ice in global climate models". *Geophysical Research Letters*, **35**, L04502. 73, 119

England, J., Lakeman, T., Lemmen, D., Bednarski, J., Stewart, T. & Evans, D. (2008). A millennial-scale record of Arctic Ocean sea ice variability and the demise of the Ellesmere Island ice shelves. *Geophysical Research Letters*, **35**. 58

ETOP05 (1988). Global 5′ x 5′ depth and evaluation. *Technical report, National Geophysical Data Centre, NOAA, US Department of Commerce, Boulder, USA*. 61

Fetterer, F. & Untersteiner, N. (1998). Observations of melt ponds on Arctic sea ice. *Journal of Geophysical Research-Oceans*, **103**, 24821–24835. 39, 40

Fichefet, T. & Morales Maqueda, M.A. (1999). Modelling the influence of snow accumulation and snow-ice formation on the seasonal cycle of the Antarctic sea-ice cover. *Climate Dynamics*, **15**, 251–268. 117

Fischer, H., Fundel, F., Ruth, U., Twarloh, B., Wegner, A., Udisti, R., Becagli, S., Castellano, E., Morganti, A., Severi, M., Wolff, E., Littot, G., Röthlisberger, R., Mulvaney, R., Hutterli, M., Kaufmann, P., Federer, U., Lambert, F., Bigler, M., Hansson, M., Jonsell, U., de Angelis, M., Boutron, C., Siggaard-Andersen, M.L., Steffensen, J., Barbante, C., Gaspari, V., Gabrielli, P. & Wagenbach, D. (2007). Reconstruction of millennial changes in dust emission, transport and regional sea ice coverage using the deep EPICA ice cores from the Atlantic and Indian Ocean sector of Antarctica. *Earth and Planetary Science Letters*, **260**. 56

Flannery, B. (1984). Energy-balance models incorporating transport of thermal and latent energy. *Journal of the Atmospheric Sciences*, **41**, 414–421. 45

REFERENCES

Flato, G. & Hibler, W. (1992). Modeling pack ice as a cavitating fluid. *Journal of Physical Oceanography*, **22**, 626–651. 47

Flocco, D. & Feltham, D. (2007). A continuum model of melt pond evolution on Arctic sea ice. *Journal of Geophysical Research-Oceans*, **112**. 50, 51

Foster, G. (2008). Seawater pH, pCO_2 and $[CO_2^{-3}]$ variations in the Caribbean Sea over the last 130 kyr: A boron isotope and B/Ca study of planktic foraminifera. *Earth and Planetary Science Letters*, **271**, 254–266. 6

Garzione, C., Dettman, D., Quade, J., DeCelles, P. & Butler, R. (2000). High times on the Tibetan Plateau: Paleoelevation of the Thakkhola graben, Nepal. *Geology*, **28**, 339–342. 20

Garzione, C., Molnar, P., Libarkin, J. & MacFadden, B. (2006). Rapid late Miocene rise of the Bolivian Altiplano: Evidence for removal of mantle lithosphere. *Earth and Planetary Science Letters*, **241**, 543–556. 20

Gent, P. & McWilliams, J. (1990). Isopycnal mixing in ocean circulation models. *Journal of Physical Oceanography*, **20**, 150–155. 61

Ghosh, P., Garzione, C. & Eiler, J. (2006). Rapid uplift of the Altiplano revealed through ^{13}C-^{18}O bonds in paleosol carbonates. *Science*, **311**, 511–515. 20

Gibbard, P., Head, M. & Walker, M. (2010). Formal ratification of the Quaternary System/Period and the Pleistocene Series/Epoch with a base at 2.58 Ma. *Journal of Quaternary Science*, **25**, 96–102. 3

Giles, K., Laxon, S. & Ridout, A. (2008). Circumpolar thinning of Arctic sea ice following the 2007 record ice extent minimum. *Geophysical Research Letters*, **35**. 44

Goldner, A., Herold, N. & Huber, M. (2014). The challenge of simulating the warmth of the mid-Miocene climatic optimum in CESM1. *Climate of the Past*, **10**, 523–536. 29

Gordon, C., Cooper, C., Senior, C.A., Banks, H., Gregory, J.M., Johns, T.C., Mitchell, J.F.B. & Wood, R.A. (2000). The simulation of SST, sea ice extents and ocean heat transports in a version of the Hadley Centre coupled model without flux adjustments. *Climate Dynamics*, **16**, 147–168. 2, 59, 60, 61, 62, 63, 64, 65, 75, 122, 141, 142, 188, 189

Graversen, R. & Wang, M. (2009). Polar amplification in a coupled climate model with locked albedo. *Climate Dynamics*, **33**, 629–643. 45

Gregory, D. & Morris, D. (1996). The sensitivity of climate simulations to the specification of mixed phase clouds. *Climate Dynamics*, **12**, 641–651. 60

Gregory, D., Shutts, G. & Mitchell, J. (1998). A new gravity-wave-drag scheme incorporating anisotropic orography and low-level wave breaking: Impact upon the climate of the UK Meteorological Office Unified Model. *Quarterly Journal of the Royal Meteorological Society*, **124**, 463–493. 60, 142

Gregory, J., Stott, P., Cresswell, D., Rayner, N., Gordon, C. & Sexton, D. (2002). Recent and future changes in Arctic sea ice simulated by the HadCM3 AOGCM. *Geophysical Research Letters*, **29**. 34, 44, 65

Grenfell, T. & Perovich, D. (2004). Seasonal and spatial evolution of albedo in a snow-ice-land-ocean environment. *Journal of Geophysical Research-Oceans*, **109**. 38

Grumet, N., Wake, C., Mayewski, P., Zielinski, G., Whitlow, S., Koerner, R., Fisher, D. & Wollett, J. (2001). Variability of sea-ice extent in Baffin Bay over the last millennium. *Climatic Change*, **49**, 129–145. 56

Haggblom, A. (1982). Driftwood in Svalbard as an indicator of sea ice conditions . *Geografiska Annaler Series a-Physical Geography*, **64**, 81–94. 58

Hakkinen, S. & Mellor, G. (1992). Modeling the seasonal variability of a coupled Arctic ice-ocean system. *Journal of Geophysical Research-Oceans*, **97**, 20285–20304. 48

Hall, A. (2004). The role of surface albedo feedback in climate. *Journal of Climate*, **17**, 1550–1568. 45

Hanesiak, J., Barber, D., de Abreu, R. & Yackel, J. (2001). Local and regional albedo observations of Arctic first-year sea ice during melt ponding. *Journal of Geophysical Research-Oceans*, **106**, 1005–1016. 38, 39

Hansen, J., Lacis, A., Rind, D., Russell, G., Stone, P., Fung, I., Ruedy, R. & Lerner, J. (1984). Climate sensitivity: Analysis of feedback mechanisms. *Climate Processes and Climate Sensitivity*, **29**, 130–163. 45

Haq, B., Hardenbol, J. & Vail, P. (1987a). Chronology of fluctuating sea levels since the Triassic. *Science*, **235**, 1156–1167. 18

Haq, B., Hardenbol, J. & Vail, P. (1987b). The new chronostratigraphic basis of Cenozoic and Mesozoic sea level cycles. *Cushman Foundation for Foraminiferal Research Special Publication*, 7–14. 18

Hays, J.D., Imbrie, J. & Shackleton, N.J. (1976). Variations in the earth's orbit: Pacemaker of the ice ages. *Science*, **194**, 1121–1132. 31, 32, 33

Haywood, A. & Valdes, P. (2004). Modelling Pliocene warmth: contribution of atmosphere, oceans and cryosphere. *Earth and Planetary Science Letters*, **218**, 363–377. 25, 26, 73, 140

Haywood, A. & Valdes, P. (2006). Vegetation cover in a warmer world simulated using a dynamic global vegetation model for the Mid-Pliocene. *Palaeogeography Palaeoclimatology Palaeoecology*, **237**, 412–427. 25

Haywood, A., Sellwood, B. & Valdes, P. (2000a). Regional warming: Pliocene (3 Ma) paleoclimate of Europe and the Mediterranean. *Geology*, **28**, 1063–1066. 25

Haywood, A., Valdes, P. & Sellwood, B. (2000b). Global scale palaeoclimate reconstruction of the middle Pliocene climate using the UKMO GCM: initial results. *Global and Planetary Change*, **25**, 239–256. 25

Haywood, A., Valdes, P., Sellwood, B., Kaplan, J. & Dowsett, H. (2001). Modelling middle Pliocene warm climates and environments of the U.S.A. *Palaeontol. Electron.*, **4**. 25

Haywood, A., Valdes, P., Francis, J. & Sellwood, B. (2002). Global middle Pliocene biome reconstruction: A data/model synthesis. *Geochemistry Geophysics Geosystems*, **3**. 26

Haywood, A., Deken, P., Ravelo, A. & Williams, M. (2005). Warmer tropics during the mid-Pliocene? Evidence from alkenone paleothermometry and a fully coupled ocean-atmosphere GCM. *Geochemistry Geophysics Geosystems*, **6**, 1–20. 25, 26

Haywood, A., Valdes, P. & Peck, V. (2007). A permanent El Nino-like state during the Pliocene? *Paleoceanography*, **22**. 25, 26

Haywood, A., Chandler, M., Valdes, P., Salzmann, U., Lunt, D. & Dowsett, H. (2009). Comparison of mid-Pliocene climate predictions produced by the HadAM3 and GCMAM3 General Circulation Models. *Global and Planetary Change*, **66**, 208–224. 25

Haywood, A., Dolan, A., Pickering, S., Dowsett, H., McClymont, E., Prescott, C., Salzmann, U., Hill, D., Hunter, S., Lunt, D., Pope, J. & Valdes, P. (2013a). On the identification of a Pliocene time slice for data–model comparison. *Global and Planetary Change*, **371**. 31

Haywood, A.M., Dowsett, H.J., Otto-Bliesner, B.L., Chandler, M.A., Dolan, A.M., Hill, D.J., Lunt, D.J., Robinson, M.M., Rosenbloom, N., Salzmann, U. & Stoll, D.K. (2011a). Pliocene Model Intercomparison Project (PlioMIP): experimental design and boundary conditions (Experiment 1). *Geosci. Model Dev.*, **3**, 227–242. 29, 70, 93, 95

Haywood, A.M., Dowsett, H.J., Robinson, M.M., Stoll, D.K., Dolan, A.M., Lunt, D.J., Otto-Bliesner, B.L. & Chandler, M.A. (2011b). Pliocene Model Intercomparison Project (PlioMIP): experimental design and boundary conditions (Experiment 2). *Geosci. Model Dev.*, **4**, 571–577. 29, 30, 70, 76, 93, 95, 141, 143, 189

Haywood, A.M., Hill, D.J., Dolan, A.M., Otto-Bliesner, B.L., Bragg, F.J., Chan, W.L., Chandler, M.A., Contoux, C., Dowsett, H.J., Jost, A., Kamae, Y., Lohmann, G., Lunt, D.J., Abe-Ouchi, A., Pickering, S.J., Ramstein, G., Rosenbloom, N.A., Salzmann, U., Sohl, L., Stepanek, C., Ueda, H., Yan, Q. & Zhang, S.Z. (2013b). Large-scale features of Pliocene climate: results from the Pliocene Model Intercomparison Project. *Clim. Past*, **9**, 191–209. 1, 3, 29, 30, 73, 92, 140, 141

Hebbeln, D. & Wefer, G. (1991). Effects of ice coverage and ice-rafted material on sedimentation in the Fram Strait. *Nature*, **350**, 409–411. 55

Heinemann, M., Jungclaus, J.H. & Marotzke, J. (2009). Warm Paleocene/Eocene climate as simulated in ECHAM5/MPI-OM. *Climate of the Past*, **5**, 785–802. 28

Henehan, M., Rae, J., Foster, G., Erez, J., Prentice, K., Kucera, M., Bostock, H., Martinez-Boti, M., Milton, J., Wilson, P., Marshall, B.J. & Elliott, T. (2013). Calibration of the boron isotope proxy in the planktonic foraminifera Globigerinoides ruber for use in palaeo-CO_2 reconstruction. *Earth and Planetary Science Letters*, **364**, 111–122. 6

Herman, G. & Johnson, W. (1978). Sensitivity of the general circulation to Arctic sea ice boundaries - a numerical experiment. *Monthly Weather Review*, **106**, 1649–1664. 34, 36

Herold, N., Huber, M. & Müller, R. (2011). Modeling the Miocene Climatic Optimum. Part I: Land and Atmosphere*. *Journal of Climate*, **24**, 6353–6372. 29

Hibler, W.D. (1979). A dynamic-thermodynamic sea ice model. *Journal of Physical Oceanography*, **9**, 815–846. 47, 48, 49, 62, 75, 117, 142, 188

Hildebrandsson, H. (1914). Quelques recherches sur les centres d'action de l'atmosphère. *Kung Sven. Vetenskap Hand.*, **51**, 3–16. 35

Hill, D., Haywood, A., Hindmarsh, R. & Valdes, P. (2007). Characterizing ice sheets during the Pliocene: evidence from data and models. *Deep-Time Perspectives on Climate Change: Marrying the Signal from Computer Models and Biological Proxies*, 517–538. 24, 25

Hill, D.J., Haywood, A.M., Lunt, D.J., Hunter, S.J., Bragg, F.J., Contoux, C., Stepanek, C., Sohl, L., Rosenbloom, N.A., Chan, W.L., Kamae, Y., Zhang, Z., Abe-Ouchi, A., Chandler, M.A., Jost, A., Lohmann, G., Otto-Bliesner, B.L., Ramstein, G. & Ueda, H. (2014). Evaluating the dominant components of warming in Pliocene climate simulations. *Climate of the Past*, **10**, 79–90. 117, 123, 146, 153, 165

Hillaire-Marcel, C. & de Vernal, A. (2008). Stable isotope clue to episodic sea ice formation in the glacial North Atlantic. *Earth and Planetary Science Letters*, **268**, 143–150. 54, 55

Hillaire-Marcel, C., de Vernal, A., Polyak, L. & Darby, D. (2004). Size-dependent isotopic composition of planktic foraminifers from Chukchi Sea vs. NW Atlantic sediments - implications for the Holocene paleoceanography of the western Arctic. *Quaternary Science Reviews*, **23**, 245–260. 55

Hillenbrand, C. & Ehrmann, W. (2005). Late Neogene to Quaternary environmental changes in the Antarctic Peninsula region: evidence from drift sediments. *Global and Planetary Change*, **45**, 165–191. 24

Hodson, D., Keeley, S., West, A., Ridley, J., Hawkins, E. & Hewitt, H. (2013). Identifying uncertainties in Arctic climate change projections. *Climate Dynamics*, **40**, 2849–2865. 117

Holland, D., Mysak, L., Manak, D. & Oberhuber, J. (1993). Sensitivity study of a dynamic thermodynamic sea ice model. *Journal of Geophysical Research-Oceans*, **98**, 2561–2586. 48

Holland, M., Bitz, C. & Tremblay, B. (2006). Future abrupt reductions in the summer Arctic sea ice. *Geophysical Research Letters*, **33**. 44

Holland, M.M. & Bitz, C.M. (2003). Polar amplification of climate change in coupled models. *Climate Dynamics*, **21**, 221–232. 40, 41, 45, 46, 119

Holland, M.M. & Stroeve, J. (2011). Changing seasonal sea ice predictor relationships in a changing Arctic climate. *Geophysical Research Letters*, **38**, L18501. 93

Holland, M.M., Bailey, D.A., Briegleb, B.P., Light, B. & Hunke, E.C. (2011). Improved sea ice shortwave radiation physics in CCSM4: The impact of melt ponds and aerosols on Arctic sea ice. *Journal of Climate*, **25**, 1413–1430. 71, 83, 94, 118

Hönisch, B. & Hemming, N. (2005). Surface ocean pH response to variations in pCO_2 through two full glacial cycles. *Earth and Planetary Science Letters*, **236**, 305–314. 6

Houghton, J., Meira Filho, L., Callander, B., Harris, N., Kattenberg, A. & Maskell, K. (1996). The science of climate change. *Climate change 1995*. 64

Howell, F.W., Haywood, A.M., Dolan, A.M., Dowsett, H.J., Francis, J.E., Hill, D.J., Pickering, S.J., Pope, J.O., Salzmann, U. & Wade, B.S. (2014). Can uncertainties in sea ice albedo reconcile patterns of data-model discord for the Pliocene and 20th/21st centuries? *Geophysical Research Letters*, **41**, 2011–2018. 117, 140, 144, 151, 154

Howell, F.W., Haywood, A.M., Otto-Bliesner, B.L., Bragg, F., Chan, W.L., Chandler, M.A., Contoux, C., Kamae, Y., Abe-Ouchi, A., Rosenbloom, N.A., Stepanek, C. & Zhang, Z. (2015). Arctic sea ice in the PlioMIP ensemble: is model performance for modern climates a reliable guide to performance for the past or the future? *Climate of the Past Discussions*, **11**, 1263–1312. 141, 162, 165

Hu, Z.Z., Kuzmina, S.I., Bengtsson, L. & Holland, D.M. (2004). Sea-ice change and its connection with climate change in the Arctic in CMIP2 simulations. *Journal of Geophysical Research: Atmospheres*, **109**, D10106. 65

Huber, M. & Sloan, L.C. (2001). Heat transport, deep waters, and thermal gradients: Coupled simulation of an Eocene greenhouse climate. *Geophysical Research Letters*, **28**, 3481–3484. 28

Huber, M., Sloan, L.C. & Shellito, C. (2003). Early Paleogene oceans and climate: A fully coupled modeling approach using the NCAR CCSM. *Geological Society of America Special Papers*, **369**, 25–47. 28

Hudson, S., Granskog, M., Sundfjord, A., Randelhoff, A., Renner, A. & Divine, D. (2013). Energy budget of first-year Arctic sea ice in advanced stages of melt. *Geophysical Research Letters*, **40**, 2679–2683. 41

Hunke, E.C. (2010). Thickness sensitivities in the CICE sea ice model. *Ocean Modelling*, **34**, 137–149. 40, 71, 73, 94, 116, 119

Hunke, E.C. & Bitz, C.M. (2009). Age characteristics in a multidecadal arctic sea ice simulation. *Journal of Geophysical Research: Oceans*, **114**, C08013. 83

Hunke, E.C. & Dukowicz, J.K. (1997). An elastic-viscous-plastic model for sea ice dynamics. *Journal of Physical Oceanography*, **27**, 1849–1867. 49, 71, 94, 117

Hunke, E.C. & Lipscomb, W.H. (2008). CICE: The Los Alamos sea ice model user's manual, version 4.0. *Tech. Rep. LA-CC-06-012, Los Alamos, New Mexico.*, 76. 117

Hurrell, J.W., Kushnir, Y. & Visbeck, M. (2001). The North Atlantic Oscillation. *Science*, **291**, 603–605.

Imbrie, J. & Kipp, N. (1971). A new micropaleontological method for quantitative paleoclimatology: Application to a Late Pleistocene Caribbean core. *The Late Cenozoic Glacial Ages*, **Yale University Press, New Haven, Connecticut**, 71–181. 10

Imbrie, J., Boyle, E.A., Clemens, S.C., Duffy, A., Howard, W.R., Kukla, G., Kutzbach, J., Martinson, D.G., McIntyre, A., Mix, A.C., Molfino, B., Morley, J.J., Peterson, L.C., Pisias, N.G.,

Prell, W.L., Raymo, M.E., Shackleton, N.J. & Toggweiler, J.R. (1992). On the structure and origin of major glaciation cycles 1. Linear responses to Milankovitch forcing. *Paleoceanography*, **7**, 701–738. 32

IPCC (2007). Climate Change 2007: The Physical Science Basis. Contribution of Working Group I to the Fourth Assessment Report of The Intergovernmental Panel on Climate Change. *Cambridge University Press, Cambridge, UK & New York*, 906pp. 44, 73

Johns, T., Carnell, R., Crossley, J., Gregory, J., Mitchell, J., Senior, C., Tett, S. & Wood, R. (1997). The second Hadley Centre coupled ocean-atmosphere GCM: Model description, spinup and validation. *Climate Dynamics*, **13**, 103–134. 59, 60, 61

Johnson, M., Gaffigan, S., Hunke, E. & Gerdes, R. (2007). A comparison of Arctic Ocean sea ice concentration among the coordinated AOMIP model experiments. *Journal of Geophysical Research: Oceans*, **112**, C04S11. 93

Johnson, M., Proshutinsky, A., Aksenov, Y., Nguyen, A.T., Lindsay, R., Haas, C., Zhang, J., Diansky, N., Kwok, R., Maslowski, W., Häkkinen, S., Ashik, I. & de Cuevas, B. (2012). Evaluation of Arctic sea ice thickness simulated by Arctic Ocean Model Intercomparison Project models. *Journal of Geophysical Research: Oceans*, **117**, C00D13. 93

Joussaume, S. & Braconnot, P. (1997). Sensitivity of paleoclimate simulation results to season definitions. *Journal of Geophysical Research: Atmospheres*, **102**, 1943–1956. 32, 33

Justwan, A. & Koc, N. (2008). A diatom based transfer function for reconstructing sea ice concentrations in the North Atlantic. *Marine Micropaleontology*, **66**, 264–278. 53

K-1 Model Developers (2004). K1 Coupled Model (MIROC) Description: K1 Technical Report 1, edited by: Hasumi, H. and Emori, S. *34 pp., Center for Climate System Research, University of Tokyo*. 71, 94, 118

Kamae, Y. & Ueda, H. (2011). Evaluation of Simulated Climate in Lower Latitude Regions during the Mid-Pliocene Warm Period Using Paleovegetation Data. *SOLA*, **7**, 177–180. 25

Kamae, Y. & Ueda, H. (2012). Mid-Pliocene global climate simulation with MRI-CGCM2.3: set-up and initial results of PlioMIP Experiments 1 and 2. *Geoscientific Model Development*, **5**, 793–808. 71, 94

Kaplan, J. (2001). Geophysical applications of vegetation modelling, PhD Thesis, Lund University. *PhD Thesis, Lund University*. vii, 21

Kaufman, D. & Brigham-Grette, J. (1993). Aminostratigraphic correlations and paleotemperature implications, Pliocene-Pleistocene, high sea level deposits, northwestern Alaska. *Quaternary Science Reviews*, **12**, 21–33. 57

Kellogg, W. (1975). Climatic feedback mechanisms involving the polar regions. *Climate of the Arctic*, 111–116. 34, 73, 140

Kelly, P. (1979). An Arctic sea ice data set, 1901-1956. *Glaciological Data 5, World Data Center A for Glaciology (Snow and Ice), Boulder*, 101–106. 42

Kim, S. & Crowley, T. (2000). Increased Pliocene North Atlantic Deep Water: Cause or consequence of Pliocene warming? *Paleoceanography*, **15**, 451–455. 25

Kim, J.H., Schouten, S., Hopmans, E.C., Donner, B. & Damsté, J.S.S. (2008). Global sediment core-top calibration of the TEX_{86} paleothermometer in the ocean. *Geochimica et Cosmochimica Acta*, **72**, 1154 – 1173. 13

Knies, J., Cabedo-Sanz, P., Belt, S.T., Baranwal, S., Fietz, S. & Rosell-Melé, A. (2014). The emergence of modern sea ice cover in the Arctic Ocean. *Nat. Commun.*, **5:5608**. 53, 58, 115, 116, 124, 140, 166

Knudsen, K., Eiriksson, J., Jansen, E., Jiang, H., Rytter, F. & Gudmundsdottir, E. (2004). Palaeoceanographic changes off North Iceland through the last 1200 years: foraminifera, stable isotopes, diatoms and ice rafted debris. *Quaternary Science Reviews*, **23**, 2231–2246. 55

Koenigk, T., Devasthale, A. & Karlsson, K.G. (2013). Summer sea ice albedo in the Arctic in CMIP5 models. *Atmospheric Chemistry and Physics Discussions*, **13**, 25219–25251. 83

Krantz, D. (1991). A chronology of Pliocene sea level fluctuations - The United States middle Atlantic coastal plain record. *Quaternary Science Reviews*, **10**, 163–174. 18

Krapp, M. & Jungclaus, J.H. (2011). The Middle Miocene climate as modelled in an atmosphere-ocean-biosphere model. *Climate of the Past*, **7**, 1169–1188. 29

Kraus, E. & Turner, J. (1967). A one-dimensional model of the seasonal thermocline II. The general theory and its consequences. *Tellus*, **19**, 98–105. 61

Krebs, U., Park, W. & Schneider, B. (2011). Pliocene aridification of Australia caused by tectonically induced weakening of the Indonesian throughflow. *Palaeogeography Palaeoclimatology Palaeoecology*, **309**, 111–117. 25, 27

Kumar, A., Perlwitz, J., Eischeid, J., Quan, X., Xu, T., Zhang, T., Hoerling, M., Jha, B. & Wang, W. (2010). Contribution of sea ice loss to Arctic amplification. *Geophysical Research Letters*, **37**. 34, 45, 82, 151

Kürschner, W., van der Burgh, J., Visscher, H. & Dilcher, D. (1996). Oak leaves as biosensors of late neogene and early pleistocene paleoatmospheric CO2 concentrations. *Marine Micropaleontology*, **27**, 299–312. 6, 189

Kwok, R. (2000). Recent changes in Arctic Ocean sea ice motion associated with the North Atlantic Oscillation. *Geophysical Research Letters*, **27**, 775–778. 121

Kwok, R. (2004). Annual cycles of multiyear sea ice coverage of the Arctic Ocean: 1999-2003. *Journal of Geophysical Research-Oceans*, **109**. 39, 41

Kwok, R. & Untersteiner, N. (2011). The thinning of Arctic sea ice. *Physics Today*, **64**, 36–41. 41

Kwok, R., Cunningham, G.F., Wensnahan, M., Rigor, I., Zwally, H.J. & Yi, D. (2009). Thinning and volume loss of the Arctic Ocean sea ice cover: 2003-2008. *Journal of Geophysical Research*, **114**, C07005. 40, 112

Langen, P. & Alexeev, V. (2005). Estimating $2\times CO_2$ warming in an aqua-planet GCM using the fluctuation- dissipation theorem. *Geophysical Research Letters*, **32**. 45

Laskar, J., Robutel, P., Joutel, F., Gastineau, M., Correia, A. & Levrard, B. (2004). A long-term numerical solution for the insolation quantities of the Earth. *Astronomy and Astrophysics*, **428**, 261–285. 67, 81, 143, 189

Laskar, J., Fienga, A., Gastineau, M. & Manche, H. (2011). La2010: A new orbital solution for the long term motion of the Earth. *Astronomy and Astrophysics*, **532**, 89–103. 32

Lawrence, D., Slater, A., Tomas, R., Holland, M. & Deser, C. (2008). Accelerated Arctic land warming and permafrost degradation during rapid sea ice loss. *Geophysical Research Letters*, **35**. 34, 81

Lea, D.W., Mashiotta, T.A. & Spero, H.J. (1999). Controls on magnesium and strontium uptake in planktonic foraminifera determined by live culturing. *Geochimica et Cosmochimica Acta*, **63**, 2369 – 2379. 11

Legates, D. & Willmott, C. (1990). Mean seasonal and spatial variability in global surface air temperature. *Theor. Appl. Climatol.*, **41**, 11–21. 64, 65, 158

Lemke, P. & Ren, J. (2007). Observations: Changes in snow, ice and frozen ground. *Climate Change 2007: The Physical Science Basis*, 337–383. 37, 44

Levermann, A., Mignot, J., Nawrath, S. & Rahmstorf, S. (2007). The role of Northern sea ice cover for the weakening of the thermohaline circulation under global warming. *Journal of Climate*, **20**, 4160–4171. 37

Lindsay, R. & Rothrock, D. (1994). Arctic sea ice albedo from AVHRR. *Journal of Climate*, **7**, 1737–1749. 38, 39

Lisiecki, L. & Raymo, M. (2005). A Pliocene-Pleistocene stack of 57 globally distributed benthic δ^{18}O records. *Paleoceanography*, **20**. 4, 5

Lisitzin, A. (2002). Sea-ice and iceberg sedimentation in the ocean, recent and past. *Springer-Verlag, Berlin*, 563pp. 55

Liu, J., Schmidt, G.A., Martinson, D., Rind, D.H., Russell, G.L. & Yuan, X. (2003). Sensitivity of sea ice to physical parameterizations in the GISS global climate model. *Journal of Geophysical Research*, **108**, 3053. 71, 94

Liu, Y., Key, J. & Wang, X. (2009). Influence of changes in sea ice concentration and cloud cover on recent Arctic surface temperature trends. *Geophysical Research Letters*, **36**. 1, 34, 45

Lunt, D., Foster, G., Haywood, A. & Stone, E. (2008a). Late Pliocene Greenland glaciation controlled by a decline in atmospheric CO_2 levels. *Nature*, **454**, 1102–U41. 25, 26

Lunt, D., Valdes, P., Haywood, A. & Rutt, I. (2008b). Closure of the Panama Seaway during the Pliocene: implications for climate and Northern Hemisphere glaciation. *Climate Dynamics*, **30**, 1–18. 25

Lunt, D., Haywood, A., Foster, G. & Stone, E. (2009). The Arctic cryosphere in the Mid-Pliocene and the future. *Philosophical Transactions of the Royal Society a-Mathematical Physical and Engineering Sciences*, **367**, 49–67. 25, 26

Lunt, D., Haywood, A., Schmidt, G., Salzmann, U., , Valdes, P. & Dowsett, H. (2010). Earth system sensitivity inferred from Pliocene modelling and data. *Nature Geoscience*, **3**, 60–64. 3, 25, 26

Lunt, D.J., Dunkley Jones, T., Heinemann, M., Huber, M., LeGrande, A., Winguth, A., Loptson, C., Marotzke, J., Roberts, C.D., Tindall, J., Valdes, P. & Winguth, C. (2012). A model-data comparison for a multi–model ensemble of early Eocene atmosphere-ocean simulations: EoMIP. *Climate of the Past*, **8**, 1717–1736. 28

Luthje, M., Feltham, D., Taylor, P. & Worster, M. (2006). Modeling the summertime evolution of sea-ice melt ponds. *Journal of Geophysical Research-Oceans*, **111**, 1–17. 50, 51

Mahajan, S., Zhang, R. & Delworth, T. (2011). Impact of the Atlantic Meridional Overturning Circulation (AMOC) on Arctic surface air temperature and sea ice variability. *Journal of Climate*, **24**, 6573–6581. 34, 121

Manabe, S. & Stouffer, R. (1980). Sensitivity of a global climate model to an increase of CO_2 concentration in the atmosphere. *Journal of Geophysical Research-Oceans and Atmospheres*, **85**, 5529–5554. 45

Markwick, P. (2007). The palaeogeographic and palaeoclimatic significance of climate proxies for data-model comparisons. *London: The Geological Society*, 251–312. 19, 20

Marlowe, I. (1984). Lipids as palaeoclimatic indicators. *Doctoral Thesis, University of Bristol*. 12

Marsland, S.J., Haak, H., Jungclaus, J.H., Latif, M. & Röske, F. (2003). The Max-Planck-Institute global ocean/sea ice model with orthogonal curvilinear coordinates. *Ocean Modelling*, **5**, 91–127. 71, 94, 117

Martinez-Boti, M., Foster, G., Chalk, T., Rohling, E., Sexton, P., Lunt, D., Pancost, R., Badger, M. & Schmidt, D. (2015). Plio-Pleistocene climate sensitivity evaluated using high-resolution CO_2 records. *Nature*, **518**, 49–54. 3, 6, 7

Mashiotta, T., Lea, D. & Spero, H. (1999). Glacial-interglacial changes in Subantarctic sea surface temperature and δ^{18}O-water using foraminiferal Mg. *Earth and Planetary Science Letters*, **170**, 417–432. 11, 12

Maslanik, J., Fowler, C., Stroeve, J., Drobot, S., Zwally, J., Yi, D. & Emery, W. (2007). A younger, thinner Arctic ice cover: Increased potential for rapid, extensive sea-ice loss. *Geophysical Research Letters*, **34**. 44

Massé, G., Rowland, S., Sicre, M.A., Jacob, J., Jansen, E. & Belt, S. (2008). Abrupt climate changes for Iceland during the last millennium: Evidence from high resolution sea ice reconstructions. *Earth and Planetary Science Letters*, **269**, 564–568. 52

Massé, G., Belt, S., Crosta, X., Schmidt, S., Snape, I., Thomas, D. & Rowland, S. (2011). Highly branched isoprenoids as proxies for variable sea ice conditions in the Southern Ocean. *Antarctic Science*, **23**, 487–498. 53

Masson-Delmotte, V., Schulz, M., Abe-Ouchi, A., Beer, J., Ganopolski, A., González Rouco, J., Jansen, K., Lambeck, K., Luterbacher, J., Naish, T., Osborn, T., Otto-Bliesner, B., Quinn, T., Ramesh, R., Rojas, M., Shao, X. & Timmerman, A. (2013). Information from Paleoclimate Archives. In: *Climate Change 2013: The Physical Science Basis. Contribution of Working Group I to the Fifth Assessment Report of the Intergovernmental Panel on Climate Change* [Stocker, T.F., D. Qin, G.-K. Plattner, M. Tignor, S.K. Allen, J. Boschung, A. Nauels, Y. Xia, V. Bex and P.M. Midgley (eds.)]. Cambridge University Press, Cambridge, United Kingdom and New York, NY, USA. 19

Massonnet, F., Fichefet, T., Goosse, H., Bitz, C.M., Philippon-Berthier, G., Holland, M.M. & Barriat, P.Y. (2012). Constraining projections of summer Arctic sea ice. *The Cryosphere Discussions*, **6**, 2931–2959. 92, 114, 119, 125

Matthiessen, J., de Vernal, A., Head, M., Okolodkov, Y., Zonneveld, K. & Harland, R. (2005). Modern organic-walled dinoflagellate cysts in Arctic marine environments and their (paleo-) environmental significance. *Palaeontologische Zeitschrift*, **79**, 3–51. 54

Mauritsen, T., Stevens, B., Roeckner, E., Crueger, T., Esch, M., Giorgetta, M., Haak, H., Jungclaus, J., Klocke, D., Matei, D.,

Mikolajewicz, U., Notz, D., Pincus, R., Schmidt, H. & Tomassini, L. (2012). Tuning the climate of a global model. *Journal of Advances in Modeling Earth Systems*, **4**, M00A01. 119

Maykut, G. (1978). Energy exchange over young sea ice in the central Arctic. *Journal Of Geophysical Research - Oceans*, **83**, 3646–3658. 34, 40, 41, 73, 140

Maykut, G. & Untersteiner, N. (1971). Some results from a time-dependent thermodynamic model of sea ice. *Journal of Geophysical Research*, **76**, 1550–1575. 46, 47, 48, 50, 61, 142, 188

McMillan, M., Heller, P. & Wing, S. (2006). History and causes of post-Laramide relief in the Rocky Mountain orogenic plateau. *Geological Society of America Bulletin*, **118**, 393–405. 20

Meehl, G. & Stocker, T. (2007). Global Climate Projections. *Climate Change 2007: The Physical Science Basis*, 747–845. 45

Meinardus, W. (1906). Periodische Schwankungen der Eistrift bei Island. *Ann. Hydrograph. Marit. Meteorol*, **34**, 148–162, 227–239, 278–285. 34

Mellor, G.L. & Kantha, L. (1989). An ice-ocean coupled model. *Journal of Geophysical Research-Oceans*, **94**, 10937–10954. 50, 71, 94, 117, 122

Milankovitch, M. (1941). Kanon der Erdbestrahlung und seine Andwendung auf das Eiszeiten-problem. *Royal Serbian Academy, Belgrade*. 31

Miles, M.W., Divine, D.V., Furevik, T., Jansen, E., Moros, M. & Ogilvie, A.E.J. (2014). A signal of persistent Atlantic multidecadal variability in Arctic sea ice. *Geophysical Research Letters*, **41**, 463–469, 2013GL058084. 121

Miller, K., Wright, J., Browning, J., Kulpecz, A., Kominz, M., Naish, T., Cramer, B., Rosenthal, Y., Peltier, W. & Sosdian, S. (2012). High tide of the warm Pliocene: Implications of global sea level for Antarctic deglaciation. *Geology*, **40**, 407–410. 3, 18, 19

Milton, S. & Wilson, C. (1996). The impact of parameterized subgrid-scale orographic forcing on systematic errors in a global NWP model. *Monthly Weather Review*, **124**, 2023–2045. 60

Moran, K., Backman, J., Brinkhuis, H., Clemens, S.C., Cronin, T., Dickens, G.R., Eynaud, F., Gattacceca, J., Jakobsson, M., Jordan, R.W., Kaminski, M., King, J., Koc, N., Krylov, A., Martinez, N., Matthiessen, J., McInroy, D., Moore, T.C., Onodera, J., O'Regan, M., Pälike, H., Rea, B., Rio, D., Sakamoto, T., Smith, D.C., Stein, R., St John, K., Suto, I., Suzuki, N., Takahashi, K., Watanabe, M., Yamamoto, M., Farrel, J., Frank, M., Kubik, P., Jokat, W. & Kristoffersen, Y. (2006). The Cenozoic palaeoenvironment of the Arctic Ocean. *Nature*, **441**, 601–605. 74, 92, 124, 140, 181

Mosbrugger, V. & Utescher, T. (1997). The coexistence approach a method for quantitative reconstructions of Tertiary terrestrial palaeoclimate data using plant fossils. *Palaeogeography, Palaeoclimatology, Palaeoecology*, **134**, 61–86. 17, 28

Moss, S. & Johnson, D. (1994). Aircraft measurements to validate and improve numerical model parametrisations of ice to water ratios in clouds. *Atmospheric Research, Vol 34, Nos 1-4, June 20, 1994: Special Issue: 11th International Conference on Clouds and Precipitation, Part III*, 1–25. 60

Müller, J., Wagner, A., Fahl, K., Stein, R., Prange, M. & Lohmann, G. (2011). Towards quantitative sea ice reconstructions in the northern North Atlantic: A combined biomarker and numerical modelling approach. *Earth and Planetary Science Letters*, **306**, 137–148. 51, 52

Müller, P., Kirst, G., Ruhland, G., von Storch, I. & Rosell-Melé, A. (1998). Calibration of the alkenone paleotemperature index $U^{k'}_{37}$ based on core-tops from the eastern South Atlantic and the global ocean (60°N - 60°S). *Geochimica Et Cosmochimica Acta*, **62**, 1757–1772. 12

Murray, R. & Simmonds, I. (1995). Responses of climate and cyclones to reductions in Arctic winter sea ice. *Journal of Geophysical Research - Oceans*, **100**, 4791–4806. 36

Nicolaus, M., Katlein, C., Maslanik, J. & Hendricks, S. (2012). Changes in Arctic sea ice result in increasing light transmittance and absorption. *Geophysical Research Letters*, **39**. 41

Notz, D. (2009). The future of ice sheets and sea ice: Between reversible retreat and unstoppable loss. *Proceedings of the National Academy of Sciences of the United States of America*, **106**, 20590–20595. 40

Nrnberg, D., Bijma, J. & Hemleben, C. (1996). Assessing the reliability of magnesium in foraminiferal calcite as a proxy for water mass temperatures. *Geochimica et Cosmochimica Acta*, **60**, 803 – 814. 11

Oberhuber, J. (1993). Simulation of the Atlantic circulation with a coupled sea ice mixed layer isopycnal general circulation model. I. Model Description. *Journal of Physical Oceanography*, **23**, 808–829. 48

Overland, J., Spillane, M., Percival, D., Wang, M. & Mofjeld, H. (2004). Seasonal and regional variation of pan-Arctic surface air temperature over the instrumental record. *Journal of Climate*, **17**, 3263–3282. 44

Pagani, M., Liu, Z., LaRiviere, J. & Ravelo, A.C. (2010). High Earth-system climate sensitivity determined from Pliocene carbon dioxide concentrations. *Nature Geoscience*, **3**, 27–30. 6, 8, 73, 92, 140, 189

Parkinson, C. & Washington, W. (1979). A large-scale numerical model of sea ice. *Journal of Geophysical Research - Oceans and Atmospheres*, **84**, 311–337. 47, 48

Parkinson, C.L., Vinnikov, K.Y. & Cavalieri, D.J. (2006). Evaluation of the simulation of the annual cycle of Arctic and Antarctic sea ice coverages by 11 major global climate models. *Journal of Geophysical Research: Oceans*, **111**, C07012. 93

Parkinson, C.L. (2008). Recent trend reversals in Arctic sea ice extents: possible connections to the North Atlantic Oscillation. *Polar Geography*, **31**, 3–14. 121

Parkinson, C.L. & Comiso, J.C. (2013). On the 2012 record low Arctic sea ice cover: Combined impact of preconditioning and an August storm. *Geophysical Research Letters*, **40**, 13561361. 44, 92

Parkinson, C.L., Cavalieri, D.J., Gloersen, P., Zwally, H.J. & Comiso, J.C. (1999). Arctic sea ice extents, areas, and trends, 1978-1996. *Journal of Geophysical Research-Oceans*, **104**, 20837–20856. 42

Pegau, W. & Paulson, C. (2001). The albedo of Arctic leads in summer. *Annals of Glaciology*, **33**, 221–224. 38

Pelejero, C. & Calvo, E. (2003). The upper end of the $U_{37}^{k'}$ temperature calibration revisited. *Geochemistry Geophysics Geosystems*, **4**. 13

Perovich, D. & Polashenski, C. (2012). Albedo evolution of seasonal Arctic sea ice. *Geophysical Research Letters*, **39**. 39, 40, 41, 74, 83, 144, 176, 177

Perovich, D., Maykut, G. & Grenfell, T. (1986). Optical properties of ice and snow in the polar regions. I: Observations. *Proc. SPIE Ocean Optics VIII*, **637**, 232–241. 38, 39

Perovich, D., Grenfell, T., Light, B. & Hobbs, P. (2002). Seasonal evolution of the albedo of multiyear Arctic sea ice. *Journal of Geophysical Research-Oceans*, **107**. 39

Perovich, D., Jones, K., Light, B., Eicken, H., Markus, T., Stroeve, J. & Lindsay, R. (2011). Solar partitioning in a changing Arctic sea-ice cover. *Annals of Glaciology*, **52**, 192–196. 39, 41

Perovich, D.K., Nghiem, S.V., Markus, T. & Schweiger, A. (2007). Seasonal evolution and interannual variability of the local solar energy absorbed by the arctic sea iceocean system. *Journal of Geophysical Research: Oceans*, **112**, C03005. 74

Pfirman, S., Lange, M., Wollenburg, I. & Schlosser, P. (1990). Sea ice characteristics and the role of sediment inclusions in deep-sea deposition: Arctic-Antarctic comparisons. *Geological History of the Polar Oceans : Arctic Versus Antarctic*, **308**, 187–211. 55

Polashenski, C., Perovich, D. & Courville, Z. (2012). The mechanisms of sea ice melt pond formation and evolution. *Journal of Geophysical Research: Oceans*, **117**, C01001. 74, 83, 177

Polyak, L., Alley, R.B., Andrews, J.T., Brigham-Grette, J., Cronin, T.M., Darby, D.A., Dyke, A.S., Fitzpatrick, J.J., Funder, S., Holland, M.M., Jennings, A.E., Miller, G.H., O'Regan, M., Savelle, J., Serreze, M., St John, K., White, J.W.C. & Wolff, E. (2010). History of sea ice in the Arctic. *Quaternary Science Reviews*, **29**, 1757–1778. 51, 55, 57, 58, 74, 92, 124, 140, 166, 181

Polyakov, I. & Johnson, M. (2000). Arctic decadal and interdecadal variability. *Geophysical Research Letters*, **27**, 4097–4100. 46

Polyakov, I., Alekseev, G., Bekryaev, R., Bhatt, U., Colony, R., Johnson, M., Karklin, V., Makshtas, A., Walsh, D. & Yulin, A. (2002). Observationally based assessment of polar amplification of global warming. *Geophysical Research Letters*, **29**. 46

Pope, J., Collins, M., Haywood, A., Dowsett, H., Hunter, S., Lunt, D., Pickering, S. & Pound, M. (2011). Quantifying Uncertainty in Model Predictions for the Pliocene (Plio-QUMP): Initial results. *Palaeogeography Palaeoclimatology Palaeoecology*, **309**, 128–140. 25, 27

Pope, V., Gallani, M., Rowntree, P. & Stratton, R. (2000). The impact of new physical parametrizations in the Hadley Centre climate model: HadAM3. *Climate Dynamics*, **16**, 123–146. 22, 59, 64, 65

Potvin, E., Rochon, A. & Lovejoy, C. (2013). Cyst-theca relationship of the Arctic dinoflagellate cyst *Islandinium minutum* (Dinophyceae) and phylogenetic position based on SSU rDNA and LSU rDNA. *Journal of Phycology*, **49**, 848–866. 54

Prahl, F. & Wakeham, S. (1987). Calibration of unsaturation patterns in long-chain ketone compositions for palaeotemperature assessment. *Nature*, **320**, 367–369. 12

Prahl, F., Muehlhausen, L. & Zahnle, D. (1988). Further evaluation of long-chain alkenones as indicators of paleoceanographic conditions. *Geochimica Et Cosmochimica Acta*, **52**, 2303–2310. 12

Prescott, C., Haywood, A., Dolan, A., Hunter, S., Pope, J. & Pickering, S. (2014). Assessing orbitally-forced interglacial climate variability during the mid-Pliocene Warm Period. *Earth and Planetary Science Letters*, **400**, 149–163. 31

Rankin, A., Wolff, E. & Martin, S. (2002). Frost flowers: Implications for tropospheric chemistry and ice core interpretation. *Journal of Geophysical Research-Atmospheres*, **107**. 56

Raymo, M., Grant, B., Horowitz, M. & Rau, G. (1996). Mid-Pliocene warmth: Stronger greenhouse and stronger conveyor. *Marine Micropaleontology*, **27**, 313–326. 189

Rayner, N.A., Parker, D.E., Horton, E.B., Folland, C.K., Alexander, L.V., Rowell, D.P., Kent, E.C. & Kaplan, A. (2003). Global analyses of sea surface temperature, sea ice, and night marine air temperature since the late nineteenth century. *Journal of Geophysical Research-Atmospheres*, **108**, 4407, d14. 42, 66, 76, 79

Reynolds, R. & Smith, T. (1995). A high-resolution global sea-surface temperature climatology. *Journal of Climate*, **8**, 1571–1583. 15, 29

Ridley, J., Lowe, J., Brierley, C. & Harris, G. (2007). Uncertainty in the sensitivity of Arctic sea ice to global warming in a perturbed parameter climate model ensemble. *Geophysical Research Letters*, **34**. 34

Rigor, I., Colony, R. & Martin, S. (2000). Variations in surface air temperature observations in the Arctic, 1979-97. *Journal of Climate*, **13**, 896–914. 45

Riihela, A., Mannien, T. & Laine, V. (2013). Observed changes in the albedo of the Arctic sea-ice zone for the period 1982-2009. *Nature Climate Change*, **3**, 895–898. 39, 144, 176

Rind, D., Healy, R., Parkinson, C. & Martinson, D. (1995). The role of sea ice in $2\times CO_2$ climate model sensitivity, Part I: The total influence of sea ice thickness and extent. *Journal of Climate*, **8**, 449–463. 38, 40, 41

Roberts, M., Marsh, R., New, A. & Wood, R. (1996). An intercomparison of a Bryan-Cox-type ocean model and an isopycnic ocean model. 1. The subpolar gyre and high-latitude processes. *Journal of Physical Oceanography*, **26**, 1495–1527. 61

Robinson, M., Dowsett, H., Dwyer, G. & Lawrence, K. (2008). Reevaluation of mid-Pliocene North Atlantic sea surface temperatures. *Paleoceanography*, **23**. 11, 12, 27

Rochon, A., de Vernal, A., Turon, J., Matthiessen, J. & Head, M. (1999). Distribution of dinoflagellate cyst assemblages in surface sediments from the North Atlantic Ocean and adjacent basins and quantitative reconstruction of sea-surface parameters. *Special Contribution Series. American Association of Stratigraphic Palynologists, n° 35, College Station, Texas*. 54

Rosell-Melé, A. (1998). Interhemispheric appraisal of the value of alkenone indices as temperature and salinity proxies in high-latitude locations. *Paleoceanography*, **13**, 694–703. 13

Rosell-Melé, A. & McClymont, E. (2007). Biomarkers as Paleoceanographic Proxies. *Proxies in Late Cenozoic Paleoceanography*, **1**, 441–490. 12

Rosenbloom, N.A., Otto-Bliesner, B.L., Brady, E.C. & Lawrence, P.J. (2013). Simulating the mid-Pliocene Warm Period with the CCSM4 model. *Geoscientific Model Development*, **6**, 549–561. 71, 94

Röthlisberger, R., Mulvaney, R., Wolff, E., Hutterli, M., Bigler, M., de Angelis, M., Hansson, M., Steffensen, J. & Udisti, R. (2003).

Limited dechlorination of sea-salt aerosols during the last glacial period: Evidence from the European Project for Ice Coring in Antarctica (EPICA) Dome C ice core. *Journal of Geophysical Research-Atmospheres*, **108**. 55

Röthlisberger, R., Crosta, X., Abram, N., Armand, L. & Wolff, E. (2010). Potential and limitations of marine and ice core sea ice proxies: an example from the Indian Ocean sector. *Quaternary Science Reviews*, **29**, 296–302. 56

Rothrock, D., Yu, Y. & Maykut, G. (1999). Thinning of the Arctic sea-ice cover. *Geophysical Research Letters*, **26**, 3469–3472. 44

Rowley, D., Pierrehumbert, R. & Currie, B. (2001). A new approach to stable isotope-based paleoaltimetry: implications for paleoaltimetry and paleohypsometry of the High Himalaya since the Late Miocene. *Earth and Planetary Science Letters*, **188**, 253–268. 20

Sakamoto, T., Komuro, Y., Nishimura, T., Ishii, M., Tatebe, H., Shigoama, H., Hasegawa, A., Toyoda, T., Mori, M., Suzuki, T., Imada, Y., Nozawa, T., Takata, K., Mochizuki, T., Ogochi, K., Emori, S., Hasumi, H. & Kimoto, M. (2012). MIROC4h - A new high-resolution atmosphere-ocean coupled general circulation model. *Journal of the Meteorological Society of Japan. Ser. II*, **90**, 325–359.

Salzmann, U., Haywood, A., Lunt, D., Valdes, P. & Hill, D. (2008). A new global biome reconstruction and data-model comparison for the Middle Pliocene. *Global Ecology and Biogeography*, **17**, 432–447. 17, 21, 22, 23, 28, 77, 144, 191

Salzmann, U., Dolan, A., Haywood, A., Chan, W.L., Voss, J., Hill, D., Abe-Ouchi, A., Otto-Bliesner, B., Bragg, F., Chandler, M., Contoux, C., Dowsett, H., Jost, A., Kamae, Y., Lohmann, G., Lunt, D., Pickering, S., Pound, M., Ramstein, G., Rosenbloom, N., Sohl, L., Stepanek, C., Ueda, H. & Zhang, Z. (2013). Challenges in quantifying Pliocene terrestrial warming revealed by data-model discord. *Nature Climate Change*, **3**, 969–974. 1, 27, 28, 73, 77, 81, 84, 140, 144, 166

Schell, I. (1956). Interrelations of Arctic ice with the atmosphere and the ocean in the North Atlantic-Arctic and adjacent areas. *Journal of Meteorology*, **13**, 46–58. 36

Schell, I. (1970). Arctic ice and sea temperature anomalies in the northeastern North Atlantic and their significance for seasonal foreshadowing locally and to the eastward. *Monthly Weather Review*, **98**, 833–850. 36

Scherhag, R. (1936). Eine bemerkenswerte Klimaänderung über Nordeuropa. *Ann. Hydrograph. Marit. Meteorol*, **64**, 96–100. 35

Schlesinger, M. & Ramankutty, N. (1994). An oscillation in the global climate system of period 65-70 years. *Nature*, **367**, 723–726. 46

Schmidt, G.A., Reto, R., Hansen, J.E., Aleinov, I., Bell, N., Bauer, M., Bauer, S., Cairns, B., Canuto, V., Cheng, Y., Del Genio, A., Faluvegi, G., Friend, A.D., Hall, T.M., Hu, Y., Kelley, M., Kiang, N.Y., Koch, D., Lacis, A.A., Lerner, J., Lo, K.K., Miller, R.L., Nazarenko, L., Oinas, V., Perlwitz, J.P., Perlwitz, J., Rind, D., Romanou, A., Russell, G.L., Sato, M., Shindell, D.T., Stone, P.H., Sun, S., Tausnev, N., Thresher, D. & Yao, M.S. (2006). Present-day atmospheric simulations using GISS ModelE: Comparison to in situ, satellite, and reanalysis data. *Journal of Climate*, **19**, 153–192. 118

Schouten, S., Hopmans, E.C., Schefuss, E. & Damsté, J.S.S. (2002). Distributional variations in marine crenarchaeotal membrane lipids: a new tool for reconstructing ancient sea water temperatures? *Earth and Planetary Science Letters*, **204**, 265 – 274. 13

Schouten, S., Hopmans, E.C. & Damsté, J.S.S. (2013). The organic geochemistry of glycerol dialkyl glycerol tetraether lipids: A review. *Organic Geochemistry*, **54**, 19 – 61. 13

Schröder-Adams, C., Cole, F., Medioli, F., Mudie, P., Scott, D. & Dobbin, L. (1990). Recent Arctic shelf foraminifera - seasonally ice covered vs. perennially ice covered areas. *Journal of Foraminiferal Research*, **20**, 8–36. 54

Scott, D., Mudie, P., Baki, V., MacKinnon, K. & Cole, F. (1989). Biostratigraphy and late Cenozoic paleoceanography of the Arctic Ocean: foraminifera, lithostratigraphic, and isotopic evidence. *Geological Society of America Bulletin*, **101**, 260–277. 54

Scott, D., Schell, T., St-Onge, G., Rochon, A. & Blasco, S. (2009). Foraminiferal assemblage changes over the last 15,000 years on the Mackenzie-Beaufort Sea Slope and Amundsen Gulf, Canada: Implications for past sea ice conditions. *Paleoceanography*, **24**, PA2219. 54

Screen, J. & Simmonds, I. (2010a). Increasing fall-winter energy loss from the Arctic Ocean and its role in Arctic temperature amplification. *Geophysical Research Letters*, **37**. 45, 82, 151

Screen, J. & Simmonds, I. (2010b). The central role of diminishing sea ice in recent Arctic temperature amplification. *Nature*, **464**, 1334–1337. 45, 82

Screen, J., Deser, C. & Simmonds, I. (2012). Local and remote controls on observed Arctic warming. *Geophysical Research Letters*, **39**. 34, 45

Sedláček, J., Knutti, R., Martius, O. & Beyerle, U. (2012). Impact of a reduced Arctic sea ice cover on ocean and atmospheric properties. *Journal of Climate*, **25**, 307–319. 44

Seidenkrantz, M.S. (2013). Benthic foraminifera as palaeo sea-ice indicators in the subarctic realm - examples from the Labrador Sea-Baffin Bay region. *Quaternary Science Reviews*, **79**, 135–144. 54

Seki, O., Foster, G.L., Schmidt, D.N., Mackensen, A., Kawamura, K. & Pancost, R.D. (2010). Alkenone and boron-based Pliocene pCO_2 records. *Earth and Planetary Science Letters*, **292**, 201–211. 6, 7, 8, 73, 92, 140, 189

Sellers, W. (1969). A global climate model based on the energy balance of the earth-atmosphere system. *Journal of Applied Meteorology*, **8**, 392–400. 46

Semtner, A.J. (1976). A model for the thermodynamic growth of sea ice in numerical investigations of climate. *Journal of Physical Oceanography*, **6**, 379–389. 47, 48, 49, 61, 62, 75, 117, 142, 188

Serreze, M. & Barry, R. (2011). Processes and impacts of Arctic amplification: A research synthesis. *Global and Planetary Change*, **77**, 85–96. 45, 46

Serreze, M. & Francis, J. (2006). The Arctic amplification debate. *Climatic Change*, **76**, 241–264. 45, 46

Serreze, M., Maslanik, J., Scambos, T., Fetterer, F., Stroeve, J., Knowles, K., Fowler, C., Drobot, S., Barry, R. & Haran, T. (2003). A record minimum Arctic sea ice extent and area in 2002. *Geophysical Research Letters*, **30**. 44

Serreze, M., Barrett, A., Stroeve, J., Kindig, D. & Holland, M. (2009). The emergence of surface-based Arctic amplification. *Cryosphere*, **3**, 11–19. 45

Shackleton, N., Hall, M. & Pate, D. (1993). Pliocene stable isotope stratigraphy of Site 846. *Proceedings of the ODP Scientific Results*, **138**, 42pp. 18

Shackleton, N., Hall, M. & Pate, D. (1995). Pliocene stable isotope stratigraphy of Site 846. *Proceedings of the Ocean Drilling Program, Scientific Results*, **138**, 337–355. 5

Shellito, C.J., Sloan, L.C. & Huber, M. (2003). Climate model sensitivity to atmospheric CO_2 levels in the Early–Middle Paleogene. *Palaeogeography, Palaeoclimatology, Palaeoecology*, **193**, 113 – 123. 28

Shellito, C.J., Lamarque, J.F. & Sloan, L.C. (2009). Early Eocene Arctic climate sensitivity to pCO_2 and basin geography. *Geophysical Research Letters*, **36**, L09707. 28

Shu, Q., Song, Z. & Qiao, F. (2015). Assessment of sea ice simulations in the CMIP5 models. *The Cryosphere*, **9**, 399–409. 93, 111, 112, 162

Sloan, L., Crowley, T. & Pollard, D. (1996). Modeling of middle pliocene climate with the NCAR GENESIS general circulation model. *Marine Micropaleontology*, **27**, 51–61. 25

Sloan, L.C., Walker, J.C.G. & Moore, T.C. (1995). Possible role of oceanic heat transport in Early Eocene climate. *Paleoceanography*, **10**, 347–356. 28

Sluijs, A., Schouten, S., Pagani, M., Woltering, M., Brinkhuis, H., Damste, J., Dickens, G., Huber, M., Reichart, G., Stein, R., Matthiessen, J., Lourens, L., Pedentchouk, N., Backman, J., Moran, K. & the Expedition 302 Scientists (2006). Subtropical Arctic ocean temperatures during the Palaeocene/Eocene thermal maximum. *Nature*, **441**, 610–613. 28

Sohl, L., Chandler, M., Schmunk, R., Mankoff, K., Jonas, J., Foley, K. & Dowsett, H. (2009). PRISM3/GISS topographic reconstruction. *U.S. Geological Survey Data Series*, **419**, 6pp. 19, 20, 23, 24, 191

Solomon, S., Qin, D., Manning, M., Chen, Z., Marquis, M., Averyt, K., Tignor, M. & Miller (eds.), H. (2007). Contribution of Working Group I to the Fourth Assessment Report of the Intergovernmental Panel on Climate Change. *Cambridge University Press*, 996pp. 45

Sonzogni, C., Bard, E., Rostek, F., Dollfus, D., Rosell-Melé, A. & Eglinton, G. (1997). Temperature and salinity effects on alkenone ratios measured in surface sediments from the Indian Ocean. *Quaternary Research*, **47**, 344–355. 13

Stein, R. & Fahl, K. (2013). Biomarker proxy shows potential for studying the entire Quaternary Arctic sea ice history. *Organic Geochemistry*, **55**, 98–102. 53

Stein, R., Fahl, K. & Müller, J. (2012). Proxy reconstruction of Arctic Ocean sea ice history: from IRD to IP_{25}. *Polarforschung*, **82**. 53

Stepanek, C. & Lohmann, G. (2012). Modelling mid-Pliocene climate with COSMOS. *Geoscientific Model Development*, **5**, 1221–1243. 71, 94

Stranne, C. & Bjork, G. (2012). On the Arctic Ocean ice thickness response to changes in the external forcing. *Climate Dynamics*, **39**, 3007–3018. 40

Stroeve, J., Holland, M.M., Meier, W., Scambos, T. & Serreze, M. (2007). Arctic sea ice decline: Faster than forecast. *Geophysical Research Letters*, **34**, L09501. 44, 74, 79, 93

Stroeve, J., Serreze, M., Holland, M., Kay, J., Maslanik, J.A. & Barrett, A. (2012a). The Arctic's rapidly shrinking sea ice cover: a research synthesis. *Climatic Change*, **110**, 1005–1027. 38, 40, 43

Stroeve, J., Barrett, A., Serreze, M. & Schweiger, A. (2014). Using records from submarine, aircraft and satellites to evaluate climate model simulations of Arctic sea ice thickness. *The Cryosphere*, **8**, 1839–1854. 93, 112

Stroeve, J.C., Kattsov, V., Barrett, A., Serreze, M., Pavlova, T., Holland, M.M. & Meier, W.N. (2012b). Trends in Arctic sea ice extent from CMIP5, CMIP3 and observations. *Geophysical Research Letters*, **39**, L16502. 1, 44, 74, 92, 93

Taylor, P. & Feltham, D. (2004). A model of melt pond evolution on sea ice. *Journal of Geophysical Research-Oceans*, **109**, 149–163. 50, 51

Thompson, R. & Fleming, R. (1996). Middle Pliocene vegetation: Reconstructions, paleoclimatic inferences, and boundary conditions for climate modeling. *Marine Micropaleontology*, **27**, 27–49. 20, 21, 158, 191

Thomsen, H. (1947). The annual reports on the Arctic sea ice issued by the Danish Meteorological Institute. *Journal of Glaciology*, **1**, 140–141. 42, 111

Tremblay, L., Mysak, L. & Dyke, A. (1997). Evidence from driftwood records for century-to-millennial scale variations of the high latitude atmospheric circulation during the Holocene. *Geophysical Research Letters*, **24**, 2027–2030. 58

Uttal, T., Curry, J.A., McPhee, M.G., Perovich, D.K., Moritz, R.E., Maslanik, J.A., Guest, P.S., Stern, H.L., Moore, J.A., Turenne, R., Heiberg, A., Serreze, M.C., Wylie, D.P., Persson, O.G., Paulson, C.A., Halle, C., Morison, J.H., Wheeler, P.A., Makshtas, A., Welch, H., Shupe, M.D., Intrieri, J.M., Stamnes, K., Lindsey,

R.W., Pinkel, R., Pegau, W.S., Stanton, T.P. & Grenfeld, T.C. (2002). Surface heat budget of the Arctic Ocean. *Bulletin of the American Meteorological Society*, **83**, 255–276. 39, 42

Vare, L., Massé, G., Gregory, T., Smart, C. & Belt, S. (2009). Role of Arctic sea ice in global atmospheric circulation: A review. *Quaternary Science Reviews*, **28**, 1354–1366. 52

Vaughan, D., Comiso, J., Allison, I., Carrasco, J., Kaser, G., Kwok, R., Mote, P., Murray, T., Paul, F., Ren, J., Rignot, E., Solomina, O., Steffen, K. & Zhang, T. (2013). Observations: Ocean. In: *Climate Change 2013: The Physical Science Basis. Contribution of Working Group I to the Fifth Assessment Report of the Intergovernmental Panel on Climate Change* [Stocker, T.F., D. Qin, G.-K. Plattner, M. Tignor, S.K. Allen, J. Boschung, A. Nauels, Y. Xia, V. Bex and P.M. Midgley (eds.)]. Cambridge University Press, Cambridge, United Kingdom and New York, NY, USA. 1

Vogt, P.R. & Parrish, M. (2012). Driftwood dropstones in Middle Miocene Climate Optimum shallow marine strata (calvert cliffs, Maryland coastal plain): Erratic pebbles no certain proxy for cold climate. *Palaeogeography, Palaeoclimatology, Palaeoecology*, **323**, 100 – 109. 55

Visbeck, M., Marshall, J., Haine, T. & Spall, M. (1997). Specification of eddy transfer coefficients in coarse-resolution ocean circulation models. *Journal of Physical Oceanography*, **27**, 381–402. 61

Wagenbach, D., Ducroz, F., Mulvaney, R., Keck, L., Minikin, A., Legrand, M., Hall, J. & Wolff, E. (1998). Sea-salt aerosol in coastal Antarctic regions. *Journal of Geophysical Research-Atmospheres*, **103**, 10961–10974. 56

Walker, G. (1947). Arctic conditions and world weather. *Quarterly Journal of the Royal Meteorological Society*, **73**, 226–256. 35

Walsh, J. & Johnson, C. (1979). An analysis of Arctic sea ice fluctuations. *Journal of Physical Oceanography*, **9**, 580–591. 42

Walsh, J. & Timlin, M. (2003). Northern Hemisphere sea ice simulations by global climate models. *Polar Research*, **22**, 75–82. 46

Walsh, J.E. & Chapman, W.L. (2001). 20th-century sea-ice variations from observational data. *Annals of Glaciology*, **33**, 444–448. 42, 111

Wang, M. & Overland, J. (2009). A sea ice free summer Arctic within 30 years? *Geophysical Research Letters*, **36**. 146, 178

Wang, M. & Overland, J.E. (2012). A sea ice free summer Arctic within 30 years: An update from CMIP5 models. *Geophysical Research Letters*, **39**, L18501. 44, 92

Washington, W. & Meehl, G. (1996). High-latitude climate change in a global coupled ocean-atmosphere-sea ice model with increased atmospheric CO_2. *Journal of Geophysical Research-Atmospheres*, **101**, 12795–12801. 45

Whitehead, J. & Bohaty, S. (2003). Pliocene summer sea surface temperature reconstruction using silicoflagellates from Southern Ocean ODP Site 1165. *Paleoceanography*, **18**. 24

Wiese, W. (1924). Polareis und Atmospharische Schwankungen. *Geograf. Ann.*, **6**, 273–299. 35

Winguth, A., Shellito, C., Shields, C. & Winguth, C. (2010). Climate Response at the Paleocene–Eocene Thermal Maximum to Greenhouse Gas Forcing–A Model Study with CCSM3. *J. Climate*, 2562–2584. 28

Winton, M. (2006). Amplified Arctic climate change: What does surface albedo feedback have to do with it? *Geophysical Research Letters*, **33**. 45, 46

Wolfe, J. (1993). A method of obtaining climatic parameters from leaf assemblages. *U.S. Geological Survey Bulletin*, **2040**, 1–71. 17

Wolff, E., Rankin, A. & Röthlisberger, R. (2003). An ice core indicator of Antarctic sea ice production? *Geophysical Research Letters*, **30**. 56

Wolff, E., Fischer, H., Fundel, F., Ruth, U., Twarloh, B., Littot, G., Mulvaney, R., Röthlisberger, R., de Angelis, M., Boutron, C., Hansson, M., Jonsell, U., Hutterli, M., Lambert, F., Kaufmann, P., Stauffer, B., Stocker, T., Steffensen, J., Bigler, M., Siggaard-Andersen, M., Udisti, R., Becagli, S., Castellano, E., Severi, M., Wagenbach, D., Barbante, C., Gabrielli, P. & Gaspari, V. (2006). Southern Ocean sea-ice extent, productivity and iron flux over the past eight glacial cycles. *Nature*, **440**, 491–496. 56

Yukimoto, S., Adachi, Y., Hosaka, M., Sakami, T., Yoshimura, H., Hirabara, M., Tanaka, T.Y., Shindo, E., Tsujino, H., Deushi, M. *et al.* (2012). A new global climate model of the Meteorological Research Institute: MRI-CGCM3–model description and basic performance. *Journal of the Meteorological Society of Japan*, **90**, 23–64.

Zhang, J. & Rothrock, D. (2000). Modeling Arctic sea ice with an efficient plastic solution. *Journal of Geophysical Research*, **105**, 3325–3338. 71, 94, 117

Zhang, J., Lindsay, R., Schweiger, A. & Steele, M. (2013a). The impact of an intense summer cyclone on 2012 Arctic sea ice retreat. *Geophysical Research Letters*, **40**, 720–726. 6, 7, 8, 44, 68, 92, 140, 143

Zhang, R. & Jiang, D. (2014). Impact of vegetation feedback on the mid-Pliocene warm climate. *Advances in Atmospheric Sciences*, **31**, 1407–1416. 25

Zhang, Z., Nisancioglu, K., Chandler, M., Haywood, A., Otto-Bliesner, B., Ramstein, G., Stepanek, C., Abe-Ouchi, A., Chan, W., Bragg, F., Contoux, C., Dolan, A., Hill, D., Jost, A., Kamae, Y., Lohmann, G., Lunt, D., Rosenbloom, N., Sohl, L. & Ueda, H. (2013b). Mid-Pliocene Atlantic Meridional Overturning Circulation not unlike modern. *Climate of the Past*, **9**, 1495–1504. 121, 183

Zhang, Z.S., Nisancioglu, K., Bentsen, M., Tjiputra, J., Bethke, I., Yan, Q., Risebrobrakken, B., Andersson, C. & Jansen, E. (2012). Pre-industrial and mid-Pliocene simulations with NorESM-L. *Geoscientific Model Development*, **5**, 523–533. 71, 94